

JAERI - M
93-193

ANNUAL REPORT OF NAKA FUSION RESEARCH ESTABLISHMENT
FOR THE PERIOD FROM APRIL 1, 1992 TO MARCH 31, 1993

October 1993

Naka Fusion Research Establishment

日本原子力研究所
Japan Atomic Energy Research Institute

JAERI-Mレポートは、日本原子力研究所が不定期に公刊している研究報告書です。
入手の問い合わせは、日本原子力研究所技術情報部情報資料課（〒319-11茨城県那珂郡東海村）あて、お申しこしてください。なお、このほかに財団法人原子力弘済会資料センター（〒319-11茨城県那珂郡東海村日本原子力研究所内）で複写による実費頒布をおこなっております。

JAERI-M reports are issued irregularly.

Inquiries about availability of the reports should be addressed to Information Division
Department of Technical Information, Japan Atomic Energy Research Institute, Tokai-
mura, Naka-gun, Ibaraki-ken 319-11, Japan.

©Japan Atomic Energy Research Institute, 1993

編集兼発行 日本原子力研究所
印 刷 いばらき印刷機

Annual Report of Naka Fusion Research Establishment
for the period from April 1, 1992 to March 31, 1993

Naka Fusion Research Establishment

Japan Atomic Energy Research Institute
Naka-machi, Naka-gun, Ibaraki-ken

(Received September 6, 1993)

Research and development activities at Naka Fusion Research Establishment, JAERI, are reported for the period from April 1, 1992 to March 31, 1993.

The main objectives of JT-60U experiments in FY1992 were to improve plasma confinement properties and to study non-inductive current drive. High- β_p H-mode performance obtained in March 1993 was highlighted, in particular, a world-record fusion-triple-product of $1.1 \times 10^{21} \text{ m}^{-3} \cdot \text{s} \cdot \text{keV}$, and record values for JT-60 of neutron yield rate of $5.6 \times 10^{16} \text{ s}^{-1}$, stored energy of 8.3 MJ, and H-factor of 3.6. The JFT-2M continued to study divertor biasing and ergodic limiter experiments, and disruption control by ECH.

The study in Plasma Theory and Computation focused on scaling laws of the thermal energy confinement and the bootstrap current, the iron temperature gradient instability, the MHD stability, the rotation damping by external magnetic error field, and the burning plasma of D- ^3He fusion.

As for the fusion engineering research, the vacuum technology advanced the development of a high resolution quadrupole mass spectrometer, etc. The super-conducting Demo Poloidal Coil achieved pulsed operation with 7 T in 0.5 s, and newly developed conductors made of Nb_3Al and Nb_3Sn showed 40 kA at 12 T and 82 kA at 13.6 T, respectively. A high energy H $^-$ beam of 350 kV, 0.17 A was produced with a current density of 10 mA/cm^2 .

Editors: M. Ohta (in chief), K. Shimizu, T. Fujii, M. Nishi, T. Matoba,
T. Kanazawa

Much effort was made in developing the ECH gyrotron with an output power of 460 kW at 120 GHz for 100 ms. The main progress in the Tritium Systems Test Assembly (a US/Japan collaboration) was continuous loop run for 25 days. The developed plasma facing components posed no problem under a heat flux of 20 MW/m² for 30 s over 1000 thermal cycles.

The ITER Engineering Design Activities Agreement and Protocol 1 were signed on July 21, 1992 and the organization of its project was fixed. The Joint Central Team proposed the preliminary design in March 1993.

Keywords: Fusion Research, JAERI, JT-60U, JFT-2M, DIII-D, Plasma Physics, Fusion Engineering, ITER, FER, Fusion Reactor Design, Annual Report

那珂研究所年報（平成4年度）

日本原子力研究所
那珂研究所

（1993年9月6日受理）

原研・那珂研究所における平成4年度（1992年4月～1993年3月）の研究開発活動について報告する。

1992年度のJT-60Uの主な実験目的は、プラズマ閉じ込めの改善と非誘導電流駆動の研究であった。1993年3月に得られた高 β_p ・Hモードプラズマの成果は顕著であった。特に核融合積は世界記録の $1.1 \times 10^{21} \text{m}^{-3} \cdot \text{s} \cdot \text{keV}$ 、中性子発生率、蓄積エネルギー及びHファクターは、それぞれJT-60での最大値 $5.6 \times 10^{19} \text{s}^{-1}$ 、8.3J及び3.6であった。JFT-2Mは、ダイバータパイアスやエルゴディックリミタの実験、ECHによるディスラプション制御の研究を継続した。

プラズマ理論・数値解析では、熱エネルギー閉じ込めの比例則、有限アスペクト比のトカマクでのブートストラップ電流、イオン温度勾配不安定性、MHD安定性、外部から加えられた不整磁場による回転の減衰、D-³He核融合の燃焼プラズマを研究した。

核融合工学については、真空技術では、高分解能四極子質量分析器などの開発を進めた。超電導実証ポロイダル・コイルでは0.5秒で7Tまで立ち上げるパルス運転を達成した。新たに開発したニオブアルミとニオブズ製の導体を用いて、それぞれ12Tで40kA、13.6Tで82kAの通電を達成した。高エネルギー負イオンビームの開発では、 10mA/cm^2 の電流密度で350kV、0.17Aの発生に成功した。ECH用ジャイロトロンの開発では120GHeで460kWを100msの間発生させた。トリチウムシステム試験施設（日米協力）では、25日間の連続運転が大きな進展であった。 20MW/m^2 で30秒間加熱する1000回以上の試験に耐えた第一壁を開発した。

ITER工学設計活動の協定と議定書1が1992年7月21日に調印され、その組織が決まった。中央チームは予備設計を1993年3月に提案した。

FOREWORD

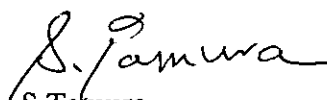
The JT-60U project progressed deeply into the mature study of plasma confinement and non-inductive current drive. The results obtained in high- β_p H-mode plasmas in March 1993 were highlighted, in particular, a world-record fusion-triple-product of $1.1 \times 10^{21} \text{ m}^{-3} \cdot \text{s} \cdot \text{keV}$, JT-60 record values of neutron yield rate of $5.6 \times 10^{16} \text{ s}^{-1}$, stored energy of 8.3 MJ, and H-factor up to 3.6.

The ITER Engineering Design Activities Agreement and Protocol 1 were signed by four parties, the Government of Japan, the European Atomic Energy Community, the Government of the United States of America and the Government of the Russian Federation. The organization of the project was fixed and the design activities were commenced at the three Co-centers; Naka, San Diego and Garching.

Various engineering fields remain to be studied in the course of the construction of the ITER and a fusion reactor. Much effort at JAERI Naka was devoted to the development of vacuum technology, super-conducting magnets, high-energy neutral beam injection, radio-frequency heating, tritium handling, blanket technology, plasma facing components, etc. Main topics are the achievement of pulsed operation with 7T in 0.5s, an H⁻ beam output of 350kV, 0.17A for 1s, and continuous loop run for 25 days in the Tritium System Test Assembly (a US/Japan collaboration).

The JFT-2M and DIII-D (a US/Japan collaboration) continued to advance the understanding of mainly divertor physics and disruption control, and the works on plasma theory and fusion reactor design also progressed.

We are looking forward to more progress in the fusion research and development in the next fiscal year.



S. Tamura

Director General
Naka Fusion Research Establishment
JAERI

Contents

I. JT-60 Program	1
1. Overview	1
2. Operation of JT-60 Upgrade	2
2.1 Tokamak	2
2.2 Control System	4
2.3 Power Supply	5
2.4 Neutral Beam Injection System	7
2.5 Radio-frequency System	8
2.6 Diagnostic Systems	11
3. Experimental Results and Analysis	15
3.1 Disruptions and Plasma Control	15
3.2 Energy Confinement Properties in Ohmic, L-mode and H-mode .	18
3.3 High Poloidal-beta Confinement	20
3.4 Transport and MHD Studies	22
3.5 Impurity and Divertor Characteristics	25
3.6 Fast Ion Studies	27
3.7 LHRF and ICRF Experiments	28
3.8 Development of Fusion Plasma Analysis Codes	30
4. Related Developments and Maintenance	33
4.1 Boronization System using Decaborane	33
4.2 In-vessel Inspection System	34
4.3 Development of Real-time Plasma Shape Visualization System	35
4.4 Development of New Type DC Interrupting System	36
4.5 Negative-ion-based Neutral Beam Injection System	38
4.6 Developments of Diagnostics for LHCD Launcher	39
II. JFT-2M Program	40
1. Toroidal Confinement Experiments	40
1.1 Overview	40
1.2 Experimental Results	40
2. Operation and Maintenance	45
2.1 Introduction	45
2.2 Operation and Maintenance	45
2.3 Development of Equipments and Instruments	46

III. Plasma Theory and Computation	47
1. Introduction	47
2. Analyses of Confinement and Heating Processes	47
2.1 Confinement Scaling of Thermal Energy	47
2.2 Scaling of Bootstrap Current in Finite Aspect Ratio Tokamak	48
2.3 Self-organized Profile Relaxation by Ion Temperature Gradient Instability in Toroidal Plasma	49
2.4 Linear Dispersion Analysis of Toroidal Ion Temperature Gradient Mode in Entire Complex Frequency Plane	50
2.5 Beam Orbit Analysis in Focusing Wiggler by using Non-canonical Perturbation Method	50
3. MHD Equilibrium and Stability Analyses	51
3.1 Stability Analysis of Small Aspect Ratio Tokamak	51
3.2 Rotation Damping by External Error Field	51
3.3 Effect of Electron and Ion Viscosity on Sawtooth Crash in Tokamak	51
4. Analyses of Burning Plasma in Tokamaks	52
4.1 Study of Combined NBI and ICRF Enhancement of D- ³ He Fusion Yield with Fokker-Planck Code	52
4.2 Effects of Radio-frequency-induced Radial Diffusion on Triton Burn-up	52
5. Development of Numerical Codes and Plasma Simulator	52
5.1 Finite Element Calculation of Outer Region Matching Data ..	52
5.2 Development of Inverse Equilibrium Solver	53
5.3 Improvement of TSC Code	53
5.4 MHD Simulation Code Based on Toroidally Incompressible Plasma Model	54
5.5 Parallel Processing of Particle Simulation Codes	54
IV. Cooperative Program on DIII-D (Double III) Experiment	55
1. Introduction	55
2. Highlights of FY1992 Research Results	55
3. JAERI Collaboration	56
V. Technology Development	58
1. Vacuum Technology and Fuel Injection	58
1.1 Introduction	58
1.2 Progress in Ceramic Vacuum Pump Development	58

1.3	Research on High Resolution Quadrupole Mass Spectrometer (QMS)	58
1.4	Progress in Ceramic Coating and Joining Technology	59
1.5	Study on Railgun Pellet Injector using Laser-induced Plasma Armature	62
1.6	Design, Fabrication and Test of Elemental Components for Large-size Turbomolecular Pump	63
2.	Superconducting Magnet Development	64
2.1	Introduction	64
2.2	Demo Poloidal Coil (DPC) Program	64
2.3	40-kA Nb ₃ Al Conductor Development	67
2.4	ITER-EDA Works	68
3.	Beam Technology	74
3.1	Introduction	74
3.2	Negative Ion Beam Technology	74
3.3	Application of High Current Ion Beam Technology	77
4.	RF Technology	78
4.1	Introduction	78
4.2	Development of High Power Gyrotron and ECH Components	78
4.3	Development of LHCD and ICRF Launcher	79
4.4	Millimeter Wave Free Electron Laser	80
4.5	Design Study of RF Heating and Current Drive Launcher for ITER	80
5.	Tritium Technology	82
5.1	Development of Tritium Processing Technology under US-Japan Collaboration	82
5.2	Development of Tritium Processing Technology in TPL	84
5.3	Tritium System Design and Analysis	85
5.4	Development of Tritium Handling Technology	85
6.	High Heat Flux Technology	88
6.1	Introduction	88
6.2	Activities on Divertor Plate Development	88
6.3	Development of First Wall	90
6.4	Study of Plasma Surface Interaction	90
7.	Reactor Structure Development	92
7.1	Introduction	92
7.2	R&D Activities for Reactor Structure	92
7.3	R&D Activities for Remote Maintenance	93

8. Blanket Technology	94
8.1 Introduction	94
8.2 Fabrication of Blanket Box Structure integrated with First Wall	94
8.3 Out-of-reactor Testing	96
8.4 Design of Tritium Breeding Blanket	97
VI. International Thermonuclear Experimental Reactor (ITER)	99
1. Introduction	99
2. ITER Engineering Design Activities (EDA)	100
2.1 Review of Detailed Technical Objectives of ITER	100
2.2 Preliminary Design proposed from Director	101
2.3 Organization of Japanese Home Team	104
VII. Fusion Reactor Design	106
1. Introduction	106
2. FER Design	106
3. Fusion Reactor Design	106
4. Safety Analysis	108
Appendices	109
A.1 Publication List	109
A.2 Personnel and Financial Data	121

目 次

I. JT-60計画	
1. 概 要	1
2. JT-60Uの運転	2
2.1 トカマク装置本体	2
2.2 制御システム	4
2.3 電 源	5
2.4 中性粒子入射装置	7
2.5 高周波装置	8
2.6 計測装置	11
3. 実験結果と解析	15
3.1 ディスラプションおよびプラズマ制御	15
3.2 オーミック, LモードおよびHモードのエネルギー閉じ込め特性	18
3.3 高 β p閉じ込め	20
3.4 輸送とMHD研究	22
3.5 不純物とダイバータ特性	25
3.6 高速イオンの研究	27
3.7 LHRFとICRF実験	28
3.8 炉心プラズマ解析コードの開発	30
4. 関連技術開発および装置の保守	33
4.1 デカボロンを用いたボロン化システム	33
4.2 真空容器内観察装置	34
4.3 実時間プラズマ形状可視化システムの開発	35
4.4 新型直流遮断システムの開発	36
4.5 負イオン中性粒子入射装置	38
4.6 LHCDランチャ用計測器の開発	39
II. JFT-2M計画	
1. 閉じ込め実験	40
1.1 概 要	40
1.2 実験結果	40
2. 運転と保守	45
2.1 はじめに	45
2.2 運転と保守	45

2.1	はじめに	64
2.2	実証ポロイダル・コイル (DPC)計画	64
2.3	40kA Nb ₃ Al導体の開発	67
2.4	ITER EDA開発	68
3.	ビーム技術	74
3.1	はじめに	74
3.2	負イオンビーム技術	74
3.3	大電流イオンビーム応用技術	77
4.	RF技術	78
4.1	はじめに	78
4.2	大電力ジャイロトロンおよび電子サイクロトロン加熱用部品の開発	78
4.3	LHCDとICRFランチャの開発	79
4.4	ミリ波帯自由電子レーザ	80
4.5	ITER用高周波加熱と電流駆動ランチャの設計研究	80
5.	トリチウム技術	82
5.1	日米協力でのトリチウムプロセス技術の開発	82
5.2	トリチウムプロセス研究棟のトリチウムプロセス技術の開発	84
5.3	トリチウムシステムの設計と解析	85
5.4	トリチウム取扱技術の開発	85
6.	高熱流束技術	88
6.1	はじめに	88
6.2	ダイバータ板の開発	88
6.3	第一壁の開発	90
6.4	プラズマ壁相互作用の研究	90
7.	炉構造の開発	92
7.1	はじめに	92
7.2	炉構造の研究開発活動	92
7.3	遠隔保守の研究開発活動	93
8.	ブランケット技術	94
8.1	はじめに	94
8.2	第一壁を内蔵したブランケットボックス構造部の製作	94
8.3	炉外試験	96
8.4	トリチウム増殖ブランケットの設計	97
VI.	国際熱核融合実験炉 (ITER)	
1.	はじめに	99
2.	ITER工学設計活動 (EDA)	100

2.1	ITERの詳細技術目的の審査	100	
2.2	所長提案の予備設計	101	
2.3	日本のホームチーム組織	104	
VII. 核融合炉の設計			
1.	はじめに	106	
2.	FER設計	106	
3.	核融合炉の設計	106	
4.	安全解析	108	
付 録			109
A.1	論文リスト	109	
A.2	人員および予算に関するデータ	121	

I. JT-60 PROGRAM

1. Overview

Upgraded JT-60(JT-60U) is capable of producing single-null divertor discharges with plasma current of 6 MA, with high power heating and current drive: neutral beam heating power of up to 40 MW, lower hybrid current drive (LHCD) power of up to 10 MW, and ion cyclotron resonance heating (ICRF) power of up to 5MW. Features of JT-60U are a high aspect ratio (4.0), a high toroidal magnetic field (4 T) and divertor plates with beveled edges. From the view point of divertor heat load, 40 MW of heating power in JT-60U corresponds to alpha heating power in ITER, making ITER-relevant experiments feasible. The main objectives of JT-60U experiments are: (1) confinement improvement, (2) impurity control and divertor studies, (3) steady-state studies, and (4) high energy particle confinement. Through the pursuit of these goals, we aim to contribute to the ITER Physics R&D, and provide data essential for the concept development of fusion power reactors like SSTR.

JT-60U experiment was commenced in March 1991. After four months in July, deuterium operation was started. Well-controlled equilibrium in the diverted configuration was successfully achieved for $I_p \leq 5$ MA by the discharge optimization of elongated plasmas and the understandings of operational characteristics, such as MHD, disruption, edge-radiation, and profile effects. The NB power was increased up to 33 MW with perpendicular and tangential injectors. The power of ICRF with a frequency range of 110-130 MHz were also increased up to 5 MW with two antennas. The 4-pellet injector was successfully operated with 2.3 km/s for hydrogen pellets and 1.8 km/s for deuterium pellets.

The newly-developed boronization equipment using decaborane gas vaporized by heating solid decaborane ($B_{10}H_{14}$) at 100 °C was installed in July, and it was very effective for optimization of the vacuum-wall conditioning and for reduction of particle recycling at the wall. During November and December, another multi-junction LHCD launcher with power capability of 7 MW was newly installed. In early 1993 LHCD experiments were started toward 10-MW level in combination with the old previously- installed multi-junction launcher.

The main objectives of JT-60U experiments during April 1992 to March 1993 were to improve confinement properties and to study non- inductive current drive, and the following experiments were performed: 1) optimization of highly-heated discharges, 2) confinement improvement and studies of its characteristics, 3) MHD and disruption studies, 4) impurity control and divertor studies, 5) studies of ripple loss, high energy particle and D-D reaction product, 6) studies of NBCD and bootstrap-current and 7) LHCD and ICRF experiments.

High- β_p H-mode performance obtained in March 1993 was especially highlighted among these experiments. The fusion-triple-product $1.1 \times 10^{21} \text{m}^{-3} \cdot \text{s} \cdot \text{keV}$ was achieved in the high- β_p H-mode in which the confinement was improved in the edge region as well as the core region by

the combination of the high- β_p mode and H-mode. The highly improved confinement in the high- β_p H-mode with both the centrally peaked profile and the edge pedestal in the pressure led to the significant H-factor up to 3.6. In the mode, the highest stored energy of 8.3 MJ and the highest neutron yield of $5.6 \times 10^{16} \text{sec}^{-1}$ were also achieved.

2. Operation of JT-60 Upgrade

2.1 Tokamak

2.1.1 Operation results of machine components

The operation of the JT-60 Upgrade machine has been carried out almost on schedule in this fiscal year. During shutdown in May, the regular inspection and maintenance of the high pressure gas facility, the residual gas analysis system, etc. were performed. The linkage test of the pellet injection system and the JT-60U control system was performed in June, followed by the first pellet injection experiment in JT-60U.

The power test of the toroidal field coil was carried out to examine the lateral deformation under the overturning loading up to 400 ton/coil. Two laser displacement monitors were attached to measure the deformation of the upper support structure. The measured values were about 3 mm for 400 ton which agrees well with the designed one.

A new in-situ boronization system using decaborane was installed in July. The anode of the glow discharge cleaning system was also attached to the opposite side of the original one for efficient boronization. The boronizations were carried out in July and September successfully. Measurement of the boron coating thickness was made after the second boronization and the result showed rather nonuniform distribution due to a single decaborane gas injection port.

In October, the water leakage was observed from one of the toroidal coils (TC-9). Inspections of the leak channel and location were carried out in November through December during the regular shutdown. The bottom of the coil case was drilled to drain leaked water inside the coil case, followed by the drying operation by supplying hot water to non-leaked channels. The sniffer leak detection method was applied to detect the leak point. The finally confirmed leak point was the inboard mid plane of the 16th conductor of the pancake winding. Fortunately the leaked conductor has two parallel cooling channels, so that the heat load in the normal operation can be removed by the non-leaked cooling channel alone without producing large thermal stress in the windings. The electrical resistance was measured after repair and showed the allowable value. The withstand voltage test was also carried out successfully. The toroidal field coils have been operated within the rated current since January 1993 without any trouble.

During this shutdown, modifications of the glow discharge cleaning system were carried out to increase the applied current up to 10 A. The baking heaters were attached around tangential neutral beam injection ports to outgas the port wall. Twelve in-vessel decaborane gas feed lines

were also installed during this vent by distributing pipes, about 10 mm in diameter, under the first wall, in order to attain more uniform boron coating in the toroidal direction. The third boronization was carried out in February 1993. The measured thicknesses of the coating samples inserted at two toroidal positions showed improved uniformity with maximum/minimum thickness ratio of 4.

2.1.2 Operation results of plasma facing components

Figure I.2.1-1 shows a typical view of the divertor tiles after operation until October 1992, where the inboard and outboard striking zones are coated with redeposited carbon-based material. No serious damage such as cracking or fracture of divertor tiles was observed. However, shallow erosions were observed on a large number of divertor tiles located at the outboard striking point in lower X-point distance operations. The erosion pattern shows clear toroidal periodicity, which suggests that heat and particle fluxes are enhanced at the eroded positions due to the field ripple of the toroidal field coils. The erosion profile was measured using 3-D Laser Sensor inside the vacuum vessel. The typical erosion depth and gradient of the eroded surface are 0.4 mm and 1/50, respectively.

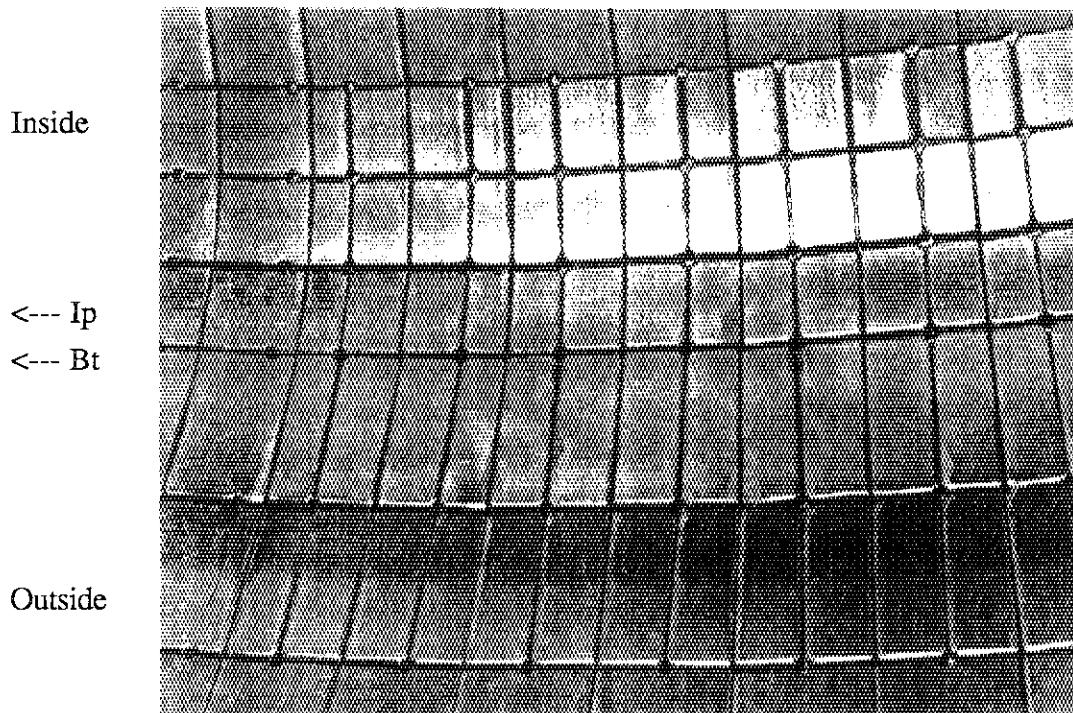


Fig. I.2.1-1 Typical view of the divertor tiles after operations until October 1992, showing no significant damage except for slight erosions at tile edges due to field ripple effect (Typical tile size is 107 mm x 40 mm)

Four Rogowski loops were installed under the divertor tiles to measure halo current induced during disruption. The initial measurement showed that the Halo current is about 20 % of the plasma current.

One loose-jointed divertor tile was found. The tile surface was eroded due to protrusion during operation. The eroded depth was about 1.4 mm. Many small craters were observed on two graphite tiles located at the opposite side of the pellet injector. The radioactive analysis of the removed tiles showed that the highest residual activity is Be-7 which appears at the inboard divertor striking zone. Residual tritium analysis was also carried out and indicated that tritium is concentrated in the surface layer at least within 0.2 mm which is the limitation of sampling.

One row of the divertor tiles located at the outboard striking point was replaced by B₄C-converted ones to maintain boronized surface for a longer operation period. These B₄C-converted tiles have graded boronized surface layer with a thickness of 0.05 - 0.2 mm. The B₄C layer is formed by the chemical reaction process of gaseous boron oxide and carbon/carbon (C/C) composite at a temperature of about 2000 °C. These tiles were taper-shaped before the conversion process to reduce heat flux concentration at tile edges. The B₄C-converted isotropic graphite tiles were also installed in the first wall region around large ports where plasma wall interactions are enhanced due to large openings and field ripple effect. These B₄C-converted graphite possess favorable surface characteristics, that is, lower sputtering yield and lower release temperature of retained deuteriums, with sufficient heat load durability compared to those of graphite.

2.2 Control system

The VME-bus (IEEE std. P1014/D1.2) based multiprocessor system for plasma position and current control (FBCC) [2.2-1] can implement multivariable PD control with cycle time of 250/500 μs. Stable divertor plasmas were obtained by the non-interacting control method in this system. In the present scheme of plasma position control, however, the coil current signals are put into the FBCC and the direct digital controllers of the poloidal field power supply (P-DDCs) via their own signal transducers (isolation amplifiers and 12-bit ADCs) independently as shown in Fig. I.2.2-1(a). The differences between the coil current data observed in the FBCC and those in the P-DDCs are 6-8 bits at maximum, which corresponds to 200-270 A in the case of the vertical field coil current. These differences lower the control performance consequently. Then, in order to solve the problem we added a new control scheme in the feedback control system, where the coil current signals are used only in the FBCC as shown in Fig. I.2.2-1(b). The time optimal control algorithm to obtain the desired coil current was moved from the DDC to the FBCC in this control scheme. For this modification one of the three VME based RISC processors MVME181 with a CPU clock of 20 MHz was superseded by MVME187 with that of 25 MHz.

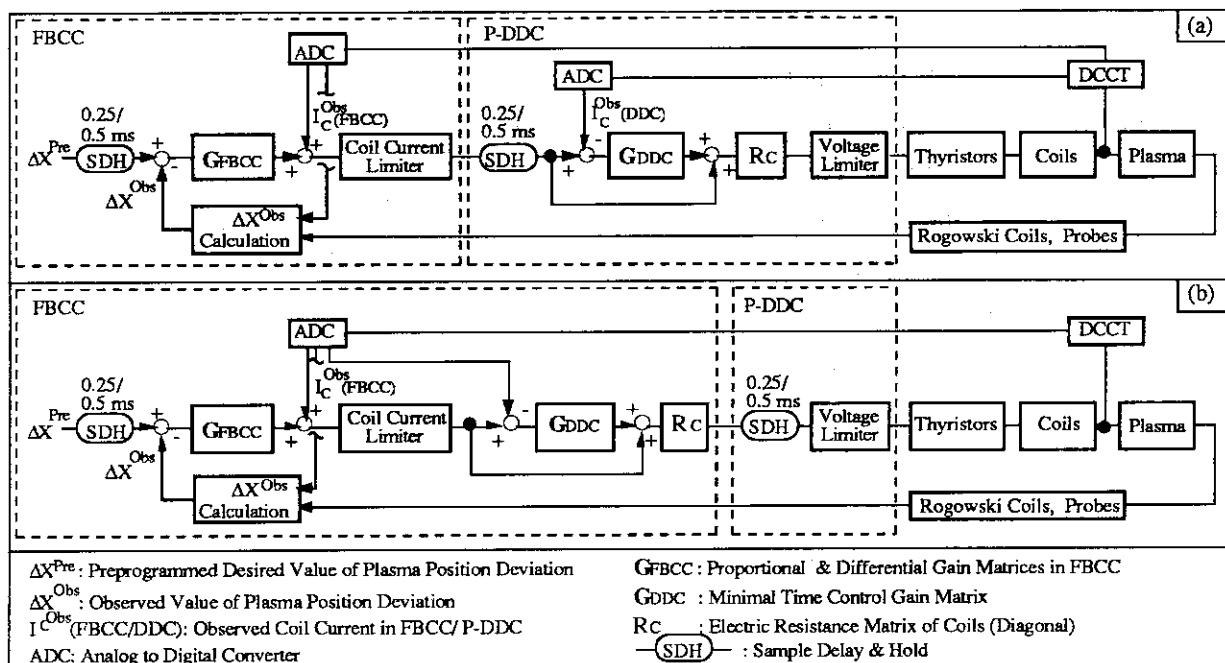


Fig. I.2.2-1 Block diagram of the original plasma position feedback control (a) and that of modified scheme (b). In the scheme (a), the difference of the coil current values observed in the FBCC and P-DDC deteriorates the plasma control performance. Since the coil current signals are used only in the FBCC in the scheme (b), the deterioration doesn't arise.

In the workstation based man/machine interface system [2.2-2], some of the Sun-3 workstations were superseded by SPARC Stations from the view point of the processing speed in the setting of discharge condition parameters and display of discharge result data. Improvements in the functions of automatic decision of the parameters and reasonability check in the setting discharge condition parameters were continued corresponding to the progress of the JT-60U operation.

References

- [2.2-1] T. Kimura, et al., IEEE Trans. on Nuclear Science 35 (1989) 1554.
 [2.2-2] I. Yonekawa, et al., Proc. 14th Symp. on Fusion Engineering, San Diego, 1991, pp.798-801.

2.3 Power supply

In this period of FY 1992, the poloidal field power supply (PFPS), the toroidal field power supply (TFPS) and the motor-generator for the additional heating system (H-MG) were operated satisfactorily. The power distribution system, the emergency power supply and the secondary cooling system were also operated satisfactorily in this period. The motor generators (MGs) in the TFPS, the PFPS and the H-MG were operated for 1,296, 1,392 and 1,555 hours, respectively. In the TFPS-MG a slight increase of the vibration level of the rotating shaft were continuously observed. In the re-acceleration phase of the MG, the vibration magnitude sometimes exceeded

the alarm levels, which are 0.33 mm for the vibration at the upper position, 0.82 mm at the middle and 0.57 mm at the lower. (See Fig. I.2.3-1.) Then, the following countermeasures in the operation were adopted to reduce the shaft vibration. First, the MG was made to run idle for over 30 minutes after the rotating speed reaches its standby level (420 rpm). Second, the toroidal field strength in the daily first shot was restricted within 3 T, which corresponds to the top speed of the MG being 564 rpm (94 % of the rated value).

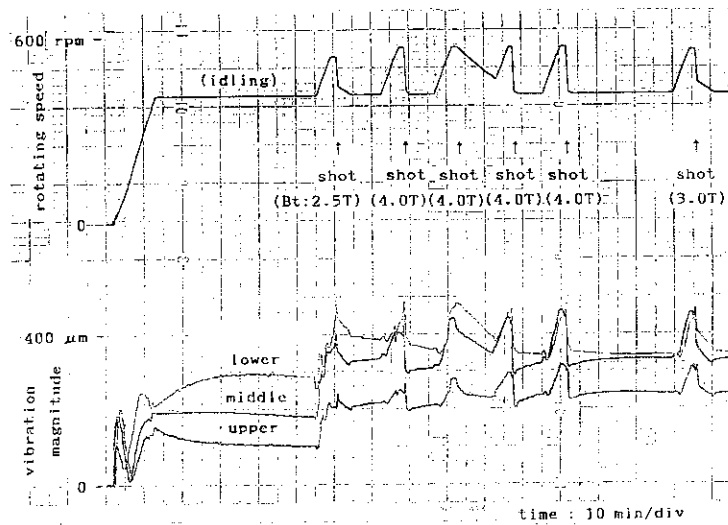


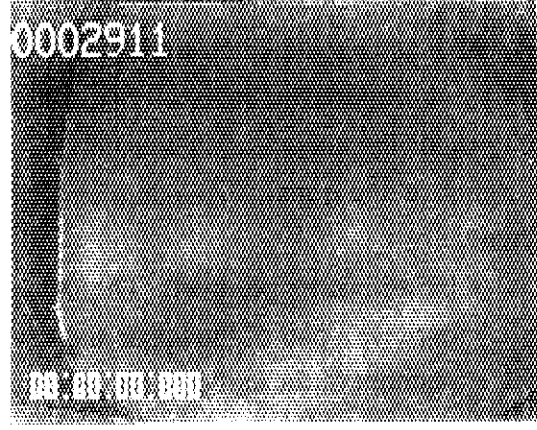
Fig. I.2.3-1 The vibration magnitude of the rotating shaft of the TFPS-MG increases with increasing rotating speed. The magnitude decreases gradually in the idling phase at the speed of 420 rpm.

Some improvements were made in the PFPS for increasing the efficiency of wall cleaning in the Taylor-type discharge cleaning (TDC) operation, where the ohmic heating (OH) and vertical field (V) coils are normally connected with their dedicated power supplies as shown in Fig. I.2.3-2(a). In this operation, the one-turn loop voltage induced in the outer region of the vacuum vessel cross-section is very low because the mutual coupling between the OH- and V-coils is strong. Hence, the TDC plasma is initiated only in the inner region of the vacuum vessel as shown in Fig. I.2.3-2(a), and the TDC with this connection is not powerful to clean up the outer region of the wall. Then, two kinds of operation modes were added to the PFPS for increasing the effect of the TDC operation. One is the "OH- and V-coil anti-parallel connection mode", where the V-coil is connected with the OH power supply in parallel but inverse direction to the OH-coil as shown in Fig. I.2.3-2(b). The other is the "D-coil closed circuit mode", where the divertor (D) coil is formed to be a closed circuit apart from its power supply. These modes can be selected easily by some additional disconnecting switches. In the former-mode TDC operation, the loop voltage in the outer region is induced sufficiently and the plasma expands to the outer region of the wall as shown in Fig. I.2.3-2(b). This mode has been proved to be very effective for reducing the residual gas in the first wall of the vacuum vessel. The efficiency for exhausting oxygen is 3-5 times larger than that in the normal-mode operation. In the latter-mode operation, the D-coil current is induced in the same direction with that of plasma current. Hence, the plasma column is attracted to the divertor plate and cleans up divertor plate effectively.



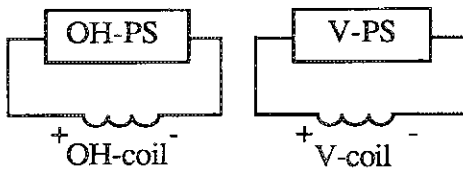
outer side of v.v.

inner side of v.v.

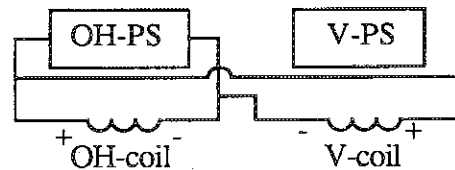


outer side of v.v.

inner side of v.v.



(a) Normal connection. The TDC plasma touches only the inner region of the vacuum vessel.



(b) "Anti-parallel" connection. The plasma is initiated in the entire region of the vacuum vessel.

Fig. I.2.3-2 Two patterns of connection of OH- and V-coils with the power supplies and their corresponding TDC plasmas.

2.4 Neutral beam injection system

Reorientation of 4 units out of the original 14 quasi-perpendicular beamline units was completed to inject beams in co- and counter-tangential directions [2.4-1].

^3He beams were injected with 5 quasi-perpendicular beamlines for the D- ^3He fusion experiment. ^3He gas was pumped out by a cryo-sorption with an argon-condensed layer, where argon gas was fed through the neutralizer gas-feeding system before every ^3He beam extraction. ^3He beams were injected into 24 tokamak discharges. Maximum beam energy and power were 78 keV and 1.3 MW/unit, respectively.

The JT-60 neutral beam injection system was designed to inject hydrogen beams with 75 keV of beam energy in the standard-rated operation; therefore, the ion sources are air-insulated with short and long ceramic insulators for the first- and second-stage accelerations, respectively. Consequently, in the recent operation aiming at 120-keV deuterium beam extraction, we observed frequent flashovers on the outer-surface of the short ceramic insulators succeeding to the inter-electrode breakdowns in the second-stage acceleration. Such a surface-flashover gradually contaminates the surface and hence deteriorates the voltage holding characteristics. Since there is a structural difficulty to fill up an insulating gas such as SF_6 in the ion source enclosure, we added a set of sphere gap to bypass the surge current for each beamline unit. Together with the improvement of the neutralization efficiency by increasing the gas flow rate into the neutralizers, we achieved up to 33 MW injection with 90 to 95 keV of beam energy.

The integrated beam pulse required to decrease the reionization loss at the NBI ports below 10% was greatly reduced by a glow discharge cleaning. The required beam pulse lengths after recent vents are listed in Table I.2.4-1. The total beam pulse as long as 125 sec was required in the port aging of the tangential NBI ports in July 1992. This is about three times longer than in the port aging of the quasi-perpendicular NBI ports in April 1992. The possible reasons are the differences of

- Beam power per port. The beam power per port for tangential beamlines is doubled because a pair of the upper and lower tangential beamlines use the same NBI port.
- Amount of the carbon tiles. The area of the carbon tiles in the tangential port is about 5.5 m²/port while that in the quasi-perpendicular port is about 1.2 m²/port.

In the port aging in January 1993, the required integrated beam pulse was dramatically shortened; several seconds for the quasi-perpendicular NBI ports and 10 seconds for the tangential NBI ports, which are about one-tenth of the previous port aging. This is due to the glow discharge performed for the cleaning of the JT-60U vacuum vessel. In the glow discharge cleaning before the beam injection in January 1993, the glow current was increased to about 10 A, which is about 5 times higher than that in the previous operation. Accordingly, the intense glow discharge spread well into the NBI ports and hence the required beam pulse was greatly shortened.

References

[2.4-1] M. Kuriyama et al., Proc. of 13th Symp. on Fusion Engineering, Knoxville (1989).

Table I.2.4-1 Integrated beam pulse required to decrease the reionization loss below 10%.

date	pulse length	NB
April 1992	~50 sec	quasi-perpendicular
July 1992	~125 sec	tangential
January 1993	several seconds	quasi-perpendicular
January 1993	~10 sec	tangential

2.5 Radio-frequency system

2.5.1 LHCD system

The JT-60U LH system consists of three sub-systems to inject ~10 MW at frequencies of around 2 GHz. Each sub-system has eight klystrons and can control the frequency, power and the phase between adjacent klystrons during an RF pulse [2.5-1]. One of the sub-systems has been operated at a power level of 2~3 MW by using the 24 x 4 multijunction launcher with standard waveguides (CD-1') which is the same type of multijunction launcher of JT-60. Two other sub-systems have been arranged to drive the simple launcher (CD-2) with oversized waveguides for delivering ~7 MW into plasmas. The CD-1' is featured by a wide controllability of wave spectrum

in the range of $N_{||peak} = 1$ to 3 with high directivity. In 1992, the CD-1' launcher was used to investigate the wave spectrum dependencies of various plasma characteristics.

On the other hand, the CD-2 launcher has been developed to simplify the LHCD system for JT-60U. The power dividers are not employed in the transmission lines of the latter two sub-systems, so that the output power of the klystron is directly guided to one multijunction module in the CD-2 launcher as shown in Fig. I.2.5-1. The CD-2 launcher consists of 4 (toroidal) x 4 (poloidal) multijunction modules to excite very sharp wave spectra for efficient current drive and profile control. Each module utilizes a single oversized waveguide to divide the RF power toroidally into 12 sub-waveguides. The number of the sub-waveguides are 48 in the toroidal direction and 192 in total in this launcher. The CD-2 launcher has been installed on JT-60U at the end of 1992.

A coupling property was studied in the preliminary experiment. It is found that a very low reflection coefficient less than 2 % is obtained even though the plasma is ~100 mm away from the first wall. The effect of the higher modes in the oversized waveguides is negligible as far as the reflection coefficients less than 10% according to the study on the mock-up test. Therefore, the simple launcher with oversized waveguides may work well on JT-60U LHCD experiments.

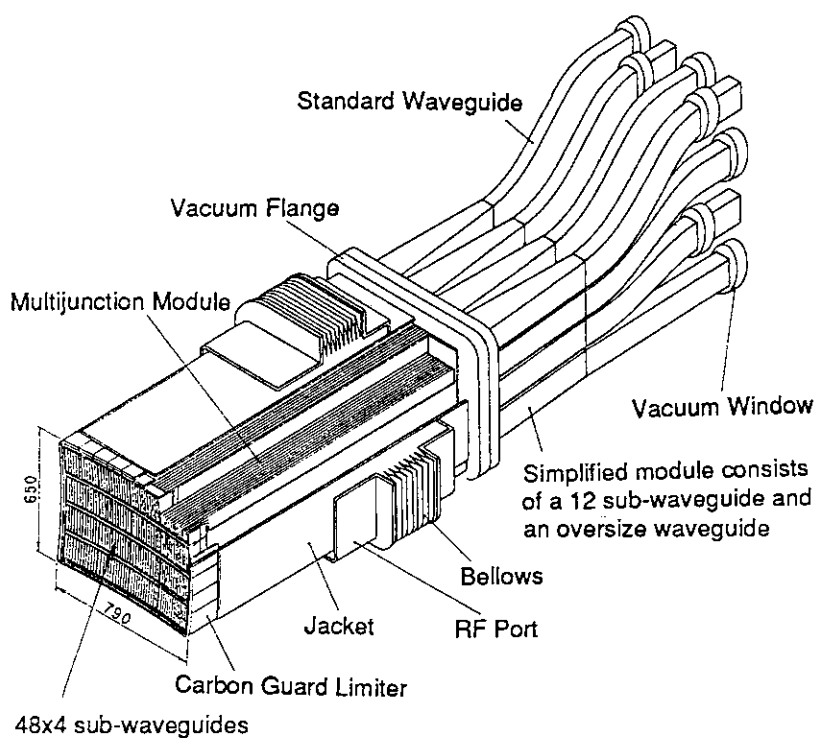


Fig. I.2.5-1 48 x 4 sub-waveguide multijunction (CD-2) launcher

Reference

[2.5-1] Y. Ikeda, M. Seki et al., Proc. 17th Symp. on Fusion Tech., Rome (1992)

2.5.2 ICRF heating system

The ion cyclotron range of frequencies (ICRF) heating system for JT-60U was modified in 1992. Its major specifications are : a frequency range is 108 - 132 MHz, total output power of eight generators is 6 MW for 10 sec and the launcher is two 2 x 2 loop element antennas.

After adjustment of its protection circuits, the operation of the ICRF heating system has started in earnest from April, 1992. Figure I.2.5-2 shows the history of the injected power into JT-60U plasmas for about 250 shots from April to October. The highest power of 3.6 MW was achieved after only 60 conditioning shots in very short period of about a week. This value is

higher than the maximum power of 3.1 MW in JT-60 obtained for three years. The coupling properties of the antenna was examined in the middle phase of the operation term so that high power injection was not required. It is found that the antenna has a very high coupling even in $(\pi,0)$ phasing (out-of-phase of loop element currents) [2.5-2]. Experiments of sawtooth stabilization by ICRF heating and combined ICRF and LHRF heating were carried out at power levels of 3 MW in September and October. The power level is limited by experimental conditions, and it might be increased up to 5 MW with appropriate antenna conditioning because the maximum voltage in the antenna system is fairly low levels of less than 30 kV.

During no operation term for ICRF experiments from November to December, 1992, we increased the output power of the generators up to 8 MW for 3 sec with a matched dummy load by selecting higher screen grid voltage and fine tuning of the final stage of tetrode amplifiers. This work was quite difficult because the power level is a marginal level of the tetrode (Eimac 8973) beyond the maximum rating. Its successful result was brought by detailed analyses of the operation data and mastery of high power tetrode technologies for several years.

Reference

[2.5-2] T. Fujii, K. Ushigusa, M. Saigusa et al., 10th Top. Conf. on RF Power in Plasmas, Boston (1993) .

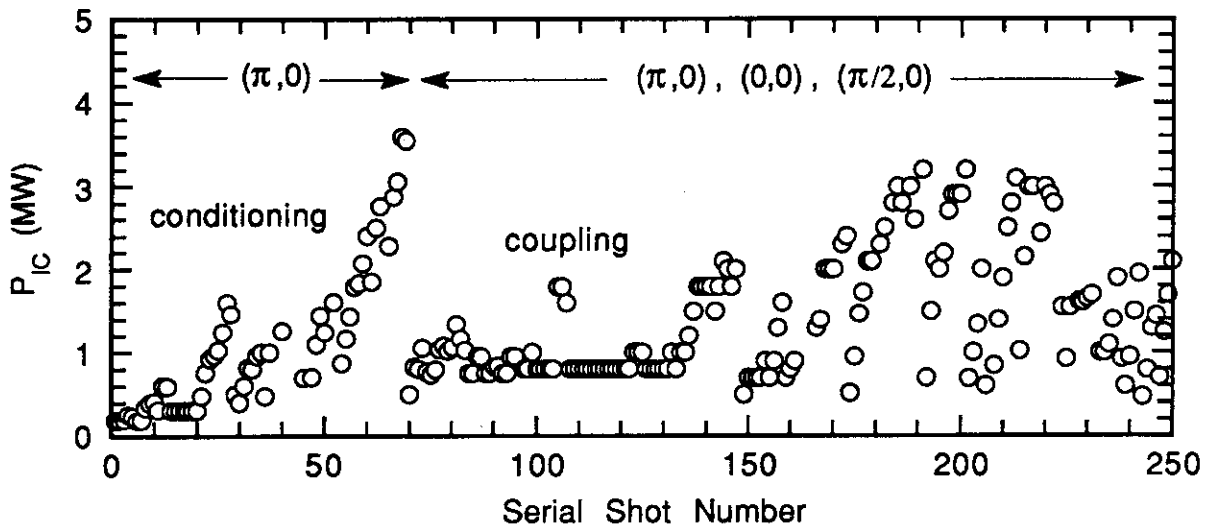


Fig. I.2.5-2 History of the injected power from April to October, 1992 just after upgrade of the ICRF heating system.

2.6 Diagnostic systems

During the period from April 1992 to March 1993, the performance of JT-60U had been progressed. The JT-60U diagnostic systems and their status at the end of March 1993 are summarized in Tab.I.2.6-1. Some improvements of the systems are described in Ref.2.6-1~2.6.3. The newly operated or installed systems in this period are the tangential CO₂ laser interferometer [2.6-4], the motional Stark spectrometer[2.6-5], the α particle charge exchange analyzer and the X-ray Image TV etc. The α particle charge exchange analyzer and the X-ray Image TV are described in section I.2.6.1~2.6.2.

2.6.1 Alpha particle charge exchange analyzer

In a collaboration between the A.F.Ioffe Physical-Technical Institute(Russian Federation) and JAERI, the alpha particle diagnostics in JT-60U has been investigated since 1990. Based on the successful collaboration, the Alpha Particle Charge Exchange Analyzer was introduced to JT-60U from Ioffe Institute on March 1993.

A schematic view of the analyzer is shown in Figure I.2.6-1. The charge stripping of atoms coming into the analyzer from the plasma is performed by a carbon foil of 400Å. The energy and mass of the secondary ions after the stripping is resolved by a deflection magnet and an electrostatic condenser (E//B type analyzer). The analyzer has eight signal channels with CsI(Tl) scintillation detectors whose light emission is measured by a photo multiplier tube. The minimum neutron sensitivity of the detector is 10^{-7} [count/neutron]. The energy range for alpha particle is 0.5~4 MeV with a dynamic range(the ratio of maximum energy to minimum energy, E_{\max}/E_{\min}) of 4.08. The energy resolution($\Delta E/E$) is 8 % to 12 %. The detection efficiency for alpha particle over 1 MeV is 30 % to 40 %. These basic parameters were obtained in the calibration experiment using a cyclotron accelerator at Ioffe Institute.

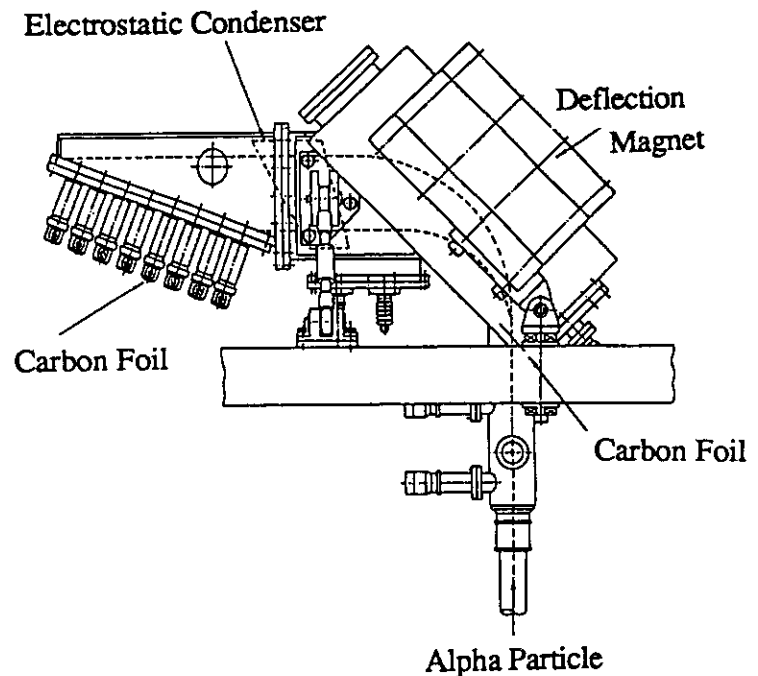


Fig. I.2.6-1: A schematic view of the analyzer.

2.6.2 X-ray image TV

In order to monitor a shape of high temperature plasma and to observe a behavior of high energy electron generated in LHCD experiments, the X-ray image TV has been designed and

installed. The schematic view of the X-ray Image TV is shown in Fig.I.2.6-2. X-ray photons emitted from high temperature plasmas are converted into visible light photons in a CsI(Tl) scintillator ($\phi 101.6$ mm and 3 mm^t, the front and back are covered with a beryllium film of 0.3 mm^t and a Pyrex glass plate of 0.3 mm^t) through a beryllium window of $\phi 30$ mm and 0.3 mm^t, and a lead pin-hole of $\phi 4$ mm (or $\phi 2$ mm). The thin scintillator is used as a X-ray to visible light convertor and is located in the vacuum vessel which has a hard X-ray shield of lead 10 mm^t for the prevention of neutron and γ -ray noise. The converted visible image is led to ICCD (Image intensified Charged Coupled Device) TV camera through a image guide optical fiber scope with a focus lens. The neutron shield (polyethylene: 300mm^t [max.], 200mm^t [min.]) and γ -ray shield (lead: 200mm^t [max.], 100mm^t [min.]) were installed to prevent the ICCD camera from neutron and γ -ray noises, because of the high detective efficiency. The X-ray image signals on ICCD TV camera in the JT-60 torus hall are transferred to video tape recorder (VTR) in the shield room by an optical data link through an optical fiber, and are recorded in VTR tapes. The total detective efficiency for X-ray extends to a wide energy range from 5 keV to 500 keV.

Figure I.2.6-3 shows a X-ray image of LHCD plasmas of $I_p=3.6$ MA observed by the X-ray image TV. The image is processed to a contour plot after a filtering process and includes an effect of line integral because a reconstruction process is not performed. Figure IV.2.6-4 shows a viewing area of the X-ray image TV in the JT-60U vacuum vessel(an inside of a circle). A black filled part shows a shadow obstruction by an inside of a port-box.

References

- [2.6-1] T. Sugie, et al., JAERI-M 93-057, p347.
- [2.6-2] M. Sato, et al., JAERI-M 93-057, p359.
- [2.6-3] S. Ishida, et al., JAERI-M 93-057, p363.
- [2.6-4] Y. Kawano, et al., JAERI-M 93-057, p351.
- [2.6-5] H. Kubo, et al., JAERI-M 93-057, p355.

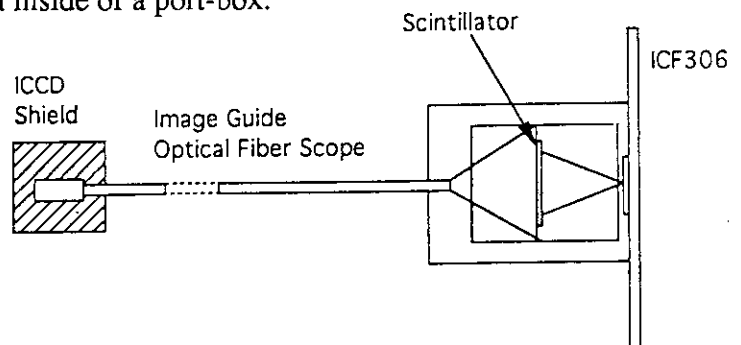


Fig. I.2.6-2 Schematic view of the X-ray Image TV.



Fig. I.2.6-3 A X-ray image of LHCD plasma observed by the X-ray image TV.

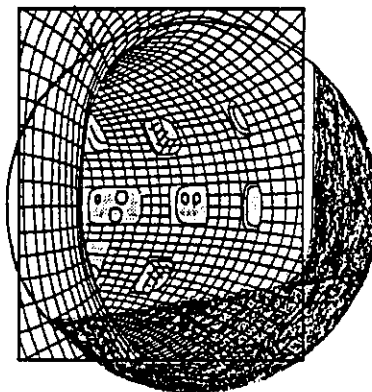


Fig. I.2.6-4 A viewing area of the X-ray image TV in the JT-60U vacuum vessel (an inside of a circle).

Tab.I.2.6-1 Status of JT-60U diagnostic systems

Diagnostic System	Subsystem	Specification	Status Mar.1993
<i>Electron Density</i>	FIR Interferometer	CO ₂ Pumped CH ₃ OH Laser Vertical 2 chords	Operational
	CO ₂ Laser Interferometer	Tangential 1 chord	Operational
	Millimeter Wave Reflectometer	2 density points fluctuation	Operational
	Electromagnetic Wave Scattering	2 points, $0.5 < k\theta\rho_1 < 4.5$, $\Delta f \sim 5\text{MHz}$	Under construction
<i>Electron Temperature</i>	Thomson Scattering	50 points $\Delta z = 8 \sim 22\text{mm}$, 2 Ruby Lasers, 2ms at burst mode	Operational
	ECE Michelson Interferometer	512 Points, $\Delta t \sim 20\text{ms}$, $\Delta f \sim 3.7\text{GHz}$	Operational
	ECE Grating Polychromator	20 Points, $\Delta t \sim 20\mu\text{s}$, $\Delta f \sim 2\text{GHz}$	Operational
	ECE Heterodyne Radiometer	12 Points, $\Delta t \sim 20\mu\text{s}$, $\Delta f \sim 0.5\text{GHz}$	Under construction
<i>Ion Temperature</i>	Charge Exchange Recombination Spectroscopy	20 points (tangential) 8 points (perpendicular)	Operational
	First Charge Exchange Recombination Spectroscopy	6 x 2 Points, $\Delta t \sim 1\text{ms}$	Operational
	Active Beam Scattering	He Beam 200keV, 3.5A 1 point (center)	Operational
	Charge Exchange Neutral Particle Energy Analyzer Array	2 chords (tangential) 1 chord (perpendicular)	Operational
<i>Impurity</i>	X-ray Crystal Spectrometer (Doppler & Monochromator)	1 chord (vertical) Ti, Ni, Kr-K α Rotating Crystal, 0.1-0.8 nm	Operational
	VUV Spectrometer	1 chord, 0.5-130 nm (Main) 1 chord, 30-156 nm (Div.)	Operational
	Light Impurity Spectrometer (Doppler)	1 chord, 100-200 nm (Div.)	Operational
	Grazing Incidence Monochromator	1 chord, 10-130 nm Absolutely Calibrated	Operational
	Visible Monochromator	1 chord, 200-700 nm Absolutely Calibrated	Operational
	Visible Spectrometer Periphery	Mirror Scan, 200-700 nm	Operational
	Visible Spectrometer (Divertor)	Spectrometer (2 chords) Fiber Optics & Filters (38 chords)	Operational
	Visible Bremsstrahlung (Zeff)	10 chords, 523.2 nm Fiber Optics & Filters	Operational
<i>Current Profile</i>	Motional Stark Polarimeter	1 point	Operational
<i>Radiation Flux</i>	Soft X-ray PHA	1 chord, 3-110keV	Operational
	H α / D α Arrays	Poloidal 15(30) chords Toroidal 3(6) chords, $\Delta t \sim 1\text{ms}$ (Divertor 1 chord) (Outer Region 1 chord)	Operational (plan)
	pellet ablation monitor	Poloidal 8 chords Midplane 1 chord	Under construction
	Soft X-ray Arrays	Poloidal 64 chords Outer Region 4 chords	Operational
	Bolometer Arrays	Poloidal 32 chords Divertor 9 chords Toroidal 2 chords	Operational
	Hard X-ray PHA	Poloidal 7 chords Co 1 chord, (Counter 1 chord)	Operational (plan)
	X-ray Image TV	Tangential 1 chord (5-500keV)	Operational

<i>Neutron</i>	Fission Chamber	3 Points, $\Delta t \sim 10\text{ms}$	Operational
	Neutron Spectrometer(NE213)	1 chord, $\Delta E \sim 10\%$	Operational
	Neutron Spectrometer (^3He Ionization Chamber)	1 chord, $\Delta E \sim 2\%$	Operational
	Neutron Activation	1 point	Operational
	14MeV Neutron Detector	1 point	Operational
<i>α particle</i>	Neutral Particle Analyzer	1 chord(perpendicular), 0.5-4MeV, $\Delta E \sim 10\%$	Under construction
<i>Peripheral Plasma & Wall Surface</i>	Infrared TV	Divertor 1 camera, 100-1200°C	Operational
	Visible TV	Tangential 2 chords	Operational
	High Speed TV	Tangential 1 chord, 1 frame/ms	Operational
	Electromagnetic Probes (Mirnov Coils)	40 points (Poloidal & Toroidal Arrays)	Operational
	Electromagnetic Probes (Rogowski for halo current)	4 points	Operational
	Electro Static Probes	Divertor 2 X 16 probes	Operational
	Reciprocation Probe	Triple probe array, 1 sweep/shot	Under construction

3. Experimental Results and Analysis

3.1 Disruptions and plasma control

3.1.1 Disruptions in JT-60U

In tokamak fusion reactors, disruptions will determine the life time of the first wall and divertor plates, and the resultant high electromagnetic stress on the structure will impose severe constraints on their design. Then developments of avoiding and softening techniques of disruptions are indispensable. In JT-60U, five types of disruptions were observed in divertor plasmas; the locked mode disruption, the density limit disruption, the high I_i disruption during the plasma current ramp-down at high I_i and low plasma density[3.1-1], the vertical positional instability at high Shafranov lambda, and disruptions caused by the β_p -collapse. In the last ones plasmas touch the inboard first wall owing to the shift of the plasma horizontal position, and then high impurity influxes terminate discharges.

In the density limit disruptions of divertor plasmas, MARFE and the detached plasma state were always observed before the current quench at $q_{eff} > 3$. A stable MARFE of ~ 4 s was observed for OH and NB plasmas at any q_{eff} higher than 3. For OH plasmas, the duration of the detached plasma phase was 0.1~0.6s at $3 < q_{eff} < 5$, and increased a little by decreasing I_i at the start of the detachment[3.1-1]. A soft X-ray spike[3.1-2] was observed at the end of the energy quench and just before a negative spike of the one-turn voltage, that is the start of the current quench.

Low density locked modes[3.1-3] were also observed at the current flattop with $q_{eff} < 3.6$ for $n_e < 0.9 \times 10^{19} \text{m}^{-3}$ only for the excitation of the divertor coil. On the other hand divertor plasmas produced by a stray field of OH coil current without exciting the divertor coil were stable.

3.1.2 Current quench in disruptive termination

In density limit disruptions of OH divertor plasmas with $I_p = 1.5 \sim 3.0 \text{MA}$, the plasma current decay time defined by $I_p / (dI_p/dt)$ increases with the decrease in the stored energy just before the energy quench as presented in Fig.I.3.1-1[3.1-1]. Here dI_p/dt is the averaged current decay rate over an interval from the start of the quench to the time when the current has reached 50% of its flattop value. Circular and cross points show current quenches without and with runaway electrons, respectively. The current decay time becomes long when runaway electrons are generated. However only few runaway discharges were observed at the decay time of > 15 ms. The plasma current decay time at the current quench is determined by the electron temperature. Then Fig.I.3.1-1 suggests that a slower plasma current decay with a higher electron temperature is obtained with a lower stored energy just before the energy quench. If all of the stored energy is lost at the energy quench, the rise in the radiation loss at the energy quench depends on the stored energy just before the energy quench. This dependence can be shown in Fig.I.3.1-2. Here some fraction of the plasma internal magnetic energy, that is lost when the internal inductance drops at the energy quench, may contribute to the rise in the radiation loss. Radiation loss powers of

$\sim 1\text{GW}$ can be explained by a high impurity (carbon) contamination of 20~30% at a plasma density of $\sim 3 \times 10^{19} \text{m}^{-3}$ and an electron temperature of $\sim 10 \text{eV}$. It can be assumed that the plasma stored energy flows to the divertor plate at the energy quench and impurities (mainly carbon) are generated by this high heat flux to it. Because the plasma stored energy that flew to the divertor plate at the energy quench measured in JT-60 was almost the same with the stored energy just before the energy quench [3.1-4]. The same relation between the current decay time and the rise in the radiation loss during the energy quench was observed for the locked mode disruption and the high I_i disruption as presented in Fig.I.3.1-2.

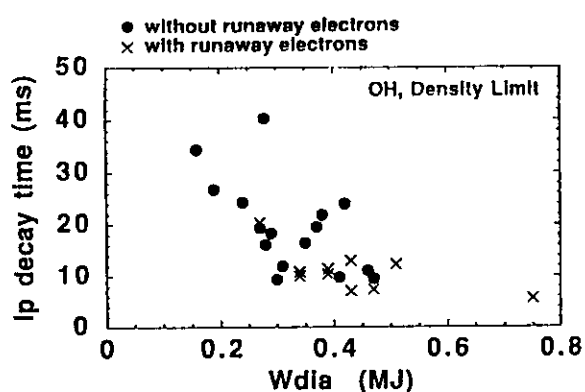


Fig.I.3.1-1 The current decay time defined by $I_p/(dI_p/dt)$ versus the stored energy just before the energy quench in the density limit disruptions for divertor OH plasmas with $I_p=1.5\sim 3.0\text{MA}$.

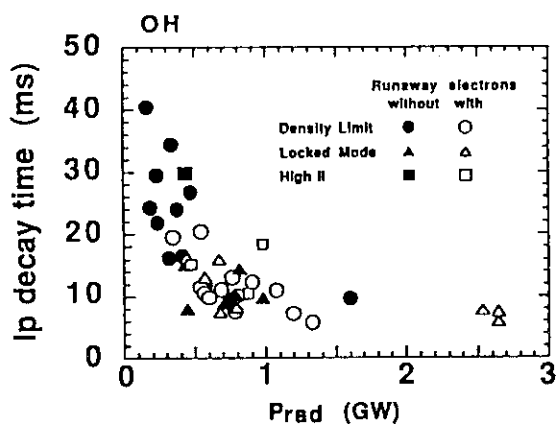


Fig.I.3.1-2 The current decay time versus the rise in the radiation loss during the energy quench in the density limit disruption, the locked mode disruption, and high I_i disruption for divertor OH plasmas with $I_p=1.5\sim 3.0\text{MA}$.

3.1.3 Softening of current quench in disruptive termination

The experimental results presented in section 3.1.2 suggest that a reduction of the drop in the electron temperature just after the energy quench is essential for reducing the current decay rate. Then the following three methods were investigated to decrease the current decay rate. 1) *Reduction of the heat flux to the divertor plate at the energy quench.* Figure I.3.1-2 suggests the necessity of low plasma stored energy just before the energy quench to decrease the current decay rate in the density limit disruption. A detached plasma state with or without minor disruptions lowers the stored energy during a short time interval of 100~600ms. A large degradation of the stored energy (e.g.~60%) can be obtained with intense gas puffing or impurity injection. 2) *Suppression of the impurity influxes at the energy quench.* No current quench was observed for divertor plasmas with $q_{\text{eff}} > 7$ in spite of many minor disruptions. However disruptive plasma terminations can be observed in limiter plasmas with $q_{\text{eff}} > 7$. This avoidance of the current quench obtained in divertor plasmas with high q_{eff} may be caused by shielding of impurities owing to the long connection length from the divertor plate to the main plasma, and by decreasing of the heat flux density at the divertor plate [3.1-4]. 3) *Additional heating of the main plasma core during the current quench.* In the detached plasma state the plasma stored energy can

be reduced in spite of the NB heating, and the current decay time can be increased with the rise of NB heating power during the current quench[3.1-1].

3.1.4 Fast Plasma Shutdown

Fast plasma shutdown from 2MA to zero with a dI_p/dt of -6MA/s was achieved successfully with an aid of the intense helium gas puffing actively producing a detached plasma state. The stored energy was reduced within a short period of the detached plasma state including the $m=1$ erosion phase. The rise in the radiation loss at the energy quench was low enough to avoid the current quench[3.1-6]. This simple plasma shutdown scenario can be used in tokamak fusion reactors at some emergencies.

3.1.5 DCW effect on disruptions

Effects of DCW(Disruption Control Winding with a principal mode of $m/n=3/2$)[3.1-7] on the density limit itself was not observed in the density limit disruption. However a phase of $m/n=2/1$ mode locking changed with the coil current of DCW at $>0\text{kA}$. No change in the phase was observed at $<0\text{kA}$. This results is consistent with the relation between the two phases of error fields produced by DCW and D-coil feeder[3-1-8]. Furthermore some modification of the location of the $m=1$ erosion just before the energy quench, and softening of the plasma current decay in the current quench were observed by the excitation of DCW coil[3-1-9].

3.1.6 Pellet injection and pulse gas puffing [3.1-10]

Modifications of NB heating profile and the resultant pressure profile were obtained by shallow pellet injection with a pulse gas puff to an OH target plasma just before NB heating. The β_p collapse driven by some ideal modes was avoided by a little broader pressure profile. The increase in the ion temperature and the pressure at the peripheral region produced an early H-mode transition. The same discharge scenarios except an intense gas puffing alone delayed the H-mode transition and a following ELMy H-mode, and made it possible to get the highest neutron yield of $5.63 \times 10^{16}/\text{s}$ in DD reactions with much enhanced confinement. Combination of the pellet injection and the following NB heating suppressed the locked mode instability. An increase in the local toroidal rotation speed at the rational surface might suppress the locked mode.

References

- [3.1-1] R. Yoshino, 14th IAEA, Wurtzburg (1992) IAEA-CN-56/G-3-1.
- [3.1-2] J.A. Wesson, et al., Nuclear Fusion 29 (1989) 641.
- [3.1-3] G.M. Fishpool, et al., in *Avoidance and Control of Tokamak Disruptions* (paper presented at the IAEA Technical Committee Meeting, Culham, 1991) IAEA, Vienna (1991) 84.
- [3.1-4] N. Hosogane, et al., Kakuyugo-kenkyu 65 (1991) 323 (in Japanese).
- [3.1-5] K. Itami, et al., 14th IAEA, Wurtzburg (1992) IAEA-CN-56/A-6-5.
- [3.1-6] R. Yoshino, et al., submitted to Nuclear Fusion.
- [3.1-7] H. Ninomiya, et al., Plasma Devices and Operations, 1 (1990) 43.
- [3.1-8] Y. Neyatani, et al., JAERI-M 93-057 (1993) p.291-294.
- [3.1-9] R. Yoshino et al., JAERI-M 93-057 (1993) p.295-297.
- [3.1-10] R. Yoshino, et al., "Pellet Injection Study in JT-60U" presented at the IAEA Technical Committee Meeting on Pellet Injection, JAERI-Naka, (1993).

3.2 Energy confinement properties in ohmic, L-mode and H-mode

3.2.1 Scaling of thermal energy in L-mode and ohmic plasmas

In order to establish the B_T dependence of thermal energy and to understand the transport mechanism in L-mode plasmas, B_T scan experiments were performed in JT-60U with the following parameters; $R \approx 3.2\text{m}$, $a \approx 0.85\text{m}$, $k \approx 1.65$, $B_t = 4.2, 3.2, \text{ and } 2.5\text{T}$, $q_{\text{eff}} \approx 4.5 \text{ and } 6.5$, $P_{\text{NB}} = 5\text{-}17\text{ MW}$ and $\bar{n}_e = 1.6\text{-}3.1 \times 10^{19}\text{m}^{-3}$. A scaling of stored thermal energy, W_{th} , was obtained, $W_{\text{th}} = C (I_i I_p)^{6/9} \bar{n}_e^{5/9} (\bar{n}_e q_{\text{eff}})^{-h/9} P_{\text{abs}}^{4/9}$, where I_p , I_i , \bar{n}_e , q_{eff} , and P_{abs} are plasma current, normalized internal inductance, line averaged density, effective safety factor, and total absorbed power, respectively.

The uncertainty in the power h , which takes the value between 0 and 1, comes from the existence of correlations, $\bar{n}_e q_{\text{eff}} \approx \text{const.}$ and $I_i^5 P_{\text{abs}} \approx \text{const.}$ This scaling is consistent with the thermal diffusivity of the form of $c = (T/eB_p) (r_p/a)^{(1-h)/2} b_p^{h/4}$, where subscript p represents "poloidal". The effect of Larmor radius is rather weak compared with gyro-Bohm type, and collisional effect is very weak.

On the basis of the above results, a scaling including size dependence is derived. The database of JT-60 with a circular cross section and of JT-60 with a lower x-point configuration are also applied. The square root dependence of mass and elongation are assumed. A weak-gyro-Borm type scaling ($h=1$) is obtained as

$$W_{\text{th}} = 0.0105 (M_i k)^{0.5} R^{19/9} (I_i I_p)^{6/9} \bar{n}_e^{5/9} P_{\text{abs}}^{4/9},$$

where W_{th} is in the unit of MJ, R in m, I_p in MA, \bar{n}_e in 10^{19}m^{-3} , and P_{abs} in MW.

This scaling covers the experimental data of both L-mode and ohmic plasmas in JT-60 and JT-60U with various configurations.

3.2.2 H-mode confinement

One explanation of the poor H-mode properties in 1991 was insufficient reduction of particle recycling and impurity. Therefore, main effort in 1992 was to reduce the recycling and impurity with 4 wall conditioning techniques; He-TDC, He-GDC, boronization, and temperature control of the vacuum vessel. The first boronization was made at the end of July, 1992.

A clear drop of D_a emission (H-mode) was observed in the case of low toroidal field ($B_T=2.5\text{ T}$). The duration of this phase was short because edge localized modes (ELMs) appeared. The ELM occurred at relatively low density ($n_e=2\text{-}3 \times 10^{19}\text{ m}^{-3}$) in JT-60U, and this threshold density increased with the plasma current (see section 3.4). This low threshold density of ELM onset restricts the improvement of plasma performance in JT-60U H-mode, though no carbon bloom was observed even at a high heating power of 28MW.

In discharges with high $q_{\text{eff}} (>4)$ at high B_T ($B_T \sim 4.2\text{ T}$), low target density operation was possible. In such a case, the discharge tended to lose clear D_a drops as shown in Fig. I.3.2-1.

However, we found that the confinement improvement was obtained with increasing edge ion temperature[3.2-1]. Formation of the edge pedestal in the ion temperature profile indicated edge transport barrier. Since this improvement was obtained in the edge region when the net input power exceeded a certain value (14-16 MW), we think of this phase as a kind of H-mode.

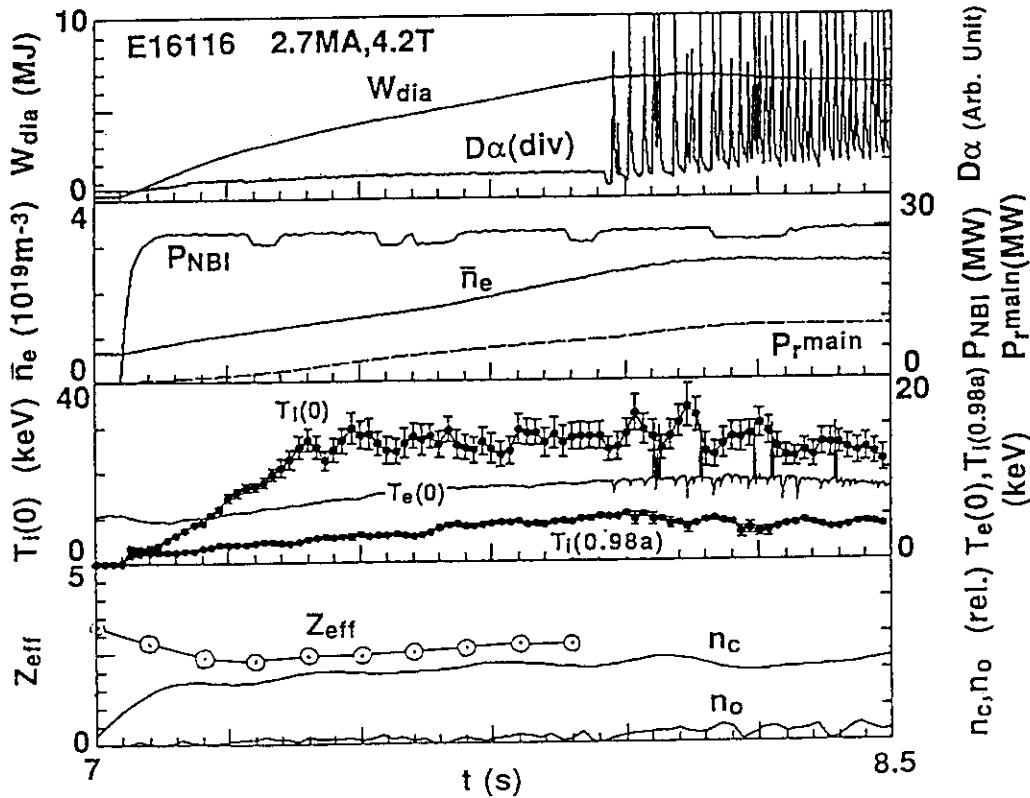


Fig.I.3.2-1 Typical Da transition-free H-mode at 2.7MA, 4.2T. High performance was terminated by strong ELM activity.

Formation of the edge transport barrier is an important property in the H-mode. The width of the edge transport barrier (d) measured by edge Thomson scattering and charge exchange recombination spectroscopy was 2.4-7 cm which seemed to become narrower with poloidal field (B_p); $d \sim 1/B_p$ [3.2-2]. The absolute value of the width is fairly close to the slowing down fast ion orbit width, $\sqrt{e}r_{pi}$, where r_{pi} is a fast ion poloidal gyro-radius and e is an inverse aspect ratio. Further investigation is necessary for confirmation.

The enhancement factor, H , increased with decrease of D_a emission in the divertor region[3.2-3], and the D_a emissions in 1992 experiments could be reduced by an order of magnitude compared with those obtained in 1991. A possible explanation for the decrease of the D_a emission is reduction of the recycling. The highest enhancement factor of 2.2 was achieved with a plasma current of 2 MA and a toroidal magnetic field of 4.2 T.

Effects of toroidal field ripple on H-mode confinement was investigated in $V_p=60, 70, 80$ m³ deuterium plasmas corresponding to $d < 0.5, 1$ and 2%, respectively, where V_p is plasma volume and d is triangularity. The plasma current was 2 and 3 MA with $B_T=4$ T, and high power

neutral beam injection was applied (D^0 , $E_b < 90$ keV, $P_{\text{perp}} < 22$ MW, $P_{\text{tang}} < 8$ MW). Estimated fraction of loss power due to the orbit loss were 5-12% with $d < 0.5\%$ and 30-35% with $d = 2\%$. All data were taken before the onset of ELMs. Experimental observations indicate that the global H-factor is not very sensitive on the magnitude of the ripple after correction of the absorbed power for additional losses due to the toroidal field ripple [3.2-4].

In summary, performance of the H-mode was extended successfully in 1992; maximum stored energy of 7.7 MJ, the highest confinement time of 0.45 s, the highest enhancement factor of 2.2 in ELM free phase and that of 1.6 in the steady state case, the highest neutron emission rate of 2.3×10^{16} /s, and the highest central ion temperature of 32 keV were achieved separately.

References

- [3.2-1] KIKUCHI, M., SHIRAI, H., TAKIZUKA, T., et al., Proc. 14th Int. Conf. Plasma Physics and Controlled Nuclear Fusion Research, IAEA-CN-56/A-3-3, Wurzburg, 1992.
- [3.2-2] Kikuchi, M., Sato, M., Koide, Y., et al., to be published, 20th European Conf. on Controlled Fusion and Plasma Physics, Lisbon, 1993.
- [3.2-3] Ninomiya, H. and JT-60 Team, JAERI-M 93-057(1993), p.5.
- [3.2-4] van Blokland, A.A.E., Azumi, M., Koide, Y., et al., to be published, 20th European Conf. on Controlled Fusion and Plasma Physics, Lisbon, 1993.

3.3 High poloidal-beta confinement

The high poloidal-beta (β_p) regime of tokamak operation attracts much interest as it may offer an alternative way for the development of a steady state tokamak reactor such as SSTR. To extrapolate the reactor plasma, the feasibility study is indispensable under the reactor-relevant conditions in a large tokamak. The JT-60U is a unique large tokamak allowing the discharges to run at a high toroidal field ($B_t = 4.4$ T) with a non-circular divertor configuration (an ellipticity of $\kappa \sim 1.7$) with a high aspect ratio ($A \sim 4.3$) similar to the SSTR concept, which is beneficial to such a reactor-oriented study. In the FY92 high β_p experiments, the high β_p enhanced confinement regime originally found in FY91 has been extended into the higher current region up to 2.4 MA to improve confinement and stability, in which the H-mode confinement has been newly achieved.

3.3.1 High- β_p mode regime

From the April and August runs in FY91, a highly enhanced regime of plasma confinement was achieved with energy confinement times up to a factor of H ~ 3 above the ITER89-P L-mode scaling for high β_p discharges at $\epsilon\beta_p \sim 0.5$ as shown in Fig.I.3.3-1 [3.3-1]. The plasma confinement in such a high β_p enhanced confinement regime was referred to as the high- β_p mode, where the plasmas were acquired with highly peaked profiles of both electron density and ion temperature. A large amount of bootstrap current of 0.8 MA corresponding to 58 % of the plasma current was obtained for a high β_p discharge with $\beta_p = 2.0$ from the 1.5-dimension transport analysis using the TOPICS code. The plasma performance in the high- β_p mode regime was characterized by high temperature of $T_i \sim 38$ keV and $T_e \sim 12$ keV, large fusion neutron rate of

2.8×10^{16} n/s, fusion triple product of $n_i(0)\tau_E T_i(0) \sim 4.4 \times 10^{20}$ m⁻³·s·keV, fusion amplification factors of $Q_{DD} \sim 1.9 \times 10^{-3}$ and equivalent Q_{DT} of ~ 0.31 .

Power dependence of the energy confinement time is found to be closely coupled with the plasma current, resulting in the apparent weak dependence against the power by changing the current according to the power level. It suggests that an optimum combination of the power and the current exists to maximize the confinement enhancement for a given toroidal field. The stability limit caused by β_p collapses was clearly reduced by decreasing the internal inductance resulting in the lower attainable $\epsilon\beta_p$ values. The β limit in the high β_p regime depends on both the Troyon factor (g-factor) and $\epsilon\beta_p$ as the attainable g-factor tends to increase with decreasing $\epsilon\beta_p$ along an approximate limit line of $g\epsilon\beta_p \sim 1.1$. Termination of the high- β_p mode was due to the occurrence of β_p collapses. Stability analysis using the ERATO-J code indicates that low-n ideal kink/ballooning modes can be unstable for a monotonic current density profile. Local T_e fluctuation measurements by 20-channel ECE grating polychromator revealed strong inside-outside asymmetry on the midplane of the plasma during the precursor oscillations prior to the β_p collapse, suggesting a ballooning mode feature (see Fig.I.3.3-2).

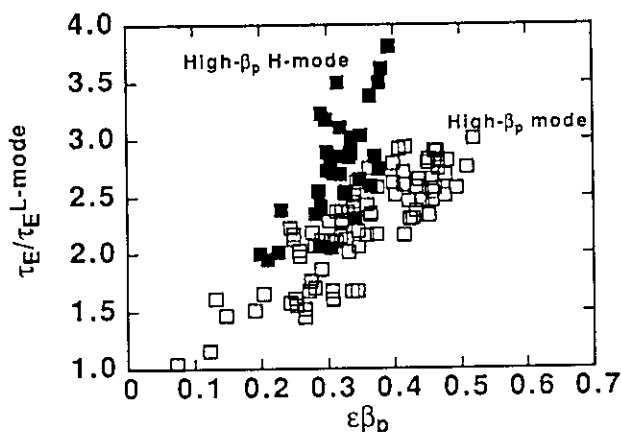


Fig.I.3.3-1 H-factor as a function of $\epsilon\beta_p$.

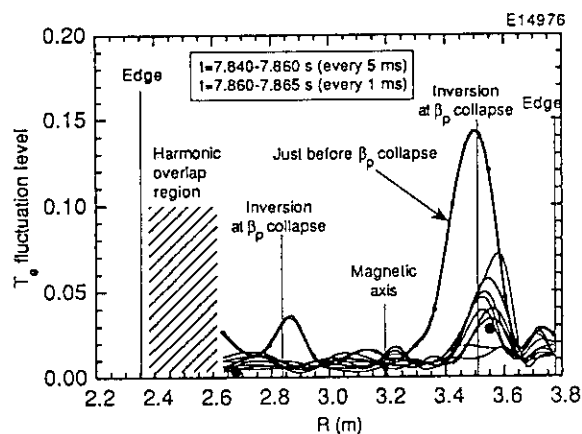


Fig.I.3.3-2 Ballooning-like precursors at $\epsilon\beta_p \sim 0.4$.

3.3.2 High- β_p H-mode regime

After extensive bolonization of the first wall to reduce impurities and deuterium recycling, a new enhanced confinement regime named as "high- β_p H-mode" has been achieved in March 1993 with high-power neutral beam injection up to 34 MW into high current plasmas over 2 MA (see Fig.I.3.3-3). A clear transition to H-mode occurred during the high- β_p mode under the high field of 4.4 T, where an apparent edge pedestal was observed with a peaked pressure profile (see Fig.I.3.3-3). Although the β_p collapses associated with kink/ballooning limits were avoided by a slight pressure profile broadening during an ELM free phase, the subsequent ELM activities degraded the confinement enhancement, in some cases leading to a stationary ELMy H-mode with H \sim 2. Across the transition, the significant increase in the edge T_i (typically, 2 to 6 keV) and the

formation of remarkable shears in the edge E_r pointed outward were observed. Thus, by achieving the H-mode confinement during the high β_p mode, the neutron rate (S_n) and the DD fusion amplification factor and fusion triple product in the high β_p regime were doubled up to $S_n \sim 5.6 \times 10^{16}$ n/s, $Q_{DD} \sim 4 \times 10^{-3}$ and a new world record of $n_i(0)\tau_E T_i(0) \sim 1.1 \times 10^{21}$ m⁻³·s·keV, respectively (see Fig.I.3.3-4).

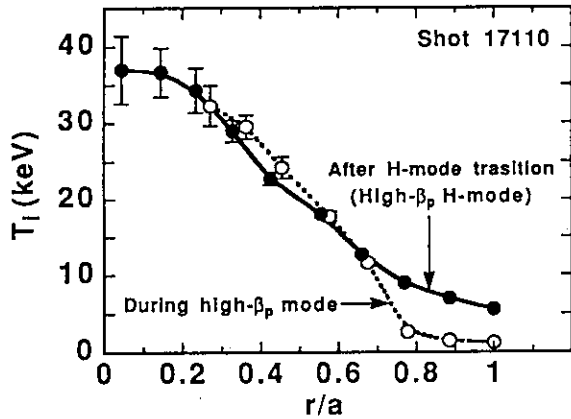


Fig.I.3.3-3 T_i profiles before and after H-mode transition

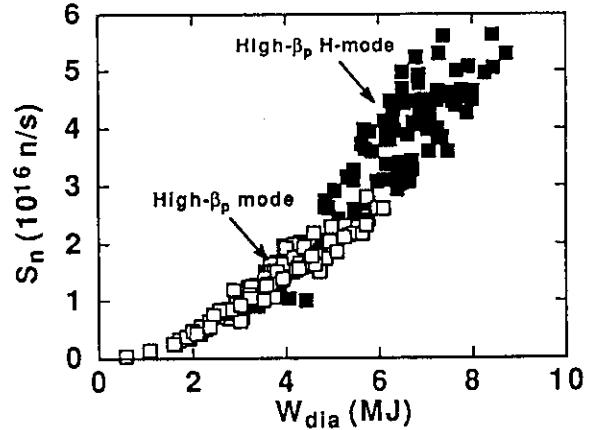


Fig.I.3.3-4 Neutron rate as a function of W_{dia}

References

- [3.3-1] S. Ishida et al., in Proc. of 14th Int. Conf. on Plasma Physics and Controlled Fusion Research, Wurzburg 1992, IAEA-CN-56/A3-5.

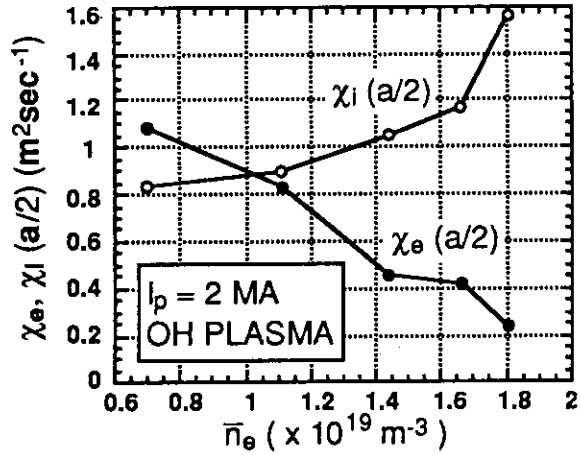
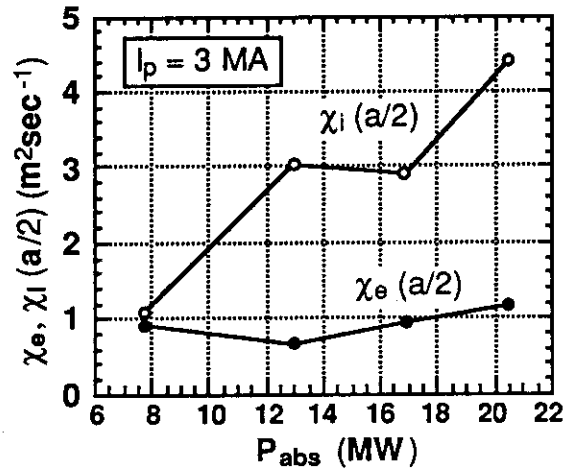
3.4 Transport and MHD studies

3.4.1 Transport

Understanding of various aspects of plasma transport; particle transport, heat transport and momentum transport is one of the important subjects in designing a reactor-size tokamak. Characteristics of transport in JT-60U plasmas in ohmic, L-mode, H-mode and hot ion mode have been studied from the standpoint of steady state analysis and by using perturbation methods.

The particle transport was studied in ICRF heating phase. In equations of electron density and temperature evolution, off-diagonal transport terms were taken into account. The particle flux was described as $\Gamma/n = -D/n \partial n/\partial r - \alpha/T \partial T/\partial r$ and there was no external particle source in the core plasma during ICRF heating. The perturbation analysis of n_e evolution after the sawtooth collapse showed that $\alpha/D \approx -1$; i.e. the off-diagonal term is comparable with the diagonal term. The transport of high energy electron generated by the LHCD discharge was studied in the pellet injection phase. The time evolution of hard X-ray intensity just after the pellet injection was simulated by using the density equation considering the slowing down process of high energy high energy electron, D_h , we obtained electron. By changing the diffusion coefficient of $D_h \leq 1$ m²s⁻¹.

In the ohmically heated plasmas, short-pulsed (< 100 msec) neutral beams were used for the evaluation of the T_i profile. The local heat transport analysis in $I_p = 2$ MA and 3 MA plasmas shows that χ_e at $r = a/2$ is large in low densities and decreases with \bar{n}_e , while χ_i at $r = a/2$ is small in low densities and increases with \bar{n}_e (Fig.I.3.4.-1). The local heat transport coefficients in low P_{abs} neutral beam heated L-mode plasmas were also studied in $I_p = 2$ MA and 3 MA plasmas and were compared with the results of ohmic heating phase and high P_{abs} phase. The χ_i continuously increases from ohmic to high P_{abs} plasmas, while the χ_e is almost unaffected by P_{abs} and remains in the range of $\chi_e \sim 1$ m²s⁻¹ (Fig.I.3.4.-2). The deposition profile dependence of χ_e and χ_i was studied in on- and off-axis tangential neutral-beam heated plasmas. The T_e profile is not sensitive to the profile of the NBI power deposition to electrons. There seems to be the profile resiliency in the electron temperature. On the other hand, the T_i profile is very sensitive to the power deposition profile.

Fig. I.3.4-1 Density dependence of $\chi_{e,i}$ Fig.I.3.4-2 Power Dependence of $\chi_{e,i}$

As for the momentum transport, toroidal and poloidal rotations have been measured extensively by the CXRS. In the tangential neutral beam injection, the toroidal rotation direction coincides with the direction of momentum input. Interesting feature of co-perpendicular beam injection is that plasmas rotate in the counter direction. In the modulated beam experiment, the ctr-rotation propagates inwardly from the edge region. This ctr-rotation is larger with higher q_{eff} and larger toroidal field ripple. It is deduced that the ctr-rotation is driven by inwardly directed radial electric field caused by the ripple-loss. Another interesting feature is the co-directed plasma rotation in LHW-driven plasmas, which suggests the formation of an outwardly radial electric field, because an external momentum input from LHW is given to electrons and the direction of the momentum input is opposite to the plasma current direction. The toroidal momentum transport coefficient, χ_ϕ , in the tangential NBI heating phase was studied using momentum balance equation. Results from the periodical momentum input experiment in off-axis NBI showed that the inward flow velocity of momentum is comparable to the momentum diffusivity ($\chi_\phi \sim 1$ m²/s,

$V_{in}^{\phi} \sim 1$ m/s). Momentum transport study has just begun, and the systematic parameter dependence of momentum transport coefficients will be clarified in near future.

3.4.2 MHD studies

To demonstrate the attractiveness of the tokamak fusion reactor, the following conditions should be satisfied steadily and simultaneously; high H-factor for ignition, high- β_p for high bootstrap current fraction, high- β_N for high fusion power density, short τ_p , disruption-free and dense & cold divertor condition. Since MHD activities play important roles for all of these conditions, the final goal of MHD research is to optimize the above performance by control of MHD activities. In particular, from the view point of steady state, active controlling the instabilities (frequency, perturbed area etc.) is necessary rather than suppression for non-disruptive instabilities. This section lists the outline of the MHD research in JT-60U in 1992 toward this goal.

1) sawteeth and $m/n=1/1$ mode [3.4-1 - 3.4-3]

The condition for appearance of sawteeth is given by a clear boundary on q_{eff} - l_i diagram. A scaling of the inversion radius r_{inv} was given by a function of q_{eff} and l_i . The sawtooth period τ_{sw} is basically given by a function of resistive diffusion time. These results are important to optimize the high performance discharges in tokamaks. Monster sawteeth ($\tau_{sw} \sim 2$ s) were studied by ICRH.

2) medium m/n modes at low β [3.4-1 - 3.4-4]

The condition for high- l_i disruption and low- l_i locked mode were given by clear boundaries on the q_{eff} - l_i diagram. Systematic works of minor and major disruptions were reported. High- l_i and low- l_i disruptions were avoided by growing and dwindling a_p . Locked modes and QSM at low n_e were studied including error field effects.

3) ELMs [3.4-1, 3.4-3]

The ELM frequency and the n_e -threshold for ELM-on condition were related to the ballooning parameter. The ELM frequency is an increasing function of NB heating power.

4) β -limit; ($\beta_N=3.5$, $\beta_p=3$; H-factor=2; ELMy H-mode) [3.4-1]

The β -limit was increased by broad $p(r)$ and peaked $j(r)$ (increase in l_i). Energy confinement was limited by pressure driven medium m/n modes.

5) high- β_p mode; ($\beta_p=3$, $\epsilon\beta_p < 0.7$, bootstrap fraction ($\sim 58\%$)) [3.4-1, 3.4-5, 3.4-6]

Achievable β_p was limited by the β_p -collapse under peaked $p(r)$ with broad $j(r)$, which is caused by kink-balloon type medium m/n modes. An MHD design study for the optimized high β_p reactors reported that hollow q -profiles have advantages for the high- β operation..

6) L-mode and H-mode [3.4-1 - 3.4-3]

Concerning L-mode confinement, H-factor is almost proportional to $l_i^{0.8}$ for $q_{eff}=2-14$. The reason of confinement degradation at low- q ($q_{eff} < 4 \sim 5$) was quantitatively confirmed as effects of l_i and sawtooth. The degradation due to sawteeth is stronger at lower q_{eff} . A new confinement

scaling law for the H-factor (H_{SC}) in L-mode is obtained by including the effects of I_i and sawteeth. This study was expanded to H-mode including ELM effects.

References

- [3.4-1] JT-60 Team, 'Review of JT-60U Experimental Results from March to October, 1992' JAERI-M 93-057, Japan Atomic energy Research Institute (1993)
 [3.4-2] KAMADA Y., et al., Nucl. Fusion. **33** (1993) 225.
 [3.4-3] KAMADA Y., et al., in Proc. Int. Conf. Plasma Phys. Controlled Nucl. Fusion Research (14-th Int. Conf. Wurzburg 1992) IAEA-CN-56/A-7-13.
 [3.4-4] YOSHINO, R., et al., ibid. IAEA-CN-56/G-3-1.
 [3.4-5] ISHIDA, S., et al., ibid. IAEA-CN-56/A-3-5
 [3.4-6] OZEKI, T., et al., ibid. IAEA-CN-56/D-4-1.

3.5 Impurity and divertor characteristics

Quantitative studies of particle recycling, helium, impurity and heat transport have been performed on divertor plasmas in JT-60U in light of their importance for the ITER physics R&D. Carbon fiber composite divertor plates with good alignment and beveled edges in JT-60U provided excellent power handling capability; no carbon burst has been observed during 5-s heating pulses at about 20 MW [3.5-1]. Experiments indicated that high safety factor and high density operation is favorable to reduce divertor heat load and to lower the electron temperature at the divertor with enhanced particle recycling and radiation power.

A scaling law on the peaking factor of the divertor heat flux based on a database in a heating power range of 4 MW to 16 MW [3.5-2] was found to be applicable to higher heating power of up to 25 MW [3.5-3]. The peak heat flux at the outer divertor is two to three times higher than that at the inner divertor in the L mode. The heat flux profile in the H mode was nearly symmetric. The peak heat flux during ELM-free H mode is higher than in the L mode by a factor of up to 2. However ELMs broadened the heat flux profile to L-mode levels.

The mechanism for carbon impurity generation was investigated with spatially resolved spectroscopic diagnostics [3.5-4] while the previous study was based only on total flux measurements [3.5-5]. Figure I.3.5-1 shows a measured carbon influx on the divertor plates and calculated ones in a beam heated discharge. The calculated carbon influx by physical deuterium ion sputtering, physical and chemical oxygen ion sputtering and self sputtering agrees well with the measured influx both in its profile and magnitude. The carbon and deuterium physical sputtering was dominant. The chemical sputtering by deuterium ions appears to play

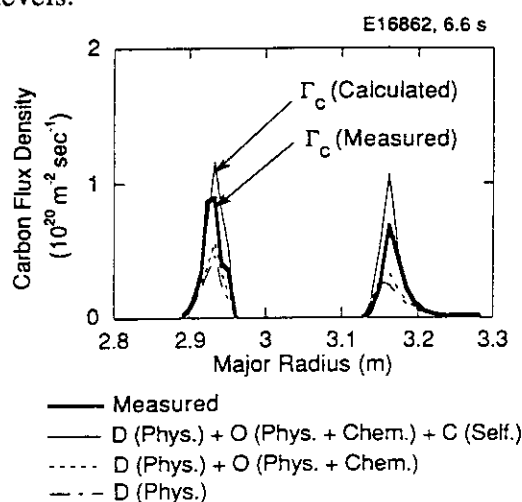


Fig. I.3.5-1 Comparison of a measured carbon influx profile and calculated ones at divertor plates.

little role since the carbon influx had no dependence on the plate temperature. The radiation loss in the divertor region was analyzed by VUV spectroscopy. It was found that a large fraction of the divertor radiation was caused by deuterium and C^{3+} .

A 2-D impurity code based on the Monte Carlo technique was developed to study impurity transport in divertor/SOL plasmas. The required plasma parameters in the SOL was provided from an interpretative divertor code [3.5-6] where fluid equations along the magnetic field were solved by using divertor Langmuir data as boundary conditions. A preliminary calculation predicted a carbon concentration in the main plasma of 1.5%, which was in a good agreement with experimental values of 2-3%. Helium transport experiments during L and H modes showed that the ratio of the helium density in the main plasma to the helium influx in the divertor saturated within 0.5 s for 2-s gas puff, which indicates that helium exhaust is plausible in the L mode and ELMy H mode only with a factor of 2.5 difference in the ratio between the two modes.

Particle influx evaluated from $D\alpha/H\alpha$ measurements [3.5-7] increased with the main density and the effective safety factor as shown in Fig.I.3.5-2. Inboard recycling and in-out asymmetry were enhanced when the ion grad-B drift was toward the X-point. The divertor electron temperature should be reduced below the sputtering threshold of about 20 eV to alleviate the erosion of plates. However the outboard particle recycling was not enhanced so much as the inboard recycling in spite of the higher heat flux to the outer strike point. The peak electron temperature and the peak electron density at the outer divertor is plotted as a function of the outboard particle flux in Fig.I.3.5-3.

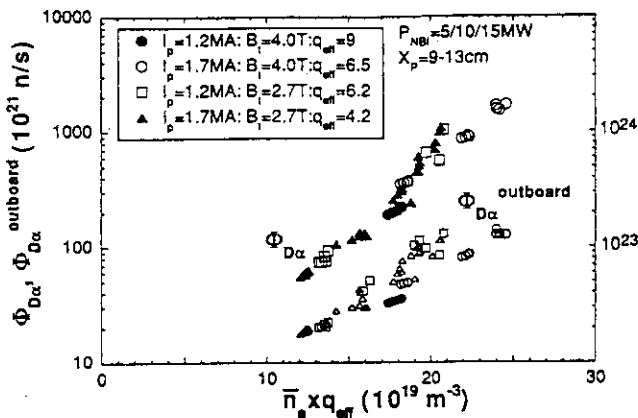


Fig. I.3.5-2 Particle influx in the outboard side and the total particle influx including inboard side as a function of the line averaged main electron density multiplied by the effective safety factor. The higher q_{eff} means longer connection length from the X-point to the divertor plates.

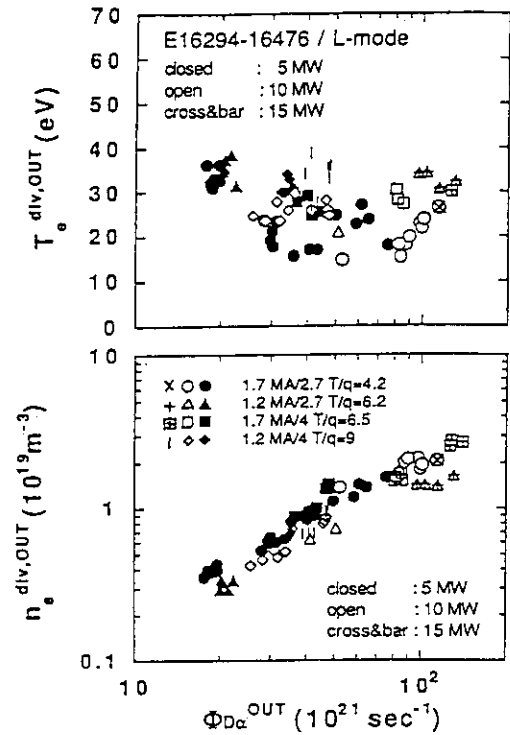


Fig. I.3.5-3 Peak values of T_e and n_e at the outer divertor as a function of the outboard particle influx.

The electron temperature at the outer divertor was reduced to around 20 eV with increasing particle flux, which was limited by the density limit. A slight increase in density or a slight drop in heating power triggered MARFE near the X-point, which obstructs particle and heat flows to the divertor and resulted in detached plasmas [3.5-8]. Thus cold divertor plasmas below 20 eV were not easy to maintain experimentally. The particle flux to the divertor in the H mode was less than that in high recycling L mode by about two orders of magnitude. The asymmetric particle recycling and the evolution to detached plasmas was analyzed with a 2-D divertor transport code, the UEDA code.

References

- [3.5-1] JT-60 team presented by M. Shimada, IAEA Wurzburg Conf. (1992) IAEA-CN-56/A-1-3.
- [3.5-2] K. Itami et al., J. Nucl. Mater. 196-198 (1992) 755.
- [3.5-3] K. Itami et al., IAEA Wurzburg Conf. (1992) IAEA-CN-56/A-6-5.
- [3.5-4] A. Sakasai et al., IAEA Wurzburg Conf. (1992) IAEA-CN-56/A-7-12.
- [3.5-5] H. Kubo et al., J. Nucl. Mater. 196-198 (1992) 71.
- [3.5-6] K. Shimizu et al., J. Nucl. Mater. 196-198 (1992) 476.
- [3.5-7] N. Asakura et al., J. Nucl. Mater. 196-198 (1992) 1069.
- [3.5-8] N. Hosogane et al., J. Nucl. Mater. 196-198 (1992) 750.

3.6 Fast ion studies

Ripple losses of NB-injected fast ions were measured by using an IRTV camera in JT-60U. Experimental data were compared with calculation results from an orbit-following Monte-Carlo (OFMC) code. The power loss fraction integrated over the hot region in the lower side of the torus (in the direction of ∇B drift) agrees well with the fraction of ripple-trapped loss calculated by the OFMC code. In order to reproduce the 2-D distribution of the heat load due to the ripple-trapped loss, the effect of $\vec{E} \times \vec{B}$ drift of ripple-trapped particles must be taken into consideration. The effect of the external electric field, the electric field between the plasma surface and the first wall, is very important to reproduce the 2-D distribution of the heat load. The integrated power loss fractions are insensitive to both internal and external electric fields. There is still a small difference between the numerical and experimental results of the 2-D distributions of the heat load. The model electric field will be improved in the near future for more precise numerical investigations.

Effect of TF ripple on triton burn-up ratio in deuterium discharges also has been checked by using OFMC. Both DD reaction neutrons with 2.45 MeV and DT reaction ones with 14.1 MeV were measured, and the burn-up ratios of 1 MeV tritons generated by DD reaction were evaluated from the ratio of both neutrons. Experimental results give 20~30 % lower values than those evaluated without any losses of tritons during their slowing-down process, while OFMC calculations with TF ripple loss give results in good agreement with experimental ones. This suggests that the TF ripple loss degrades the confinement of 1 MeV triton and reduces the triton burn-up ratio in JT-60U. Systematic parameter study on the triton burn-up ratio is now under way.

In the hot ion discharge, the ion temperature is comparable with beam energy and the coupling between the bulk ions and fast ions has to be carefully analyzed. The deuterium temperature in the discharge with carbon ion temperature 38 keV at the plasma center and beam energy of 90 keV was analyzed by solving the coupled nonlinear Fokker Planck equations for deuteriums and carbons. Assuming the ion energy confinement time of $\tau_E = \tau_{E0} [1 + (E / E^*)^{3/2}]$ and adjusting τ_{E0} such that the carbon temperature is the measured one, the effective deuterium temperature defined by $T_D^{eff} = - f / (df / dE)$ in the energy range of $E < 38$ keV with isotropic velocity distribution was evaluated. Interestingly, the results show that T_D^{eff} exceeds 38 keV for $E^* > 20$ keV, where E^* stands for the critical energy of fast ion improved confinement. The accurate determination of T_D^{eff} requires the further study of fast ion confinement property in the hot ion discharges.

3.7 LHRF and ICRF experiments

3.7.1 Lower hybrid current drive (LHCD) experiment

LHCD experiments were performed by using a 24x4 multijunction launcher with $P_{LH} \leq 2.6$ MW. The plasma current of 2 MA was driven by LHCD alone and the current drive efficiency of $2.5 \times 10^{19} m^{-2} A/W$ was achieved[3.7-1]. The observed efficiency was consistent with the empirical scaling derived in 1989[3.7-2] from JT-60 results.

By measuring the soft x-ray flux from the divertor plates during LHCD, the direct loss power through fast electrons was identified in JT-60U LHCD discharges[3.7-3]. In Fig.I.3-7-1, the direct loss power is divided by the injection power and plotted against the slowing down time of fast electrons with $v_p = c/N_{||}^{peak}$. The measured direct loss is nearly proportional to the slowing down time of fast electrons. One dimensional quasi-linear Fokker-Planck equation with a radial diffusion of fast electrons was solved numerically and the fast electron power loss was calculated under experimental conditions ($T_{e0} = 5$ keV, $n_{e0} = 2 \times 10^{19} m^{-3}$ and $N_{||}^{peak} = 1.44$). Figure I.3-7-2 shows the numerically calculated direct loss rate against $\tau_{SD}(v_p)/(a^2/D_s(v_p))$ where $\tau_{SD}(v_p)$ is the slowing down time of electrons with the velocity $v_p = c/N_{||}^{peak}$ and $D_s(v_p)$ is the radial diffusion coefficient of fast electrons at v_p .

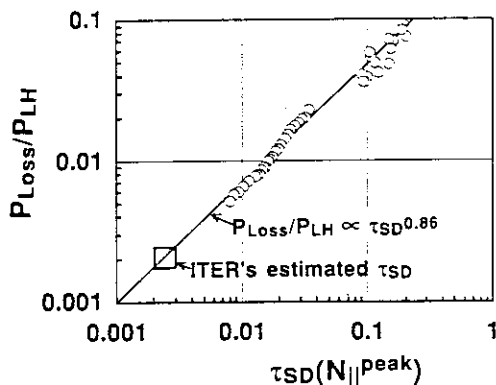


Fig. I.3-7-1 The directly lost power rate against the slowing down time of fast electrons.

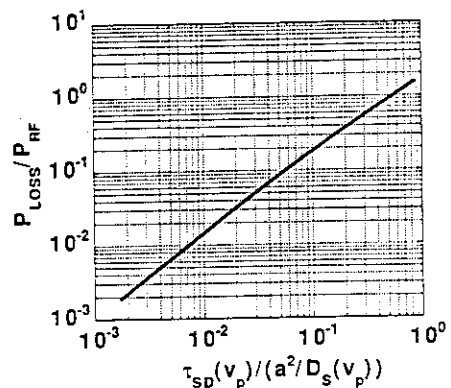


Fig. I.3-7-2 Simulated direct loss rate against the normalized slowing down time of fast electrons.

The calculated direct loss power has a similar dependence on $\tau_{SD}(v_p)$ with the experimental results. Since $P_{Loss}/P_{LH} \leq 0.1$ in the experiments, numerical modeling suggests that $D_s \leq 0.5 \text{ m}^2/\text{s}$ at $N_{||peak} = 1.44$. The similar conclusion was obtained in the analysis of response on hard x-ray signal after the pellet injection during LHCD, and in modulated LH power injection.

The validity of wave accessibility condition was confirmed. It was found that the wave accessibility condition limits the maximum electron energy accelerated by LH waves, reduces the current drive efficiency, enhances the surface wave power, the impurity content and the radiation loss. In the present condition, $N_{||acc}/N_{||peak} > 0.8$ is enough to avoid these unfavorable effects.

3.7.2 ICRF experiments

Higher harmonic ICRF heating is investigated in JT-60U. Significantly large loading resistances (~ 5 ohms) were obtained with the in-phase current mode ((0,0) mode) at a large separatrix-wall gap of 29 cm. Energetic proton tails were observed when the distance between the $2\omega_{CH}$ resonance position and the plasma center was within about 10% of the minor radius. These tails are generated by second harmonic minority ion heating so that the central plasma heating occurs with (0,0) phasing even at such a large gap.

Efficient sawtooth stabilization by $2\omega_{CH}$ heating is observed with $(\pi,0)$ phasing in relatively high-density and low-q region, $\langle n_e \rangle / P_{tot} \approx 0.8 \times 10^{19} \text{ m}^{-3}/\text{MW}$ at $q_{eff} = 4$ and $I_p = 2.4 \text{ MA}$. Figure I.3.7-3 shows a typical results of sawtooth stabilization at $P_{IC} = 2.8 \text{ MW}$ for the plasma parameters of $I_p = 2 \text{ MA}$, $B_T = 3.97 \text{ T}$, $q_{eff} = 5.3$, $\bar{n}_e \sim 2 \times 10^{19} \text{ m}^{-3}$ and helium discharge containing residual hydrogen. The central electron temperature increases from 3.1 keV to 5.5 keV and the profile peaking factor $T_e(0)/\langle T_e \rangle$ is 2.8. The increase in plasma stored energy by diamagnetic measurement is about 0.71 MJ. Then the incremental energy confinement time ($\Delta W / (P_{IC} + I_p \Delta V_L)$) is about 0.3s. This value is comparable to the results in JET at a similar plasma current [3.7-4]. This suggests that ICRF central heating does not suffer from the large toroidal field ripple of JT-60U.

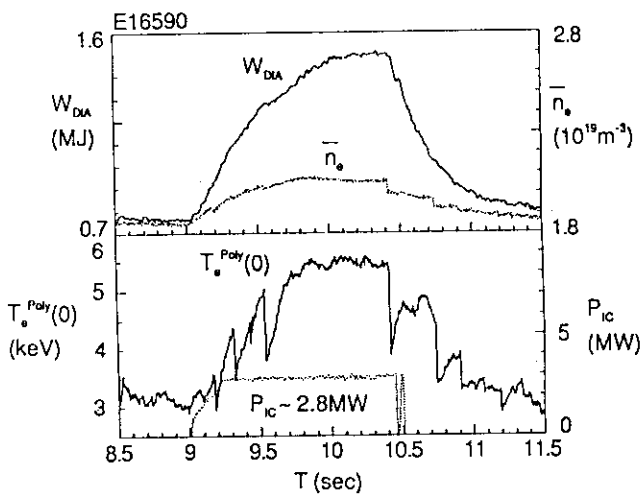


Fig. I.3.7-3 Example of sawtooth stabilization by $2\omega_{CH}$ minority ion heating alone.

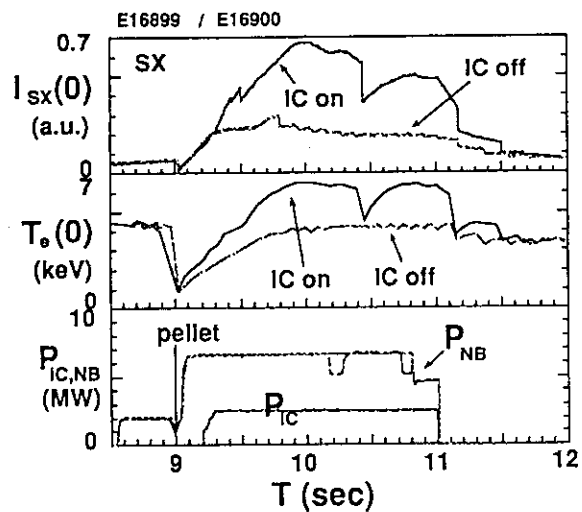


Fig. I.3.7-4 Comparison of results of pellet+ICRF+NBI with pellet+NBI.

The maximum sawtooth-free period is 0.9s for OH target plasmas and 1.7s for NB-heated target plasmas at a power of $P_{IC} \approx 3$ MW.

Combined $2\omega_{CH}$ ICRF (2.5 MW) and NBI (D beam, ~ 6 MW) heating was carried out for pellet-fueled plasmas (Fig. I.3.7-4). Preliminary results show that the pellet enhanced phase is maintained for 1.4 sec up to sawtooth crash and the energy confinement time normalized by heating power is improved by 20% compared with pellet injection and NBI heating alone. Preliminary experiments on higher harmonic beam ion acceleration including a fourth harmonic ^3He resonance [3.7-5] or a fifth harmonic deuterium resonance were also carried out. Beam acceleration in the plasma core was actually observed to some extent in both cases, and recipes for improvement were clarified.

References

- [3.7-1] T. Imai et al., Proc. 19th Int. Conf. on Contr. Fusion and Plasma Phys. (1992) Vol. 16C, Part II, p.953.
- [3.7-2] K. Ushigusa et al., Nuclear Fusion **29**, 1052 (1989).
- [3.7-3] K. Ushigusa et al., Nuclear Fusion **32**, 1977 (1992).
- [3.7-4] V.P. Bhatnagar et al., Plasma Phys. Contr. Fusion **31**, 333 (1988).
- [3.7-5] M. Yamagiwa et al., Nucl. Fusion **33**, 493 (1993).

3.8 Development of fusion plasma analysis codes

The numerical codes required for the experimental data analysis and the theoretical prediction of plasma performance in JT-60 and a tokamak reactor are systematically developed and updated. The efforts of code development and update in FY1992 have been concentrated on the more accurate evaluation and verification of the improved plasma performance, the detail analysis of physical mechanisms and the increased functions in utility softwares.

3.8.1 Experimental data time slice monitoring software : SLICE

The "SLICE" code maps various kinds of plasma experimental data measured at the different geometrical position of JT-60 and JFT-2M onto the equilibrium magnetic configuration and treats them as a function of volume averaged minor radius r . Plentiful of commands of SLICE make it easy to process the mapped data. The experimental data measured as line integrated values are also transformed by Abel inversion. The mapped data are fitted to a functional form and saved to the database MAPDB. SLICE can read the data from MAPDB and re-display and transform them. SLICE creates run data of orbit following Monte-Carlo code OFMC and tokamak predictive and interpretation code system TOPICS.

3.8.2 Tokamak prediction and interpretation code system : TOPICS

TOPICS is the 1-1/2 tokamak transport code system for the systematic transport studies in experimental data analysis and theory-based performance analysis, both in steady state and in time evolution. The system includes many modules calculating physical processes in a tokamak and is designed such that the user can pick up necessary modules for studying the underlined subject by

using the FORTRAN source organizing code SPOT. Several functions of the code system have been updated in FY 1992, according to the progress in JT-60 experiments and in the reactor design. The major effort was made for the improvement of time evaluation in nuclear reactions in JT-60 high β_p discharges, which gives the good agreement with experimental data of neutron production. The interface routines with plasma profile database and equilibrium database has been also revised for the improvement of each database. The functions of the equilibrium solver module, SELENE/MEUDAS, were also increased such that the code can meet the requirements of the tokamak machine design calculation. Several load modules are now running for both the steady state and time-evolutional analysis of transport properties based on experimental data and for studying the operation scenario in the self-ignition phase of the steady-state tokamak reactor.

3.8.3 Orbit-Following Monte-Carlo code : OFMC

A new system to evaluate the effect of the toroidal field (TF) ripple on the triton burn-up fraction has been developed. The system consists of two different orbit-following Monte-Carlo codes: one to evaluate the distribution function of neural-beam injected fast deuterons under the influence of TF ripple and one to evaluate the burnup fraction of tritons produced by beam-beam and beam-thermal D-D fusion reactions.

3.8.4 Current drive analysis code : ACCOME

As a part of the effort to improve the numerical code ACCOME for studying the steady-state properties of inductive and non-inductive current drive in a tokamak plasma, an analysis code for the electron cyclotron current drive using a ray-tracing method has been developed. The inclusion of the code into ACCOME is under way.

3.8.5 Source program organization tool : SPOT

The SPOT system was developed to control and manage large-size FORTRAN source program. SPOT builds source FORTRAN program, where unnecessary statements or modules for the model are automatically discarded, by tree analysis through plural source files and include members and specification of calculation models, according to script called SPOT DATA, and finally creates the load module. For the convenience and the timesaving of code development, three functions are added to new version : updating load module by substitution of modules in case that source files were changed locally, creating user-library used at link phase by skipping of tree analysis, and preserving fixed modules as user-library temporarily. Using these new function, the user doesn't need to wait until whole SPOT execution is done.

3.8.6 EXPERT system

EXPERT system to make the input data of ERATO code and to judge the validity of calculation results has been developed with the aid of the artificial intelligence. Linear ideal MHD stability code ERATO is useful to analyze the experimental data of JT-60 and to estimate the MHD limit of the tokamak reactor. However, users of ERATO code are quite restricted to the expert because it is difficult to select the input data and to judge the justice of results. By using EXPERT system, ERATO code can be used without the special knowledge. The EXPERT system works on the work-station SUN using the software of the artificial intelligence KEE, and ERATO code executes on the main frame of FACOM.

3.8.7 Fast analyzer for MHD equilibrium : FAME

MHD equilibria are necessary for high level processing of experimental data from tokamaks. A small scale parallel computer, FAME, has been installed in order to solve the 2D MHD equilibria at energy 0.1 sec (more than 120 times in total per shot) during the shot interval. Computational results are stored on a disk system ad the MHD equilibrium database and are also visualized by using a SUN workstation and a video disk system.

4. Related Developments and Maintenance

4.1 Boronization system using decaborane

A new type of boronization system has been installed in the JT-60U tokamak in July 1992 [4.1-1]. Decaborane $B_{10}H_{14}$, a material less hazardous than diborane B_2H_6 , has been used to deposit a pure boron film on the first wall. The purpose of the boron film is to reduce the impurity contamination in the JT-60U plasmas. The decaborane-based boronization system including a decaborane container can be located in the torus hall because of its safer features; decaborane is not explosive and less toxic than diborane and the pressure of decaborane is always subatmospheric throughout the system. This enables installation of a decaborane container near the JT-60U vacuum vessel, which shortens the delivery lines from the container to the injection port of the vacuum vessel to less than 20 m, which is a factor of five shorter than the conventional boronization system. The decaborane-based boronization has been performed under a glow-discharge using helium-decaborane gas mixture.

Three boronization sessions, so far, have been carried out in this fiscal year. In November 1992, before the third boronization, modification has been made in the gas feeding line, in which gas inlets of helium-decaborane gas mixture have been increased from one toroidal location to twelve in order to improve a deposition of boron film with better toroidal uniformity. Table I.4.1-1 shows the summary of three boronization sessions performed in this fiscal year.

Table I.4.1-1 Summary of three boronization sessions performed in this fiscal year

	1st	2nd	3rd
Date	July 30/92	September 1/92	February 17/93
Amount of decaborane consumed (g)	10	15	50
Deposition time (h)	10	10	36
Wall temperature (deg C)	300	300	250
number of gas inlets	1	1	12
Estimated boron film thickness (nm)	30	45	150
Measured thickness (nm)	—	2 - 80	100 - 400
Hydrogen content (H/B) (%)	—	10	10 - 14

Post-boronization tokamak discharges showed good performances; oxygen was reduced by an order of magnitude for ohmically-heated plasmas and its concentration was around 1 % for neutral beam heated plasmas up to 25 MW after the second boronization. The particle recycling flux was also reduced by a factor of 2 - 3 for neutral beam heated plasmas and the stored energy increased from 5.3 MJ to 7.7 MJ[4.1-2]. After the third boronization a deposition of thicker boron film with better toroidal uniformity has been achieved. With this upgraded boronization system as well as

increased neutral beam heating power of up to 33 MW and optimization of current profile and plasma pressure profile, the plasma performance improved further; the stored energy and the ion temperature increased to 8.7 MJ and 40 keV, respectively[4.1-3].

References

- [4.1-1] M. Saidoh et al., Fusion Eng. & Des. 22 (1993) 271.
- [4.1-2] M. Saidoh et al., Jpn. J. Appl. Phys. 32 (1993).
- [4.1-3] M. Mori et al., submitted to Nucl. Fusion.

4.2 In-vessel inspection system

A new in-vessel inspection system was installed in the JT-60U machine. This system consists of a movable TV camera and a lighting device which can be inserted through horizontal viewing ports during intervals of operations. Figure I.4.2-1 shows the camera head and the light inserted into the vacuum vessel for performance tests during the air vent. The TV camera is encased in the vacuum-tight cylindrical chamber with internal thermal insulation layers to protect from thermal radiation from the first wall at 300 °C. The front window of the camera chamber consists of double layers of glasses for thermal shield. The camera chamber can be rotated in the poloidal direction in the range from +90 to -90 degrees. The driving mechanism using a vacuum-tight motor is attached outside the camera chamber. The shaft of the viewing system can also be rotated around its axis in the range from +180 to -180 degrees. Although the camera head and the light source are not cooled actively, the allowable observation time is about two hours which is sufficient for the observation of the in-vessel components. The camera head and the light source can be withdrawn from the vacuum vessel and stored in the chamber which are differentially pumped continuously. The operation of this system are carried out at the central control room of JT-60 by watching the TV monitor.

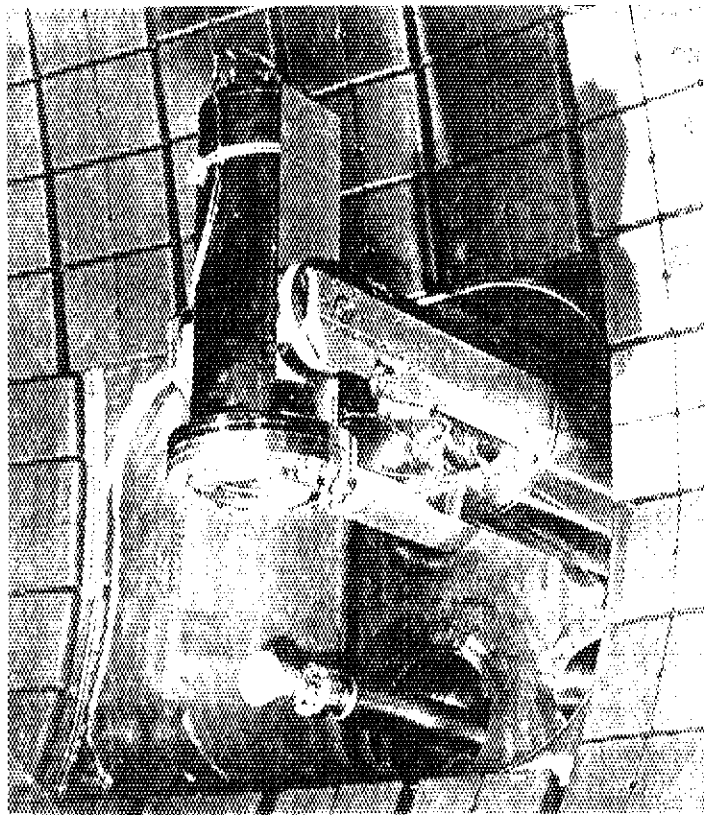


Fig. I.4.2-1 New in-vessel inspection system inserted into the vacuum vessel, consisting of the movable camera head and the lighting device (Size of the camera head is 433 mm long and 203 mm in diameter)

4.3 Development of real-time plasma shape visualization system

A prototype real-time shape visualization system has been developed, which has the following features: (a) The system can give a clear view of plasma cross-sectional configuration. It is difficult to obtain clear view with a TV camera in the vacuum vessel. (b) Plasma motion and/or vibration along with evolution of the plasma shape can be observed. It may be helpful for understanding of plasma behavior. (c) It enables us to evaluate plasma performance very effectively. If the operator records the monitor output with a video tape recorder (VTR), he can confirm the shape at any instance of discharge by replaying the tape at a selected speed after the shot.

(1) Algorithm for real-time computation

The flux function value in a vacuum region, which can be obtained by the three methods of boundary integral equation (BIE) [4.3-1], filament current plasma (FCP) [4.3-2] and Legendre-Fourier expansion (LFE) [4.3-3], is expressed as a linear combination of the measured magnetic flux, the magnetic flux density, the PF coil current and the plasma current. To visualize the plasma shape in real time, the flux function values at approximately 1000 points in the tokamak cross-section should be calculated within 10~20 ms. Then, the coefficients of the expression are calculated for all possibly utilized positions in the vessel beforehand. They are stored in the computer memory in tabular form. During a pulse of discharge, the utilized linear coefficients are fetched from the table every time when the flux function values are calculated. The algorithm to obtain the outermost magnetic surface of plasma is given in the following process.

- (a) The flux values at the fixed limiters are calculated on the three-dimensional curved surface of the flux in the vacuum region, .
- (b) The X-point of divertor plasma is searched as a saddle point of the same surface of the flux.
- (c) Among the calculated flux values at both the fixed limiters and the X-point, the smallest one indicates the plasma surface flux value.
- (d) The contour of the flux is then searched and drawn out showing the shape of the plasma.

(2) Hardware configuration

The main part of the real-time shape visualization system is composed of VME-bus (IEEE std. P1014/D1.2) devices as shown in Fig. I.4.3-1. The execution of the shape reproduction algorithm is performed in real time by a microprocessor named MVME147SC having a large-sized memory. Under control of the main processor, a fast and high resolution graphic processor, VG-1281 draws out the plasma shape. A digital input module MVME340A is equipped to receive a clock signal, which enables periodic execution of the real-time program installed in the MVME147SC. The measured data are transferred to the system via a buffer memory, DVM11WF. To develop the real-time programs and to produce a table of the coefficients for the real-time operation, SUN-3 Workstation is adopted as the host computer of the system. This WS is linked with an Ethernet to communicate with CPU in the VME rack.

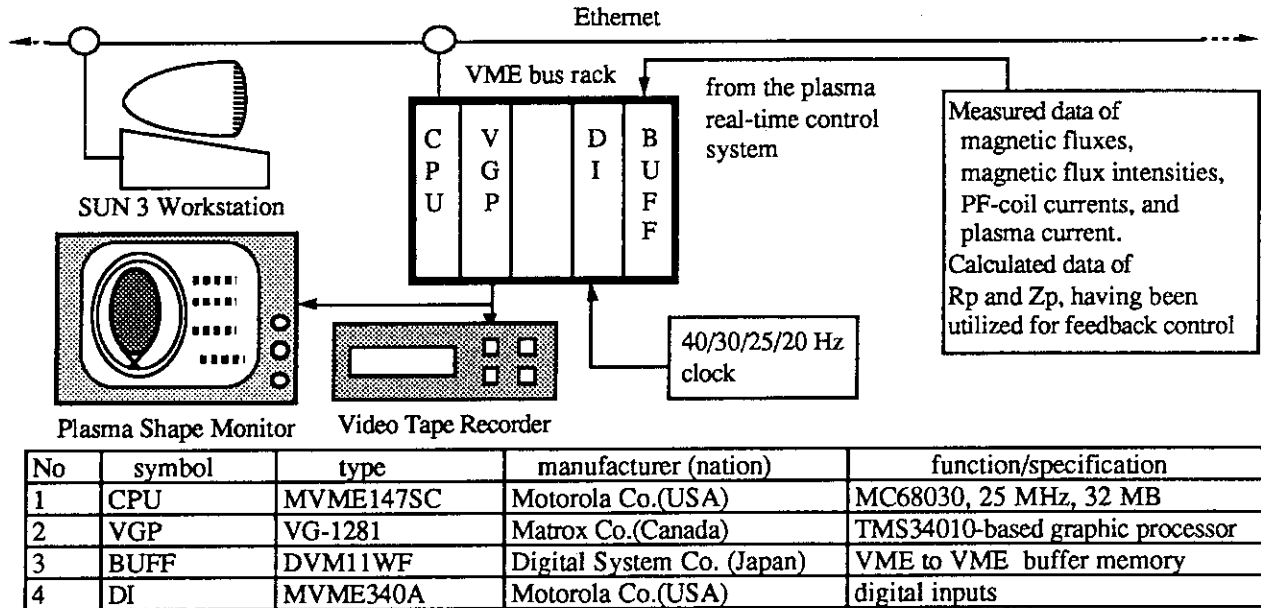


Fig. I.4.3-1 Configuration of real-time shape visualization system and hardware specifications.

(3) Test results

To evaluate the system performance, two items of tests of line drawing and system integration were executed without connecting to the actual on-line system. Plasma shape is approximated to be a 200-sided polygon of the same size with the plasma. It takes 8.0 ms to draw a 200-sided polygon (40 ms are spent for one vector drawing) using the VGP. Since the cycle time must be less than 33 ms (30 Hz) so as to visualize the shape like a movie, computation of the identification is required to be completed within less than 17 ms (= 33 - 8 x 2 (draw & erase)).

The system integration test were performed using discharge result data of JT-60U. The data is stored in the memory of CPU beforehand. In real time, the CPU reads these data and performs the shape identification. Memory size of 5 Mbytes is allocated for a set of the coefficients table in application of the FCP method to JT-60U. This table covers the region of $R = 2.2 \sim 4.6$ m and $Z = -1.7 \sim +1.7$ m with the precision of 1 cm, and 15 coefficients (1 word = 4 bytes) are memorized for each point. The processing speed of MVME147SC is not high enough to visualize the shape like a movie. It takes about 300 ms to draw the plasma shape at present. Then, improvement of the processing speed and the installation to the actual system are now under development.

References

- [4.3-1] K. Kurihara, Nuclear Fusion 33, No.3 (1993) 399.
- [4.3-2] D. W. Swain and G. H. Neilson, Nucl. Fusion 22 (1982) 1015.
- [4.3-3] K. Kurihara, Fusion Technology 22 (1992) 334.

4.4 Development of new type DC interrupting system

Interrupting high direct current (DC) is one of the key technologies for protecting superconducting magnets from quench phenomenon. The current excited in the superconducting

coils is estimated to be more than several tens of kiloampères. Circuit breakers (CBs) with a capability of breaking current of about 20 kA are commercially available at present. Although the CB which was developed for JT-60 has a capability of interrupting DC of 92 kA, it can pass the current for only 4 s at maximum. On the other hand, although a method to use many circuit breakers (CBs) connected in parallel can be considered for interrupting the high current, it is very difficult to break the CBs simultaneously. Hence, we are developing a new DC interrupting system using a saturable reactor (SR) with an iron core, which commutates the high current from a main bus including the SR to that with a CB.

The system is composed of two parts of main circuit and bias current circuit as shown in Fig. I.4.4-1.

The fundamental functions of the system are as follows:

- (a) The SR is saturated by a bias current (I_b) before the superconducting coil (SC) is excited.
- (b) The current is delivered to the SC by the main power supply (PS) through the saturated SR.
- (c) When the quench occurs, the switch SW_b is closed. At the same time, the bias current supply PS_b begins to reduce the I_b .
- (d) When the current which is passed through the CB_b decreases to almost zero, the CB_b is opened. At the same time, the protecting switch SW_0 and the DCCB are closed.
- (e) Then, the current I_b decreases with a decay time of L_2/R_b , where L_2 is the inductance of the secondary winding of the SR and R_b is the bias resistance.
- (f) When the I_b reaches to a certain low level, the state of the iron core changes from saturation to non-saturation, which makes the impedance of the SR large effectively and generates an inverse voltage on the primary winding of the SR to reduce the current passed through itself.
- (g) As the current passed through the SR primary winding decreases, the main current passed through the DCCB increases. When the current passed through the SR reaches almost zero, the switch SW_1 is opened. Then, the main current I_s is completely commutated to the path with DCCB.
- (h) At last, the DCCB interrupts several tens of kA of the direct current. Then, the current flows in the resistor R and the energy stored in the SC is consumed in the R.

We have examined the new system numerically using the computer code EMTP, and experimentally using a small model. The test results agree well with those of the computer simulation, and it has been proved that the method used in the new interrupting system can be applied to the power supply for super conducting magnets in the next step machines such as ITER.

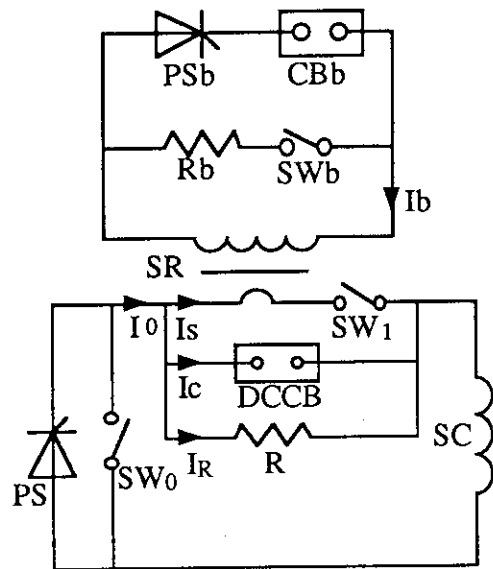


Fig. I.4.4-1 New direct current interrupting system.

4.5 Negative-ion-based neutral beam injection system

The construction of the test facility of the negative-ion-based neutral beam injection system started at the end of this fiscal year. The test facility is composed of an ion source, an ion source tank, an ion source power supply, a power supply building, and an auxiliary system. The test facility will be operational from the summer of 1994. The aim of the test facility is to make the test of the negative ion source and high voltage power supply for the JT-60 negative-ion-based neutral beam injection system (JT-60 N-NBI) shown in Fig. I.4.5-1[4.5-1]. Then the test facility will be a part of the JT-60 N-NBI together with another ion source, a neutralizer tank, an ion dump tank, which will be fabricated later. Plasma heating and current-drive experiments with the JT-60 N-NBI will start in the spring of 1996. The rated power and beam energy of the JT-60 N-NBI are 10 MW and 500 keV, respectively.

Magnetic fields in the JT-60 N-NBI were studied by making the one-tenth scale model of the magnetic shielding and coils. In the JT-60 N-NBI, the stray field from the JT-60U is shielded by high μ materials for the ion sources, the ion source tank, and the neutralizer tank. The residual ion beams after passing through the neutralizers are deflected by the magnetic field induced by a pair of air-core deflecting coils in the ion dump tank. These deflecting coils produce the magnetic field with constant strength under the varying stray field from the JT-60U. The magnetic shields

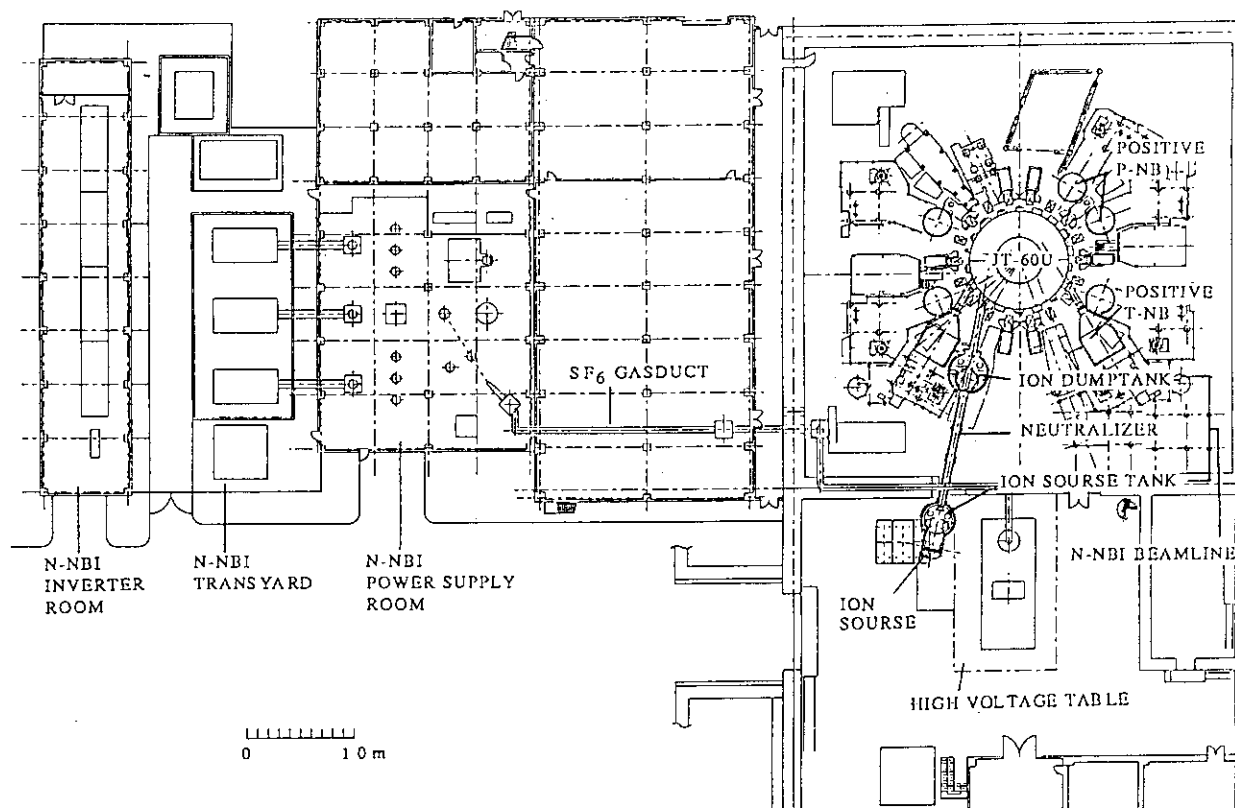


Fig. I.4.5-1 Layout of the negative-ion-based neutral beam injection system for JT-60U.

and the deflecting coils have been designed with 2D and 3D magnetic field analysis codes and a beam orbit code. The purpose of the measurement with the one-tenth model is to check the validity of the calculations.

We observed B-H characteristics are significantly deteriorated while manufacturing the high μ elements as mentioned in [4.5-2]. This effect is unable to include the calculation without measurement. We found the inner shields made of permalloy must be annealed after manufacturing while the outer shields made of SS-400 are unnecessary to be annealed in order to make the inner residual field below an object value of 5×10^{-6} T. The measured fields reasonably agree with the calculations except the deterioration of B-H curve.

References

- [4.5-1] M. Kuriyama et al., Proc. of 14th Symp. on Fusion Engineering, San Diego (1991).
 [4.5-2] J. Kim et al., Proc. of 12th Symp. on Fusion Engineering, Monterey (1987).

4.6 Developments of diagnostics for LHCD launcher

The main issue of the LHCD launcher is to couple slow waves with plasmas effectively. This requirement demands the launcher close to the plasmas. Therefore, the heat load on the launcher head is one of main concerns in operation under such plasma bombardments. On JT-60U, we have equipped a infrared (IRTV) camera to measure the heat load on the launcher head during RF injection. A whole view of the launcher head can be obtained by using two Au coating mirrors through a sapphire window. Figure I.4.6-1 shows the layout of the IRTV camera system. The calibration of the temperature is under operation.

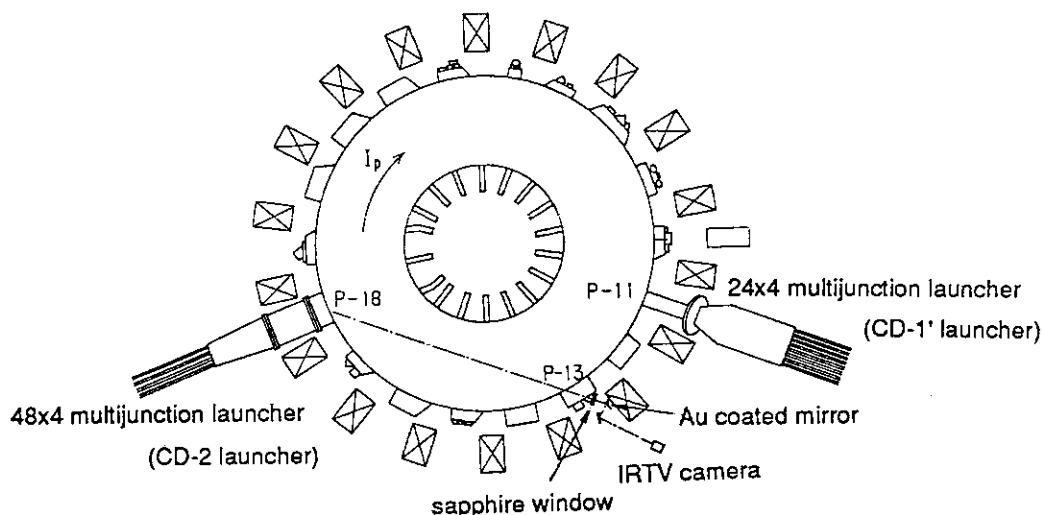


Fig. I.4.6-1 Layout of IRTV camera system for monitoring the heat load on the 48 x 4 multijunction launcher head

An electromagnetic force on the launcher during plasma disruption is one of the main keys to construct the launcher. We have equipped two acceleration monitors on the CD-2 launcher to investigate the electromagnetic force. The feasibility of the monitor is under testing.

II. JFT-2M PROGRAM

1. Toroidal Confinement Experiments

1.1 Overview

The main progress in JFT-2M program is summarized. For JFY1992, intensive divertor biasing and ergodic magnetic limiter experiments have been continued in order to investigate modification of transport properties in scrape-off layer plasmas and MHD characteristics especially with much emphasis on ($m=2/n=1$) activities. The other major efforts are put on disruption control by electron cyclotron resonance heating of ($m=2/n=1$) magnetic islands. The continuous heating of $q=2$ surface has been found to suppress ($m=2/n=1$) fluctuations and lead to disruption avoidance since last fiscal year in JFT-2M. For the present period, disruption control with feedback modulation of ECH power through magnetic probe signals has been studied extensively.

1.2 Experimental results

1.2.1 Experimental results with ergodic magnetic limiter

In JFT-2M, three types of coils are mounted outside and inside on the vacuum vessel; Ergodic Magnetic Limiter Coils which are referred simply as EML type coils, Ergodic Magnetic Limiter Coils referred as Ladder type coils, and Disruption Control Coils referred as Saddle type coils(see Fig.II.1.2-1). These sets of coils produce magnetic perturbations of broad spectra of various helicities for systematic study of plasma response to externally applied magnetic field.

1) Stationary H-mode

Plasma density and radiation loss increase continuously in an edge localized mode (ELM) -free H-mode, even without gas input. This plasma density rise was found to be suppressed by ELMs during H-mode induced by application of ergodic magnetic fields produced by EML ($m=10-16/n=\text{even}$)coils. In order to find out the helical components which effectively induce the ELMs, their repetition rates in different ergodic field coil operations have been compared. The repetition rate is high when the field of

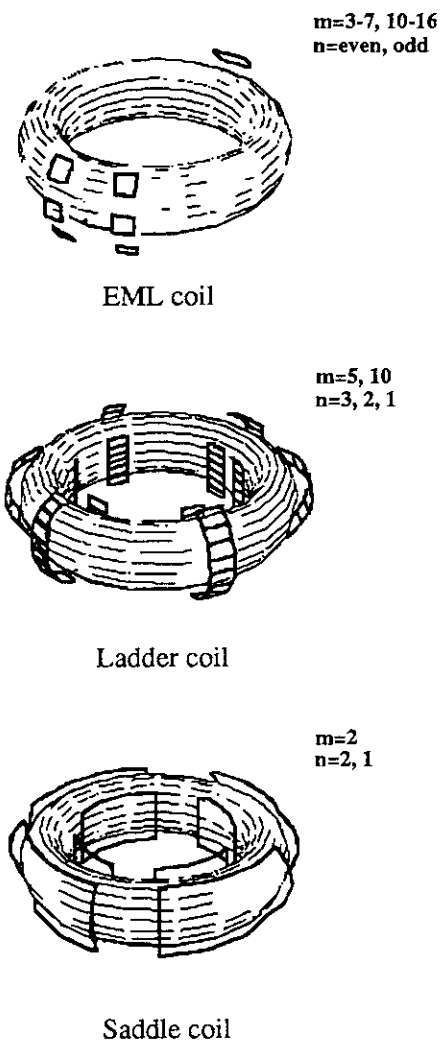


Fig.II.1.2-1 Ergodic Magnetic Limiter and Disruption Control Coils on JFT-2M

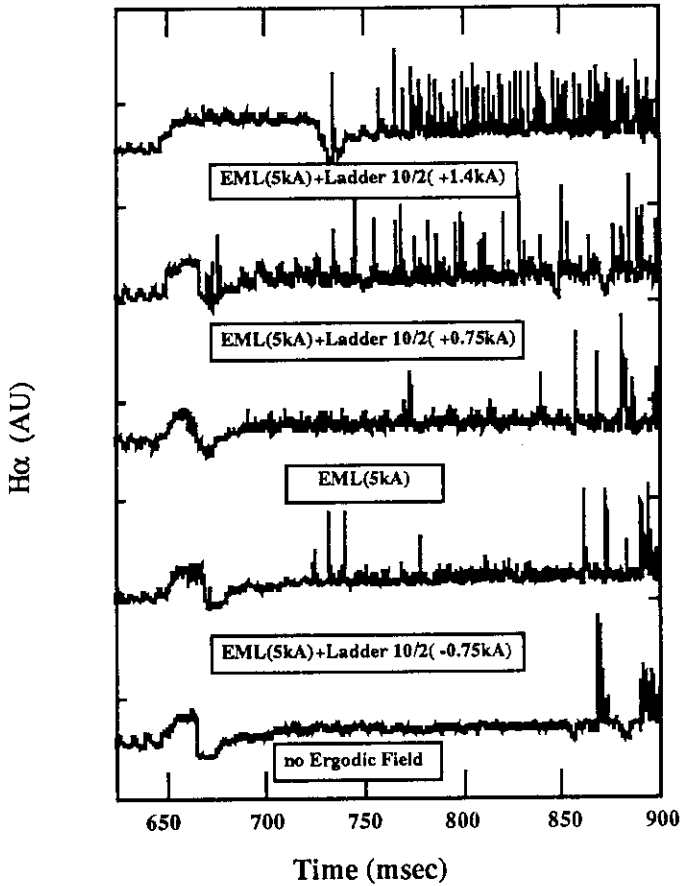


Fig.II.1.2-2 Variation of ELM Activities vs. Helical Perturbation

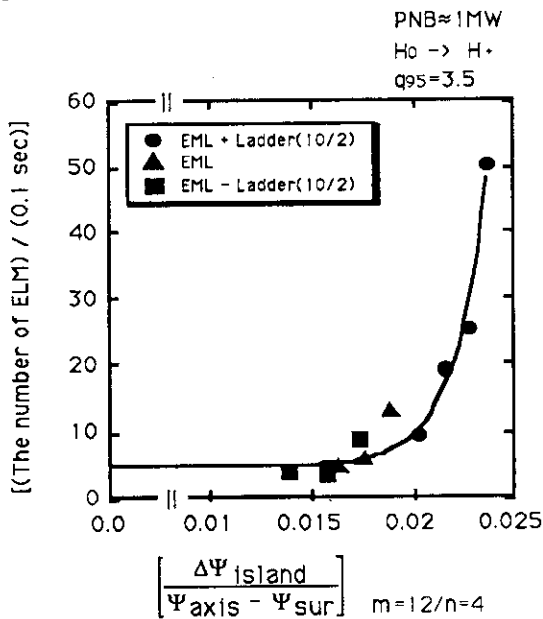


Fig.II.1.2-3 ELM Frequency vs. Island Width

the positive current in the Ladder ($m=10/n=2$) coils is added to the field of the EML ($m=10-16/n=even$) coils and is almost zero when a field of the negative current in the Ladder coils is added. Fig.II.1.2-2 shows the variation of the repetition rate with various combination of ergodic magnetic fields operations. The repetition rate of ELMs is found to be an increasing function of the ($m=16/n=4$) magnetic island width estimated from analysis of the ergodic magnetic field, as shown in Fig.II. 1.2-3. Unfortunately, same dependence is obtained from the analysis for the $m=12-20$ islands with the n -value of 4, and this means that the ($m=12-20/n=4$) helical field is one of the possible candidates for the effective field inducing ELMs.

These islands are produced on the $q=3-5$

surfaces close to the separatrix. No obvious correlation between the repetition rate and the island width at a low n -value ($n=1,2$ or 3). In conclusion, the ELMs are considered to be induced by the $n=4$ and high m ($m=12-20$) helical fields whose resonant surfaces are close to the separatrix.

2) Locked mode suppression

Plasma disruptions can be caused by the ($m=2/n=1$) locked modes during the current ramp-up phase. It has been found in JFT-2M that the application of an ergodic magnetic field can suppress this type of MHD activities. We have examined the case in which the plasma disruption occurs at 400ms because of an MHD instability

that begins to grow when surface safety factor q reaches around 4. The MHD activities have an ($m=4/n=1$) helical structure at the beginning of this instability but change to ($m=2/n=1$) at an early

stage. Following the structural change, the frequency decreases gradually from about 5 kHz with increasing amplitude. When the frequency reaches about zero and the fluctuating magnetic fields reaches about 30 G, the plasma disrupts. This type of instability is suppressed by the application of helical magnetic fields of Saddle ($m=2/n=1$) coils and as a result the disruption is avoided. EML ($m=10-16/n=\text{odd}$) coils have also the same stabilizing effect. From the analysis of the Fourier components of the applied fields, ($m=2/n=1$) field is

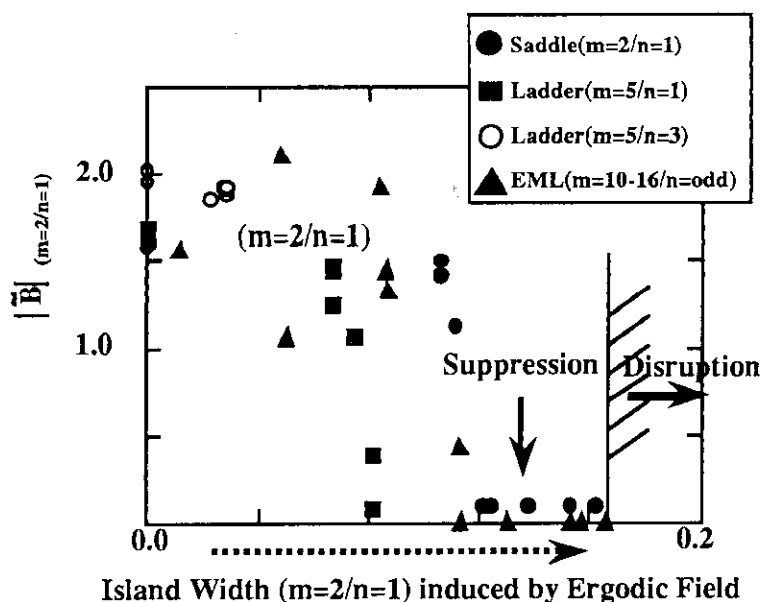


Fig.II.1.2-4 Suppression of ($m=2/n=1$) Helical Instabilities

considered to suppress the present instability, however, we can not exclude the possibility of the ($m=3/n=1$) component for the effective field from the present experiments. Fig.II.1.2-4 shows the relation between the amplitude of ($m=2/n=1$) magnetic fluctuation and the island width of ($m=2/n=1$) helical component induced by externally applied ergodic magnetic fields with various combination of coil operations.

1.2.2 Experimental results with divertor biasing

Divertor biasing experiments on JFT-2M have been performed in order to modify the tokamak boundaries and understand the L/H transition physics. It has been found on JFT-2M that the threshold power for L/H transition is reduced from 340kW to 140kW by a unipolar negative divertor biasing. In the present reporting period, the modifications in this case occurred in the scrape-off-layer (SOL) have been clarified by extensively using a movable Langmuir probe array biased in triple probe configurations. Radial profiles of floating potential, electron density, and electron temperature in SOL have been measured in detail and the flow velocity was derived from the ion saturation current collected on opposite side of another rotating probe. The measurements have shown that a negative potential gradient is produced 2 cm outside the separatrix during the L-mode phase by a unipolar negative divertor biasing. At the same position, a steep density gradient is formed; a shear-flow is created corresponding to a strong localised electric field of -110V/cm; density fluctuations are suppressed at frequencies less than

100kHz at the shear flow region. The clarification of SOL modifications with a unipolar negative divertor biasing has made a progress extensively, nevertheless, the reduction of the threshold power for L/H transition is still an open question.

1.2.3 Experimental results with electron cyclotron resonance heating

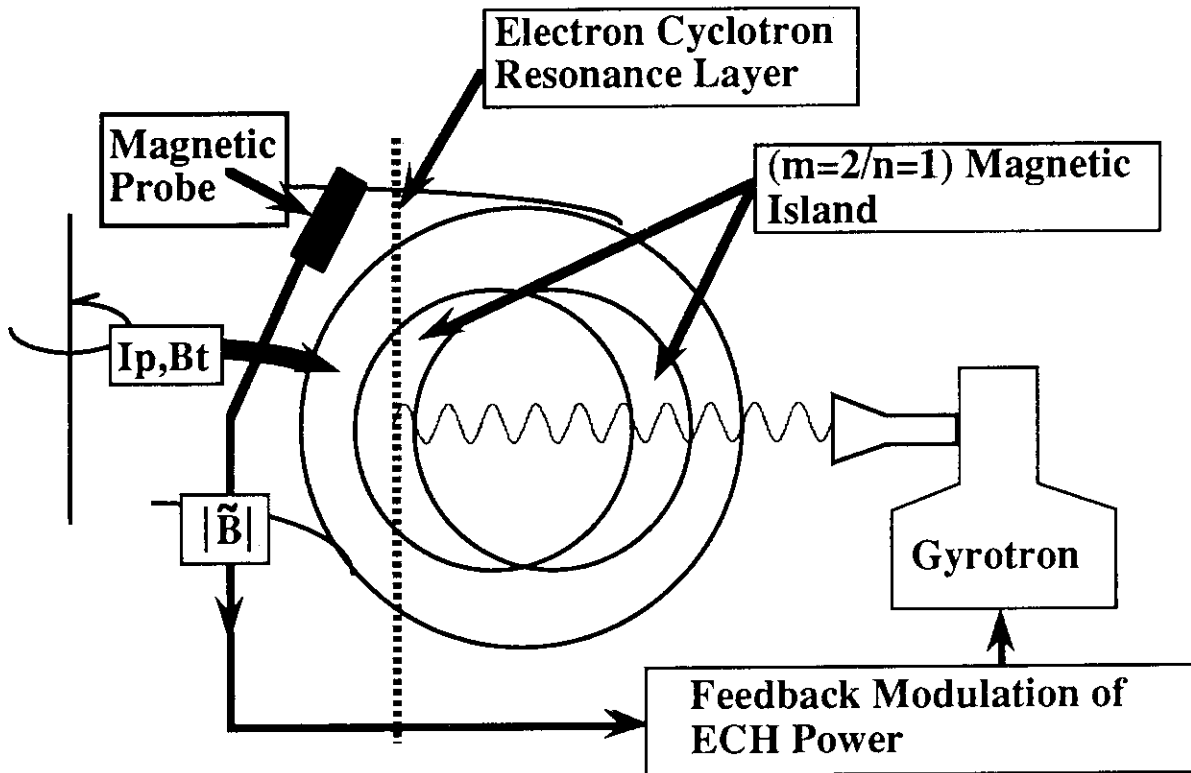


Fig.II.1.2-5 Schematic Drawings of Feedback Stabilization of $(m=2/n=1)$ Magnetic Island Using Electron Cyclotron Resonance Heating on $q=2$ Surface

In the limiter discharges with circular plasma cross section, the Mirnov oscillations which appear at the surface safety factor $q=3$ lead to the plasma disruption when the line-average plasma density is in the region of $1.1 \times 10^{19} \text{m}^{-3} < \bar{n}_e < 2.5 \times 10^{19} \text{m}^{-3}$, with constant plasma current. When the plasma density is below this density region, this MHD activity stays stationary with constant amplitude and constant frequency. This mode has a helicity of $(m=2/n=1)$ and grows as the density is raised. The plasma disrupts when the density is increased to be larger than $\bar{n}_e = 1.1 \times 10^{19} \text{m}^{-3}$. It has been found on JFT-2M that these disruptions at surface safety factor $q=3$ is avoided by local off-central (resonance layer location $r/a=0.70$) electron heating by ECH (frequency 59.8 GHz, second harmonic extraordinary mode). For the suppression, the electron cyclotron resonance layer has to be placed radially in a very narrow region of which about 1 cm near the $q=2$ surface. Both low-field side heating and high-field side heating are effective for the suppression. Fourier spectrum of the magnetic fluctuations shows that mode amplitude decreases

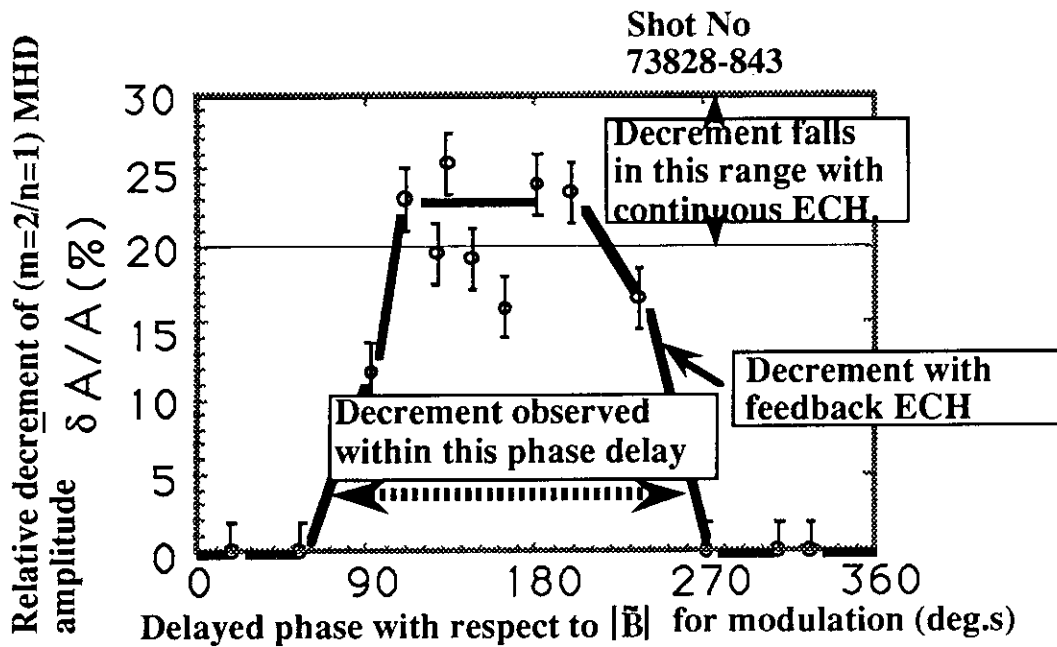


Fig.II.1.2-6 Suppression of (m=2/n=1) Magnetic Island Through O-point ECH

by ECH and disruption is avoided. Without ECH, the mode frequency decreases (mode locking) and disruption occurs. In the reporting period, pulse feedback modulation of the ECH power by a magnetic pickup signal has been performed in order to clarify whether O-point or X-point heating of (m=2/n=1) island is effective for the suppression. Fig.II.1.2-5 shows a schematic scheme of the

experiments. To see that ECH of $r/a=0.70$ acts on the m=2 island, ECH power is modulated using poloidal magnetic probe signal as reference. Experiments have been performed with the electron cyclotron layer at $r/a=-0.70$ (high field side). Firstly it has been reconfirmed that continuous ECH decreases the amplitude of the (m=2/n=1) mode. Secondly ECH power is modulated to produce pulse trains. Pulse width of a single ECH pulse is 0.1ms (10kHz, 100% modulation) and the phase delay of the modulated ECH pulse trains with respect to the probe signal can be changed from 0 deg. to 360 deg.s throughout the experiments. Suppression of the (m=2/n=1) mode is observed when the phase delay is in a particular region of angle width of 180 deg.s. In the other region of the phase delay, no suppression is observed (see Fig.II.1.2-6). From the probe analysis the O-point heating of the magnetic (m=2/n=1) island is found to be effective for the suppression, however, the X-point heating is found to be ineffective for the suppression. With ECH on the (m=2/n=1) island, amplitude of the mode decreases and the mode locking and successive disruption are avoided. It is noted that decrement of the (m=2/n=1) mode amplitude is almost the same for continuous ECH pulse; 20-30%, and for modulated ECH pulses; 15-26%. The peak power is the same; $P=92\text{kW}$, in both cases, while the average power of the modulated ECH case is only 45kW to suppress the mode effectively. The suppression of the (m=2/n=1) mode depends on the peaked power of the ECH short pulses rather than on the average power.

2. Operation and Maintenance

2.1 Introduction

The JFT-2M tokamak has been operated from 1983 in cooperation with two laboratories (Experimental plasma physics lab. and JFT-2M facility div.). The main duty of JFT-2M facility div. is to operate the facility smoothly and to develop new equipments necessary for experiments. The JFT-2M experimental plan and operation schedule are arranged every week at the group leader meeting. In this fiscal year, each apparatus was operated smoothly according to the experimental plan, and the careful examination of machine status was carried out daily and periodically. As for the development study of equipment, a boronization system based on the RF sputtering of titanium was installed.

2.2 Operation and maintenance

The summary of operation records for the main apparatuses is listed in Table II.2.2-1. The main apparatuses such as the flywheel motor-generator (MG), JFT-2M machine, neutral beam injection system (NBI), electron cyclotron heating system (ECH) and fast wave current drive system (FW) have been operated smoothly according to the experimental schedule. Air vent of the vacuum vessel to install new diagnostics and to repair in-vessel equipments were carried out three

Table II.2.2-1 Summary of operation records for main apparatus

		FY 1991	FY 1992				
			Apr-Jun	Jul-Sep	Oct-Dec	Jan-Mar	total
MG	#1MG (hour)	716	279	307	222	228	1,036
	#2MG (hour)	715	278	307	224	228	1,037
JFT-2M	Shot number (shot)	3,920	1,547	1,716	982	1,084	5,329
	TDC (hour)	152	65	72	60	55	252
	Baking (times)	2	0	1	1	1	3
	Pellet injection (day)	0	0	0	0	0	0
NBI	Operation (day)	59	24	27	12	7	70
	A-line Injection(times)	13,531	5,124	7,016	2,905	1,639	16,684
	B-line Injection(times)	12,509	6,340	10,746	4,060	1,656	22,802
ECH	Operation (day)	17	0	0	0	19	19
	Injection (times)	11,783	0	0	0	23,610	23,610
FW	Operation (day)	35	0	2	13	17	32
	Injection (hour)	259	0	7	107	142	256

times and wall conditioning (baking and TDC) followed. During the machine stop phase, necessary checks and regular examinations of the apparatuses were carried out by the help of industries.

2.3 Development of equipments and instruments

In collaboration with the experimental plasma physics lab., R & D studies have been carried out as follows. As for the divertor biasing system and the ergodic magnetic limiter system, electric insulation against arcing, plasma sputtering and deposition of sputtered materials was improved by using alumina coated covers and alumina bolts and by changing insulators from Teflon to Kapton. In particular, careful protection for plasma coating was made in the hidden side against plasma. As for the wall conditioning, the modification of the titanium RF sputtering system has been completed to use as a boron coating system. The merit of this method seems to be safe from diboran gas and to be a short operation time of about half an hour. The quality of boron coating will be checked in the next operation phase. As for the development of diagnostic neutral beam, fairly well beam characteristics were obtained such as a beam current of 5 A, a beam divergence of 1.0 degree and a peak power density of 3.0 kW/cm². The final test combined with a charge-exchange recombination diagnostics is now in preparation.

III. PLASMA THEORY AND COMPUTATION

1. Introduction

During FY1992 the theoretical and computational works were carried out extensively by putting emphases on the following problems.

As for the confinement theory scaling laws of the thermal energy confinement and the bootstrap current in finite aspect ratio tokamaks were derived. The ion temperature gradient instability was studied both numerically and analytically, especially from the viewpoint of the self-organized profile relaxation. In relation with the plasma heating analyses of a beam orbit in a focusing wiggler of an FEL were carried out. Concerning the MHD studies stability analyses of low aspect ratio tokamak plasma were carried out. In relation with the disruption phenomena rotation damping by external error field and the effect of viscosity on the sawtooth crash were studied by both analytic method and numerical simulations. As for the burning plasma analyses enhancement of the D-³He fusion by combined use of the NBI and the ICRF heatings was calculated and effects of radio-frequency-induced radial diffusion on triton burn-up was investigated. Some MHD codes were developed to be used as necessary components of the analysis system of the non-ideal MHD instabilities. The computational efficiency of the TSC code was improved and the MHD simulation code based on a toroidally incompressible plasma model was developed. In preparation for the future large scale computer simulation parallelization of a three dimensional particle simulation code was investigated.

2. Analyses of Confinement and Heating Processes

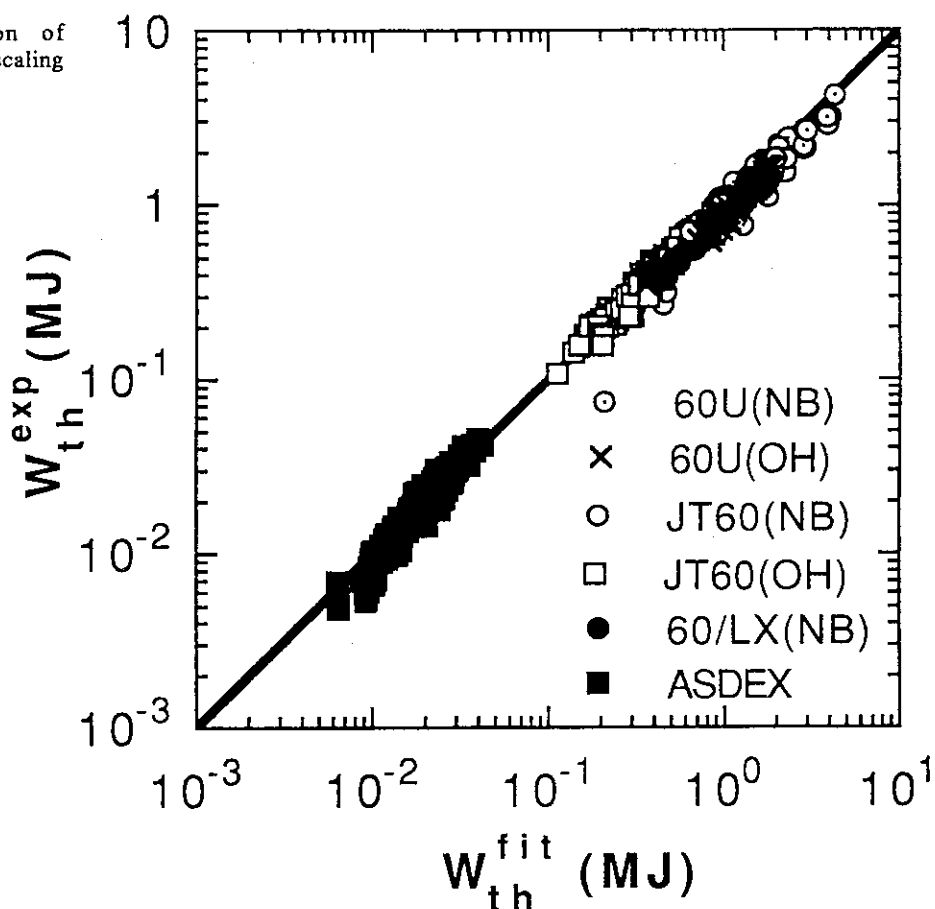
2.1 Confinement scaling of thermal energy

A scaling of thermal energy in JT-60 L-mode plasmas was given as $W_{th} = C (I_p B_t \bar{n}_e)^{1/2} P^{1/3}$ [2.1-1]. The dependence on B_t is uncertain because of small variable range of the B_t value in the database. Since the effective thermal diffusivity χ_{eff} experimentally obtained around the two third of the minor radius a is related to the thermal energy confinement time as $\tau_{th} = a^2 / 4\chi_{eff}$, we assume the form of $\chi_{eff} \propto (T/eB_t) (\rho_L/a)^\mu \beta^x (v/v_b)^y$, where ρ_L is the Larmor radius, v is the collision frequency and v_b is the bounce frequency. Fixing the power for I_p , \bar{n}_e , and P in W_{th} , the powers for B_t and for the size L become $(5+4\mu)/18$ and $(40+5\mu)/18$, respectively. Analysis of the data of JT-60 with the original and the lower x-point configurations, JT-60U, and of ASDEX gives the following scaling of thermal energy through ohmic confinement and L-mode confinement,

$$W_{th} = C M^{0.15+0.3\mu} \kappa^{1.10-0.45\mu} R^{1.07+0.73\mu} a^{1.15-0.45\mu} I_p^{1/2} \bar{n}_e^{1/2} B_t^{(5+4\mu)/18} P^{1/3},$$

where $C = 0.047 e^{-1.2\mu}$, W is in MJ, M is the ion mass number, κ the elongation, R in m, a in m, I_p in MA, \bar{n}_e in $10^{19}m^{-3}$, B_t in T, and P in MW. Experimental data are fitted well by this scaling as shown in Fig. III.2.1-1.

Fig.III.2.1-1 Comparison of experimental data with the scaling of W_{th} ($\mu=0.5$).



Reference

[2.1-1] T. Takizuka, Proc. 1992 ICPP (Innsbruck, 1992) Part I, 51.

2.2 Scaling of bootstrap current in finite aspect ratio tokamak

The bootstrap current will be utilized to reduce the current drive power in steady state tokamak reactors. A scaling of the bootstrap current fraction I_{bs}/I_p in large aspect ratio tokamak was given [2.2-1]. The finite aspect ratio changes the value of I_{bs}/I_p significantly and it is required to establish a new scaling for designing tokamak reactors with the finite aspect ratio. The coefficients L for the pressure and temperature gradients in the bootstrap current density $J_{bs} \propto L_1 d\ln P/d\rho + L_2 d\ln T/d\rho$ given by Hirshman [2.2-2] are expressed approximately as a function of local inverse aspect ratio ϵ_ρ of the form of $L \propto \epsilon_\rho^{0.5} (1 - c \epsilon_\rho^{0.4})$. On the basis of this approximation, a scaling of I_{bs}/I_p in the finite aspect ratio tokamaks is given as follows,

$$I_{bs}/I_p = \epsilon^{0.5} \beta_p \{ 1.15 (1 - 0.92 \alpha_T / \alpha_p) F - 0.68 \epsilon^{0.4} (1 - 1.79 \alpha_T / \alpha_p) G \},$$

where F and G are the simple functions of α_p and α_J . Radial profiles of temperature (T), pressure (P) and current density (J) are assumed to be $(1 - \rho^2)^\alpha$. This scaling fits well the numerical results given by ACCOME code [2.2-3] within the error of a few %.

References

[2.2-1] N. Fujisawa and T. Takizuka, JAERI-M 92-064 (1992).

[2.2-2] S.P. Hirshman, Phys. Fluids 31 (1988) 3150.

[2.2-3] K. Tani et al., J. Comput. Phys. 98 (1992) 332.

2.3 Self-organized profile relaxation by ion temperature gradient instability in toroidal plasma[2.3-1,2]

By using the toroidal particle code (TPC) the anomalous heat transport by ion temperature gradient mode was investigated computationally and analytically. The simulation by the TPC code shows strong excitation of radially extended global mode localized to the outside of the torus. The time evolution of the potential on a cross section of the torus is shown in Fig.II.2.3-1 at three time steps. It was found that by the global mode the temperature profile rapidly relaxes to that of the exponential function, $T_i(r) \sim \exp(-\kappa_T r)$, in the case of the ITG mode with flat density profile and the heat flux becomes radially independent. The profile continues to relax toward a critical state slightly above the marginal stability with the functional form of the profile unchanged. Such a self-organized relaxed state was found to provide the radially increasing heat conductivity χ_i which is consistent with the simulation result. These results were obtained by linear and quasi-linear kinetic theory. A relaxation theory based on the reductive perturbation theory in the quasi-linear equation was also developed.

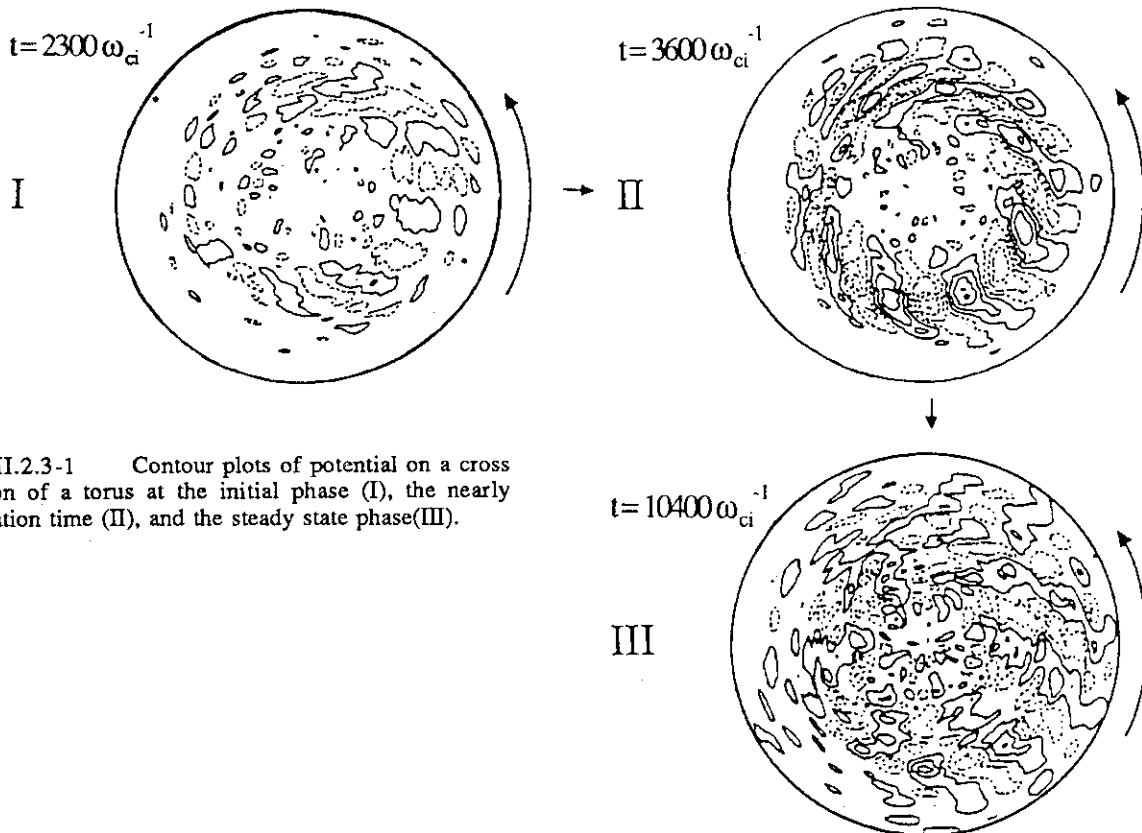


Fig.III.2.3-1 Contour plots of potential on a cross section of a torus at the initial phase (I), the nearly saturation time (II), and the steady state phase(III).

References

- [2.3-1] Y. Kishimoto, T. Tajima, M.J. LeBrun et al. IFSR #589.
 [2.3-2] T. Tajima, Y. Kishimoto, M.J. LeBrun et al., Proc. US-Japan Workshop on Ion Temperature Gradient Driven Turbulent Transport (Austin, 1993).

2.4 Linear dispersion analysis of toroidal ion temperature gradient mode in entire complex frequency plane

The kinetic dispersion analysis in a toroidal geometry has been done to analyze the mode behavior of the ion temperature gradient instability near the marginal stability which is especially important in the transient problem like a stable/unstable boundary crossing of the plasma profile. The damping problem by the resonance and phase mixing in the system where the toroidal magnetic drift resonance and Landau resonance simultaneously exist was studied. In order to obtain the explicit form of the dispersion relation which is analytically continued to $\text{Im}\omega < 0$, we originally developed the coordinate transformation method of the independent variables in velocity space so that the resonance line becomes straight. In the analysis, we found that the heat flux is sustained even if at $\text{Im}\omega = 0$ due to the kinetic contribution which comes from the resonant pole and play an important role on the heat transport at the marginal state [2.4-1].

Reference

- [2.4-1] Y. Kishimoto, T. Tajima, M.J. LeBrun et al. IFSR #589.

2.5 Beam orbit analysis in focusing wiggler by using non-canonical perturbation method

In a free electron laser with long wiggler, an additional focusing field is required to keep the electron beam from divergence. However, the large scale transverse motion induced by the arbitrary focusing field modulates the longitudinal electron motion and sometimes breaks the phase relation between electron and radiation field. Here, we employ the systematic perturbation method [2.5-1] to investigate the delicate phase relation in the wiggler with the focusing field. In the problem, coordinate transformations by using non-canonical variables are successively repeated so that the electron orbit is exactly solved up to an arbitrary order of a smallness parameter $\epsilon \equiv r_b/\lambda_w$ where r_b is beam radius and λ_w is wiggler pitch. As examples, we applied the method to a case of parabolically curved self-focusing magnet [2.5-2] as well as a case of current-wire quadrupole focusing. It is found that the self-focusing magnet maintains the axial phase relation constant up to order ϵ^7 although the quadrupole magnet breaks up the relation at order ϵ^6 . The effect of the radial space charge field on the phase relation and the beam current limitation is also investigated.

References

- [2.5-1] J.R. Cary and R.G. Littlejohn, Annals of Physics **151** (1983) 1.
 [2.5-2] K. Sakamoto, T. Kobayashi, Y. Kishimoto et al., Phys. Rev. Lett. **70** (1993) 441.

3. MHD Equilibrium and Stability Analyses

3.1 Stability analysis of small aspect ratio tokamak [3.1-1]

Aspect ratio (A) dependence of critical beta for an ideal MHD ballooning mode and available bootstrap current has been studied to clarify the MHD stability properties of a small aspect ratio tokamak. In the studies the marginal pressure profile was computed for the specified surface averaged current profile. In comparison with large aspect ratio tokamaks a small aspect ratio tokamak shows stronger shaping effects on critical beta and it becomes greater than 10 % for $\kappa = 1.6$ and $\delta = 0.3$ for the TBR-2E (aspect ratio $A = 1.5$) device parameters (κ : ellipticity, δ : triangularity).

The bootstrap current increases with increasing κ but saturates because of decrease in critical beta. The available bootstrap current for the small aspect ratio tokamak is 20 - 30 % which is comparable for the conventional tokamaks such as ITER, whereas the bootstrap current for the tokamak with $A = 5$ can be 60%.

Reference

- [3.1-1] S. Tokuda, P.H. Sakanaka, and H. Shigueoka, "MHD stability study of a small aspect ratio tokamak," US-Japan Workshop on the Theory of High b Plasmas, Nov. 11-13, 1992, San Diego, California.

3.2 Rotation damping by external error field

Linear response of rotating plasma on a resonant helical field is examined for a small amplitude limit. Current layer width and frictional force are estimated. At low frequency region, an external helical field penetrates freely into the plasma and a frictional force increases with frequency rise. Current excited by magnetic perturbation shields the external helical field when its frequency is raised and the frictional torque has its maximum value at certain frequency. The value of the maximum torque does not depend on resistivity if the coil current is fixed.

3.3 Effect of electron and ion viscosity on sawtooth crash in tokamak [3.4-1]

Effect of anomalous electron and ion viscosity induced by the stochastization of magnetic field line on sawtooth crash in a tokamak was investigated by using the reduced set of resistive MHD equations. As the perturbation grows beyond some amplitude, the most unstable mode is turned from the pure resistive mode into the one induced by the anomalous electron viscosity, and the growth rate suddenly increases, as observed in some experiments. After that the growth of perturbation is decreased due to the anomalous ion viscosity. The sawtooth crash time is prolonged in spite of the explosive growth due to the electron viscosity. However, it is not completely suppressed by the effect of anomalous ion viscosity.

Reference

- [3.4-1] G. Kurita, M. Azumi, and T. Tuda, J. Phys. Soc. Jpn. **62** (1993) 524.

4. Analyses of Burning Plasma in Tokamaks

4.1 Study of combined NBI and ICRF enhancement of D-³He fusion yield with Fokker-Planck code [4.1-1]

A two-dimensional bounce average Fokker-Planck code has been used to study the fusion yield and the wave absorption by residual hydrogen ions in higher harmonic ICRF heating of D and ³He beams in the JT-60U tokamak. Both for fourth harmonic heating of ³He beams in the D(³He) regime and of D beams in the ³He(D) regime, a few percent of hydrogen ions can deteriorate the fusion yield markedly. As the beam power to be injected and the fusion yield are sensitively dependent on the background thermal ion concentration, the lower n_e and higher T_e case is not favorable for the fusion yield enhancement at least in the low hydrogen concentration. It has also been found that the attainable fusion yield increases with the cyclotron harmonic number at or near the plasma center.

Reference

[4.1-1] M. Yamagiwa et al., Nucl. Fusion 33 (1993) 493.

4.2 Effects of radio-frequency-induced radial diffusion on triton burn-up [4.2-1]

Effects of radio-frequency(rf)-induced radial diffusion on triton burn-up have been studied for D(³He) plasmas with ion cyclotron range of frequencies heating in the fundamental minority regime. The triton distribution is determined from a Fokker-Planck equation including a radial diffusion term. Provided that the rf power is extremely localized in the plasma center, tritons are driven out from the center because of rf-induced diffusion in the second harmonic resonance and the emission profile of the 14-MeV neutrons due to D-T reactions can possibly be flattened appreciably. This may lead to verification of rf-induced radial diffusion of the ions only through neutron detection.

Reference

[4.2-1] M. Yamagiwa, US-Japan Joint Workshop on Ion Orbit Losses in Toroidal Systems, National Institute of Fusion Science, December 1-4, 1992.

5. Development of Numerical Codes and Plasma Simulator

5.1 Finite element calculation of outer region matching data [5.1-1]

A code has been developed to calculate outer region matching data of an ordinary differential equation with regular singular points by finite element method. Matching data play a central role in nonideal MHD stability analysis for a magnetically confined plasma by asymptotic matching method. In the code the Frobenius series for the big solution, the fundamental solution which is not square-integrable at the regular singular point, is prescribed. Numerical experiments

has been carried out for model equations including studies of the convergent rate of the matching data and of the effect on the data by truncating the Frobenius series at finite terms. It is shown from the experiments that the finite element method is an effective method for obtaining the matching data with high accuracy as long as the sufficient number of terms of the Frobenius series for the big solution are taken.

Reference

[5.1-1] S. Tokuda, T. Kumakura, and K. Yoshimura, JAERI-M 93-075 (1993).

5.2 Development of inverse equilibrium solver

Solution method has been formulated for the inverse equilibrium equation for computation of the big solutions and outer region matching data of a tokamak plasma in two-dimensional toroidal configuration. In the solver the solution of the Grad-Shafranov equation is expressed in the form of

$$r = r(s, \theta) = \Delta(s) + \rho(s) \cos \theta + \sum_{m=2}^M Rm(s) \cos m\theta, \quad z = z(s, \theta) = \kappa(s) \sin \theta + \sum_{m=2}^M Zm(s) \sin m\theta.$$

The poloidal angle θ is defined by the constraint that the Jacobian is independent on the poloidal angle. Equations for Δ , ρ , κ , Rm and Zm are obtained by truncating the Grad-Shafranov equation at finite terms of the Fourier series, and are expressed in a matrix form. The matrix elements are obtained by using REDUCE, a formula manipulation language. The equations are solved either as a initial value problem or as a boundary value problem.

5.3 Improvement of TSC code

A large amount of CPU time is needed to execute the TSC code (tokamak simulation code) which is useful to analyze the time-evolution of axisymmetric and deformable plasma motion, [3.2-1]. For practical use of TSC in designing a fusion reactor as ITER, especially, many grid points in the R - Z space are required to express a complicated wall configuration and the necessary CPU time becomes quite large. During FY1992 main effort was directed to improve the simulation speed as follows. (1) DFT (Discrete Fourier Transform) algorithm in the FACR (Fourier Analysis and Cyclic Reduction) routine for solving an elliptic partial differential equation was replaced by the FFT (Fast Fourier Transform) algorithm. (2) Subroutine to calculate the flux surface quantities was vectorized. The new FACR routine was tested for the analytic solution $\Psi(R, Z)$ and the corresponding source term of Grad-Shafranov equation and the almost same accuracy was attained in comparison with the result of the original version. The CPU cost reductions were evaluated as $\sim 1/10$ for both the FACR routine and the integrating routine. In total the CPU speed in typical TSC run becomes three times faster.

Reference

[3.2-1] Y. Nakamura, T. Nishino, T. Tsunematsu, M. Sugihara, JAERI-M 92-189 (1992).

5.4 MHD simulation code based on toroidally incompressible plasma model [5.4-1]

Three dimensional toroidal MHD code "AEOLUS-IT" has been developed, on a basis of a new reduced set of resistive MHD equations with the assumption of toroidal incompressibility instead of the tokamak ordering in the conventional reduced set of resistive MHD equations.

The code can carry out an overall MHD calculation with the effect of finite plasma resistivity, linear and non-linear, of low aspect ratio and low-q tokamak because the basic equations include the ideal $m=1$ mode. The implicit time integration scheme for the linear term of the perturbation is employed, dividing the variables into the equilibrium and perturbation parts. The huge CPU time due to solution of the large matrix can be reduced by high efficiency of vectorization.

Reference

[5.4-1] G. Kurita, M. Azumi, and T. Takeda, JAERI-M 93-004 (1993).

5.5 Parallel processing of particle simulation codes

In order to realize a high performance computation on a parallel computer to carry out a large scale simulation efficiently issues concerning the parallel processing are being investigated. For this purpose a three-dimensional particle simulation code was analyzed from the viewpoint of the parallel algorithm and it was reconstructed for the use on a parallel computer.

IV. COOPERATIVE PROGRAM ON DIII-D (Doublet III) EXPERIMENT

1. Introduction

The DIII-D long range research program focuses on divertor and advanced tokamak issues. The goal is to provide an integrated demonstration of well-confined high-beta divertor plasma with non-inductive current drive.

During the past year several device improvements were made to DIII-D including:

- # Installation of complete graphite interior walls.
- # Installation of a cryogenic pump in the advanced divertor.
- # Installation of a multiple feed boronization system.
- # Installation of slanted fast wave current drive antenna Faraday shield.
- # Installation of new diagnostic systems: (a) Lithium beam emission spectroscopy, (b) Divertor spectrometer and new bolometers, (c) Improvements to the multi-pulse Thomson scattering system.

The experimental program on DIII-D made significant progress during the last year. New data advanced the physics understanding of the divertor and the improved confinement regimes (VH-mode and high-inductance H-mode), including experiments in which the "n=1" coil was used to modify the radial profile of rotation to test theoretical concept of the origin of the VH-mode. The new real-time digital control system for the tokamak made new types of experiments possible, for example those in which the neutral beam heating power was controlled by feed back to generate long period of VH-mode. Currents driven by fast waves were clearly identified. New results on toroidal Alfvén eigenmode (TAE) indicating the importance of current profile control were obtained. Configurations were found in which a large fraction of the total input power was radiated in the divertor region. The effective removal of helium from the plasma by ELMs was demonstrated. New diagnostics in the divertor region have provided data which have advanced the modeling of the physics of divertors. These DIII-D results have been highly beneficial to the planning of the JT-60U experimental program emphasizing fusion parameters. DIII-D contributions to the high performance JT-60U plasmas, based on the experiences of wall conditioning including boronization, are specifically noted.

2. Highlights of FY1992 Research Results

The observed characteristics of toroidicity-induced Alfvén eigenmodes in DIII-D tokamak discharges are compared in detail with predictions of various theories of TAE mode stability, and good qualitative agreement is found [IV-1]. The observed range of unstable toroidal mode numbers ($n \sim 3-6$) is consistent with theoretical predictions. For DIII-D parameters, low mode numbers are damped by coupling to the stable Alfvén continuum, while high mode numbers are damped by electron kinetic effects including coupling to kinetic Alfvén waves. A threshold for destabilization is observed experimentally at a fast ion beta of approximately 1%. The predicted

driving and damping rates, estimated from experimental data, balance within about a factor of 2 for discharges at the threshold. It is demonstrated experimentally that the damping of TAE modes can be increased by current profile control, in this case with a peaked current profile produced by a negative current ramp, in qualitative agreement with theoretical predictions. A possible stabilizing effect of discharge elongation is also observed.

A regime of improved H-mode energy confinement, VH-mode, was obtained following boronization of the DIII-D tokamak vacuum vessel. The improved confinement in VH-mode is consistent with the extension of the region of high $E \times B$ velocity shear further in from the Plasma boundary, resulting in a larger region of turbulence suppression. The inward penetration of the $E \times B$ velocity shear is due primarily to changes in the toroidal profile. The disappearance of periodic momentum transfer events, MTEs, associated with density fluctuations may be the cause of the $E \times B$ velocity shear penetration in high confinement VH-mode discharges. Two alternative models for the confinement improvement in VH-mode are also considered: the expansion of the region with access to the second stable regime for ideal ballooning modes, and the expansion of the region with toroidal drift reversal stabilization of trapped particle modes. Both of these models are less consistent with the experimental observations than the $E \times B$ velocity shear model [IV-2]. Figure IV.2-1 shows the change in the profiles of radial electric field, E_r , $E \times B$ velocity shear, and effective thermal diffusivity, c_{EFF} , during a VH-mode discharge. The $E \times B$ velocity shear is increased in the region where the greatest reduction in c_{EFF} is computed. Also shown is the $E \times B$ velocity shear required for turbulence suppression based on turbulence measurements in the DIII-D L-mode edge using Biglari, Diamond, Terry [IV-3] expression, BDT-DIII-D EDGE. ELM-free VH-mode is terminated in a rapid global energy loss which is initiated by a mode with toroidal mode number, $n \sim 5$. Calculations indicate VH-mode discharges to be unstable to an edge localized ideal kink at the termination time.

3. JAERI Collaboration

During FY 1992 a total of four individual scientists from JAERI contributed to the DIII-D research on VH-mode physics, impurity study, divertor pumping and rf current drive experiment. These activities were of direct benefit to the DIII-D, JT-60U and JFT-2M programs.

The highest confinement discharges were observed only in the case of the high triangularity double/single null divertor configurations. There was a steady confinement improvement as triangularity increased in both single and double null divertor configurations. Detailed analysis of the steady improvement was found to have a good inverse correlation with nickel radiation. Since the outer scrape-off layer of the DIII-D shaped plasma shifts more outward as plasma shaping becomes less triangular, the increased interaction with outer Inconel walls gives reasonable explanation of the results. The bolometer data showed that the peak of the radiation profile roughly corresponded to the plateau region of the temperature profile and also the region where the

VH-mode spin-up occurred. The radiative power loss due to the nickel line emission was estimated to be the order of several tens of mW/cm³ and was comparable to the local input power. The amount of nickel contamination was approximately estimated to be the order of 0.1 % [IV-4]. The results on impurity transport simulation by MIST code gave several fundamental bases in planning future DIII-D experiments.

References

- [IV-1] E.J. Strait, et al., GA-A21037(1993).
- [IV-2] T.H. Osborne, et al., GA-A21182(1992).
- [IV-3] H. Biglari, et al., Phys. Fluids B2(1990) 1.
- [IV-4] S. Konoshima, et al., Bull. Am. Phys. Soc. 37 (1992) 1509.

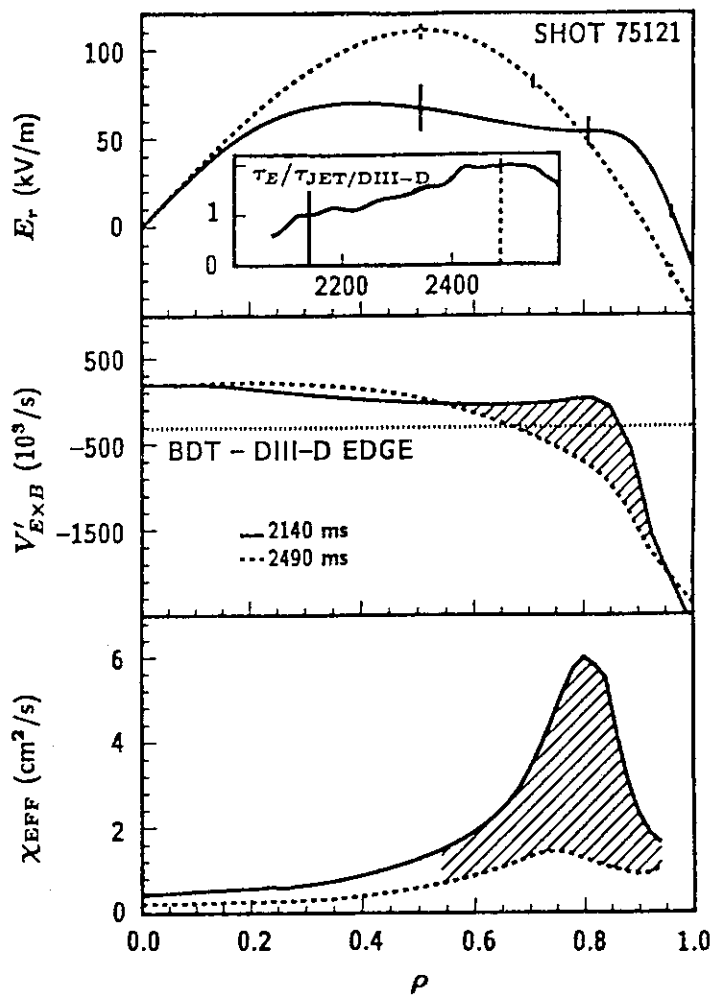


Figure IV.2-1 Change in the profiles of radial electric field, E_r ; $E \times B$ velocity shear, $V' E \times B$; and effective thermal diffusivity, χ_{EFF} ; versus the normalized radial coordinate, r , during the VH-mode discharge.

V. TECHNOLOGY DEVELOPMENT

1. Vacuum Technology and Fuel Injection

1.1 Introduction

Vacuum technology is one of the most important elements of technology for the realization of a fusion experimental reactor like ITER. R&D's of innovative vacuum components and techniques are essential in this technology area.

For this fiscal year, the research activity of a high resolution quadrupole mass spectrometer should be noted. Development of the ceramic turbo-viscous pump, ceramic coating and jointing technology, and ceramic-insulated cables was also advanced.

A new R&D program on the fueling and pumping of tokamak fusion experimental reactors was started in FY1991 to meet the ITER Engineering Design Activity. It is well known that efficient fueling and ash exhaust are essential to confine and control near-ignition fusion plasmas. In this fiscal year, detailed design considerations and some tests of elemental components were carried out to construct a rail-gun system capable of ejecting deuterium ice pellets of variable velocities between 1.5 and 5 km/s at a repetition rate of 1-2 Hz and a large-size turbomolecular pump having a pumping speed of around 25 m³/s.

1.2 Progress in ceramic vacuum pump development

The conditions needed for the torus pumping system of fusion experimental reactors are large pumping speed, large gas throughput, and robustness against radiation, tritium and high magnetic fields. To establish such a system by using dynamic oil-free pumps, for eight years we developed two types of ceramic pumps: ceramic turbomolecular pump and ceramic turbo-viscous pump.

Since the fabrication and some preliminary tests were made of a large-size turbo-viscous pump whose rotor assembly consisted of seven rotor disks 200 mm in diameter and hybrid gas bearings by the previous year, our effort was laid on the performance test of the large turbo-viscous pump.

The test showed that the pump worked in a wide pressure range from atmospheric pressure to 10⁻² Pa and had a maximum pumping speed of 1.7 m³/min for helium, in contrast to 2.8 m³/min for nitrogen. The pump tolerated sudden atmosphere rushings during operation.

1.3 Research on high resolution quadrupole mass spectrometer (QMS)

In fusion research, high resolution QMS's capable of detecting a small amount of helium (⁴He) in deuterium (D₂) are demanded to investigate the behavior of alpha particles in D₂ and to detect ⁴He leak in vacuum vessels. Two years ago, we demonstrated the possibility of the separation of ⁴He⁺ from D₂⁺ by using the condition of the second stability zone (zone II) in the Mathieu diagram [1.3-1]. In this fiscal year, some improvements were made to increase the rf

frequency up to 3.58 MHz which enabled us to detect 10^{-3} peak of ${}^4\text{He}$ in D_2 atmosphere[1.3-2]. A set of spectra at different gains in Fig. V.1.3-1 was obtained by applying the mass scan line to the condition of the upper tip in zone II. The approximate formulae for stable ion orbits at the upper tip are written as follows[1.3-3][1.3-4]:

$$x(\xi) \approx K_x(\sin 2\xi - 0.25\sin 4\xi)\sin(\beta_x\xi - \phi)$$

$$y(\xi) \approx K_y(1 - 0.5\cos 2\xi)\cos(\beta_y\xi - \phi) ,$$

where $\xi=0.5\omega t$, ω is angular frequency, $\beta_x \rightarrow 0$, $\beta_y \rightarrow 0$, and K_x , K_y and ϕ are determined by the initial x and y positions, velocities and rf phase angle.

1.4 Progress in ceramic coating and joining technology

1.4.1 Cr_3C_2 plasma spraying on in-vessel components

Fusion in-vessel components will meet severe operating conditions such as high temperatures and large electromagnetic forces induced by plasma disruptions. To reduce the disruption-induced effects on the components, it is useful to coat the surface of each component with ceramic materials having a insulation property.

On the other hand, to attain stable confinement plasmas, it is required to coincide the electric potential of the components with that of the vacuum vessel which is usually at the earth potential. In this case, every surface of the components to be touched to the vacuum vessel is coated with ceramic materials having a conduction property to reduce contact resistance between the components and the vacuum vessel.

In this fiscal year, a $\text{Cr}_3\text{C}_2/\text{NiCr}$ mixture was chosen as the conduction coating material for the stainless steel components. The vacuum plasma spray method was employed for the coating. An electrical test showed a low contact resistance to fulfill the ITER requirements. Figure V.1.4-1 shows the experimental conditions for the abrasion test of the $\text{Cr}_3\text{C}_2/\text{NiCr}$ coating samples. These were chosen by considering the operating conditions of ITER. Table V.1.4-1 shows the test results with the ITER requirements.

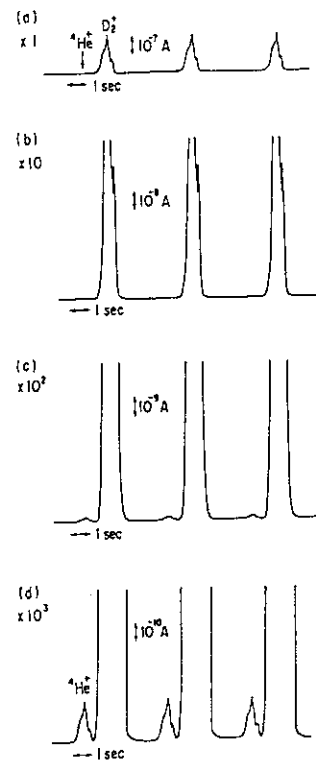
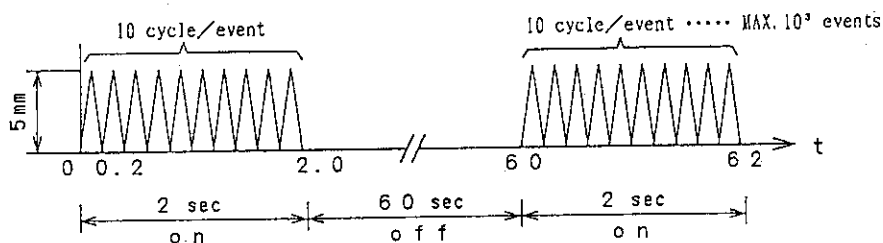


Fig. V.1.3-1 D_2^+/He^+ spectra obtained at 3.58 MHz; (a) 1×10^{-7} A/div, (b) 1×10^{-8} A/div, (c) 1×10^{-9} A/div, (d) 1×10^{-10} A/div.

Table V.1.4-1 Test results of the conduction coatings compared with ITER requirements

Properties	Cr ₃ C ₂ Plasma spraying	ITER Requirements
1) Tensile strength (kgf•mm ⁻²)	> 1.9 (125 μm) > 2.2 (125 μm)	>5.0
2) Thermal shock resistance	No damage (125 μm)	>10 Cycles (RT ≥ 77°K)
3) Tolerant bending angle (°)	10 (125 μm) 10 (125 μm)	-
4) Thermal conductivity (J•cm ⁻¹ •°C ⁻¹ •sec ⁻¹)	0.1422	>2.5 × 10 ⁻⁴
5) Resistivity (Ω•cm)	4.8 × 10 ⁻⁵	<2.0 × 10 ⁻³
6) Abrasion resistance (cycles; 50MPa, 350°C)	7.0 × 10 ³ (300μm)	>10 ⁴
7) Coefficient of friction (RT ~ 350°C)	0.6~0.7	-

- (1) Environment : N₂ gas atmosphere
 (2) Sample temperature : 350°C
 (3) Contact pressure : 50 MPa
 (4) Cycle speed : 50 mm•sec⁻¹
 (5) Cycle pattern : See below

Fig. V.1.4-1 Abrasion test conditions for the Cr₃C₂/NiCr coatings.

1.4.2 Si₃N₄-to-Si₃N₄ joining using ultra-fine particles

The ceramics-to-ceramics joining is a fundamental technique for the production of large-size ceramic components. In a conventional joining technique, some reactive metals are used as the bonding material to seal, increase bonding strength and release thermal stresses. However, the conventional technique has an inevitable problem, i.e., the joined body is not proof against such high temperatures as the ceramics themselves can withstand. An ideal joining would be to unite ceramic parts to be joined using a similar bonding material, as when metallic parts are joined by welding.

Several years ago, we proposed a novel joining technique which featured the use of ultra-fine particles (UFP) [1.4-1]. The chemical composition of the UFP material is very similar to that

of the ceramics to be joined. This technique is based on the idea that the UFP would react at somewhat lower temperatures than the bulk of the same material does.

In our long course of R&D, we tried to join two Si_3N_4 ceramic rods, 15mm×15mm cross section, by using Si_3N_4 UFP in FY1992. In the joining process, fresh UFP's were inserted in between the two ceramic rods and then heated to 1700°C at 10^8 Pa in nitrogen atmosphere. The average bending strength of the joined body showed 86 kg/mm² in contrast to 110 kg/mm² for the bulk Si_3N_4 .

1.4.3 Ceramic-insulated multi-wired cable and its connectors

The ceramic-insulated wires developed [1.4-2] are now widely used in bakable vacuum vessels. The wires are also applied to special motors and magnetic bearings which work in high vacuum, at high temperature or in a radiation environment. On the other hand, multi-wired cables are required to connect these devices to their controlling units. In this fiscal year, we proceeded to develop a ceramic-insulated multi-wired cable and its connectors. The newly fabricated 8-wired cable is illustrated in Fig. V.1.4-2(a), where each ceramic-insulated wire [1.4-2] is covered with a ceramic fiber braiding and the 8 wires are bundled with another metal braiding. The cable is 8.4 mm in diameter and has a breakdown voltage between neighboring wires of over 1 kV. The cable is compact, flexible, yielding no corrosive and toxic gases, and nonflammable as demonstrated in Fig. V.1.4-2(b).

In addition, a pair of 8-pin connectors was fabricated for the

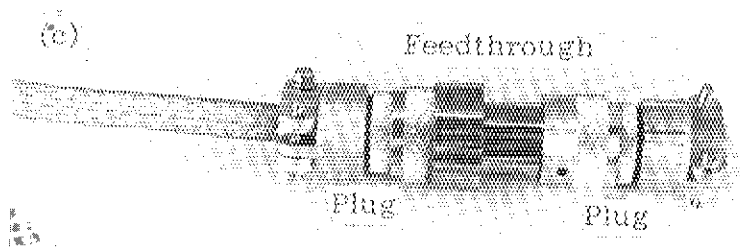
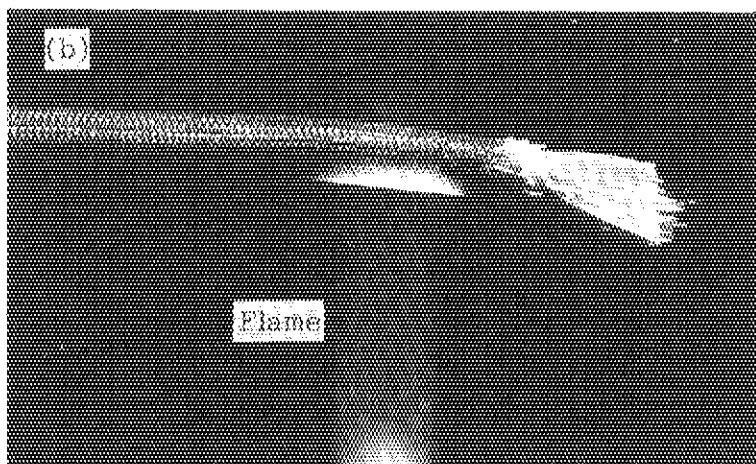
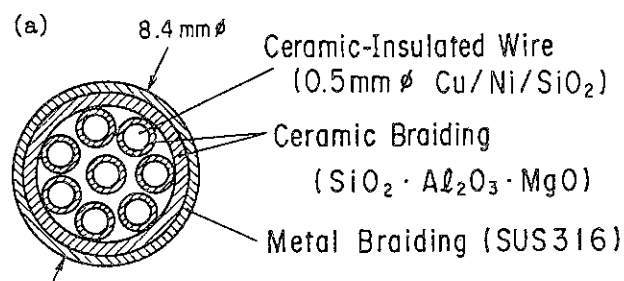


Fig. V.1.4-2 Ceramic-insulated multi-wired cable and its connectors; (a) crosssection of the cable, (b) view of a flame test, (c) connectors joined to the multi-wired cable.

multi-wired cable. A jointed view is shown in Fig. V.1.4-2(c), where the connectors are composed of a vacuum feedthrough and two common plugs. Alumina (Al₂O₃) is used for the insulators. The feedthrough can be welded to a vacuum flange.

1.5 Study on railgun pellet injector using laser-induced plasma armature

A two-stage type railgun injector was studied to develop a repeating-type, high-velocity pellet injector for a reactor-like plasmas. A final goal of this R&D is to develop the injector with the following characteristics:

- 1) Pellet speeds can be variable in the range of 1.5-5 km/s during a repeating injection.
- 2) Pellets can be repeatedly ejected at 1-2 Hz.
- 3) A plasma armature is produced by a laser, so the supplied voltage to the rails is reduced and rail erosion becomes small.

The railgun system, which is used for study, consists of the pneumatic pre-accelerator, a single-stage pipe-gun for the first acceleration stage, and a railgun for the second acceleration stage. Specifications for this system are shown in Table V.1.5-1.

In this fiscal year, solid hydrogen pellet acceleration tests were initiated. A 3mmφ×7mmL hydrogen pellet is produced in the pipe-gun and ejected. The initial speed of the pellet is 0.7-1 km/s. Figure V.1.5-1 shows the dependence of the final speed of hydrogen pellets and the supplied currents to the rails on the charging voltage to the capacitor of the Pulse-Forming-Networks power supply (PFN). In these tests, one capacitor (23.5 mF) of the PFN is used. The final pellet speeds and the supplied currents are linearly proportional to the charging voltages to the capacitor.

Table V.1.5-1 Specifications of railgun system

Type	: Laser-Prearc Railgun	
Railgun	: Bore Diameter	3mm
	: Acceleration Length	1000 mm
	: Materials	Cu or W-Alloy
Hydrogen Pellet	: Diameter	3mm
	: Length	4-7mm
	: Material	Solid-Hydrogen
Dummy Pellet	: Diameter	3mm
	: Length	3-6 mm
	: Materials	Poly-Carbonate, Luan, Balsa
Propellant Gas	: Material	Helium
	: Pressure	-4 MPa
	: Type	Pulsed YAG Laser
Laser Beam	: Pulse Energy	900mJ for 6ns
	: Wavelength	1064 nm
	: Type	Pulse-Forming-Networks
Power Supply	: Capacitors	23.5mF × 4 stages
	: Charging Voltage	~350V
	: Supplied Current	~25 kA

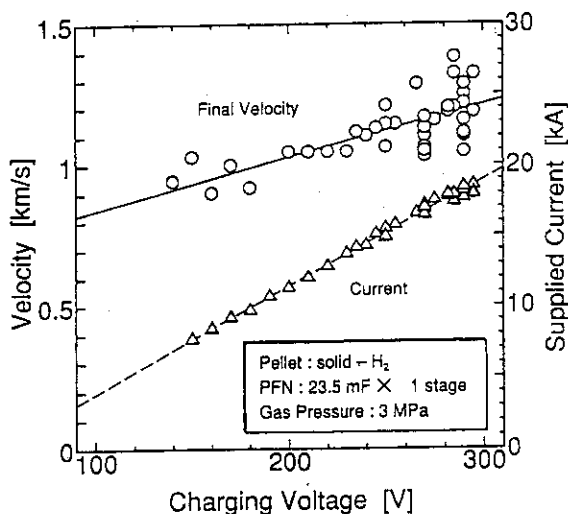


Fig. V.1.5-1 Dependence of final speeds of solid hydrogen pellets and rail currents on charging voltage to the capacitor. The capacitor is one stage and its capacity is 23.5 mF. The rail material is tungsten-alloy. The propellant gas(He) pressure of the pipe-gun is 3 MPa.

Similar results are obtained in the dummy pellet ejection tests [1.5-1]. These results mean that the pellet speed can be easily controlled by the charging voltage, i.e., rail current. In this preliminary tests, solid hydrogen pellets with about 4 mg were accelerated up to 1.4 km/s using only one capacitor.

Copper and tungsten-alloy were used as rail materials. Copper rails were used for 25 operations before they were damaged due to ablation from the plasma, while the tungsten-alloy rails lasted 40 operations. Thus, tungsten-alloy is a superior rail material. Durability of the rails will be also extended significantly by optimizing the supplied current rail length and pre-accelerated pellet speed. These investigations have been done in the collaboration with Mitsubishi Heavy Industries, Ltd.

In the future, it will be necessary to study the acceleration properties of solid hydrogen pellets, and to improve rail-durability and acceleration efficiency.

1.6 Design, fabrication and test of elemental components for large-size turbomolecular pump

The ITER torus vacuum pumping system is required to exhaust a large amount of D-T burn related gases. For this system, JAERI proposed a 25 m³/s turbomolecular pump (TMP) with magnetic bearings that can offer advantages in terms of handling, space and tritium inventory, in contrast to large cryopumps. The ceramic turbo-viscous pump will be used as its backing pump. The major design specifications of the TMP are as follows:

- pumping speed	25m ³ /s for helium
- rotor diameter and length	ca. 1000mm ϕ ×540mm
- rotational speed	8400 rpm
- magnetic bearing	5 axes control
- emergency bearing	dry type, tolerable to 8×10 ³ N
- input power of motor	6 kW
- magnet wire insulator	ceramics
- total weight	ca. 1600 kg

Several types of emergency bearings were fabricated and tested, and some dry ball bearings were found to be tolerable to 8×10³ N.

References

- [1.3-1] S. Hiroki, T. Abe and Y. Murakami, Rev. Sci. Instrum. 63 (1992) 3874.
- [1.3-2] S. Hiroki, T. Abe and Y. Murakami, J. Vac. Soc. Jpn. 36 (1993) 319 (in Japanese)
- [1.3-3] S. Hiroki, T. Abe and Y. Murakami, J. Vac. Soc. Jpn. 35 (1993) 972 (in Japanese)
- [1.3-4] S. Hiroki, T. Abe and Y. Murakami, J. Vac. Soc. Jpn. 36 (1993) 1 (in Japanese).
- [1.4-1] H.Kondoh, T. Abe, Y. Murakami, et al., J. Surface Science Soc. Jpn. 8 (1987) 415 (in Japanese).
- [1.4-2] Annual Report of Naka Fusion Research Establishment, JAERI-M 91-159 (1991) 69.
- [1.5-1] M.Onozuka et al., Int. Symp. on Simulation and Design of Applied Electromagnetic Systems, Sapporo, 1993.

2. Superconducting Magnet Development

2.1 Introduction

JAERI has been systematically developing superconducting fusion magnet technologies, composed of advanced technologies for 1) toroidal coils [DC operation, 13T, large coil with a height 15-20 m], 2) central solenoid coils [pulsed operation, 13T, 3-4m inner dia.], 3) outer ring coils [pulsed operation, 5-7T, 5-20m outer dia.], and 4) a large cryogenics system [30 kW x 4 at 4 K].

The main achievements in FY92 were as follows:

- a) Achievement of a pulsed operation to 7T in 0.5s and measurement of ramp rate limitation on the second test of the DPC-EX.
- b) Investigation of instability behavior on the DPC-U1 and U2, and improvement of its stability margin.
- c) Development of a large current Nb₃Al conductor with 40 kA at 12T.
- d) Contribution to JCT with design work of ITER coil and its model coils.
- e) Achievement of 82kA at 13.6T by a CS full-scale conductor developed for ITER.
- f) Detailed design of the 8kW refrigerator of the ITER-EDA common test facility.

2.2 Demo Poloidal Coil (DPC) program

2.2.1 Results of second experiment of DPC-EX

The Nb₃Sn demo poloidal coil (DPC-EX) was developed to demonstrate the applicability of a Nb₃Sn conductor to pulsed coils for a tokamak fusion machine. The DPC-EX was successfully charged to 6.7 T at 17 kA in 1 second during the first experiment in 1989. The second experiment was performed to get detailed data needed to design a fusion experimental reactor and to study current ramp-rate limitation in 1992. The DPC-EX achieved a rapid charging to 7.1 T at 18 kA in 0.5 second during this experiment. In addition, current sharing temperatures, AC losses, displacements, and strains were measured before and after cyclic pulsed operation, which consisted of over 250 cycles.

In the pulsed field operation, the coil is quenched at much lower current than DC critical current. This phenomenon, called current ramp-rate limitation, was found in the first experiment of the DPC-EX and systematically studied in the experiment of the United States Demo Poloidal Coil (US-DPC). This phenomenon is one of the most serious problems in the design of pulsed poloidal coils. Therefore, the systematic measurements of current ramp-rate limitation were performed during the second experiment. Figure V.2-1 shows the measured boundary of the current ramp-rate limitation in the DPC-EX. The open circles are the maximum field of non-quenched points and the solid ones are the maximum field of quenched points. The solid line shows the ramp-rate boundary between the stable and unstable charging region. In the

DPC-EX, the boundary decreases with the increase of ramp-rate up to about 5T/s. Over a ramp-rate of about 5 T/s, however, the boundary increases with the increase of ramp-rate. This results are different from the trend obtained in the US-DPC experiment as shown in Fig. V.2-1.

The results of current sharing temperature measurements before and after cyclic pulsed operation are shown in Fig. V.2-2. The open circles show current sharing temperatures before numerous-cycle pulsed operation and open triangles show the data after numerous-cycle pulsed operation. Both data show good agreement, and no degradation of the coil performance was observed in the range of less than about 250 cycles. The solid line shows a curve-fit calculated in accordance with Summer's equation using a T_{c0} of 17.0 K and a B_{c20} of 23.5 T. From the results, it is predicted that a -0.5 % strain was applied to the strand. This value is equivalent to the 29 % degradation of critical current at 10 T which corresponds to critical current measurements of verification test results. This means the DPC-EX was not damaged during the fabrication process and the fabrication procedure of a Nb₃Sn large coil for a fusion reactor was established. In addition to the current sharing temperature behavior, the cyclic operation (consisting of over 250 cycles) was not observed to affect the measured values for AC losses, displacements, or strains.

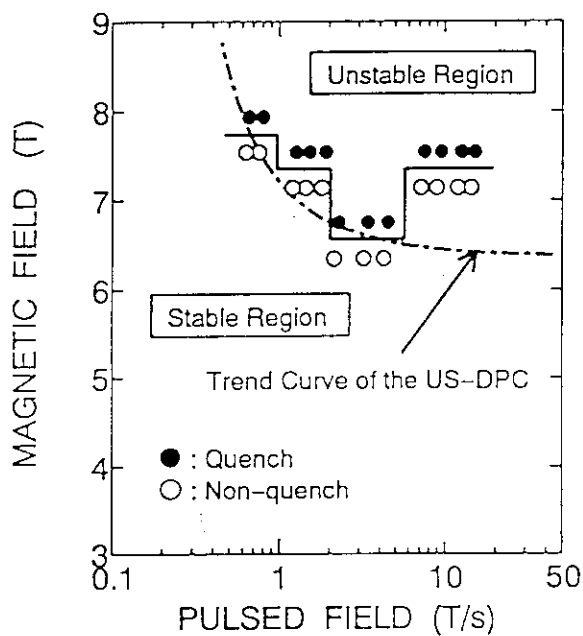


Fig. V.2-1 The results of current ramp-rate limitation of the DPC-EX. The open circles are the maximum field of non-quenched points and solid ones are the maximum field of quenched points.

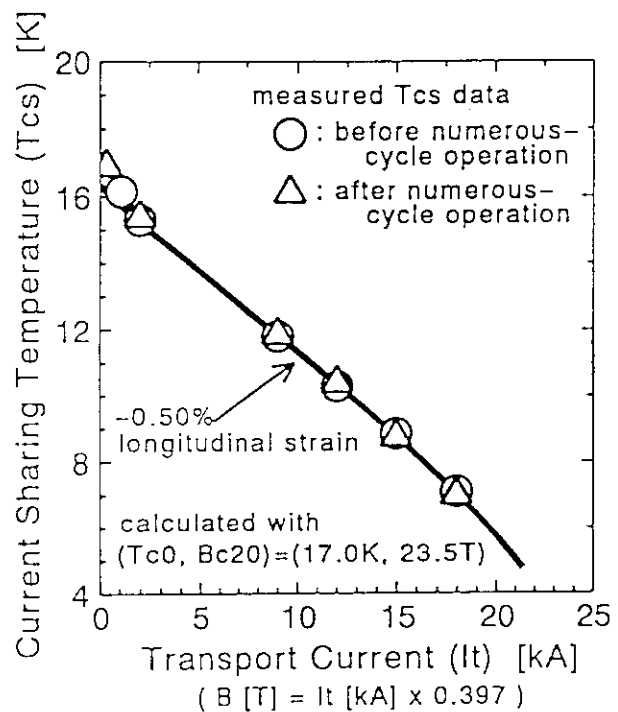


Fig. V.2-2 Relation between current sharing temperature and transport current. The open circles and triangles show current sharing temperatures before and after numerous pulsed operation, respectively.

2.2.2 Improvement of stability of the DPC-U

2.2.2.1 Characteristic of DPC-U and its instability

In the DPC project, two forced-flow cooled NbTi coils, DPC-U1 and DPC-U2, were fabricated to provide the background magnetic field for a test coil to be installed between DPC-U1 and -U2 (hereafter referred to as "DPC-U"). DPC-U was designed to be capable of both DC and pulsed operations up to 7 T with a current of 30 kA. For achievement of a pulsed operation of 7 T/s, the key issue was to reduce a.c. loss. Therefore, the coupling time constant of the DPC-U strand was reduced below 1 ms ; furthermore, the strand surface was coated by formvar to reduce the coupling loss between the strands. These techniques were successfully demonstrated in a NbTi, 30-kA, pool-boiling cooled coil[2.2-1]. The DPC-U conductor was composed 486 twisted strands whose diameter was 1.12 mm. The photograph of the DPC-U conductor is shown in Fig.V. 2-3.

However, the DPC-U exhibited an instability : in many cases the coil quenched at a current of one-tenth the conductor critical current, although DPC-U can reach the designed current of 30 kA by spending quite a long time for a charge. An experiment to clarify this instability was carried out in the fifth DPC experiment. From these experimental results, it was found that this instability was caused by a non-

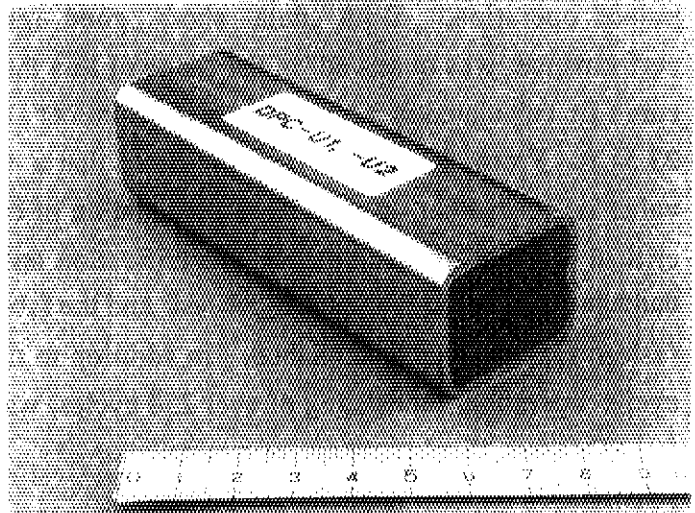


Fig. V.2-3 The DPC-U conductor.

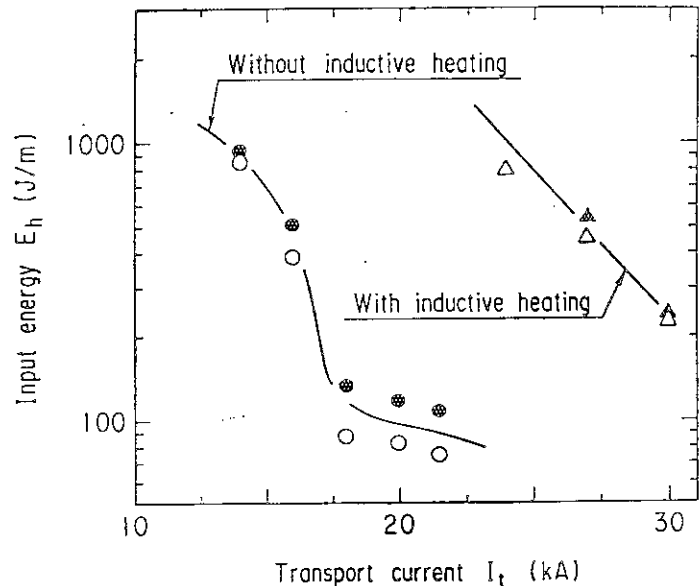


Fig. V.2-4 Stability margins of DPC-U1. Open and close symbols show recovery and quench points, respectively.

uniform current distribution and a long time constant of current redistribution in the conductor. It was also shown that the current distribution in the DPC-U conductor can be made uniform by applying inductive heating pulses without a coil quench. The instability of DPC-U can be improved using this effect [2.2-2].

2.2.2.2 Improvement of the instability of DPC-U

Based on the above results, the inductive heaters were attached to the DPC-U1 conductor: A coil charge to 30 kA was attempted, putting inductive heating pulses to the conductor during the charge in the sixth DPC experiment. We could stably charge DPC-U1 up to 30 kA during a much shorter time than the charge without using inductive heaters. The stability margins of DPC-U1 were also measured after charging with and without inductive heating. Figure. V. 2-4 shows the results of the stability experiment. The stability margin was dramatically enhanced after a charge with inductive heating. Therefore, the instability of DPC-U can be improved using inductive heaters.

Reference

- [2.2-1] Shimamoto S. et al. Proc. of ICEC 13
Butterworth Heinemann UK (1990) 23
- [2.2-2] Koizumi N, et al. Cryo. Eng. Japan
Vol.27 3 (1993)

2.3 40-kA Nb₃Al conductor development

Presently, Nb₃Sn is mainly used for high-field superconductors (more than 12 T) and is commercially available

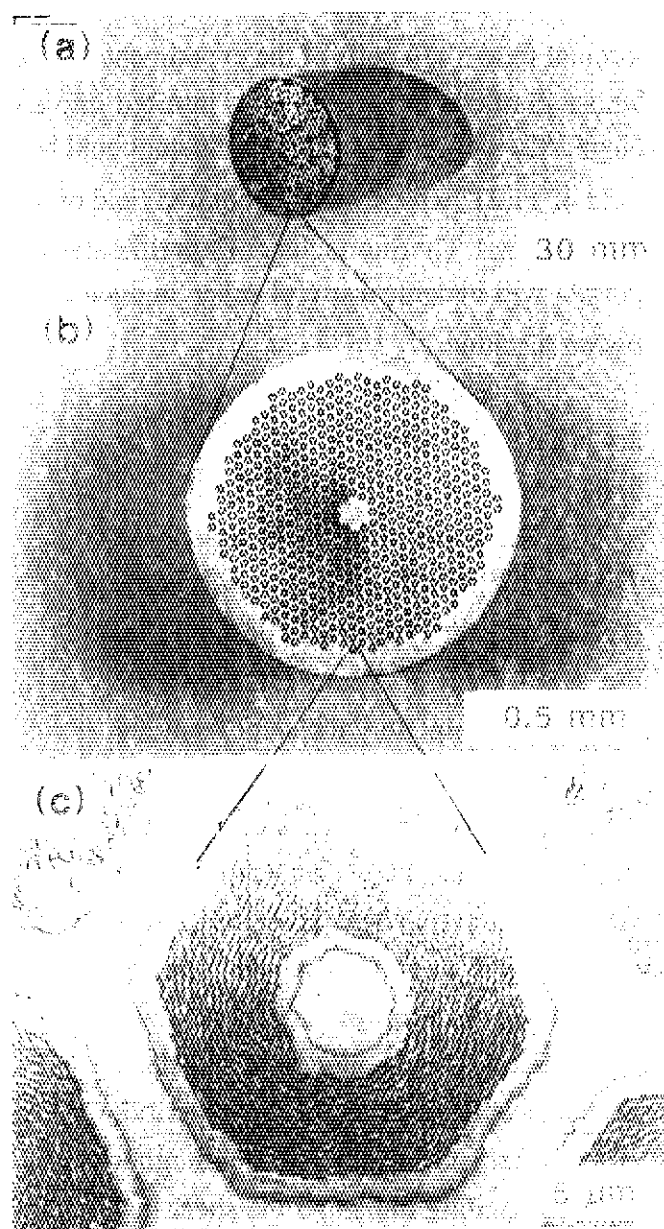


Fig.. V.2-5 40-kA Nb₃Al cable-in-conduit conductor: (a) the conductor, (b) Nb₃Al strand, (c) Nb₃Al filament.

in various types. However, a serious disadvantage of Nb_3Sn is that its critical current is very sensitive to strain and the fabrication of the Nb_3Sn coil must be carried out very carefully. On the other hand, the degradation of the critical current of Nb_3Al is one sixth the that of Nb_3Sn . Therefore, Nb_3Al has excellent mechanical performance and could be very useful for the toroidal field coil which are operated under large electromagnetic forces. However, Nb_3Al use is not practical use at present due to the difficulty of its fabrication.

A 40-kA Nb_3Al conductor, shown in Fig. V.2-5, was developed and tested for the toroidal field (TF) coils of the experimental fusion reactor. The conductor consists of 405 strands, whose diameter is about 1 mm, inserted into a CuNi conduit. The strands are multifilamentary $\text{Nb}_3\text{Al}/\text{Cu}$ composites. This conductor could be operated up to the current of 46 kA at an external field of 11.2T, which was the required field of the TF coils in the conceptual design activity in the International Thermonuclear Experimental Reactor (ITER). According to this development, Nb_3Al will become a useful superconductor for large-scale, high-field applications, such as the fusion machine.

2.4 ITER-EDA works

2.4.1 Design of ITER coils

The concept of the International Thermonuclear Experimental Reactor (ITER) magnet system was proposed by the Joint Central Team (JCT). This concept is completely different from the concept of the Conceptual Design Activity (CDA). In the CDA concept, the toroidal field (TF) coils are supported by wedging them together. Therefore, stress analysis was done to discover whether the ITER magnet system was mechanically strong enough to withstand the allowable stresses. In this period, stress analysis of the whole magnet system, winding units and the shear key was carried out. Stress analysis of the whole magnet system at the end of burn (EOB) stage was described as follows.

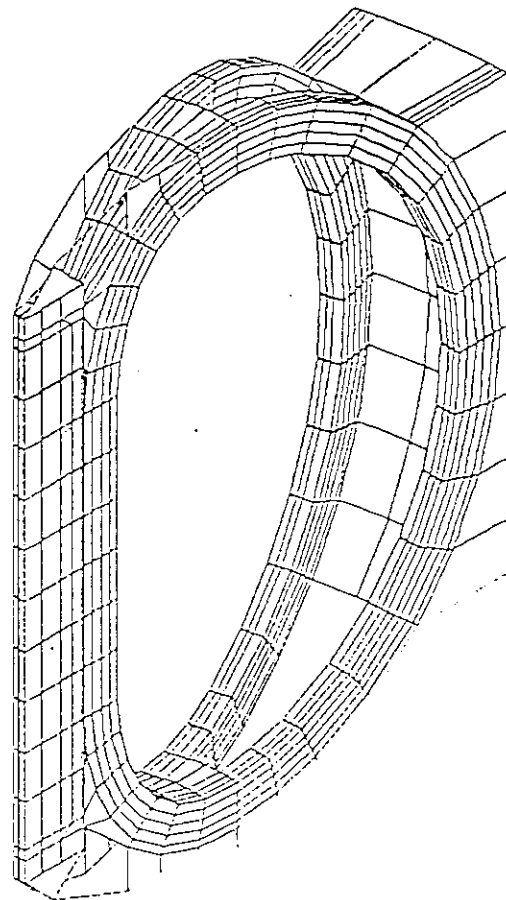


Fig.V.2-6. FEM analysis model which is equivalent to a 15-degree section of magnet system in a toroidal direction.

The ITER magnet system is composed of TF coils, central solenoid (CS) coils, bucking cylinders, insulators and an outer support structure. The finite element method (FEM) analysis model we used is shown in Fig. V.2-6 This model is composed of halves of two adjacent TF coils and a connecting slice of outer support structure. Moreover, the model is equivalent to a 15-degree section of the magnet system in a toroidal direction. TF coils have a composite construction of shear disks, insulator and conductor jackets.

Stresses of Toroidal Field Coil: The maximum Tresca stress of 392 MPa in the TF coil is generated at the upper and lower parts of the inboard. The maximum point is located at the inside of the coil and between TF coils.

The maximum shear stress τ_{xy} is 47.0 MPa at the bottom of coil. The maximum shear τ_{yz} and τ_{zx} is -39.9 MPa and -139 MPa at the bottom of the inboard, respectively. The maximum shear stress and τ_{xy} are located at the inside in the cross section of the maximum stress plane. However, the maximum shear stresses of τ_{yz} and τ_{zx} are located on the outside in the cross sections.

Stresses of Central Solenoid Coil: The maximum Tresca stress of 496 MPa and the maximum shearing stress of -42.8 MPa are at the top and the outside of the coil due to the huge electromagnetic forces in the CS coil in the vertical direction.

Stresses of Other Structures: The maximum Tresca stress is 624 MPa in the outer structural band at the bottom. This value is the largest value in the magnet system.

Summary of Stress at EOB: The maximum stress values in the magnet system at the EOB are the Tresca stress of 624 MPa in the outer structural band and the shearing stress of -139 MPa in the TF coil. The maximum values of this stress analysis are summarized in Table V. 2-1

Table V.2-1 List of the Maximum Stresses at EOB

	TF coil	CS coil	Bucking Outer	Cylinder Structure
(unit : MPa)				
Principal stress				
Max. Tresca	392	496	540	624
Max. σ_1	376	411	366	538
Max. σ_2	66.5	144	-201	128
Max. σ_3	-184	-145	-316	-232
Shearing Stress				
Max. τ_{xy}	47	-42.8		
Max. τ_{yz}	-39.9	41.7		
Max. τ_{zx}	-139	-63.2		

2.4.2 Design of ITER model coils

2.4.2.1 Toroidal field model coil

The main issue concerning the ITER TF coils are mechanical behaviors, especially shear stresses between shear plates and between TF coils. We designed the TF model coil in order to simulate the stress behavior of the full scale TF coil. The TF model coil is a race-track shape and the global size is 4.5 m x 3.5 m. The TF model coil which consists of layer wound conductors and shear plates is called a side-by-side coil because of a LCT coil adjacent to the TF model coil. A spacer is located between the TF coil and the LCT coil at the straight part of the TF coil. The analysis model of the side-by-side coil system is shown in Fig. V.2-7

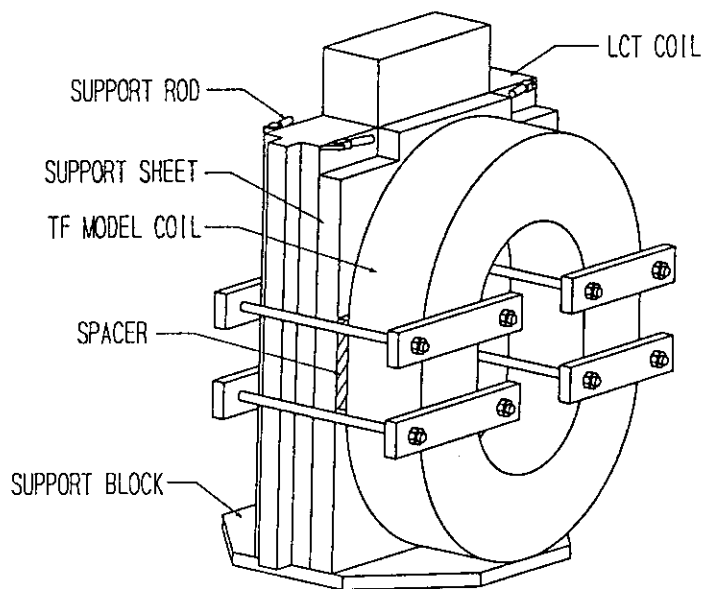


Fig.V.2-7 Test configuration of ITER-TF Model coil with EC-LCT coil

We carried out stress analysis for several load cases. The results clarify the following things :

- 1) It is possible to generate shear stresses that are equivalent to the full scale coil in this model coil. The shear stress between shear plates is 46 MPa in this model coil while 60 MPa in the full scale coil.
- 2) It is possible to simulate stress behaviors (Tresca, principal stress) of the full scale coil in this model coil. The maximum Tresca stress is 348 MPa in this model coil while 368 MPa in the full scale coil.

2.4.2.2 Central solenoid model coil

The Central Solenoid (CS) Model Coil is a solenoid of about 2 meter inner diameter, 2 meter height, and capable of reaching a nominal field of 13 Tesla with ITER-relevant ramp rate. The CS model coil will be capable of accepting a replaceable layer insert to simulate relevant operating conditions for the conductor. Because the CS model coil will be in a tensile hoop stress whereas the full scale CS operation is in a compressive state. The insert will use CS and TF conductor to simulate the expected radial and hoop compression.

The design of the CS model coil is in progress through the magnet workshop and ITER Joint Central Team. The Main design concern is how to simulate the full scale CS coil with 19.5 ton strand. The layer and pancake winding methods are proposed for manufacturing methods of CS model coil which is also influenced from the results of manufacturing feasibility study. The

layer winding method has many difficulties to scale up 12 m full size CS coil, but the pancake winding method has week point of outer joint area and maintenance of joints. The layer and pancake method will be selected by full scale CS coil design.

2.4.3 Development of CS conductor

JAERI has conducted a trial manufacture of a CS full-scale conductor with a length of more than 30 m, JAERI has also produced several kinds of test samples using the conductors of two industrial companies in order to demonstrate manufacture and to evaluate the characteristics of the conductor. The CS conductor is composed of 675 ~ 768 Nb₃Sn strands and a Ti conduit. The strands were made by a bronze process and have a 0.92-mm diameter and Cr-plated surface.

As the first experiment of the test samples, critical current of the full-scale conductor was measured. Typical results from the experiments are shown in Fig.V.2-8. The measured value of critical current in a background field of 13.6 T is 82 kA and it seems that degradation of critical current is small

due to heterogeneous current distribution and damage by cabling and jacketing. This is a good information for coil design with respect to critical current.

Other experiments, such as an AC loss measurement, a stability margin measurement and so on, will be made in the near future.

2.4.4 Cryogenic system for common test facility

Cooling requirements for the Test Facility were determined by the ITER Joint Central Team (ITER JCT) when the CS coil concept of the ITER EDA was significantly changed from that of the ITER CDA. The requirements concerned with the cryogenic facility are listed in Table V.2-2. According to the requirements, the substantial heat loads for the cryogenic system were considered again, resulting in the rated capacity of around 2.6 kW at 4.5 K with a

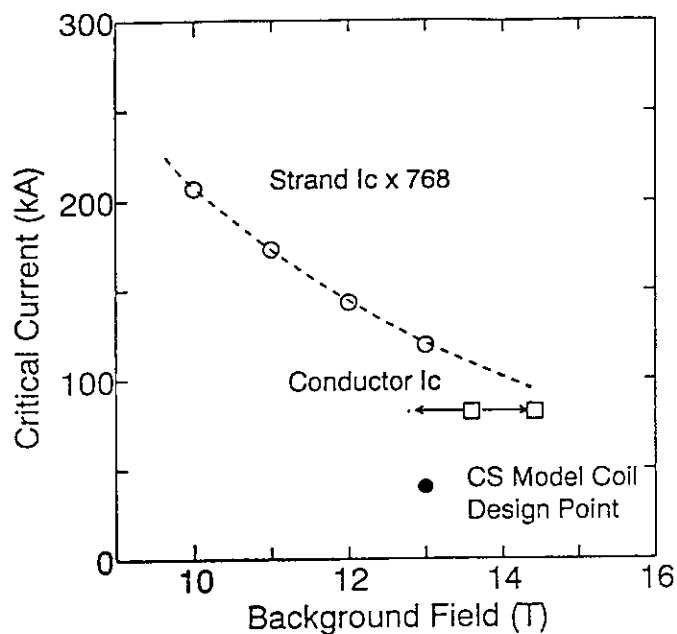


Fig.V.2-8. Typical results from critical current measurement of a cs full-scale conductor

liquefaction rate of 380 l/h as shown in table V.2-3. The capacity load curve is also shown in Fig. V.2-9. Based on this criteria, a design study has been performed and the detail specifications have been determined. The substantial components and their major specifications are shown in Table V.2-4 and their configuration in Fig. V.2-10. It will be difficult to develop key cryogenic machinery expecting to the ITER cryogenic system such as large-scale turbo-expander, cryogenic pump, and cold compressor. The thermodynamic process design, however, remains the same, as well as

the previous design, which is supposed to be used in the ITER cryogenic system.

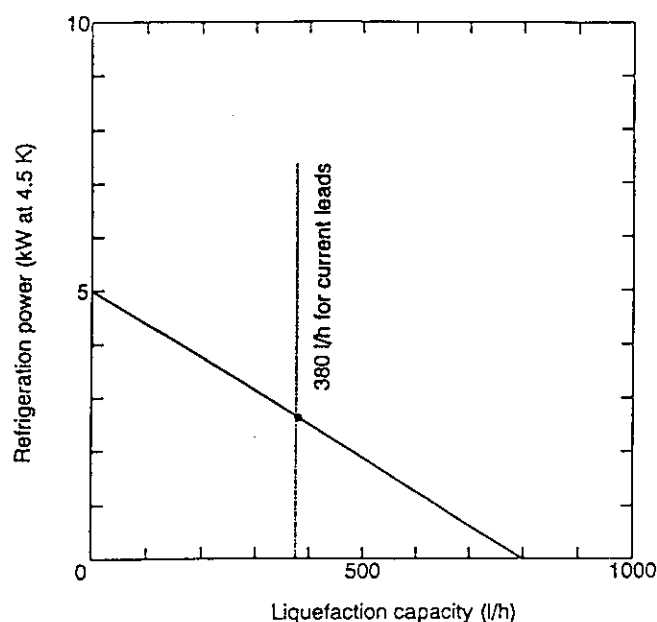


Fig.V.2-9 Refrigeration and liquefaction load for the cryogenic system.

Table V.2-2 Cooling requirements proposed by ITER JCT

(1) Cooldown time	40day (target 20 days)
(2) Pulse repetition	@1pulse/ 30 minutes for a only solenoid coil @10000 cycles/ 3 months for a insert coil with 50 kA constant in a solenoid coil
(3) Operating temperature	4.5 K
(4) Helium flow rate	@50 g/s per channel @350 g/s for coil
(5) Average AC losses	600 W for coil and structure
(6) Max. operation pressure	7 bar
(7) Max. pressure drop	4 bar (Pressure drop measurement only)
(8) Average pump work	400 W into cold circuit
(9) Max. helium volume	2000 liters in coil

Table V.2-3 Required heat loads for the helium cryogenic system

(1)Static heat loads	500 W
(2)AC losses	600 W for coils 100 W for coil structure
(3)Cold pump work	1070 W (350g/s for coil + 100 g/s for structure with pump head of 0.2 MP, a pump efficiency of 60%)
(4)Others	350 W (Cold compressor work, Joule heating at coil joints)
(5)Current leads (2 pairs)	380 l/h
Total heat loads at rated condition	2620 W + 380 l/h

Table V.2-4 Substantial components and their major specifications

(1) Cold box Refrigeration power Liquefaction power	5kW at 4.5 K at maximum 800 liters/hour at maximum
(2) Helium compressor Total mass flow rate Suction pressure Discharge pressure Isothermal efficiency	750 g/s at maximum 300 mmHg at rated 1.6 MPa at rated more than 55%
(3) Purifier* Inlet Air contamination ratio Outlet Air contamination ratio Mass flow capacity	1000 ppm less than 1 ppm 20 g/s
(4) Helium gas storage and recovery unit* Helium gas storage Gas recovery compressor	700m ³ at 2.0MPa at maximum 20 g/s
(5) Primary liquid helium storage tank*	20000 liters
(6) Auxiliary cold box * Supercritical helium (SHe) flow rate SHe temperature SHe pressure SHe circulation head	500 g/s at maximum as low as 4.0 K 0.5 - 1.0 MPa as high as 0.2 MPa
(7) Liquid nitrogen tank*	100000 liters

* : They are supposed to re-install existing one which has been used for 5 -10 years.

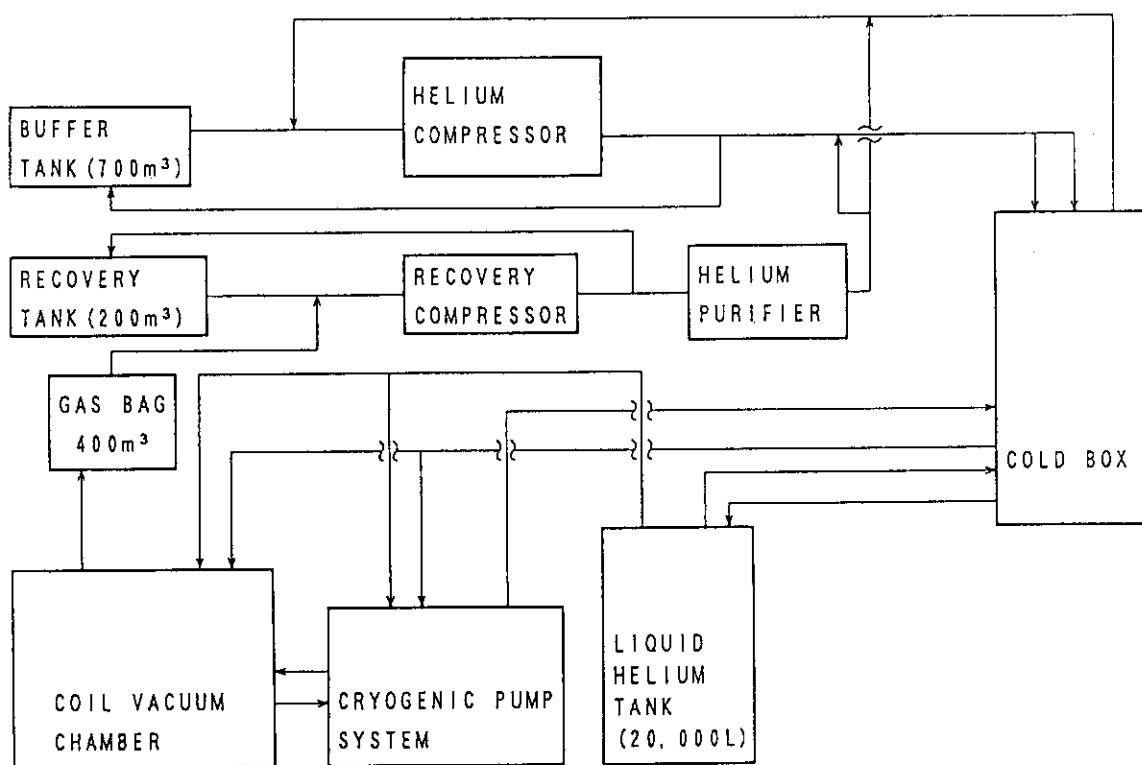


Fig.V.2-10 Cryogenic system for ITER common test facility

3. Beam Technology

3.1 Introduction

Development of a high power negative ion source is an important key to realizing negative ion based neutral beam injectors for JT-60 and ITER. R&D efforts have been concentrated on high energy acceleration, beam optics study and production of negative ions with high efficiency. Positive ion beam technology has also been developed for a high brightness ion source for accelerator applications.

3.2 Negative ion beam technology[3.2-1]

3.2.1 High energy acceleration of H^- ions[3.2-2,3]

High energy acceleration of H^- ions has been studied using a 350 keV negative ion source. A schematic of the ion source is shown in Fig. V.3.2.-1. The ion source consists of a cesium seeded multi-cusp plasma generator, whose inner dimensions are 22 cm in diameter and 17 cm in depth, and an electrostatic multi-aperture accelerator with 9 apertures. The diameters of the apertures in the extractor and the accelerator are 14 mm and 16 mm, respectively. The accelerator has an extraction gap of 5.7 mm and two stage acceleration gaps of 83 mm and 57 mm.

By optimizing electrostatic lens and electric field configurations in the accelerator, a high energy H^- beam of 350 keV, 0.17 A was produced for 1s with a good beam divergence of smaller than 5 mrad. This is a world record of the H^- beam produced in the electrostatic accelerator. The current density of the accelerated H^- beam was 10 mA/cm^2 . A picture of the beam is shown in Fig. V.3.2-2.

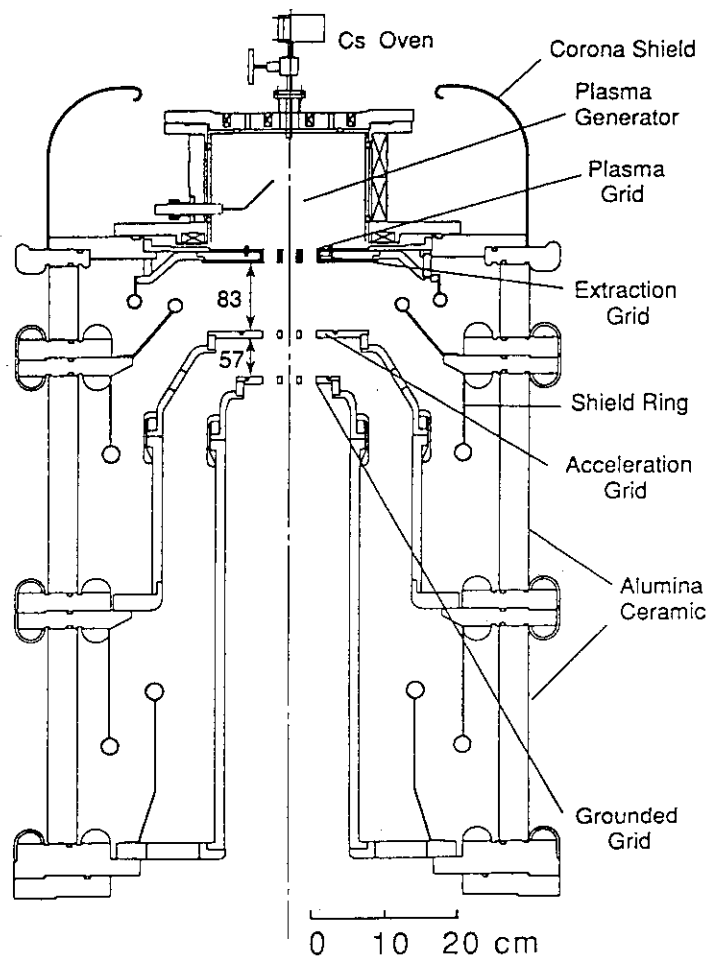


Fig. V.3.2-1: A schematic of the 350 keV H^- ion source. The source consists of a cesium seeded multicusp plasma generator and an electrostatic multiaperture accelerator. The H^- ions produced in the plasma generator are extracted and accelerated by 9 apertures of 14mm in diameter each.

Heat loads in the accelerator grids were confirmed to be mainly due to stripped electrons from the H^- ions in the accelerator. Direct interception of the H^- beam was found to be very small. These results showed that heat loads can be lowered by reducing the operating pressure in the ion source. Heat loads in the accelerator grids were lower than 6 % of the electric power required for beam acceleration at the filling pressure of 0.5 Pa. A power density of 250 W/cm^2 in the grids during the 350 keV operation is an allowable value for designing long pulse accelerator grids.

After these experiments, the power supply system was upgraded so as to accelerate 1A negative ion beams up to 400keV. A 400 keV, 1A negative ion source with a 3-stage electrostatic accelerator was designed based on the experimental data obtained from the 350 keV ion source.

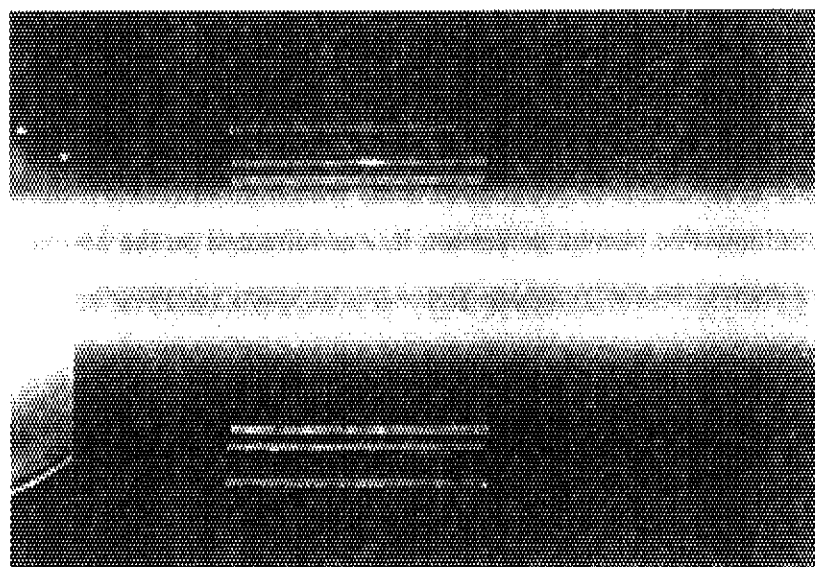


Fig. V.3.2-2: A picture of the accelerated H^- beam produced from 9 apertures. Three lines of beam correspond to three rows of the multi-apertures. We can easily distinguish the beamlet because of its small divergence.

3.2.2 H^- beam optics study

Beam merging technology is one of the important subjects to make the NBI system compact. A collaborative experiment on the negative ion beam acceleration using the ESQ (Electro Static Quadrupole) accelerator will be started at LBL(Lawrence Berkeley Laboratory, USA) in 1993. The pre-accelerated converged beam is required for the ESQ accelerator. The experiment on beam merging using a semi-spherical grid system was performed as an initial step of the collaboration. The H^- beam extracted from an area of 5 cm in diameter was successfully converged to a parallel beam with a beam diameter of 2.5 cm. The obtained beam energy and current were 60 keV and 80 mA.

Based on the experimental results, an ion source which can produce a converged beam for the ESQ accelerator was designed and fabricated.

3.2.3 Long pulse operation of an ampere-class beam [3.2-4]

The pulse length of the N-NBI system for JT-60 was designed to be 10 s. To demonstrate such a long pulse operation for the ampere beam, a 50 keV, 2 A H⁻ beam was produced for 10 s. A stable beam was produced during the pulse and the heat load on the accelerator grid was found to be smaller than the allowable value.

3.2.4 Improvement of H⁻ production efficiency by configuration of a plasma generator

It was found that a large plasma volume is favorable to enlarge the enhancement factor of H⁻ production at Cs seeded operation. To investigate the effect precisely, a large cylindrical plasma generator was fabricated and tested. The dimensions of the generator are 30 cm in diameter and 23 cm in depth. The experimental results showed that the large plasma volume with a good confinement is favorable to produce H⁻ ions with high efficiency during the operation with Cs. After optimizing this plasma generator, it was mounted on the 350 keV ion source and used for the beam acceleration study.

3.2.5 Improvement of H⁻ production efficiency by PG filter

To increase H⁻ production efficiency, a PG filter, which is a new type of magnetic filter developed at JAERI, was adopted in the multi-ampere negative ion source. The PG filter produces a transverse magnetic filter field by flowing the current through the plasma grid itself, while the magnetic filter was produced by a set of strong permanent magnets in the original configuration. The H⁻ current up to 7 A with a current density of 26 mA/cm² was produced at an arc discharge power of 35 kW. The H⁻ production efficiency (the ratio of H⁻ current to arc discharge power) was increased from 0.18 A/kW to 0.2 A/kW. This type of filter is to be adopted in the JT-60 N-NBI ion source.

3.2.6 Design of a MeV test stand

High energy acceleration of a large current of negative ions should be investigated to realize high power NBIs. To study the beam acceleration of an ampere negative ion beam up to 1 MeV, the MeV test stand was designed. The test stand consists of a power supply system for an ion source and an X-ray shield room. The high voltage power supply for beam acceleration is a 1 MV, 1 A Cockcroft-Walton power supply driven by a high frequency inverter of 3 kHz. The power supply can be operated for 1 min pulse with a duty cycle of 1/60. The high voltage power supply and the ion source are installed in pressurized tanks filled with SF₆ gas. The tanks are built in the shield room. The construction of the test stand was contracted.

References

- [3.2-1] Y. Okumura, et al., Proc. 1st Meeting on the Ion Engineering Society of Japan, Tokyo, 1992.
- [3.2-2] S. Maeno, et al., Proc. 3rd Symp. on Beam Engineering of Advanced Material Syntheses, Tokyo, 1992.
- [3.2-3] M. Mizuno, et al., 6th Symp. on the Production and Neutralization of Negative Ions and Beams, Brookhaven, 1992.
- [3.2-4] M. Hanada, et al., Proc. 3rd Symp. on Beam Engineering of Advanced Material Syntheses, Tokyo, 1992.

3.3 Application of high current ion beam technology

3.3.1 Development of a high brightness ion source for the proton linear accelerator[3.3-1,2]

A prototype ion source has been designed and tested for the 10 MeV, 10 mA, CW proton linear accelerator called the Basic Technology Accelerator (BTA), which is to be constructed at JAERI. A 100 kV test facility for the ion source was constructed. A target for the development of the ion source is to produce a 100 keV, 120 mA proton beam with a normalized emittance of as low as $0.5 \pi \text{mm.mrad}$ (90 %).

After optimization of the ion source, a 100 keV, 140 mA beam was produced with a beam divergence of 8 mrad. Emittance estimated from the beam divergence was $0.5 \pi \text{mm.mrad}$ (90 %).

3.3.2 Plasma production by RF[3.3-3]

Production of a high density plasma by Radio Frequency wave (2MHz) was studied for long life ion sources and industrial applications. A high density plasma of 10^{12} cm^{-3} was produced by RF power of 20 kW in the multi-cusp plasma generator whose inner diameter is 20 cm. This technology is also useful for the development of a plasma neutralizer.

3.3.3 Study of a steady state cryopump

A steady state cryopump is required for the ITER NBI. As a preliminary experiment for the development, a gas condensation limit was investigated using a small cryopump which has a panel area of 0.13 m^2 . The condensation limit was $2 \times 10^5 \text{ Pa.m}^3/\text{m}^2$ at the tank pressure of 0.1 Pa. The limit tended to extend by reducing the pressure in the tank. It is remarkable that the limit is ten times as large as that for the JT-60 NBI cryopump even when the pressure (0.1 Pa) is five times higher than the designed pressure for ITER.

References

- [3.3-1] H. Oguri, et al., JAERI-M 92-024, 1992.
- [3.3-2] Y. Okumura, et al., 16th Inter. Linac Conference, Ottawa, 1992.
- [3.3-3] Y. Suzuki, et al., JAERI-M 92-156, 1992.

4 RF Technology

4.1 Introduction

Radio-frequency (RF) waves are key tools for the heating and current drive of the tokamak fusion reactor. The R&D of RF technology is indispensable to establish the engineering base for ITER and next generation tokamaks. Development of a high efficiency RF source for the Electron Cyclotron Heating (ECH), the Lower Hybrid Current Drive (LHCD), the high performance Launching system for LHCD, and the Ion Cyclotron Heating (ICH) are the main efforts of JAERI RF Technology. The major activities in 1992 are the development of a high power gyrotron at the 100 GHz band and the Japan-France collaborative experiment of a LH launcher module for the next generation tokamak. The output of 460 kW for 100ms from the developed gyrotron at 120 GHz was successfully obtained and the first step outgassing experiment of the LH module was successfully completed.

4.2 Development of high power gyrotron and ECH components

Research and development of a 100GHz band gyrotron has been carried out for applications in an electron cyclotron resonance heating (ECH) in the JT-60U and ITER. In ITER, 100GHz band gyrotrons with a power of up to 1MW / tube during continuous operation is demanded. As a first step of the JAERI gyrotron development program, a high power gyrotron (E3970), which has an oscillation frequency of 120GHz, was developed. The oscillation mode is TE_{12,2}, the whispering gallery mode (WGM), and a quasi-optical mode converter is installed inside the tube (built-in type) to extract RF power as a gaussian-like beam. The high power generation of more than 500kW was demonstrated for a short pulse operation in 1990.

In 1992, a pulse extension experiment was carried out on the JAERI Gyrotron Test Facility. Stable oscillation up to 100ms, which was a design value, was obtained at an output power of 460kW. Longer pulse operation of 215ms with an oscillation power of 250kW was also performed. No evidence of RF breakdown at the output window or inside the tube was observed throughout the experiment of 100ms level pulse duration. A photograph of the gyrotron E3970 installed in a super conducting magnet for a long pulse experiment is shown in Figure V.4.2-1.

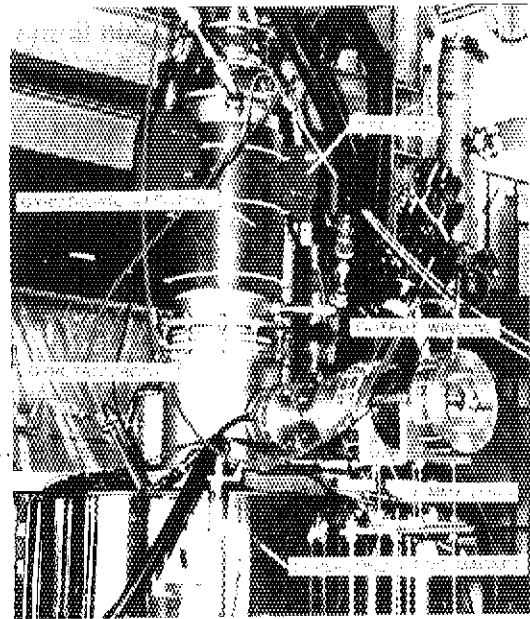


Fig. V.4.2-1 : The photograph of gyrotron E3970 installed in super conducting magnet for a long pulse experiment.

Also, the upgrade gyrotron E3971 with 110GHz for a long pulse operation ($> 1\text{sec}$) was developed and a preliminary test was made with a short pulse (1msec). As a result, oscillations of 500 ~ 600kW were obtained.

The oscillation mode was estimated to be TE_{22,2} WGM. Long pulse operation up to 1sec will be tested in 1993.

A single disk window cooled at the edge for a 1MW class and CW RF power with an HE11 mode in a corrugated waveguide was developed for shielding tritium and radioactive dust from the tokamak. The specifications for the RF window are shown in Table V.4.2-1.

Table V.4.2-1 : Specification for RF window.

Material	Sapphire
Structure	Single disk
Cooling	Edge cooling
Frequency	110 GHz
Transmitted Power	1 MW
RF Mode	HE11
Dia. of Waveguide	60.3 mm
Thickness of Disk	1.33 mm
Pressure in Waveguide	$< 0.1\text{ Pa}$

The cryo-window system consists of a sapphire disk, a vacuum insulated cryostat having a small cryo-cooler, corrugated waveguides, an arc detector and a gate valve. Figure V.4.2-2 shows a side-view of the cryo-window system.

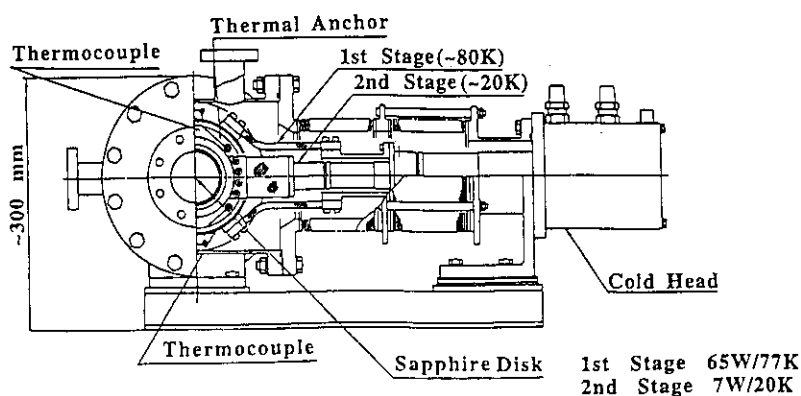


Fig. V.4.2-2 : Side-view of the cryo-window system.

Firstly, a cooling-down test of the cryo-window system was made. A window disk temperature of 13 K has been obtained by using a cryo-refrigerator capable of 7W cooling capacity at 20K. Thermal analysis of the window disk has indicated that continuous operation for 110GHz, 1MW RF power transmission is feasible. The high RF power and the long pulse operation will be tested in 1993.

4.3 Development of LHCD and ICRF launcher

To establish the design base of the LHRF launcher for the next generation tokamak, we need the outgassing data of the antenna module under high RF power and long pulse operation. The first test with a 4way-divided waveguide was done under the cooperative activities between JAERI and CEA-Cadarache. This module, which is made from Dispersion Strengthened Copper (DSC), was designed and fabricated by JAERI. CEA provided the lower hybrid test bed facility of Cadarache which included a frequency range of 3.7 GHz with a CW 500 kW klystron. The main results are as follows :

- 1) the key parameter is the module temperature

- 2) high temperature baking and RF conditioning are effective in reducing the outgassing rate
- 3) after conditioning, a low outgassing rate was measured:
 $< 3.10^{-9} \text{ T.l.s}^{-1} \text{ cm}^{-2}$ at $T=400^\circ \text{C}$
- 4) low stationary outgassing was obtained with water cooling:
 $< 2.10^{-10} \text{ T.l.s}^{-1} \text{ cm}^{-2}$ at $T=150^\circ \text{C}$ during a 30 mn injection at 15 kW/cm^2

As for the ICRF launcher, a new type fast wave current drive (FWCD) antenna, "spiral antenna" for a fusion reactor, is proposed. It is difficult to control the toroidal refractive index spectrum accurately and to match all antenna impedances at the same time in the conventional loop antenna array, because of the mutual coupling. The benefits of a "spiral antenna" are: an optimum toroidal refractive index spectrum excited by the same antenna currents, and the correct phase differences with an easy matching operation. The mock-up of a "spiral antenna" is being constructed for checking RF properties.

4.4 Millimeter wave free electron laser

Construction of a new induction linac for FEL research was started in 1992. In Fig.V.4.4-1, the conceptual view of the new induction linac is shown.

Characteristics are:

- 1) beam energy : 2MeV
- 2) beam current : 3kA
- 3) pulse width : 160ns

The construction will be completed in 1993. With the linac, high power millimeter FEL (30 ~ 140GHz) of gigawatt level output power is expected, and with this, a fusion heating experiment at JFT-2M is planned.

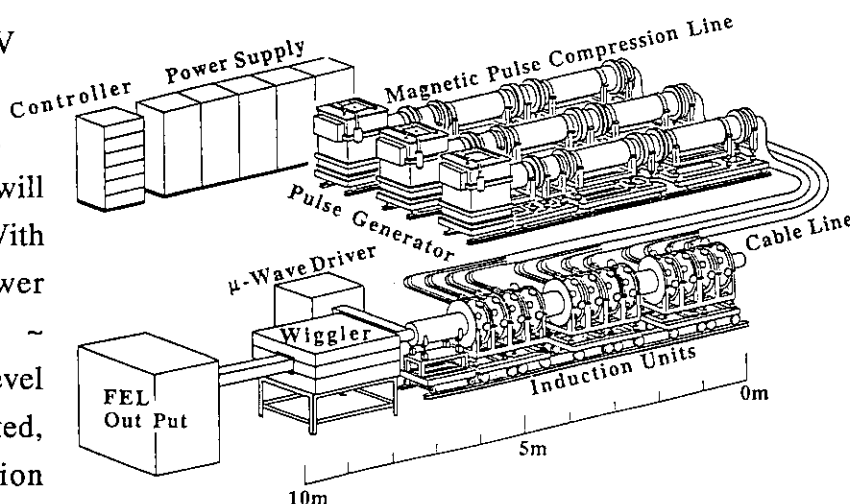


Fig. V.4.4-1 New Induction Linac.

4.5 Design study of RF heating and current drive launcher for ITER

Design study of the ceramics-free antenna feeder using the ridged waveguide was done for the ITER ion cyclotron wave system in 1991. The concept is possible over the frequency range of 15-80 MHz and within the constraints of ITER[4.5-1]. The whole metal antenna system can be thus formed compactly inside the cryostat by using the concept of locally-supporting coaxial lines by the ridged waveguide of short-length. In 1992, a quarter-scale model for such a ceramics-free antenna feeder concept for ITER was manufactured. Electric characteristics, especially power reflection at the connection

between the coaxial transmission line and the ridged waveguide will be tested by the realistic model.

For the vacuum window between the torus and the transmission lines in the LHRF system, a geometrical design at the vacuum window and a thermal analysis of the vacuum windows were done. Concerning the replacement of vacuum window by the remote handling, the construction is composed of 4 ceramics modules, each ceramic module consisting of 12 vacuum windows. The main parameters of the vacuum window, which is called a "pillbox window", are as follows:

- 1) the linked waveguide : WR-187 (47.55 X 22.15 mm)
- 2) the pillbox size : Length = 96.2 mm, Radius = 44.0 mm
- 3) the ceramics : BeO ($\epsilon_r = 6.7$), Width = 3.0 mm,
 $\tan\delta = 1.64 \times 10^{-3}$

It is found that this window can withstand the heat load and the thermal stress due to RF power of 1MW,CW within the $\tan\delta$ value of 1.64×10^{-3} by cooling the edge of the ceramics.

Reference

[4.5-1] H.Kimura et al., Proc. Europhysics Topical Conference on RF Heating and Current Drive of Fusion Devices (Brussel, 1992), EPS, Vol. 16E, 41 (1992)

5. Tritium Technology

Major progress on the development of fusion fuel technology was the successful, extended operation of the Tritium Systems Test Assembly (TSTA) at the Los Alamos National Laboratory (LANL), conducted for 25 days, with the Japanese-made plasma exhaust process J-FCU (JAERI Fuel Cleanup), US-FCU and the ISS (isotope separation system). The Annex IV collaboration was completed and extended for 2 years. In the TPL, studies on plasma exhaust processing, thermal diffusion columns, cryogenic distillation, implantation-driven permeation, and tritium recovery from a solid breeder blanket were continued. Development on a new type of tritium containment system was initiated using a polyimide membrane. The new tritium transport containers based on ZrCo were fabricated and tested. Safety analysis and the procedure to obtain license for international transportation with them were continued. Facility of the Tritium Process Laboratory was operated safely. Design studies were performed on the blanket and ITER tritium systems.

5.1 Development of tritium processing technology under US-Japan collaboration

Joint operation of TSTA at LANL under Annex IV completed the original 5-year collaborative program and was extended for two years for further studies on the development of the fusion fuel cycle. The most significant accomplishment in this year was the extended loop run that involved the continuous operation of a simulated fusion fuel loop for 25 days. Continuous processing of simulated plasma exhaust (DT and H mixture, He, CH₄ and N₂) was successfully demonstrated. Impurity processing was tested by two different techniques. US developed Fuel Cleanup System (FCU) purifies DT by cryogenic molecular sieve beds and decomposes tritiated water by Magnesium beds. Japanese developed J-FCU is based on purification by permeation through a palladium alloy membrane and vapor electrolysis with a ceramic electrolyte cell. Both separated impurity elements and recovered hydrogen isotopes as expected. Figure V.5-1 shows the permeation ratio of hydrogen isotopes through the palladium diffuser, that provided pure hydrogen to the ISS in the run. The diffuser was stably operated

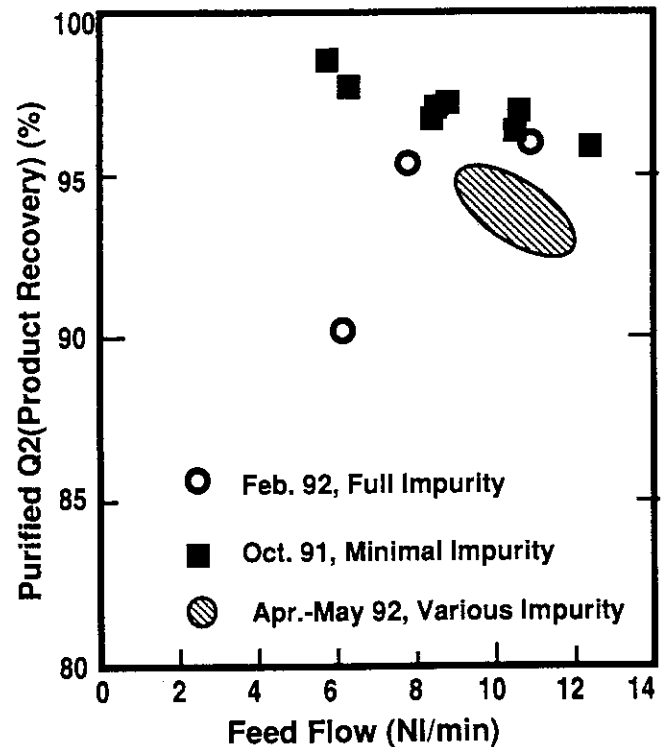


Fig. V.5-1 Permeation ratio of hydrogen isotopes through palladium diffuser in the J-FCU.

with more than 6 liter/min, which is the design capacity and 1/5 of ITER equivalent.

The isotope Separation System was stably operated with four interlinked columns and continuously produced pure tritium and deuterium stream while exhausting protium impurity. Real-time analysis in the ISS process was demonstrated with the laser Raman Spectroscopy. Mean hydrogen isotope composition during the run was about H:D:T = 1:7:2 with ~100 grams of

tritium. The processing throughput of ~6 liter/min was equivalent to approximately 1/5 of ITER.

All safety systems worked effectively and no significant tritium release from the TSTA was observed. All the tritium used in the test was corrected and accounted for. About 12 grams of tritium of >99.7% purity was off-loaded. The result demonstrated the safe and stable operation of the reactor-scale fusion fuel loop in a steady state.

The major purpose of the study under the extension is to study non-steady operation of the fuel cycle to interface with more realistic tokamaks, and to test some configurations for recovery of tritium from the breeding blanket (Breeding Blanket Interface, BBI). The cryogenic distillation column in the Isotope Separation System was modified for this purpose to include side cut stream for recycle in order to improve separation characteristic. Cold molecular sieve beds in the FCU were tested to study the feasibility of this component for recovery of low partial pressure tritium in the helium stream as a part of the BBI. Figure V.5-2 is a typical break-through curve of the hydrogen through the cold molecular sieve bed in the FCU. The result suggests that this technique is feasible and attractive for the purpose of tritium recovery from the breeding blanket.

The tritium testing of the oil-free roughing pump developed by JAERI continued. We have already pointed out that some of the oil-free vacuum pumps do not work well with light gas species such as hydrogen or helium. As shown in the figure V.5-3, different pumping characteristics were observed for each species of gas, and the behavior of tritium was similar to that for helium.

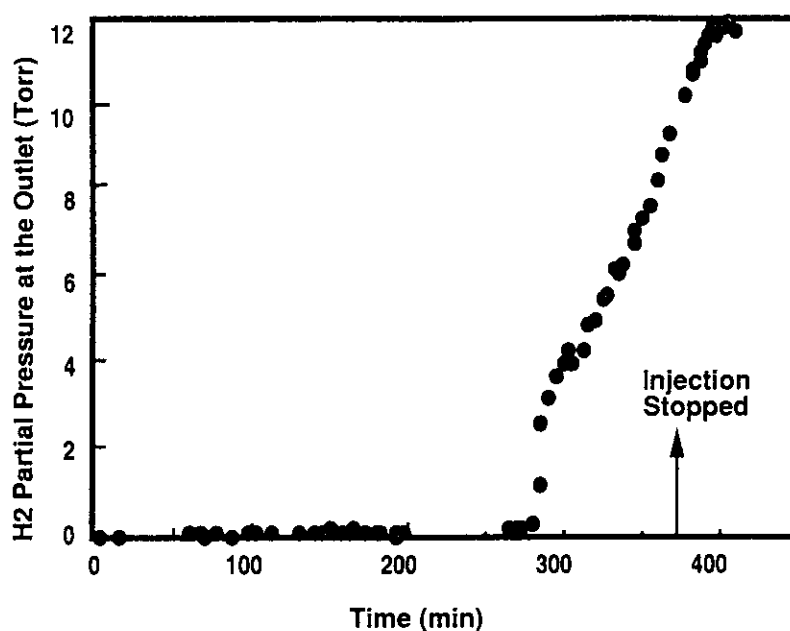


Fig. V.5-2 Break-through curve of the hydrogen through the cold molecular sieve bed in the FCU.

5.2 Development of tritium processing technology in TPL

In the TPL, experiments on plasma exhaust processing, cryogenic distillation, thermal diffusion columns, tritium analysis and measurement of tritium-materials interaction were performed.

The fuel clean up system (FCU) experiment was continued on a new process configuration to handle the tritiated impurities in the batch process and to minimize the generation of tritiated water. This process utilizes a ceramic electrolysis cell to decompose tritiated water vapor in the plasma exhaust, and the produced hydrogen is continuously removed by the palladium diffuser. This configuration will be particularly suitable for the relatively small amount of tritium processing assumed for early operation of ITER and other DT-operated tokamaks.

Experimental studies for cryogenic distillation have been continued with the H-D-T system (1.5 g of tritium). One of the significant achievements was the interfacing of this system with the FCU. A ZrCo bed that stores the HDT mixture for the distillation experiment was regenerated, and the gas was transferred to the FCU and thermal diffusion column experiment for accounting and analysis. This operation was the first integrated operation at the TPL to simulate the fusion fuel processing loop and actual accounting of tritium.

To establish system control and tritium inventory accounting in fusion fuel processing systems, development of a real time and in-situ process gas analyzer using laser Raman

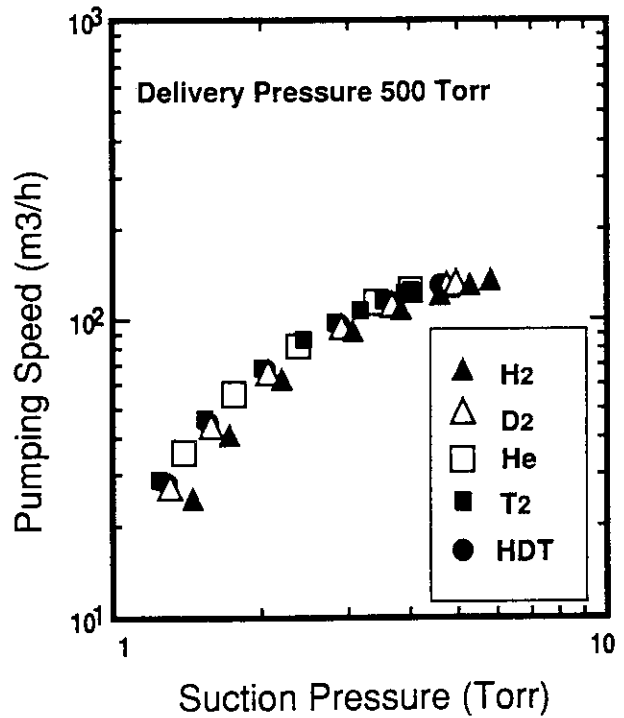


Fig. V.5-3 Pumping characteristics of the oil-free vacuum pump

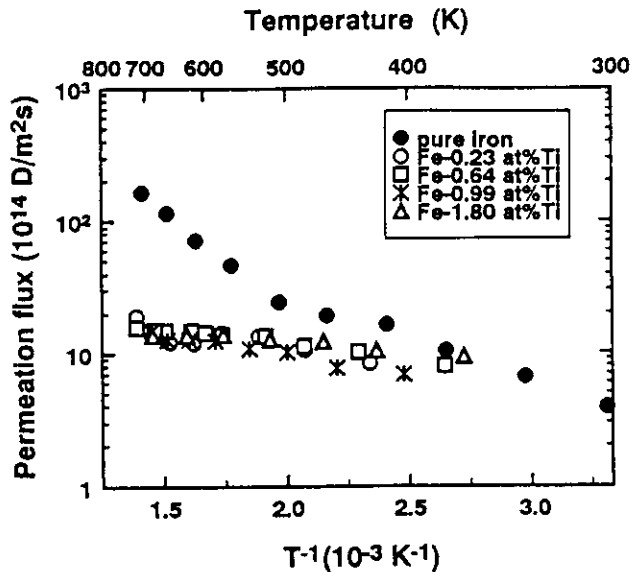


Fig. V.5-4 Permeation of deuterium ion injected at 300eV

spectroscopy was continued with a tritium-CO mixture.

Permeation of hydrogen isotopes through metals were measured with a deuterium beam. Stainless steel, titanium, iron, Fe-Ti alloy, palladium etc. were tested and the results were summarized. Figure V.5-4 shows the comparison of the permeation of deuterium ion with the incident energy at 300eV through pure iron and a Fe-Ti alloy. While permeation through pure iron was observed even at room temperature, the Fe-Ti alloy showed no permeation at room temperature, and the temperature dependence of the permeation flux was small. This can be understood this way: the deuterium was trapped by titanium in the alloy, and the permeation phenomena was controlled by the recombination process at both surfaces of the metal membrane.

5.3 Tritium system design and analysis

Numerical simulation studies on the cryogenic distillation columns were continued on the configuration with recycled flow from a side cut stream. Application for the recovery of tritium from the breeding blanket that includes a relatively small concentration of tritium in the protium was also studied.

The fuel cycle for ITER was designed and studied from the aspect of tritium accounting and inventory control. The result suggested that the ITER fuel cycle should be considered and improved if the inventory control is to be a major issue.

5.4 Development of tritium handling technology

5.4.1 Development of compact tritium confinement system

In order to establish a compact and cost-effective tritium confinement system, a new system using a gas separation membrane has been studied at TPL. Feasibility tests have been carried out using a polyimide hollow-filament membrane, which has selective permeability of hydrogen gas and water vapor. The result showed that 1) the gas separation membrane system could reduce processing volume of tritium-contaminated gas to two orders of magnitude compared with the conventional system, and that 2) most of tritiated water vapor could be directly recovered by a water trap installed just behind the membrane. In order to investigate more detailed characteristics of several gas separation plane membranes and hollow-filament modules, an experimental apparatus was installed and some experiments were initiated.

In a typical tritium monitoring system for the gloveboxes in TPL, an ion chamber was installed outside of the glovebox with a circulation pump and long piping. The monitoring function works well; however, there are some difficulties for maintenance of pumps etc. and for tritium memory in the long piping. Therefore, TPL has developed a nude type tritium monitor as a prototype. Characteristics of this nude type tritium monitor were investigated in the glovebox and compared with the original monitor. A good linearity was obtained between the current

detected by the nude type ion chamber and the tritium concentration of the original monitor.

5.4.2 Development of metal getter (ZrCo) type transport package of tritium

A tritium transport package (TPL-92Y-450K) has been designed and developed. The maximum tritium transport ability of this package is 25 g as a form of ZrCo tritide. During last year, the demonstration tests were completed under the accident test condition regulated by IAEA. Using these test results, a safety analysis report was summarized this year and submitted to STA-Japan and Canada with an official application to obtain the approval of this package.

5.4.3 Other related research and development

An oil-free reciprocating vacuum pump has been developed for various use in tritium service. In order to obtain good ultimate pressure, a prototype pump with electromagnetic valves was fabricated and tested. Figure V.5-5 shows a comparison of evacuation performances between this electromagnetic valve type and the original check valve type. The results showed that the ultimate pressure of this electromagnetic valve pump was improved about one order of magnitude. Therefore, the good combination of electromagnetic valve pump and drag pump was demonstrated without any performance loss.

As a part of a long-term reliability test for ZrCo tritide, the release behavior of decay helium (^3He) from ZrCo tritide has been investigated for three years by the application of radio-gas chromatography. The ^3He release fractions were less than 3 % and almost constant over 2 years. In the 3rd year, however, the increase of ^3He release fractions of more than 15 % was observed under operating temperatures 293K and 423 K, an initial atom-mole tritium to compound (T/ZrCo) ratio of 1.4, and one hydrogenation-dehydrogenation cycles before tritiation. The result shows that ZrCo tritide retains large quantities of ^3He in the solid phase just like other metal tritides (uranium, titanium, erbium etc.), and that the ^3He capacity in ZrCo tritide was more than 0.15 as a ratio of ^3He and ZrCo ($^3\text{He}/\text{ZrCo}$). This $^3\text{He}/\text{ZrCo}$ ratio of 0.15, where the increase of ^3He release fraction was observed, almost corresponds to the $^3\text{He}/\text{U}$ ratio when the rapid release of ^3He was also reported from uranium tritide (UT_3). The initial small release fraction of ^3He from ZrCo tritide would be caused by the recoil emission due to the tritium

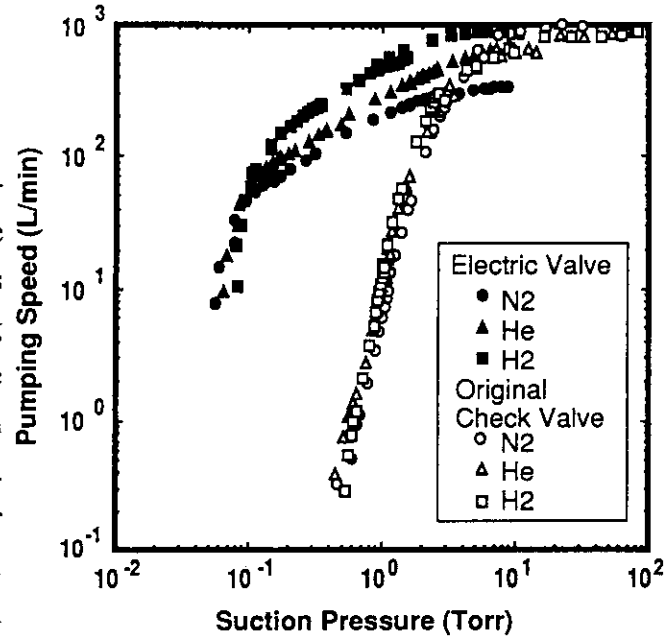


Fig.V.5-5 Comparison of pumping speed between electromagnetic valve and original check valve in the oil-free reciprocating pump

decay.

5.4.4 Operation of tritium safety systems

The safety systems of TPL were fully in tritium service without any off-normal tritium release. The operation of the Glovebox gas Purification System (GPS) was carried out for 7,200 hrs. The processing of tritium contaminated gases was performed by the Effluent tritium Removal System (ERS) for 1,250 m³ and by the Air Cleanup System (ACS) for 38,500 m³. The regeneration of molecular sieve beds and the maintenances for the above systems were also carried out safely. Figure V.5-6 shows the monthly tritium release amount from the stack at TPL in FY 1992. The total released tritium from the stack at TPL was less than 0.2 Ci.

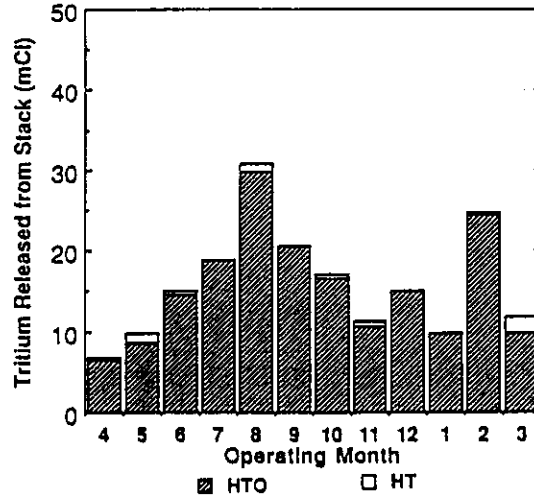


Fig.V.5-6 Monthly release of tritium from TPL

6. High heat flux technology

6.1 Introduction

Next step fusion devices such as the International Thermonuclear Experimental Reactor (ITER) will produce a nuclear fusion power of over 1000 MW. These fusion power will be finally absorbed by plasma facing components (PFCs) which will directly face the reactor plasmas. The development of the plasma facing components has been one of the key issues of ITER. The plasma facing components consists of two major parts; the divertor plate and the first wall. JAERI has extensively been conducting the development of PFCs.

In FY 1992, we successfully developed divertor elements that could endure a heat load of 20 MW/m² for 30 s for over 1000 thermal cycles, whose heat flux exceeds that of ITER conditions. This is the world record. As part of the extended R&D, divertor mock-ups in length of 1 m were also fabricated and tested, which was the first trial in the world. Preliminary results show that the deformation of the mock-ups agrees well with numerical predictions. Research and development on the plasma facing components in JAERI has greatly progressed in FY 1992.

6.2 Activities on divertor plate development

6.2.1 Development of divertor elements

Design conditions of the ITER divertor plate is as follows;

- (1) Heat loads should be 15 ~ 30 MW/m², steady state with one-side heating.
- (2) The surface of the divertor plate should be covered with low-Z armor materials such as carbon based materials.
- (3) In the case of carbon based materials, the surface temperature of the armor should be around 1000 °C, and the thickness of an armor tile should be over 1 cm.

Carbon fiber reinforced carbon composite (CFC) materials have been selected for the armor materials based on successful operations in present tokamaks. Satisfying conditions (1) and (2), the armor tile should be brazed onto a cooling structure to obtain a good thermal contact. Therefore the development of joining technology between the armor materials and the cooling structure has been one of the most important R&D issues. We developed a new braze interface geometry that can produce low residual stresses, which is shown in Figure V.6.2-1. The divertor element with an armor tile thickness of 1 cm was fabricated

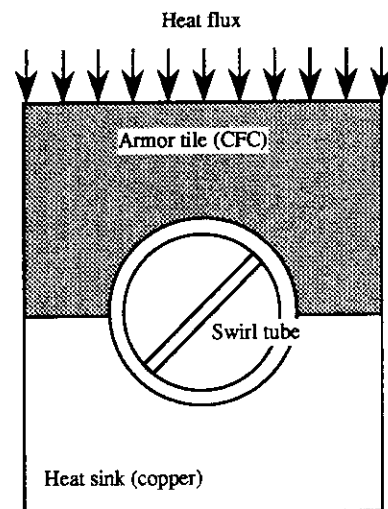


Figure V.6.2-1 Cross section of a new braze interface geometry

and tested in the electron beam test facility, JEBIS. The element tested successfully endured a deposited surface heat load of 20 MW/m^2 for 30 s for over 1000 thermal cycles [6.2-1]. No cracks and defects were found in the armor and the braze interface after the tests. The surface temperature of the element showed around $1000 \text{ }^\circ\text{C}$. This divertor element was the first element in the world that could fully satisfy the ITER design conditions.

Comprehensive surveys on materials combinations have also been made for reducing the residual stresses. We found that the combination of high thermal conductivity 1-D CFCs and W-Cu pseudo alloys would be preferable for reducing the residual stresses. Braze trials on this material combination have been made and tested in JEBIS. The 1-D CFCs brazed onto the W-Cu pseudo alloys show no defect at the braze interface after the heating tests. Based on these promising results, divertor elements with the new material combination were fabricated.

Out of above activities, international collaborations have successfully been performed. A divertor element prepared by the NET Team was tested in JEBIS.

6.2.2 Development of 1 m long divertor plate

Since the divertor plate of ITER will be over 3 m in length, it will become quite important to reduce the deformation of the divertor plate. To develop the support structure of the divertor plate which can reduce the deformation, 1 m long divertor plates with the support structure were fabricated and tested in JEBIS. The support structures developed are as follows; a rail sliding support, a pin sliding support. The deformations of both support structures show good agreement with numerical predictions.

6.2.3 Heat removal technology

Since the divertor plate is heated from the plasma, it is necessary to establish heat transfer correlations for one-side heating conditions. The existing heat transfer correlations, however, have been obtained in a uniformly heated condition, and few correlations are available for the one-side heating conditions [6.2-2]. To establish the heat transfer correlations under one-side heating conditions, small heat transfer test pieces have been manufactured, as shown in Figure V.6.2-2, and tested in the ion beam

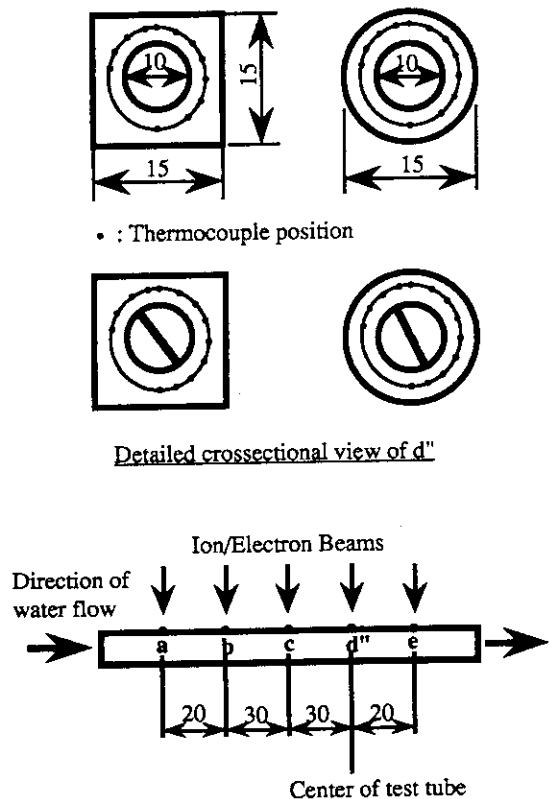


Figure V.6.2-2 Heat transfer test pieces

test facility, PBEF [6.2-3]. The tests have already been performed and the data is under analyses.

Critical heat flux (CHF) experiments were carried out at Sandia National Laboratories in the US to see the effects of the inlet coolant temperature on CHF.

References

- [6.2-1] H. Tsuji, M. Akiba, E. Tada, et al., Proc. of IAEA 1992
 [6.2-2] M. Araki, M. Ogawa, M. Akiba, et al., proc. of Fusion Technol., 21 (1992)1835-1839
 [6.2-3] S. Ikeda, M. Araki, M. Ogawa, et al., JAERI-M 93-070

6.3 Development of first wall

6.3.1 Development of first wall element

Since the ITER first wall should endure a heat flux of 0.6 MW/m^2 , the development of an attachment structure of the armor tile has been extensively conducted in JAERI. A newly designed tile attachment structure with a ceramic bolt was fabricated and tested in JEBIS. The new attachment structure could successfully endure a heat flux of 0.7 MW/m^2 . Even after continuous irradiation for 30 minutes, no serious damage was observed.

6.3.2 Development of first wall mock-ups

The first wall is made of stainless steel and has rectangle cooling channels. A Hot Isostatic Press (HIP) technique is one of the promising technologies for the fabrication of the first wall. JAERI has been developing the HIP technique for the first wall.

The HIP technique for fabricating a curved first wall mock-up was developed in FY 1992. The technique developed could successfully fabricate the first wall mock-up with a curvature radius of 40 mm.

6.4 Study of plasma surface interaction

The surface of the plasma facing components are subjected to ion sputtering and a heat load during plasma disruptions. The evaluation of erosion losses induced by these loads is critical for estimating the lifetime of the armor tiles. JAERI has been studying the plasma surface interaction in a sputtering test stand and in the electron beam test facility, JEBIS [6.4-1,2].

In the study of sputtering losses, most of our efforts this year concentrated on modifying the ion source to obtain higher ion beam fluxes at a low beam energy level. The new ion source resulted in an ion flux of about $10^{17} \text{ ions/cm}^2\cdot\text{s}$ at an energy level of 1000 V, which was one order higher than the old one. The development of a heating machine was also carried out, which could heat up test pieces up to $1500 \text{ }^\circ\text{C}$ for obtaining the sputtering yield at high temperature.

In the study of erosion losses induced by plasma disruption heat loads, the effects of a number of disruptions on the erosion loss have been investigated. The disruption heat loads were simulated by a short pulse electron beam produced in JEBIS. The erosion loss after 10 shots was

about one-half times smaller than that obtained in the single electron beam shot. This may be explained by the fact that particle emission caused by residual gases in the test sample becomes smaller because of the reduction in residual gases in the sample after 10 shots.

The disruption simulation experiments in a plasma gun facility were carried out at the University of New Mexico in the US. Preliminary data showed that the erosion loss in the plasma gun facility was about 10 times smaller than that in JEBIS, which may be caused by the vapor shielding effect.

References

- [6.4-1] K.Nakamura, M. Akiba, S. Suzuki, et al., Journal of Nuclear Materials 196-198(1992)627-632
- [6.4-2] M.Akiba, M.Araki, S.Suzuki, et al., Journal of Nuclear Materials 191-194(1992)373-376

7. Reactor Structure Development

7.1 Introduction

The reactor structure of the tokamak machine is composed of a plasma vacuum vessel, a tritium breeding blanket, a divertor system and a vacuum chamber for the superconducting magnet system. As to the next generation machine, the reactor structure components would inevitably be large scaled sizes and massive. The major task of the reactor structure R&D is to establish the manufacturing technology and the remote assembling/disassembling technology.

7.2 R&D activities for reactor structure

The vacuum vessel is a key containment structure to provide the first barrier of tritium. In addition, the vacuum vessel has to provide one-turn toroidal resistance and nuclear shielding functions, and should be sufficiently tough against the electromagnetic loads. The double walled structure reinforced by the toroidal and poloidal ribs, and the toroidally uniform resistance were employed as the most promising concept. As shown in Fig.V.7.2-1, the 1m x 1m sized segments with a total wall height of 300 mm and a wall thickness of 20 mm have been fabricated and tested under the internal pressure, in-plane shear, compression and bending loads. The test results show that the fabrication error due to welding can be controllable and that the double wall structure has sufficient mechanical toughness as well as a large margin for plastic yield load. On the other hand, the R&D activity of the nondestructive inspection methods for on-site welding under the radiation condition (10^7 R/h) has been started. Qualification tests to detect standard cracks initiated in the thick stainless steel samples(base metal and weldments) were carried out by using the ultrasonic and eddy current inspection systems.

A hydro-driven cotter system was selected and designed as the locking mechanism for supporting in-vessel replaceable components. Two different types of the cotter driver have been developed, namely the piston/cylinder type for the divertor support and the metallic balloon (dilatation tube) type for the blanket support. The titanium alloy (Ti-6Al-4V) was selected for the metallic balloon material because of its excellent super plasticity. Based on the successful results of the fabrication and driving test of the metallic balloon, a full-scaled but segmented model (1m x 1.5m x 2m) of the blanket support structure has been fabricated. On the other hand, the piston/cylinder type with a long stroke (170 mm) was also fabricated with particular attention to the selection of a material combination for the pressure ring and its guide. The cotter itself has survived 1000 operation cycles without any adhesive or abrasive wear on the cotter surface. Furthermore, a full-scaled divertor support structure was fabricated and the mechanical test was carried out to measure the locking/unlocking forces, positioning tolerance and self-locking property under seismic loads. According to the test results, the feasibility of the divertor support structure was verified.

7.3 R&D activities for remote maintenance

From the viewpoint of a maintenance scheme, all the reactor components are classified into three categories: scheduled maintenance components, unscheduled maintenance components and permanent components. The classification and the maintenance concept have been developed.

The in-vessel vehicle system was selected for the scheduled maintenance components such as plasma facing components. In the rail-mounted vehicle maintenance system, the rail is expanded sequentially and supported by four arms from the respective 90-degree horizontal ports so as to provide stable and reliable operation. The half torus model of the rail-mounted vehicle system of one-fifth scale was manufactured. Feasibility of this concept(especially the transfer of rail to and from the vacuum vessel) was confirmed. Furthermore, we have designed and fabricated a full-sized model of a divertor handling manipulator with telescopic arm and rotational mechanism, which is a key component of system as shown in Fig.V.7.3-1. The loading test using the full-sized manipulator model was carried out, and we have confirmed the design specifications which are the payload capacity of 1.2ton and the operating area to handle the upper and lower divertor plates. As the next step, the full scaled divertor assembling test shall be carried out by using this apparatus and full-scaled divertor support structure mentioned in former chapter.

Concerning the unscheduled maintenance component, the tritium breeding blanket is the largest (15 m) and the heaviest (80 ton) among the in-vessel components. We have conducted a conceptual design of the blanket handling system, which consist of stiffness rink. The blanket handling in narrow space has been successfully demonstrated with computer posture control by a one-fifth scale,twin manipulator system .

As a widely common technology, the welding and cutting procedures for the cooling pipes of the in-vessel replaceable components should be established. The internal-access concept for welding/cutting pipes was employed because of the closeness of the pipes. The welding /cutting head with CO₂ laser beam, which consists in a vehicle mounted with a traveling mechanism along the pipe and a focusing lens, has been manufactured and applied to a 200A(Sch40) SUS pipe. The feasibility of this concept has been demonstrated.

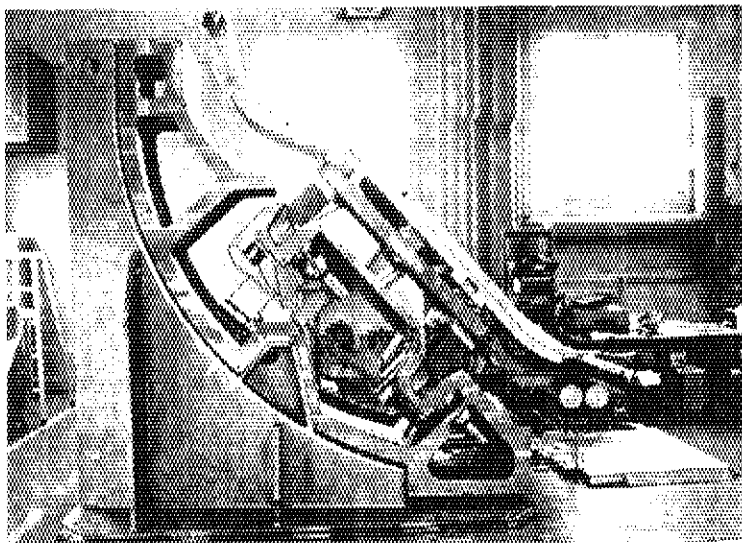


Fig.V.7.2-1 Full scaled model of divertor support structure system

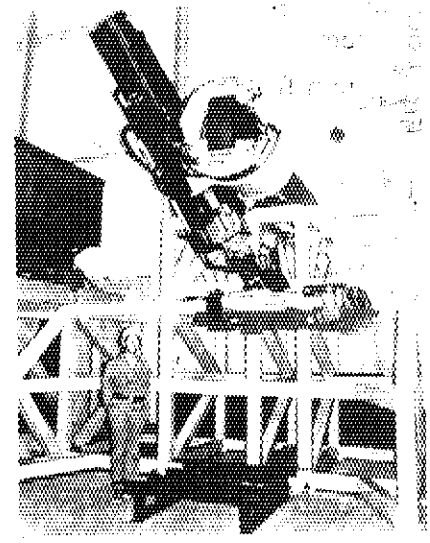


Fig.V.7.3-1 Full scaled model of divertor handling vehicle

8. Blanket Technology

8.1 Introduction

The blanket is a component which generates tritium as the fuel gas of a thermonuclear reaction, and changes the kinetic energy of neutrons to thermal energy. It is one of the key components for energy-producing fusion reactors. In experimental reactors, the blanket is mainly utilized for tritium breeding, while DEMO reactor blankets must fulfill the above functions.

In this fiscal year, R&D efforts were mainly focused on preliminary material development and out-of-reactor tests due to the delay of ITER/EDA. A partial 1/2 scaled mockup of the outboard blanket box structure was successfully fabricated by trial, and an engineering data base was accumulated for the fabrication procedure by HIP process.

A new building of the blanket out-of-reactor testing was completed, and a number of test apparatus were transported from the Tritium Processing Lab. and installed in this building. A blanket loop test facility was partially constructed, and is to be continued and completed in the next fiscal year. A set of material handling apparatus, composed of hoods and related ventilation systems, was also newly constructed for applications to blanket material testing.

Design work has been also continued on the layered pebble bed solid breeder concept, on the shielding blanket concept made of steel and water, and on the DEMO blanket concept. For in-reactor tests, design efforts for in-reactor mockups and consideration of test facilities have been continued, assuming JMTR to be an irradiation reactor.

8.2 Fabrication of the blanket box structure integrated with first wall [8.2-1]

The blanket structure integrated with first wall and shield was also investigated for a fusion experimental reactor. The blanket is divided into modules from the assembly/maintenance point of view, and the size of each module is over 10 m high and about 1 m wide. A fabrication accuracy on the order of 10 mm is required for the remote assembling scheme. The box wall has a thickness of 15 mm for the first wall and 30 mm for the side wall to withstand the enormous electromagnetic load (about 10 MN/m). The first wall must have cooling channels in it to remove nuclear heating (about 15 MW/m³) and surface heat (about 0.2 MW/m²). We adopted an advanced technique for the fabrication of the first

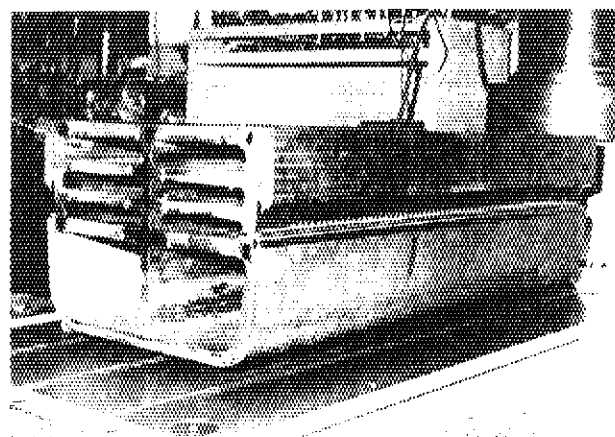


Fig.V.8.2-1. Appearance of partial 1/2 scaled mockup of blanket/first wall box structure made by HIP after welding rear wall (~1m height, ~0.5m width, ~0.4m thickness)

wall-panel, i.e. diffusion bonding of rectangular tubes with two flat plates by HIP (Hot Isostatic Pressing) bonding. It has the advantages of small deformation, small residual stress and good physical and mechanical properties similar to the base metal. We fabricated a 1/2-scale partial mock-up for the outboard side-module near the midplane without the internal structure of the breeding region, to demonstrate the feasibility of the fabrication technique (including the advanced procedure described above).

The fabricated mock-up is shown in Fig.V.8.2-1. The structural material is 316SS, and the mock-up has a dimension of 1000 mm (height in the poloidal direction) x 480 mm (width of the first wall in the toroidal direction) x 355 mm (thickness from the first wall to the back wall). In addition to the HIP bonding, EB and TIG weldings were adopted to join the center rib, the partitioning plates, the side walls and the back wall with the first wall-panel, and the overall fabrication procedure was demonstrated.

Together with the above trial fabrication of a 1/2-scale partial mockup of the outboard blanket box structure, improvement in the fabrication procedure of the HIP process was tried using small-scale partial specimen, as shown in Fig.V.8.2-2. Specimens (1) and (2) are the sandwiching rectangular channels for the first wall composed of two flat plates with 3 mm and 7 mm thick. Specimens (3) and (4) are for the side wall, made of two flat plates with 3 mm and 22 mm thick. In the case of the specimens (1) and (3), smooth-faced type flat plates were applied, while corrugated type flat plates were used for the bonding surface of the flat plates in the case of the specimens (2) and (4). As shown in Fig.V.8.2-2, it was found that the deformation by the HIP process was reduced drastically by using the corrugated type.

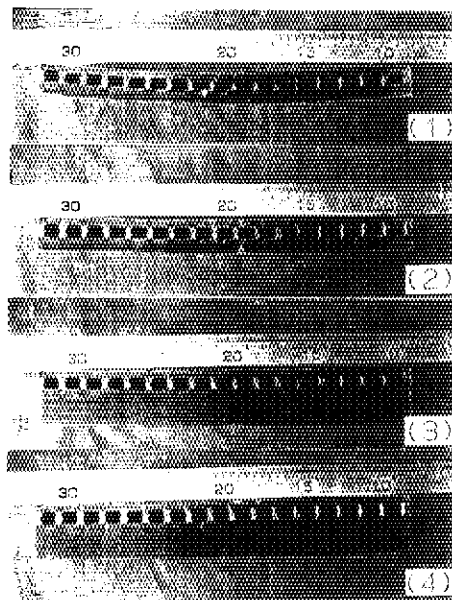


Fig.V.8.2-2. Appearance of small scaled partial specimens made by HIP

Through the trial fabrication study, the following results were obtained:

- (1) The practical fabrication data such as welding deformation were obtained to apply HIP, EBW and TIG to the fabrication of the box. The deformation during the HIP process can be reduced drastically by choosing the optimal configuration and using a jig for restricting deformation.
- (2) The feasibility of fabrication technologies was successfully demonstrated for a 1 m-scale box structure, including the first wall-panel with cooling channels by means of HIP, EBW and TIG. Further R&D is required for fabricating a 10 m-scale box structure, including the development of a poloidal joining technique and a non-destructive test method.

References

[8.2-1] T.Hashimoto et al., to be published as JAERI-M (1993)

8.3 Out-of-reactor testing

8.3.1 Installation of blanket cooling water test loop

A new building for the blanket out-of-reactor testing was completed in December 1992. The new building has three rooms, which are to be used for basic engineering tests, for basic material tests and for medium-scale blanket loop tests. After the completion of the building, three kinds of test apparatuses were transported and installed: the effective thermal conductivity measurement apparatus, the blanket pebble packing test apparatus and the cooling water distribution test apparatus. A 50 kW class cooling water loop was installed as part of the medium scale blanket loop test facility. A newly-installed cooling water loop enabled to perform the heat removal during various tests of a medium-scale blanket mockup unit, and also can be utilized to test the coolant flow rate distribution effect on the heat removal from the blanket. A set of hoods and related ventilation systems were also newly installed in the basic material test room for various blanket material tests.

8.3.2 Measurement of effective thermal conductivity of beryllium sphere packed bed

The detailed structure and dimension of the blanket should be designed to meet acceptable temperature ranges of each material in the blanket, based on the measured physical properties of the real materials. The effective thermal conductivity of Be sphere packed beds is one of the most important physical properties of the thermal design of the pebble-layered blanket. From this view point, the effective thermal conductivity of the packed beds was measured with Be spheres, whose diameter is about 1 mm to 3 mm.

Measurement of the effective thermal conductivity was performed using a cylindrical test cell whose diameter was about 100 mm. The test cell has a cooling tube at the center and was heated from outside by an infrared image furnace up to an average bed temperature of about 500°C. The net amount of sphere used for the measurement was about 2000 cm³. Helium gas was used as the purge gas. Water or air was used as a coolant. The Be sphere was fabricated by a rotating electrode method. Also, the intermediate-product Be sphere with 2 and 3 mm diameter was applied for the thermal conductivity measurement of packed beds.

The temperature and sphere diameter dependence on the effective thermal conductivity was measured in a stagnant He atmosphere. Although the measured dependencies were qualitatively the same as expected by the modified Schlunder's model, the values of 2.2, 2.6 and 2.8 W/mK at 300°C for 1, 2 and 3 mm diameter were almost halves of the expected values. This may be attributed to heat loss in the axial direction and a packing fraction variation from 55% to 50% during each measurement run. Further experiments and analysis are planned to examine the above discrepancy between expected and experimental values.

8.3.3 Durability tests of Lithium breeder under rapid thermal cycling

Ceramic breeders are to serve in a severe thermal cycle for the pulsed operation of the fusion experimental reactor. A lithium ceramic breeder is necessary to keep initial integrity under such an operation condition. In order to get the data base, thermal cycling durability tests of lithium ceramic were conducted in the temperature range between 200 and 800°C and up to 5000 cycles at a rate of 800 seconds per cycle. The measured fracture ratio of lithium ceramics after the thermal cycling test is shown in Fig.V.8.3-1.

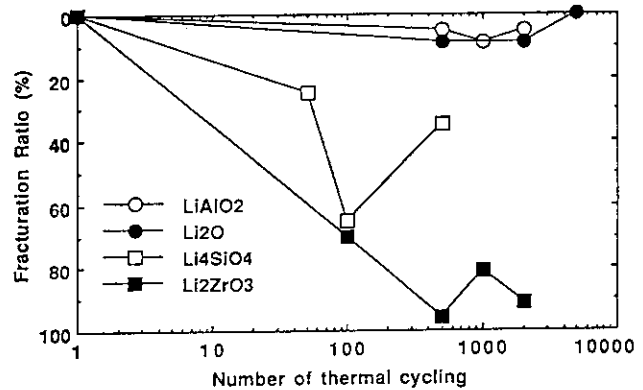


Fig.V.8.3-1. Measured fracture ratio of lithium ceramics after thermal cycling test

In the examined lithium ceramics, Li₂O and LiAlO₂ showed good durability up to 5000 cycles. Li₂ZrO₃ and Li₄SiO₄ showed granulation with thermal cycle operation. This kind of test generally depends on the fabrication method and processing, and further examination will be required.

8.4 Design of tritium breeding blanket

An analytical study was continued to refine the layered pebble bed blanket [8.4.1] proposed for ITER. Steady-state and transient thermo-mechanical analyses were performed with a finite element code to investigate the mechanical integrity of the blanket box structure against thermal stress during normal operation, loss-of-flow accident (LOFA), and maintenance. Two-dimensional neutronics and thermal analyses were performed to examine the spatial temperature distribution in breeder and multiplier pebble bed zones.

The fabrication and assembly process for the blanket box structure were studied. Poloidal segmentation of the blanket module was considered taking the capacity of the available hot isostatic pressing (HIP) device into account. The fabrication feasibility of the side wall and the top/bottom wall was examined, considering the arrangement of coolant paths in the walls and the position of coolant plenums. The present status of the welding technology, such as electron beam welding and laser welding, was investigated to clarify the applicability of that technology to poloidal joining of the segmented units into the integrated module.

A design study of the DEMO blanket was also performed. Two kinds of blankets (a pin-type concept [i.e. breeder-in-tube type] and a tube-in-shell concept [breeder-out-of-tube type]) were studied, keeping the DEMO reactor such as SSTR in mind. A preliminary conceptual design of the ITER blanket test modules, which correspond to the above two DEMO blanket concepts, was performed, and basic blanket performances were evaluated.

The mechanical design of a non-breeding shield blanket, which is considered as an alternative to a breeding blanket, was performed. The mechanical strength of the blanket box structure was examined and fixing methods of the shielding material (i.e. steel panel) were proposed.

References

[8.4.1] H. Takatsu et al., Layered Pebble Bed Concept for ITER Breeding Blanket, Proceeding of 17th SOFT Rome, 1504-1508, (1992)

VI. INTERNATIONAL THERMONUCLEAR EXPERIMENTAL REACTOR (ITER)

1. Introduction

The ITER Engineering Design Activities (EDA) Agreement and Protocol 1 were signed on July 21, 1992 by the four Parties, the European Atomic Energy Community, the Government of Japan, the Government of the Russian Federation and the Government of the United States of America. With the signing and the designations of ITER Council members, the IAEA Director General declared that ITER EDA had begun.

The overall programmatic objective of ITER, which shall guide the EDA, is to demonstrate the scientific and technological feasibility of fusion energy of peaceful purposes. In accordance with the ITER EDA Agreement, the four parties shall conduct jointly the EDA to produce a detailed, complete, and fully integrated engineering design of ITER and all technical data necessary for future decisions on the construction of ITER. The EDA, being conducted under the auspices of the International Atomic Energy Agency (IAEA), will have a duration of six years.

The organization prescribed by the ITER EDA Agreement for this purpose is outlined in Fig.VI.1.1. The ITER Council has responsibility for the overall direction of the EDA and exercises overall supervision of its execution. At the first meeting the Council elected Dr. E.P. Vellikhov as Chairman and Dr. M. Yoshikawa as Co-Chairman of the Council. The ITER Director shall direct and

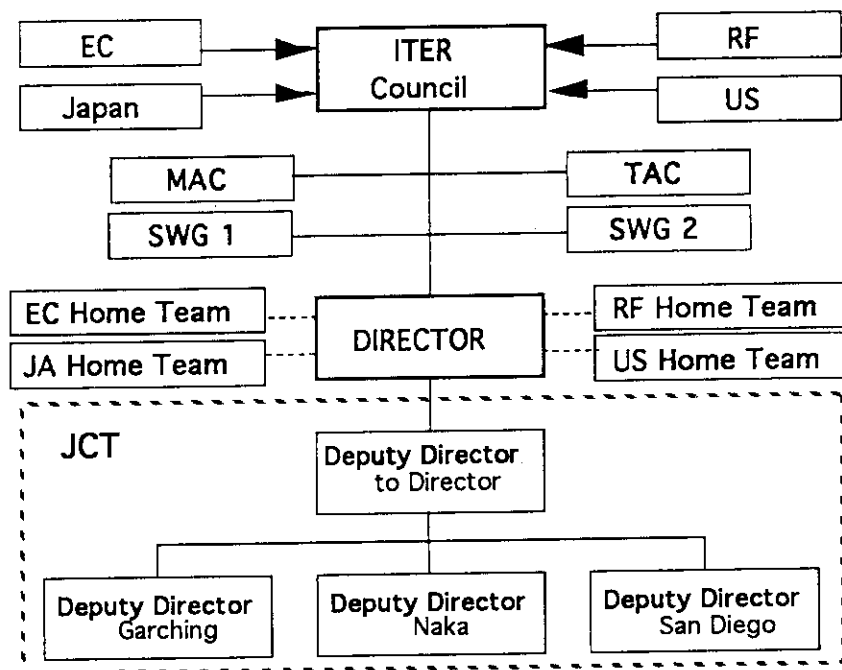


Fig.VI.1.1 ITER EDA Organization

coordinate the performance of all activities pertinent to the EDA and organize, direct and supervise the Joint Central Team. Dr. P.H. Rebut was appointed as Director by the Council.

The Technical Advisory Committee (TAC) shall, upon request by the Council, advise it on technical matters and perform such other tasks as the Council may request it to undertake. The Council designated Dr. P. Rutherford as Chairman of the TAC. The Management Advisory Committee (MAC) shall advise the Council in management and administrative matters,

including finance, personnel, and assignment of tasks to the Home Teams in appropriately equal shares and to the Joint Central Team. The council appointed Dr. M. Yoshikawa as Chairman of the MAC.

The Joint Central Team (JCT) assists the Director in the definition, direction and coordination of the performance of the engineering design activities. It also integrates all scientific and technological contributions into a coherent design. The JCT is located at the Joint Work Sites: Garching near Munich, Naka (Ibaraki), and San Diego (California). The Council agreed that the Parties should provide a total of 150 professionals to the JCT by the end of Protocol 1 (March 1994), with the buildup done as fast as possible. Home Teams, each party establishes and organizes, perform the tasks assigned to them in accordance with the EDA Work Programme.

Special Working Groups (SWGs) were established by means of the Protocols to the Agreement or by decision of the Council. They are entrusted with specific tasks which are outside the responsibilities of the Director. SWG-1 and SWG-2 were established by means of Protocol 1. SWG-1, based on the Conceptual Design Report, reviews the detailed technical objectives along with technical approaches including appropriate safety margins to determine the best practicable way to achieve the programmatic objectives of ITER. The results of the review should be compatible with the aim of maintaining the cost of the device within the limits comparable to those indicated in the final report of ITER CDA, as well as keeping its impact in the long-range fusion programme. SWG-2 submits guidelines for implementation of task assignments by the Home Teams to the Council for approval at its second meeting. This SWG also drafts Protocol 2 to the ITER EDA Agreement and submit a draft to the Council not later than by 21 May 1993.

2. ITER Engineering Design Activities (EDA)

2.1 Review of detailed technical objectives of ITER

SWG-1 conducted the review of the ITER Conceptual Design. As a general guideline for SWG-1, the ITER Council recommended that the reviewed technical objectives and technical approaches, including appropriate safety margins should be compatible with the aim of maintaining the cost of the device within the limits comparable to those indicated in the final report of ITER CDA, as well as keeping its impact in the long-range fusion programme.

The Group had in-depth discussions of the ITER technical objectives and approaches and the views of the ITER Parties on the critical issues of the Engineering Design. On the basis of these discussions and also taking into account the views on guidelines for ITER presented to the Group by ITER Director, SWG-1 prepared the Review Report. The Council accepted the

Review Report and the recommendations contained in it were adopted, in the second ITER Council Meeting, on 15-16 December 1992.

In this report SWG-1 recommended that ITER should:

- demonstrate controlled ignition and extended burn for a duration sufficient to achieve stationary conditions on all time-scales characteristic of plasma processes and plasma wall-interactions, and sufficient for achieving stationary conditions for nuclear testing of blanket components. This can be fulfilled by pulses with flat top duration in the range of 1000s. For testing particular blanket designs, pulses of approximately 2000s are desirable;
- aim at demonstrating steady-state operation using non-inductive current drive in reactor-relevant plasmas;
- demonstrate the availability of technologies essential for a fusion reactor;
- test components for a reactor;
- test design concepts of tritium breeding blankets relevant to the reactor. The foreseen on modules include the demonstration of a breeding capability that would lead to tritium self-sufficiency in a reactor, the extraction of high-grade heat, and electricity generation.

SWG-1 also recommended that the ITER operation should be divided into two phases:

- The first phase, the Basic Performance Phase, is expected to last a decade including a few thousand hours of DT operation. This phase should address the issues of controlled ignition, extended burn, steady-state operation and the testing of blanket modules. Function tests of blanket modules in this phase should consist of a few thousand hours of integral burn time, including continuous test campaigns of 3-6 days at a neutron wall loading of about 1MW/m².
- The second phase, the Extended Performance Phase, is also expected to last a decade, with emphasis placed on improving overall performance and carrying out a higher fluence component and material testing programme. Operation during this phase should include continuous testing campaigns lasting 1-2 weeks and should accumulate a fluence of at least 1MWa/m².

2.2 Preliminary design proposed from Director

In the Third ITER Council Meeting, held in Tokyo on 21-22 April 1993, the Council deliberated on the preliminary design proposed from the Director. The Council endorses the recommendations made by TAC, described later. In particular, it invites the Director to make all efforts to streamline the preliminary design so as to confirm for the next Council Meeting its ability to satisfy simultaneously the three conditions on cost, technical objectives and safety margins, as requested at the previous Council Meeting. In the complex problem area of first wall, blanket/shield, structure and coolant, the Council considers that the JCT should continue to evaluate a broad range of options with the aim of respecting the cost limitations.

The guiding principles followed by the Director are: (1) the flexibility associated with the long lead time before operation; (2) the reliability necessary for the operation of key systems without fault over a period of 30 years; (3) the safety required for the operation of a nuclear device; (4) the attempt to use wherever possible reactor-relevant technology. These principles translate into the design by increasing, wherever possible, the safety and technical margins, the reliability and simplicity of each component and by lowering the tritium inventory and the activation of the overall structures. Costs of the device must be commensurate with the capital cost of the other energy sources. The comparison between the CDA design and the device parameters proposed from the Director is in the following.

Table VI.2.1 Comparison of design parameters between CDA and Director's proposal

Parameters	CDA design	Director's Proposal
Major radius (m)	6.0	7.75
Minor radius (m)	2.2	2.8
Plasma current (MA)	22	25
Elongation	2.0	1.6
Burn time (s)	400	1000
Fusion power (GW)		
Normal operation	1	1.5
Extended operation	2	3

The overall design concept outlined in the Preliminary Design Report is for an ITER EDA device that is somewhat larger, overall, than the CDA device. The increase in size arises partly from the need for increased voltseconds to provide a 1000 s inductive pulse, as specified in the SWG-1 report, partly from increasing the plasma current (from 22 MA to 25 MA), and partly from maintaining confinement capability while adopting a lower, more conservative value for plasma elongation and increased allowance for impurities and helium accumulation. A partially compensating factor is an increase in the strength of the toroidal field, both at the coils and at the plasma, relative to their values in the CDA design. On the basis of empirical confinement scalings developed during the CDA, the present EDA design would have slightly more confinement capability than the CDA device.

A new design concept is presented for the toroidal field and poloidal field coils, using layer-wound cable-in-conduit conductors to allow all connections to be external to the core of the tokamak. Structurally, the toroidal-field coils and central solenoid are mutually supported against a bucking cylinder. This approach is intended to provide greater compactness, possibly at the cost of more difficult manufacturability and added complexity.

Emphasis is placed on the divertor design and the mode of divertor operation. A single-null divertor is adopted, both for simplicity and to provide the maximum space for the divertor assembly. Although the details of the mode of divertor operation are not yet provided, the

concept is for a "gaseous" divertor employing recycled gas reinjected perpendicular to the divertor channels which, in high-density operation, can "extinguish" the plasma in front of the divertor-plate, thereby distributing the power flow by radiation and charge-exchange over the entire surface area of the divertor channels. The present design concept includes the use of beryllium as the high heat-flux plasma-facing material for divertor components.

A number of options are being considered by the JCT for first-wall materials and coolants, although the evaluation of these options is not yet complete. The requirement for high-temperature bakeout and moderately-high-temperature operation of the first wall, as well as safety concerns relating to lithium compatibility, high coolant pressures and tritium permeation, have led to de-emphasis of water as the coolant, in favour of other options including liquid-metal coolants. In the presently preferred concept, lithium is used as the breeder in the blanket modules, which are cooled by tubes containing either another liquid-metal coolant or high-pressure helium gas. The first-wall, like the divertor-plate, would be beryllium-coated. The present design concept thus excludes all graphite first-wall materials, thereby eliminating a potential safety concern, reducing in-vessel tritium inventory, and improving neutron fluence capability in view of the degradation in thermal conductivity of graphites under intense neutron irradiation. Safety and environmental factors are given prominence in the design approach.

The major TAC's recommendations are summarized as follows.

Machine Parameters: The present machine parameters provide an adequate basis for further development of the ITER design at this time.

Divertor: The approaches to divertor concept development need further modeling work and extended verification on present devices.

Neutron Flux: The objective of 1 MW/m² should remain the reference design value.

Manufacture of the Coils: In regard to the keys, possible different designs for the keys should be examined with a simpler structure, e.g., having two flanges on adjacent coils with cylindrical keys between them, and having insulation fitted to machined plates before impregnation. In parallel with the present design, with the help of certain Home Teams interested in this task, the JCT should examine a completely different design with pancake windings, and select the final design following a detailed comparison of the alternatives.

Overall Concept of in-vessel components: In view of the concern that the only credible near-term solution for the shield was low-temperature water-cooled stainless steel, an R&D plan is needed to establish the scale of R&D required for more ambitious solutions.

First-Wall/Blanket/Shield: An evaluation should be made of an independent first wall. Further work is required before a choice can be made between beryllium and carbon-based materials, or other low-Z coatings, for the plasma-facing components. TAC is concerned that adequate tests should be made of proposed solutions. The JCT should continue to evaluate the full range of firstwall/blanket/shield, structure, and coolant options.

Cost: If the total cost of the presently conceived ITER that meets the objectives formulated by SWG-1 for the Basic Performance Phase, including the costs of additional equipment for the Basic Performance Phase, were to become significantly larger than that projected in the CDA, a lower-cost machine, involving reduced margin for meeting the objectives, should be considered by the Joint Central Team.

2.3 Organization of Japanese Home Team

As a government committee, the promotion and the planning of the entire fusion program will be continued by the Fusion Council of Atomic Energy Commission. The Fusion Council has recently established ITER Technical Committee which will advise on the technical matters of ITER program to the Fusion Council. Thus, the government is ready to be fully supportive of ITER for the execution of this unprecedented international collaboration.

Following the signing of the ITER EDA Agreement, the Japanese Government designated Japan Atomic Energy Research Institute (JAERI) as the implementing organization. JAERI established a new task force, named JAERI ITER Project to form a core of the Japanese Home Team, lead by Director General of Naka Research Establishment for the efficient execution of ITER tasks, as shown in Fig.VI.2.1. It consists of five teams, and each team is also subdivided into some units. The JAERI ITER Project includes Department of ITER Project, a newly organized department for EDA and Department of Fusion Engineering Research which covers most of the component necessary for ITER technology R&D. In addition there are three other establishments in JAERI to be involved in EDA, for instance, fusion

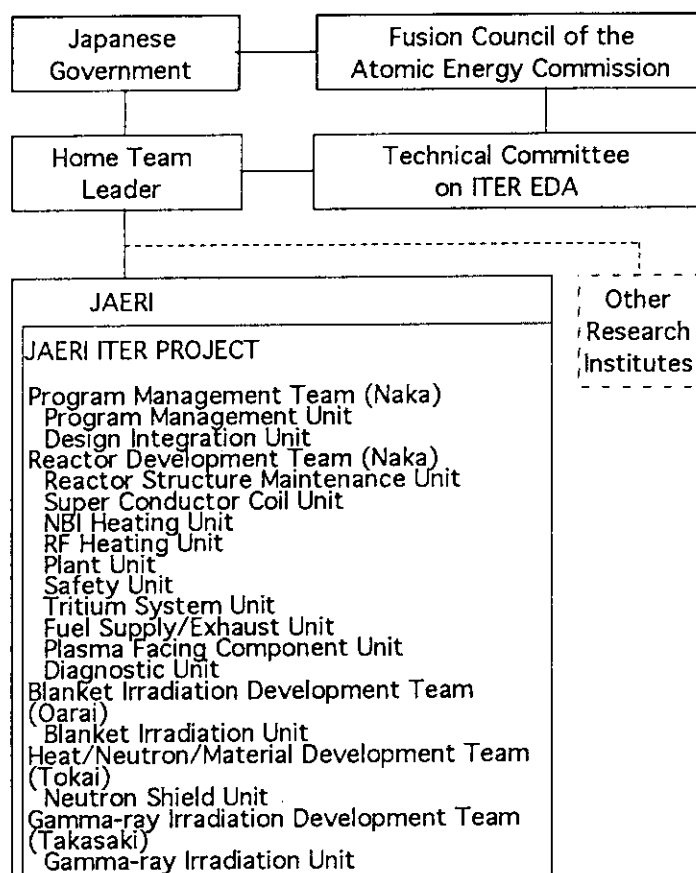


Fig. VI.2.1 Organization of Japanese Home Team

neutronics laboratory for 14 MeV neutron studies at Tokai Research Establishment, blanket irradiation and analysis laboratory for blanket development including fission reactor irradiation at Oarai Research Establishment, or gamma-ray irradiation at Takasaki Research Establishment. There will be some other units to be organized in near future. The involvement of other research

institutes is open as future possibility. The number of persons nominated as JAERI ITER Project members is about 100 and will be increased depending upon the tasks assigned to Japanese Home Team.

JAERI has been so far encouraging the participation of industries to the development of fusion research, because it has been mutually beneficial and is also expected to be quite effective in the ITER EDA. Likely participation of industries to the EDA are envisaged in the following three types. First, under the design contract with the Home Team, industries may undertake a part of the design work. Second, through the procurement contract of the ITER Technology R&D, industries can participate in the fabrication of components. Third, personnel in industries may temporarily be hired as JAERI employee through the contract of employment etc. in order to participate in the Home Team or Joint Central Team activities.

The results of the ITER Technology R&D are described in the Chapters V and VII.

VII FUSION REACTOR DESIGN

1. Introduction

Fusion reactor design and related activities are conducted to clarify the goal of fusion research, i. e. to establish attractive reactor concepts in terms of safety, environmental and economic aspects. In this chapter, the design activities on the domestic fusion experimental reactor concept FER, the DREAM Reactor concept which was derived from the basic concept of the Steady State Tokamak Reactor, SSTR and an safety analysis methodology development are introduced.

2. FER Design

In 1992, in relation to the preparation for the siting of a fusion experimental reactor in Japan, safety and environmental aspects evaluations as well as the plant system designs of FER were carried out. In the safety design study, accident sequences were selected and necessary safety devices to prevent or mitigate the propagation of the accident sequences were identified. The importance criteria of the reactor components and subsystems with regard to seismic design were studied. The conceptual studies of the reactor building, radwaste disposal facility and the primary cooling system were carried out. With regard to the reactor building, the electrically insulated iron bars were developed to prevent the corrosion due to the induced eddy current formation and seismic isolation of the building was studied.

3. Fusion Reactor Design

In order to improve the availability of the Steady State Tokamak Reactor (SSTR)^(3.1), an innovative reactor concept called the DREAM (DRastically EAsy Maintenance) Reactor was proposed. The overview of the DREAM concept is shown in Fig. VII.3.1 and major reactor parameters are compared with those of SSTR in Table VII.3.1.

For the easy maintenance of in-vessel reactor components, a plasma configuration with high aspect ratio (with slender doughnut shape) around 6 and a small number of torus sectoring of 12 are introduced to extract the 1/12 sector of the torus by a single straight radial motion through the adjacent toroidal field coils. The adjacent torus sectors are mechanically jointed by a bolt/flange structure.

A plasma vacuum region is comprised of a cryostat system and 12 horizontal access doors. The toroidal field coil system is embedded in the reactor building and in time of need repaired independent of the torus structure.

The key component for the feasibility of a tokamak reactor is the divertor. The divertor configuration improvement of the SSTR was studied. As the result, the divertor configuration with baffle plates near the divertor plasma is found to lower temperature and increase the particle density of the divertor plasma and to reduce the peak heat flux at the divertor plates.^(3.2)

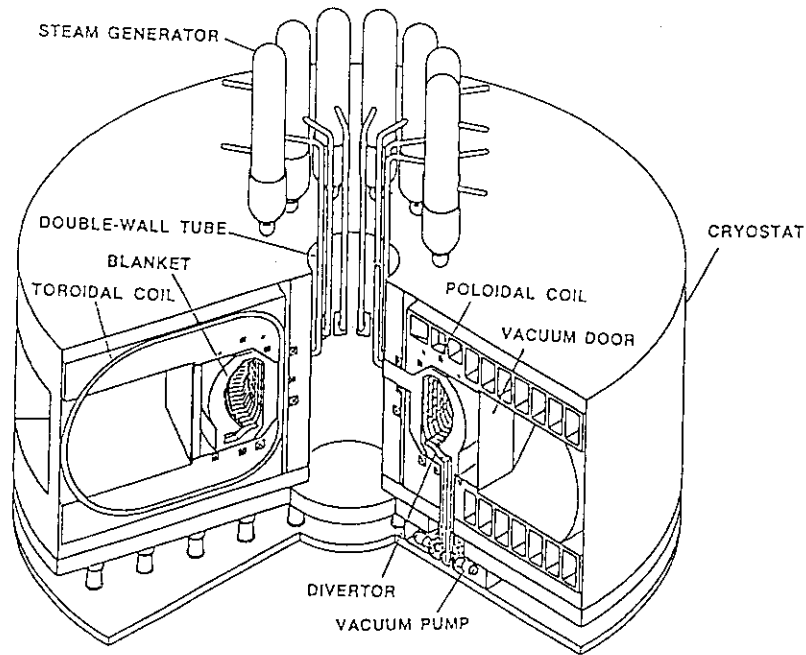


Fig. VII.3.1 Overview of the DREAM Reactor capable of achieving load factor of 85% by the easy maintenance of the in-vessel reactor components

Fundamental experiments on solid particulates suspended in helium gas cooling was carried out with the collaboration with Kyushu University.

Table VII.3.1 Comparison of major parameters for DREAM and SSTR

Item	DREAM	SSTR
Fusion power	3 GW	3 GW
Major radius	12.9 m	7.0 m
Minor radius	1.8 m	1.75 m
Aspect ratio	7.1	4
Elongation	1.6	1.8
Number of toroidal field coils	12	16
Plasma current	6.7 MA	12 MA
Bootstrap current fraction	100%	75%
Divertor	Single null at the bottom	Double null
Maintenance scheme	Single straight radial motion of 1/12 sector	Vertical replacement of six blanket pieces per 1/16

[3.1] Fusion Reactor System Laboratory, "Concept Study of the Steady State Tokamak Reactor (SSTR)", JAERI-M 91-081 (1991)

- [3.2] Moriyama, K., Nishino, T., Seki, Y. and Yamasaki, S., "Improvement Study of the Divertor Configuration of the Steady State Tokamak Reactor", JAERI-M 93-030 (1993)

4. Safety Analysis

A comprehensive safety evaluation methodology which aims to identify and to quantitatively estimate the dominant risks for designing safe fusion reactor plant was continued.

In 1992, a simplified point model plasma transient analysis code is developed and combined with a one dimensional thermalhydraulic analysis code for the evaluation of plasma facing components and blankets. With this code, the effect of plasma transients on plasma facing components and blanket was evaluated. This development will be carried out under the framework of the IEA Implementing Agreement on International Co-operation of Environmental, Safety and Economics Aspects of Fusion Power which was signed June 4, 1992.

Some fundamental experiments were carried out on the Loss of Vacuum Events in the vacuum vessel of a fusion reactor.^(4.1)

- [4.1] Ogawa, M., Kunugi, T. and the ITER/FER Safety Group, "Experiments on Exchange Flow through Two Breaches during Loss of Vacuum Accident in Nuclear Fusion Experimental Reactor", Proc. 10th Topical Meeting Technology of Fusion Energy, Boston, June 7-12, 1992, Fusion Technology, 21 (1992) 2036

APPENDICES

A.1 Publication List (April 1992 - March 1993)

A.1.1 List of JAERI-M report(Fusion Facility)

- 1) Okumura Y. and Watanabe K., "Design of a High Brightness Ion Source for the Basic Technology Accelerator", JAERI-M 92-024.
- 2) Nakamura K., Akiba M., Suzuki S., et al., "High Heat Flux Experiment on B4C-Overlaid C/C composites for Plasma Facing Materials of JT-60U", JAERI-M 92-052
- 3) Murakami Y., Horiike H., Kuroda T., et al., "Comparison Between a Steady state Fusion Reactor and an Inductively Driven Pulse Reactor", JAERI-M 92-056
- 4) Zimin, S., Sato S., Maki K., et al., "Some ITER Shield Problems Examination", JAERI-M 92-063.
- 5) Fujisawa, N. and Takizuka, T., "Bootstrap Current Profiles and Scaling in Large Aspect Ratio Tokamaks", JAERI-M 92-064.
- 6) H. Yoshida, R. Shige, M. Hasegawa et al. "Preliminary Test of Liquid metal Induced Embrittlement in LiPb and Stainless-steel systems " JAERI - M, 92-066
- 7) Yoshida H., Enoda M., Hirata S., et al., "Test Apparatus for ITER Blanket Cooling Water Distributor Design", JAERI-M 92-070.
- 8) JT-60 Team, "Review of JT-60U Experimental Results from March to October, 1991", JAERI-M 92-073.
- 9) Kurihara K. and Kimura T., "Tokamak Plasma Shape Identification Based on the Boundary Integral Equations", JAERI-M 92-075 (1992) (in Japanese).
- 10) H. Yoshida, K. Ashibe, K. Ono, et al. "Measurements of Breakaway reaction Between Beryllium and water Vapor ITER Blanket Design " JAERI - M, 92-083
- 11) Wang J.P., Azumi M., Tani K. and Callen J.D., "Momentum and Heat Frictions between Fast Ions and Thermal Plasma Species", JAERI-M 92-087
- 12) H. Yoshida, Y. Naruse, M. Yamaoka, et al. "Preliminary study on Lithium - salt Aqueous Solution blanket" JAERI - M, 92-088 (in Japanese)
- 13) Abe T., Murakami Y., Hirabayashi T., et al., "A Survey on Technical Problems in Designing High-speed Rotors with Developing Materials", JAERI-M 92-092.
- 14) Sato, S., Maki, K., Takatsu, H., et al., "Heterogeneous Effects on Shielding Characteristics in Fusion Reactor Neutronics Calculations", JAERI-M 92-093 (in Japanese).
- 15) Sawa S, Kanamori N, Shimizu K, et al., "Structural Design of Cryostat and Port Penetration of International Thermonuclear Experimental Reactor(ITER)", JAERI-M 92-094.
- 16) H. Yoshida, M. Okamoto, T. Terai, " Safety Handling of Beryllium for Fusion Technology R&D" JAERI - M, 92-100 (in Japanese)
- 17) M. Enoda, H. Yoshida, S. Hirata, et al. " Test Apparatus for ITER Blanket Pebble Packing Behavior" JAERI - M, 92-104 (in Japanese)
- 18) Wang J.P., Azumi M., Callen J.D. and Tani K., "Moment Approach to Fast Ion Neoclassical Transport and Viscous Forces", JAERI-M 92-107
- 19) Okazaki T, Nishio S, Shibui M, et al., "Design to Divertor Support Structure", JAERI-M 92-108.
- 20) Kobayashi T., Sakamoto K., Watanabe A., Mushoki S., Takahashi M., Ishizuka H., et al., "FEL Experiment with a Focusing Wiggler", JAERI-M 92-109.
- 21) Ishida, S., Isei, N., M.Sato, "Operation of a 20-channel Grating Polychromator Diagnostic System and its Application to Sawtooth Observation in JT-60U", JAERI-M 92-111.
- 22) Yoshida, H., "Fabrication of beryllium spheres and its validation tests", JAERI-M 92-116.
- 23) Yoshida K., "Stability and Protection of Forced Cooling Conductor for Large Superconducting Magnet" JAERI-M 92-119
- 24) Zimin, S., "A study on radiation shielding analysis for toroidal field coils of a tokamak-type fusion reactors", JAERI-M 92-120.
- 25) Takizuka T., et al., Proceedings of the workshop of three large tokamak operation on energy confinement scaling under intensive auxiliary heating, JAERI-M 92-128 .
- 26) Obara K, Terakado T, Kakudate S, et al., "Conceptual Design of In-vessel Viewing and Inspection System(IVIS) for International Thermonuclear Experimental Reactor(ITER)", JAERI-M 92-130.
- 27) Shimizu K, Shibui M, Koizumi K, et al., "Structural Design of Shield-integrated Thin-wall Vacuum Vessel and Manufacturing Qualification Tests for International Thermonuclear Experimental Reactor(ITER)", JAERI-M 92-135.
- 28) Sugihara, M., Tada, E., Shimomura, Y., et al., "Comparative Study of Low and High Aspect Ratio Devices for ITER Design Options", AERI-M 92-136.

- 29) Shimizu, K., Shibui, M., Koizumi, K., et al., "Shield-integrated Vacuum Vessel with Uniform Resistivity", JAERI-M 92-135 (in Japanese).
- 30) Kasai S., Hasegawa K., Suzuki S., et al., "Repeating Pneumatic Pellet Injector in JAERI", JAERI-M 92-143.
- 31) Murakami, Y., Fujieda, H., Itami, K., et al., "Optimization for steady-state and hybrid operations of ITER by using scaling models of divertor heat load", JAERI-M 92-145.
- 32) Mushoki S., Sakamoto K., Watanabe A., et al., "Design of a High Power, 2.75 GHz Relativistic Peniotron Oscillator", JAERI-M 92-153
- 33) Suzuki Y., Hanada M., Okumura Y., et al., "High Density Plasma Production in a Multicusp Plasma Generator with RF Antenna", JAERI-M 92-156.
- 34) Futakawa, M., Koizumi, K., Shimizu, K., et al., "A Seismic Analysis of ITER Vacuum Vessel (1) - Modelling and Eigenvalue Analysis -", JAERI-M 92-164.
- 35) Suzuki Y., Hanada M., Okumura Y., et al., "Measurement of Work Function of a Plasma Grid in a Cesium Seeded Negative Ion Source", JAERI-M 92-168.
- 36) Hasegawa K., Kasai S., Suzuki S., et al., "Measurement of Shadowgraph of Flying Solid-hydrogen Pellets", JAERI-M 92-170 (in Japanese).
- 37) Fujieda, H., Murakami, Y., Sugihara, M., "Tokamak Plasma Power Balance Calculation Code (TPC Code) Outline and Operation Manual", JAERI-M 92-178 (in Japanese).
- 38) Nomura, Y., Okawa, Y., Naruse, H., et al., "Plant System Design of Fusion Experimental Reactors", JAERI-M 92-180 (in Japanese).
- 39) Nakamura, Y., Nishino, T., Tsunematsu, T., et al., "User's Manual of Tokamak Simulation Code", JAERI-M 92-189 (in Japanese).
- 40) Oguri H., Okumura Y., Inoue T., et al., "Development of a High Brightness Hydrogen Ion Source for the Basic Technology Accelerator", JAERI-M 92-200.
- 41) Tobita, K., "Active Neutrals Particle Diagnostics for High Temperature Plasma", JAERI-M 92-214 (in Japanese).
- 42) Yoshida, H., Okamoto, M., Odawara, O., et al., "High Temperature Chemical Compatibility of Beryllium for Fusion Reactor Material", JAERI-M 92-217.
- 43) Kurita G., Azumi M., Takeda T., "AEOLUS-IT" MHD simulation code based on a toroidally incompressible plasma model, JAERI-M 93-004 (in Japanese).
- 44) Shirai H., Hirayama T., Shimizu K. et al., "SLICE : Experimental data Time Slice Monitor Soft", JAERI-M 93-026 (in Japanese)
- 45) W. H. Shu, K. Okuno, "Ion - driven permeation of deuterium in metals " JAERI - M, 93-043
- 46) Suzuki S., Akiba M., Araki M., et al., "Electron Beam Irradiation Experiments of a Divertor Module at KFA", JAERI-M 93-048
- 47) Suzuki S., Araki M. and Akiba M., "Summary Report for IAEA CRP on Lifetime Prediction for the First Wall of a Fusion Machine", JAERI-M 93-049
- 48) JT-60 Team, Review of JT-60U Experimental JT-60 Team Results from January to October, 1992", JAERI-M 93-057.
- 49) Satoh K., Akiba M., Araki M., et al., "Electron Beam Irradiation Experiments of Monoblock Divertor Mock-up", JAERI-M 93-058
- 50) Kuriyama M., Kunieda T., Matsuoka M., et al., "Shine Through Measurements with Hydrogen Beam in JT-60", JAERI-M 93-059.
- 51) Kondho M, Shibanuma K, Kakudate S, et al., "Design and Development of Supporting System for ITER-CDA In-vessel Components", JAERI-M 93-066.
- 52) Ikeda S., Araki M., Ogawa M., et al., "Heat transfer Experiments for Divertor Plate of Fusion Reactor under One-sided Heating Conditions (1) - Circumferential Temperature Distributions of Tube Wall in Non-boiling and Nucleate Boiling Water Flows -", JAERI-M 93-070
- 53) Iwamoto S. and Ando T., "Design and Fabrication of Disruption Simulation Coil", JAERI-M 93-071
- 54) Araki M., "Experimental and Analytical Studies of High Heat Flux Components for Fusion Experimental Reactor", JAERI-M 93-070
- 55) Tokuda S., Kumakura T., Yoshimura K., Numerical experiments on finite element method for matching data, JAERI-M 93-075 (in Japanese).
- 56) Satoshi KONISHI, Takumi HAYASHI, Masahiko INOUE, et al., "JAERI Fuel Cleanup System (J-FCU) Stand-Alone Tritium Test at the TSTA - First J-FCU Test with One Gram of Tritium on June 1991 - " JAERI-M 93-080
- 57) Takumi HAYASHI, Hirofumi NAKAMURA, Satoshi KONISHI, et al., "Joint Operation of the TSTA with the J-FCU under the Collaboration between JAERI and U.S.-DOE - A First Integrated Tritium Test Between J-FCU and ISS on Oct. 1991 - " JAERI-M 93-081

- 58) Takumi HAYASHI, Hirofumi NAKAMURA, Satoshi KONISHI, et al. "JAERI Fuel Cleanup System (J-FCU) Stand-Alone Tritium Test at the TSTA -J-FCU Tritium Test with Full Impurities on Feb., 1992 -" JAERI-M 93-082
- 59) Takumi HAYASHI, Hirofumi NAKAMURA, Satoshi KONISHI, et al., "Joint Operation of the TSTA with the J-FCU under the Collaboration between JAERI and U.S.-DOE - TSTA Extended Loop Operation with 100 grams of Tritium on Apr.-May 1992 -" JAERI-M 93-083
- 60) Takumi HAYASHI, Satoshi KONISHI, Hirofumi NAKAMURA, et al., "Joint Operation of the TSTA with the J-FCU under the Collaboration between JAERI and U.S.-DOE - Detail Performance of the J-FCU (25 Days Extended TSTA Loop Operation on Apr.-May 1992) -" JAERI-M 93-084
- 61) Satoshi KONISHI, Sigeru O'HIRA, Masahiko INOUE, et al., "Joint Operation of TSTA Under the Collaboration Between JAERI and DOE-LANL -TSTA Loop Run October 1990 - from Oct 1990 Tritium Run Test Plan and Result, TTA-TP-100-19 " JAERI-M 93-085
- 62) S. Konishi, T. Hayashi, Y. Naruse et al. "Design of the JAERI Fuel Cleanup System for the Tritium Systems Test Assembly - System Design Description of the JAERI Fuel Cleanup System -" JAERI-M 93-086
- 63) S. O'hira, S. Konishi, Y. Naruse et al. "Test of the Cold Traps in the JAERI Fuel Cleanup System in the Tritium Systems Test Assembly " JAERI-M 93-087
- 64) S. Konishi, S. O'hira, T. Hayashi, et al. "Test of the Palladium Diffuser in the JAERI Fuel Cleanup System in the Tritium Systems Test Assembly" JAERI-M 93-088
- 65) S. Konishi, S. O'hira, T. Hayashi, et al. " Tests of the JAERI Fuel Cleanup System with Deuterium at the Tritium Systems Test Assembly - JFCU Stand Alone Deuterium Test - JFCU Stand Alone Deuterium Test 2" JAERI-M 93-089
- 66) S. KONISHI, H. YOSHIDA, Y. NARUSE et al. "Tritium Test of the Tritium Processing Components under the Annex III US-Japan Collaboration - Annex III Final Report -" JAERI-M 93-090
- 67) Nishio S, Shibui M, Koizumi K, et al., "Design and Development of Supporting System for ITER/CDA Blanket Box Structure", JAERI-M 93-091.
- 68) Sato S., Maki K., Seki Y., et al., "Streaming through the Gaps around Divertor Pipings in ITER", JAERI-M 93-093.
- 69) T. Hayashi, S. Konishi, S. O'hira et al. "Test of the Scroll pump in the JAERI Fuel Cleanup System in the Tritium Systems Test Assembly - JFCU Scroll Pump Test and Result - - JFCU Stand Alone Tritium Test 2 -" JAERI-M 93-094

A.1.2 List of papers published in Journals

- 1) Kurihara K., "Eddy Current Effect Study on the JT-60 Plasma Equilibrium Control", *Fusion Engineering and Design* 19 (1992) 235.
- 2) Kurihara K., "Improvement of Tokamak Plasma Shape Identification with a Legendre-Fourier Expansion of the Vacuum Poloidal Flux Function", *Fusion Technology* 22 (1992) 334.
- 3) Kurihara K., "Tokamak Plasma Shape Identification on the basis of Boundary Integral Equations", *Nuclear Fusion* 33, No.3 (1993) 399.
- 4) Ogiwara N., Jimbou R., Saidoh M., et al., "Oxygen Gettering Action of B/C Materials", *Shinku* 35 (1992) 174 (in Japanese).
- 5) Ogiwara N., Shiho M., Watanabe A., et al., "Characteristics of Spindt-type Cold Cathode", *Shinku* 35 (1992) 392 (in Japanese).
- 6) Ando T., Takatsu H., Yamamoto M., et al., "Screening Tests of Isotropic Graphites and C/C Composite for JT-60U Plasma Facing Components", *Tanso* 152 (1992) 120.
- 7) Matsukawa M., Hosogane N. and Ninomiya H., "Application of Regression Analysis to Deriving Measurement Formulas for Feedback Control of Plasma Shape in JT-60U", *Plasma Phys. Contr. Fusion* 34 (1992) 907.
- 8) Matsukawa M., Ninomiya H. and Horiike H., "Plasma Feedback Control System Design and the Results of JT-60U", *Plasma Phys. Contr. Fusion* 21 (1992) 1624.
- 9) Ando T., Kodama K., Yamamoto M., et al., "Quality Evaluation of Graphites and Carbon/Carbon Composites during Production of JT-60U Plasma Facing Materials", *J. Nucl. Mater.* 191-194 (1992) 1423.
- 10) Fujita I., Amemiya S., Ando T., et al., "Surface Analysis of JT-60 Graphite Divertor Tiles", *J. Nucl. Mater.* 196-198 (1992) 168.

- 11) Nakamura K., Akiba M., Suzuki S., et al., "High Heat Flux Experiment on B₄C-overlaid C/C Composites for Plasma Facing Materials for JT-60U", *ibid.* **196-198** (1992) 627.
- 12) Gotoh Y., Yamaki T., Ando T., et al., "Sputtering Characteristics of B₄C-overlaid Graphite for keV Energy Deuterium Ion Implantation", *ibid.* **196-198** (1992) 708.
- 13) Jimbou R., Saidoh M., Ogiwara N., et al., "Retention of Deuterium Implanted into B₄C-overlaid Isotropic Graphites and Hot-pressed B₄C", *ibid.* **196-198** (1992) 958.
- 14) Ogiwara N. and Ueda Y., "Outgassing from the Spindt-type Cold Cathode Electron Source", *Shinku* **36** (1993) 325 (in Japanese).
- 15) Uehara K., Ikeda Y. Saigusa M., et al., "Plasma coupling test of the RF heating system in JT-60", *Fusion Engineering and Design* **19** (1992) 29-40.
- 16) Fujii T., Saigusa M., Kimura H., et al., "Performance of the JT-60 ICRF antenna with an open type Faraday shield", *Fusion Engineering and Design* **19** (1992) 213-223.
- 17) Kuriyama M., Akiba M., Araki M., et al., "Operation of Neutral Beam System in JT-60", *Plasma Devices and Operation* **1** (1991) 127.
- 18) Matsuoka M., "Optimization of Beamlet Steering for Flat Beam Intensity at a Target Surface", *T. IEE Japan B-112* (1992) 829 (in Japanese).
- 19) Matsuoka M., Matsuda S., Mizuno M., et al., "Development of Acceleration Power Supplies of a Neutral Beam Injection System Using GTO Switches with Transient-Voltage Regulation Capability", *T. IEE Japan B-112* (1992) 1035 (in Japanese).
- 20) Matsuoka M. and Takamura S., "Production of a Negative Radial Electric Field in Tokamak Edge Plasmas by Perpendicularly Injected Low Energy Neutral Beams", *Nucl. Fusion* **33** (1993) 161.
- 21) Kitsunozaki A. and JT-60 Team, "Status and Plans for JT-60U", *Fusion Tech.*, **21** (1992) 1309.
- 22) Ninomiya H. and JT-60 Team, "JT-60U Latest Results and Future Prospects", *Phys. Fluids*, **B4** (1992) 2070.
- 23) Nishitani T., Takeuchi H., Kondoh T., et al., "Absolute Calibration of the JT-60U Neutron Monitors using a ²⁵²Cf Neutron Source" *Rev. Sci. Instrum.*, **63** (1992) 5270.
- 24) Ushigusa K., Kondoh T., Naito O., "Direct Loss of Energetic Electrons during Lower Hybrid Current Drive on JT-60U", *Nucl. Fusion*, **32** (1992) 1977.
- 25) Tsuji S., "Experimental Scaling of Particle Confinement in Tokamaks", *Fusion Eng. and Design* **15**(1992)311
- 26) Tsuji S., Hosogane N., Itami K. et al., "Improvement of Confinement and Remote Radiative Cooling of Beam Heated Plasmas in JT-60 with Ion Gradient-B Drift towards the X-point", *Nucl. Fusion* **32**(1992)1313
- 27) Itoh K., Itoh S.-I., Fukuyama A., Tsuji S. and Lichtenberg A.J., "Model of the Major Disruption in Tokamaks", *Nucl. Fusion* **32**(1992)1851
- 28) Hamamatsu K., Fukuyama A., Itoh S.-I. et al., "ICRF Current Drive and Helicity Injection", *J. Phys. Soc. Jpn.*, **62**(1992)113
- 29) Itoh K., Yagi M., Itoh S.-I. et al., "L-mode Confinement Model Based on Transport-MHD Theory in Tokamaks", *Plasma Phys. Control. Fusion* **35**(1993)543
- 30) Hosogane, N., Asakura, N., Kubo, H., et al. "Divertor Phenomena prior to Density Limit Disruptions", *J. Nucl. Mater.*, **196-198** (1992) 750.
- 31) Kimura, H., "Antenna for Plasma Heating and Current Drive - IOn Cycrotron Range of Frequency (ICRF) -", *Kakuyugo-Kenkyuu* **67** (1992) 310.
- 32) Nakazato, T., Kimura, H., Fukuya, J., "Analysis of Low Frequency Fast Wave Current Drive for ITER", *Nucl. Fusion* **32**, 1209.
- 33) Shimada, M., "The Present Status of Impurity Transport Investigations" *Fusion Eng. and Design* **15** (1992) 325.
- 34) Tobita, K., Tani, K., Neyatani, Y., et al., "Ripple-Trapped Loss of Neutral-beam-injected Fast Ions in JT-60U", *Phy.Rev.Lett.* **69** (1992) 3060.
- 35) Kubo, H., Sakasai, A., Koide, Y., et al., "Intensity Ratio of Lyman- ϵ Fine-structure Components of TiXXII in the JT-60 Tokamak Plasma", *Phys. Rev.* **A46** (1992) 7877.
- 36) Sakasai, A., Koide, Y., Kubo, H., et al., "Impurity Profiles and Transport Characteristics in JT-60U", *Journal of Nuclear Materials* **196-198** (1992) 472.
- 37) Kubo, H. and JT-60 Team, "Impurity Generation Mechanism and Remote Radiative Cooling in JT-60U Divertor Discharges", *Journal of Nuclear Materials* **196-198** (1992) 71.
- 38) Itami, K., Shimada, M., Hosogane, N., "Characteristics of Divertor Plasma and Scrape-off Layer in JT-60U", *Journal of Nuclear Materials* **196-198** (1992) 755.
- 39) Nakamura, H., Sakasai, A., Shimada, M., et al., "Hydrogen / deuterium recycling and initial results of helium ash study in JT-60U", *Journal of Nuclear Materials* **196-198** (1992) 642.
- 40) Shimizu, K., Itami, K., Kubo, H., et al., "Transport analysis of divertor plasma in JT-60U", *Journal of Nuclear Materials* **196-198** (1992) 476.

- 41) Asakura, N., Shimada, M., Itami, K., et al., "Particle balance and heat balance in JT-60U", *Journal of Nuclear Materials* **196-198** (1992) 1069.
- 42) Tanabe, T., Noda, N. and Nakamura, H., "Review of high Z materials for PSI applications", *Journal of Nuclear Materials* **196-198** (1992) 11.
- 43) Kawano, Y., Nagashima, A., Ishida, S., et al., "CO₂ Laser Interferometer for Electron Density Measurement in JT-60U", *Rev. Sci. Instrum* **63** (10) 1992.
- 44) Shoji T., Tamai H., Miura Y., et al., "Effects of Ergodization on Plasma Confinement in JFT-2M", *J. Nucl. Mat.* **196-198** (1992) 296-300.
- 45) Nakajima T., Kitamura A., Maeno K., et al., "Measurement of H Energy and Flux by H->D Isotope Exchange in JFT-2M Scrape-off Layer", *J. Nucl. Mat.*, **196-198** (1992) 1036.
- 46) Miura Y., Tamai H., Suzuki N., et al., "Offset Linear Scaling for H-mode Confinement", *Kakuyugo-Kenkyuu*, **67**, (1992) 352
- 47) Uehara K., Ikeda Y., Saigusa M., "Plasma Coupling Test of the RF Heating System in JT-60", *Fusion Eng. Design*, **19** (1992) 11
- 48) Ida K., Hidekuma S., Miura Y., et al., "Edge Poloidal Rotation Profiles of H-mode Plasmas in the JFT-2M Tokamak", *Phys. Fluids B4* (1992) 2552.
- 49) Miura Y., Takizuka T., Tamai H., et al., "Geometric Dependence of the Scaling Law on the Energy Confinement Time in H-mode Discharges", *Nucl. Fusion* **32** (1992) 1473
- 50) Miura Y., Okano F., Suzuki N., et al., *Phys. Rev. Lett.* **69** (1992) 2216.
- 51) Hoshino K., Mori M., Yamamoto T., et al., "Avoidance of qa=3 Disruption by Electron Cyclotron Heating in the JFT-2M Tokamak", *Phys. Rev. Lett.* **69** (1992) 2208.
- 52) Kurita G., Tuda T., Azumi M., et al., Effect of an external helical field on a rotating magnetic island, *Nucl. Fusion* **32** (1992) 1899 .
- 53) Yamagiwa M., Fusion yield in high-power D-beam injected ³He plasmas, *Plasma Phys. Control. Fusion* **34** (1992) 715.
- 54) Takeda T., Tani K., Tsunematsu T., et al., Plasma simulator METIS for tokamak confinement and heating studies, *Parallel Computing* **18** (1992) 743 .
- 55) Yamagiwa M., Effects of spatial diffusion and direct loss on burnup fractions of fast ions, *Plasma Physics and Controlled Fusion* **34** (1992) 1503 .
- 56) Tokuda S., Takeda T., Nuclear fusion research and MHD computations, *Bulletin of the Japan Society for Industrial and Applied Mathematics* **2**(1992) 2.
- 57) Takeda T., Nagamine K., Yamazaki Y., et al., Progress of muon science, *Journal of the Atomic Society of Japan* **34** (1992) 1098 (in Japanese).
- 58) Yamagiwa M., Kishimoto Y., Fujii T., et al., Study of combined NBI and ICRF enhancement of the D-³He fusion yield with a Fokker-Planck code, *Nucl. Fusion* **33** (1993) 493.
- 59) Kurita G., Azumi M., Tuda T., Effect of electron and ion viscosity on sawtooth crash in a tokamak, *J. Phys. Soc. Jpn.* **62** (1993) 524.
- 60) Shibamura K, Matsuda S, Tsuzi H, et al., "Primary Research and Development Needs for Fusion Experimental Reactor: Perspectives", *Fusion Eng. and Design* **15** (1991)
- 61) Tada E, Okuno K, Shibamura K, et al., "ITER Conceptual Design and Development Progress at JAERI", *Fusion Eng. and Design* **18** (1991) 501.
- 62) Hanada M., Inoue T., Mizuno M., et al., "Negative Ion Production in a Large Semi-Cylindrical Ion Source", *Rev. Sci. Instrum.* **63**(1992)2699.
- 63) Okumura Y., Hanada M., Inoue T., et al., "Long Pulse Operation of a Cesium-Seeded Multicusp H- Ion Source", *ibid.* **63**(1992)2708.
- 64) Tanaka S., Araki M. and Okumura Y., "Application of Aperture Displacement Technique to Producing Flat Beam Distributions", *ibid.* **63**(1992)2779.
- 65) Hiroki S., Abe T. and Murakami Y., "Separation of Helium and Deuterium Peaks with a Quadrupole Mass Spectrometer by Using the Second Stability Zone in the Mathieu Diagram", *Rev. Sci. Instrum.*, **63** (1992) 3874.
- 66) Kato T., Ebisu H., Hiyama T., et al., "Design of a 8-kW refrigeration system for ITER common test", *Cryogenics* **32** (1992) 60
- 67) Kato T., Miyake A., Kawano K., et al., "Heat transfer characteristics of a plate-fin type super critical/liquid helium heat exchanger", *ibid.* 260
- 68) Nishi M., Ando T., Tsuji H., et al., "The DPC-TJ Program-Development of a High-Current-Density Large Superconducting Coil for Fusion Machines", *Cryogenic Engineering* **27** (1992) 25 (in Japanese)
- 69) Koizumi N., Yoshida K., Isono T., et al., "Test Results of the DPC-TJ-Stability Performance", *ibid.* 51
- 70) Sugimoto M., Kato T., Kawano K., et al., "Test Results of the DPC-TJ-Thermal and Hydraulic Performances", *ibid.* 57

- 71) Nakajima H., Yoshida K., Tsuji H., et al., "The Charpy impact test as an Evaluation of 4 K Fracture Toughness", *Advances in Cryogenic Engineering* 38 (1992) 207
- 72) Ando T., Takahashi Y., Nishi M., et al., "AC losses in a multifilamentary Nb3Al/Cu composite Superconductor made by a jelly roll process", *ibid.* 813
- 73) Hawng I.S., Morra M.M., Ballinger R.G., et al., "Charpy Absorbed energy and JIc as measures of cryogenic fracture toughness", *Journal of Testing and Evaluation* 20 (1992) 248
- 74) Inoue T., Matsuda Y., Ohara Y., et al., "Effect of Filament Material and Area on the Extracted Current from a Volume H- Ion Source", *Plasma Source Sci. Technol.* 1(1992)75.
- 75) Shibanuma K., Matsuda S., Tsuji H., et al., "Primary Research and Development Needs for Fusion Reactors: Perspectives", *Fusion Engineering and Design* 15(1992)377.
- 76) Araki M., Akiba M., Seki M., et al., "Experimental and analytical results of carbon based materials under thermal shock heat loads for fusion application", *Fusion engineering and Design*, 19 (1992) 101-109
- 77) Ogawa M., Araki M., Seki M., et al., "Experimental study on melting evaporation of metal exposed to intense hydrogen ion beam", *Fusion engineering and Design*, 19 (1992) 193-202
- 78) Watanabe K., Mizuno M., Ohara Y., et al., "Dc Voltage Holding Experiments of Vacuum Gap for High Energy Ion Sources", *J. Appl. Phys.* 72(1992)3949.
- 79) Ito Y., Mitsunaka Y., Sakamoto K. and Nagashima T., "Experimental Study on a quasi-optical mode converter for transforming the whispering gallery mode into a circularly polarized hollow radiation beam", *Int.J.Infrared and MM waves*, Vol.13, No.9,1353(1992).
- 80) Sakamoto K. "Numerical analysis method of the radiation pattern from the aperture field", *Int.J.Infrared and MM waves*, Vol.13, No.9, 1360(1992).
- 81) T. Hayashi, K. Okuno, Y. Naruse, " Permeation behavior of deuterium Implanted into Pure Aluminium " *J. Alloys and compounds*, 189 (1992) 195
- 82) Mori S., Seki Y., Shimizu A., et al., "Preliminary Design of a Solid Particulate Cooled Blanket for the Steady State Tokamak Reactor(SSTR)", *Fusion Technology*, 21(3) Part 2A, (1992)PP.1744-1748
- 83) Araki M., Ogawa M., Akiba M., et al., "Experimental and analytical evaluations on critical heat flux under one-sided heating condition for fusion applications", *Fusion Technology* 21 (1992) 1835-1839
- 84) Suzuki S., Akiba M., Araki M., et al., "Thermal cycling experiments of monoblock divertor modules for fusion experimental reactors", *Fusion Technology* 21 (1992) 1858-1862
- 85) Kunugi T., Akiba M., Ogawa M., et al., "Sensitivity study on some parameters of disruption erosion analysis", *Fusion Technology* 21 (1992) 1863-1867
- 86) Kunugi T., Akiba M., Ogawa M., et al., "The simulation of the energy deposition from runaway electrons in plasma facing components with EGS4", *Fusion Technology* 21 (1992) 1868-1872
- 87) W. M. Shu, K. Okuno, Y. Hayashi, et al. " Implantation Driven Permeation of Deuterium through Pure molybdenum " *Fusion Technology*, 21 (1992) 1934
- 88) A. Matsumoto, T. Yamanishi, K. Okuno, et al. " Characteristics of the "Cryogenic-wall" thermal Diffusion Column for Separation of Hydrogen Isotopes " *Fusion Technology*, 21 (1992) 1959
- 89) J. Barnes, K. Duerre, J. Anderson, et al. " Knowledge collection and Operator Training Using an Artificial Intelligence System " *Fusion Technology*, 21 (1992) 1968
- 90) J. E. Nasise, J. L. Anderson, Y. Naruse " Molecular Sieve Regeneration System for Assaying HTO from Detritiation System " *Fusion Technology*, 21 (1992) 1974
- 91) T. Hayashi, S. Konishi, H. Nakamura, et al. " Recent Tritium Experience of the JAERI Fuel Cleanup system (JFCU) At the Tritium Systems Test Assembly (TSTA) " *Fusion Technology*, 21 (1992) 1979
- 92) J. Barnes, W. Harbin, J. Anderson, et al. " Experience with Maintenance of a tritium Contaminated Test Component at TSTA " *Fusion Technology*, 21 (1992) 1984
- 93) T. Yamanishi, E. Sada, K. Okuno, et al., "Analysis of Characteristics of cryogenic Distillation Column in Separation of Hydrogen Isotopes " *J. Chem. Eng. Jpn.*, 26 (1992) 1
- 94) Araki M., Akiba M., Dairaku M., et al., "Thermal response of bonded CFC/OFHC divertor mock-ups for fusion experimental reactors under large numbers of cyclic high heat loads", *J. Nuclear Science and Technology*, 29 (1992) 901-908
- 95) Akiba M., Araki M., Suzuki S., et al., "Experimental and analytical studies on thermal erosion of carbon-based materials with high thermal conductivity", *J. Nuclear Materials*, 191-194 (1992) 373-376
- 96) T. hayashi, K. Okuno, Y. Naruse, " Permeation Behavior of Deuterium Implanted into Aluminum - Lithium Alloys " *J. Nucl. Mater.*, 191-194 (1992) 1065
- 97) Tanaka S., Ohira T. and Nakamura K., "Production of high density plasma and study on the influence of a nonuniform magnetic field on the particle transport in the SOL region", *Journal of Nuclear Materials* 196-198 (1992) 357-362
- 98) Linke J., Akiba M., Bolt H., et al., "Simulation of disruption on coatings and bulk materials", *Journal of Nuclear Materials* 196-198 (1992) 607-611
- 99) Laan J., Klippel H., Akiba M., et al., "Effects of short pulse high heat fluxes on carbon base plasma facing materials for ITER", *Journal of Nuclear Materials* 196-198 (1992) 612-617

- 100) Hiroki S., Abe T., Murakami Y., et al., "Development of a QMS with a Ceramic Single-Piece Quadrupole", *Vacuum*, 44 (1993) 71.
- 101) Hiroki S., Abe, T. and Murakami Y., "Ion Orbit Analysis for Quadrupole Mass Spectrometer(II)", *J. Vac. Soc. Jpn.*, 36 (1993) 1 (in Japanese).
- 102) Hiroki S., Abe, T. and Murakami Y., "Deuterium and Helium Peaks Separation by Using a High Resolution Quadrupole Mass Spectrometer", *J. Vac. Soc. Jpn.*, 36 (1993) 263 (in Japanese).
- 103) Hamazaki M., Abe T. and Murakami Y., "Fabrication of Electromagnetic Force Balance for Vacuum Applications", *J. Vac. Soc. Jpn.*, 36 (1993) 263 (in Japanese).
- 104) Okuno K., Takahashi T., Tsuji H., et al., "AC loss Performance of 1-m-bore, large-current Nb₃Sn Superconducting coil in JAERI Demo Poloidal Coil Project", *IEEE Trans. on Applied Superconductivity* 3 (1993) 602
- 105) Hosono F., Sugimoto M., Tsukamoto H., et al., "AC loss of the Toroidal Model Pancake (TMP)", *ibid.* 535
- 106) Takahashi Y., Koizumi N., Wadayama Y., "Experimental results of stability and current sharing of NbTi Cable-in-conduit conductors for the poloidal field coils", *ibid.* 610
- 107) Sasaki T., Koizumi N., Nishi M., "Stability performance of the DPC-TJ, Nb₃Sn cable-in-conduit large superconducting coil", *ibid.* 523
- 108) Isono T., Hosono F., Koizumi N., et al., "Development of a (NbTi)₃Sn Strand for the ITER CS Scalable Model Coil", *ibid.* 496
- 109) Iwaki G., Sasaki S., Kamata K., et al., "Development of Bronze-Proce-Processed (NbTi)₃Sn Superconducting Wires for Central Solenoid Model Coil of ITER", *ibid.* 998
- 110) Ando T., Nakajima H., Hiue H., et al., "The Effect of Ti Conduit on the Critical Current in (NbTi)₃Sn Cable-in-conduit Conductors", *ibid.* 488
- 111) Ando T., Takahashi Y., Sugimoto M., et al., "Development of Nb₃Al Cable-in-Conduit Fusion Superconductors", *ibid.* 492
- 112) Pamela J., Fumelli M., Jequier F., et al., "Measurement of the Neutral and Charged Beam Fractions in a D-100keV 2A Neutral Beam Injector", *Nuclear Instruments and Methods in Physics Research B73*(1993)289.
- 113) Pamela J., Fumelli M., Jequier F., et al., "Energy Recovery Experiments with a Powerful 100keV D- Baed Neutral Beam Injector", *ibid.* B72(1993)296.
- 114) Saigusa, M., Yamamoto, T., Petty, C.C., et al., "Analysis of the coupling properties of the toroidal antenna array in JFT-2M by a code considering the solid septa" *Nucl. Fusion*, 33,(1993) 421.
- 115) Sakamoto K., Kobayashi K., Kishimoto Y., Kawasaki S., Mushoki S., et al, "Beam divergence with harmonic Gyroresonance in Focusing wiggler and axial field" *Phys.Rev.Lett.*, Vol.70, No.4, 441(1993).
- 116) Matsushita, S., Narusawa, M., Kurita, G., et al., "Parallel Algorithm for Non-linear MHD Plasma Simulation", *Proceedings of Johoshori-gakkai*, 33 (1992) (in Japanese).
- 117) Dietz K.J., Chappuis P., Horiike H., et al., "Experience with high heat flux components in large tokamaks", *Fusion Engineering and Design*, 16 (1991) 229.
- 118) Ioki K., Yamada M., Sakata S., et al., "Development of conductively cooled first wall armor and actively cooled divertor structure for ITER/FER", *Fusion Engineering and Design*, 16 (1991) 293.
- 119) Shibanuma K., Honda T., Kondoh M., et al., "Design study of an armor tile handling manipulator for the Fusion Experimental Reactor", *Fusion Engineering and Design*, 16 (1991) 487.
- 120) Mori S., Miura H., Yamazaki S., et al., "Preliminary design of a solid particulate cooled blanket for the Steady State Tokamak Reactor (SSTR)", *J. Fusion Technology*, 21 (1992) 1744.
- 121) Muraoka, K., Maeda, M., Matoba, T., et al., "Fusion Plasma Diagnostics by LIDAR Thomson Scattering", *The Rev. of Laser Engineering*, 20 (1992) 375 (in Japanese).
- 122) Tsunematsu, T., "Disruption and Control of Tokamak Plasmas", *Kakuyugo-Kenkyu*, 68 (1992) 140.
- 123) Matsuda, S., "Status and Plans for Japanese FER/ITER Studies", *Proc. of Fusion Technology*, Vol.21 (1992) 1370.
- 124) Tsunematsu, T., "The scaling law of energy confinement time for ITER", *Fusion Engineering and Design* Vol.15, (1992) 309.
- 125) Toda, S., Yoshikawa, K., Takagi, T., et al., "Extreme Engineering Technology Issues for Fusion Nuclear Reactor; High heat flux component, magnetomechanics, material", *J. Atomic Energy Soc. Japan*, 34, (1992) 918.
- 126) Nishio, S., Araki, M., Shinya, K., et al., "Separatrix sweeping by in-vessel coils on a fusion reactor", *Fusion Eng. and Design* 19 (1992) 203.
- 127) Tanaka, S., Ohira, T., Nakamura, K., "Production of high density plasma and study on the influence of a nonuniform magnetic field on the particle transport in the SOL region", *J. Nucl. Mat.*, 196-198 (1992) 357.
- 128) Akutsu, Y., Ohkawa, Y., Horiuchi, M., et al., "Application of epoxy-coated reinforcing bars to large electric structure for electric insulation", *Transact. of the Japan Concrete Institute*, 14 (1992) 217.

A.1.3 List of paper published in conference proceedings

- 1) Kurihara K., Kimura T., Kawamata Y., et al., "Tokamak Plasma Shape Identification Based on Boundary Integral Equations and the Real-Time Shape Visualization System", in Proceedings of the 17th Symposium on Fusion Technology, Rome, 1992, pp. 860-866.
- 2) Matsukawa M., Ninomiya H., Horiike H., et al., "Plasma Feedback Control System Design and the Results of JT-60U" Proc. of the 10th Topical Meeting on the Technology of Fusion Engineering (1992, Boston).
- 3) Ando T., Yamamoto M., Arai T., et al., "Operation Experience with JT-60U Plasma Facing Components and Evaluation Tests of B₄C-overlaid CFC/Graphites", Proc. of the 17th Symp. on Fusion Technology (1992, Rome).
- 4) Amemiya S., Masuda T., Ando T., et al., "Hydrogen Retention and Impurity Deposition of JT-60 Graphite Divertor Tiles", *ibid.*
- 5) Ogiwara N., Shiho M. and Ueda Y., "A Mass Filter with a Cold Cathode", Proc. of the 12th Intern. Vac. Congr. and 8th Intern. Conf. on Solid Surface (1992, The Hague).
- 6) Ogiwara N., Jimbou R., Saidoh M., et al., "Oxygen Gettering Effect of B/C Materials", *ibid.*
- 7) Seki M., Ikeda Y., Imai T., et al., "The Distant Coupling of LHCD Launcher in the JT-60U", Proceeding of 19th European Conf. on Controlled Fusion and Plasma Physics, Innsbruck, (1992).
- 8) Moriyama S., Fujii T., Saigusa M., et al., "First Results of JT-60U ICRF Heating System", Proceeding of 17th Symp. on Fusion Technology, Rome (1992).
- 9) Ikeda Y., Seki M., Imai T., et al., "The Upgrade of 2 GHz Lower Hybrid Current Drive System on JT-60U", Proceeding of 17th Symp. on Fusion Technology, Rome (1992).
- 10) Yamamoto T., Yokokura K., Kasugai A., et al., "Development of Cryogenic Window for High Power Millimeter Wave" Proceeding of 17th Inter. Conf. on Infrared and Millimeter Waves, Pasadena (1992).
- 11) Kuriyama M., Ohara Y., Akino N., et al., "Activities on Neutral Beam Injectors at JAERI", 17th Symp. on Fusion Technology, Rome (1992).
- 12) Mizuno M., Hanada M., Inoue T., et al., "Multi-Second H⁻ Ion Beam Production in a 350 keV Electrostatic Accelerator", 6th Int. Symp. on the Production and Neutralization of Negative Ion and Beams, Brookhaven (1992).
- 13) Ushigusa K., Imai T., Ikeda Y., et al., "Confinement and Transport of Energetic Electrons during Lower Hybrid Current Drive", in Plasma Physics and Controlled Nuclear Fusion Research, IAEA, E-1-2.
- 14) Hamamatsu K., "Profile Control of Alpha Particles by ICRF Waves", Proc. of Int. School of Plasma Phys. (Varrenna, Italy, 1992)
- 15) Ozeki T., Azumi M., Tsunematsu T. et al., "Profile Control for Stable High-Beta-Poloidal Tokamak with Large Bootstrap Current", Proc. of 14th IAEA, D-4-1
- 16) Fukuyama A., Itoh K., Itoh S.-I., Tsuji S and Lichtenberg A.J., "Stochasticity Driven Disruptive Phenomena in Tokamaks", Proc. of 14th IAEA, D-4-12
- 17) Itoh K., Itoh S.-I., Fukuyama A., Yagi M and Azumi M., "Model of the L-mode Confinement in Tokamaks", Proc. of 14th IAEA, D-4-
- 18) Wang J.P., Azumi M., Tani K. and Callen J.P., "Fast Ion Neoclassical Transport, Frictional and Viscous Forces", Proc. of 34th APS meeting
- 19) Tsuji S., Shimizu K., Asakura N. et al., "Divertor Plasma Analysis in JT-60U", Proc. of 34th APS meeting
- 20) Ozeki T. and M. Azumi M., "MHD Stability Analysis of a Tokamak with Large Bootstrap Current Fraction", Proc. of US-Japan Workshop on "Theory of High Beta Plasmas", (San Diego, 1992)
- 21) Tani K., Takizuka T. and Azumi M., "Effect of Non-Circular Plasma Cross Section on Ripple Losses of Alpha Particles", Proc. of US-Japan Workshop on "Ion Orbit Losses in Toroidal Systems", (Nagoya, 1992)
- 22) Shirai H., Hirayama T., Koide Y. and Azumi M., " Ion Temperature Simulation of JT-60 Plasmas with Ion Temperature Gradient Mode Transport Models ", Proc. of US-Japan Workshop on " Turbulent Transport ", (Texas, 1993).
- 23) Yagi M. and Azumi M., " Transport Analysis based on Eeta-i Mode in JT-60 ", tion of JT-60 Plasmas with Ion Temperature Gradient Mode Transport Models ", Proc. of US-Japan Workshop on " Turbulent Transport ", (Texas, 1993).
- 24) Kikuchi, M., Shirai, H., Takizuka, T., et al., "Çg-mode and L-mode Confinement in JT-60U", in Plasma Physics and Controlled Nuclear Fusion Research (Proc. of the 14 th International Conf. Wurzburg, 1992) IAEA, A-3-1.
- 25) Koide, Y., Tuda, T., Ushigusa, K., et al., "Spontaneous Plasma Rotation of Nearly Perpendicular NBI and LHCD in JT-60U", in Plasma Physics and Controlled Nuclear Fusion Research (Proc. of the 14 th International Conf. Wurzburg, 1992) IAEA, E-3-11.
- 26) Kamada, Y., Takizuka, T., Kikuchi, M., et al., "Effects of Current Profile on MHD Characteristics and Plasma Performance in JT-60U", in Plasma Physics and Controlled Nuclear Fusion Research (Proc. of the 14 th International Conf. Wurzburg, 1992) IAEA, A-7-13.

- 27) Yoshino, R., Hosogane, N., Neyatani, Y., et al., "Disruptions and Stable Plasma Shutdown in JT-60U", in Plasma Physics and Controlled Nuclear Fusion Research (Proc. of the 14 th International Conf. Wurzburg, 1992) IAEA, G-3-1.
- 28) Ishida, S., Matsuoka, M., Kikuchi, M., et al., "Enhanced Confinement of High Bootstrap Current Discharges in JT-60U", in Plasma Physics and Controlled Nuclear Fusion Research (Proc. of the 14 th International Conf. Wurzburg, 1992) IAEA, A-3-5.
- 29) Hosogane, N., "Experience and Plans in JT-60 - Energy Loss during the Technology Disruptions -", Workshop on Technology and PMI Processes of Tokamak Disruptions (Monterey, USA), April 3, 1992.
- 30) de Haas, J., Nagashima, K., Shirai, H., "Characteristics of Heat Pulse Propagation at JT-60U", Proc. 1992 International Conference on Plasma Physics (Joint Conference of the 19th EPS Conference on Controlled Fusion and Plasma Physics) (Innsbruck, 1992).
- 31) Nagashima, K., Sakasai, A., de Haas, J., et al., "Gas Puff Modulation Experiment on JT-60U", Proc. 1992 International Conference on Plasma Physics (Joint Conference of the 19th EPS Conference on Controlled Fusion and Plasma Physics) (Innsbruck, 1992).
- 32) Neyatani, Y., Ushigusa, K., Matsukawa, M., et al., "Disruption Behavior of Plasma and Vacuum Vessel in JT-60U", Proc. 1992 International Conference on Plasma Physics (Joint Conference of the 19th EPS Conference on Controlled Fusion and Plasma Physics) (Innsbruck, 1992).
- 33) Costley, A.E., Cripwell, P., Fukuda, T., "Measurement of the Toroidal Motion of Fine Scale Density Structures in JET Plasmas", Proc. 1992 International Conference on Plasma Physics (Joint Conference of the 19th EPS Conference on Controlled Fusion and Plasma Physics) (Innsbruck, 1992).
- 34) Kikuchi, M., "Confinement and MHD Characteristics of High- E_{\perp} JT-60U Plasma", US-Japan Workshop on Bootstrap Currents (San Diego, USA).
- 35) Kikuchi, M., "Conceptual Design of the Steady State Tokamak Reactor (SSTR) US-Japan Workshop on Bootstrap Currents (San Diego, USA).
- 36) Neyatani, Y., "Disruption Behaviour of Vacuum Vessel in JT-60U", Proc. the 8 th Fusion Reactor Materials Forum (Nagoya, 1993).
- 37) Kikuchi, M., "The Steady State Tokamak Reactor", European Workshop on Physics Issues in Fusion Reactor (Cadarache).
- 38) Kikuchi, M., "JAERI Program of Tokamak Concept Improvement", European Workshop on Physics Issues in Fusion Reactor (Cadarache).
- 39) Isei, N., Kamada, Y., Ishida, S., et al. "Sawtooth Characteristics and Electron Temperature Profiles from Electron Cyclotron Emission Measurements in JT-60U", Bulletin of the American Physical Society, Vol. 37, No. 6 (1992).
- 40) Hosogane, N. and JT-60 Team, "Confinement and Divertor Studies in JT-60U", Bulletin of the American Physical Society, Vol. 37, No. 6 (1992).
- 41) Imai, I., Ushigusa, K., Ikeda, Y., et al., "Performance of the LHCD in High Current Regime in JT-60U", Proc. 1992 International Conference on Plasma Physics (Joint Conference of the 19 th EPS Conference on Controlled Fusion and Plasma Physics) (Innsbruck, 1992).
- 42) Kondoh, T., Ide, S., Imai, T., et al., "Investigation of High Energy Electrons Produced by Lower Hybrid Waves with Measurement of the Hard X-ray in JT-60U", Proc. 1992 International Conference on Plasma Physics (Joint Conference of the 19th EPS Conference on Controlled Fusion and Plasma Physics) (Innsbruck, 1992).
- 43) Tobita, K., Tani, K., Takeuchi, H., et al., "Two-Dimensional Measurement of Heat Load on The First Wall Due to Fast Ion Ripple Loss in JT-60U with Near-Perpendicular NBI", Proc. 1992 International Conference on Plasma Physics (Joint Conference of the 19th EPS Conference on Controlled Fusion and Plasma Physics) (Innsbruck, 1992).
- 44) Kimura, H., Fujii, T., Saegusa, M., et al., "ICRF Heating Experiments in JT-60 and JT-60U", Proc. Euro Physics Topical Conference on Radio Frequency Heating and Current Drive of Fusion Devices" (Brussels, 1992).
- 45) Kimura, H., Arai, H., Saitou, Y., et al., "Ceramics-free Antenna Feeder for ITER Ion Cyclotron Wave System", Proc. Euro Physics Topical Conference on Radio Frequency Heating and Current Drive of Fusion Devices" (Brussels, 1992).
- 46) Ide, S., Imai, T., Ushigusa, K., et al., "First Results of LHCD Experiments", Proc. Euro Physics Topical Conference on Radio Frequency Heating and Current Drive of Fusion Devices" (Brussels, 1992).
- 47) Nagami, M., Miya, N., Nakajima, S., et al., "Conceptual Design Study of a Steady State Tokamak Device", Proc. 17th SOFT, Rome, (1992).
- 48) Sakasai, A. and JT-60 Team, "Impurity Generation Mechanism in JT-60U", in Plasma Physics and Controlled Nuclear Fusion Research (Proc. of the 14 th International Conf. Wurzburg, 1992) IAEA, A-7-12.
- 49) Itami, K. and JT-60 Team, "Heat Transport and Electric Current in Tokamak Boundary Plasmas of JT-60U", in Plasma Physics and Controlled Nuclear Fusion Research (Proc. of the 14 th International Conf. Wurzburg, 1992) IAEA, A-6-5.

- 50) Sugie, T., Kubo, H., Shimada, M., et al., "Impurity Reduction and Behavior in JT-60U", Bulletin of the American Physical Society, Vol. 37, No. 6 (1992).
- 51) Asakura, N., "Particle Recycling Study on JT-60U", Proc of US-Japan Workshop on "Studies on Edge Plasma Control and Transport Processes", (Tsukuba, 1992).
- 52) Kimura, H., Fujii, T., Saegusa, M., et al., "Heat Flux Studies on the JT-60U Divertor Plates", Proc of US-Japan Workshop on "Ion Orbit Losses in Toroidal Systems", (Nagoya, 1992).
- 53) Asakura, N., "Divertor Study in JT-60U", Proc of US-Japan DIII-D / JT-60U / JFT-2M Workshop, (San Diego, 1993).
- 54) Oda T., Odajima K., Takiyama K., et al., "Development of Diagnostic System for High Power Microwave(FEL) Electric Fields in the Microwave Tokamak Experiment", in Proc. 19th European Conference on Controlled Fusion and Plasma Physics, Innsburg, 1992.
- 55) Uehara K., "Plasma Transport as a Dissipative Structure", in Proc. 19th European Conference on Controlled Fusion and Plasma Physics, Innsburg, 1992.
- 56) Shoji T., Aikawa H., Annaratone B.M., et al., "Divertor Bias Experiment on JFT-2M", in Proc. 14th International Conference on Plasma Physics and Controlled Nuclear Fusion Research, Würzburg, (1992) IAEA-CN-56/A-5-5.
- 57) Mori M., Aikawa H., Asahi Y., et al., "Plasma Improvement with Ergodic Magnetic Fields in JFT-2M", in Proc. 14th International Conference on Plasma Physics and Controlled Nuclear Fusion Research, Würzburg, (1992) IAEA-CN-56/C-3-5.
- 58) Allen S.L., Casper T.A., Oasa K., et al., "Electron Cyclotron Resonance Heating in the Microwave Tokamak Experiment", in Proc. 14th International Conference on Plasma Physics and Controlled Nuclear Fusion Research, Würzburg, (1992) IAEA-CN-56 / E-1-4
- 59) Lasnier C.J., Hoshino K., "ECE measurements During Extreme High-Power ECRH", Bull. Amer. Phys. Soc., 37 (1992).
- 60) Lopez P., Casper T.A., Hoshino K., et al., "Reflectometry Observing Density Layer Motion in MTX", Bull. Amer. Phys. Soc., 37 (1992).
- 61) Wood R.D., Allen S.L., Oasa K., et al., "High Power FEL-Generated Microwave Experiments on the MTX Tokamak", Bull. Amer. Phys. Soc., 37 (1992).
- 62) Foote J.H., Oda T., Odajima K., et al., "Measurements on MTX with the FEL Microwave Electric Field Diagnostic (LAPPS)", Bull. Amer. Phys. Soc., 37 (1992).
- 63) Allen S.L., Casper T.A., Hoshino K., et al., "High Power FEL-Generated Microwave Experiments on the MTX Tokamak", Bull. Amer. Phys. Soc., 37 (1992).
- 64) Hooper E.B., Allen S.L., Hoshino K., et al., "Electron-Cyclotron Resonance (ECR) Heating and MHD Control Experiments in MTX", Bull. Amer. Phys. Soc., 37 (1992).
- 65) Yamauchi T., LeBlanc B., Dimock D., et al., "Te and ne Profiles Measured with TV Thomson Scattering System on JFT-2M", Bull. Amer. Phys. Soc., 37 (1992).
- 66) Takizuka T., Kinetic energy confinement in JT-60 L-mode plasma, 3 Large Tokamak Workshop on Energy Confinement Scaling of Intensely Heated Plasma (May 19, 1992, Naka).
- 67) Kurita G., Tuda T., Resistive instabilities in tokamak with plasma flow, IAEA Technical Meeting (June 15-17, 1992, Montréal, Canada) .
- 68) Takizuka T., Confinement scaling for kinetic energy in tokamak L-mode plasmas, Proc. 1992 ICCP (June 29, 1992, Innsbruck) Part I, 51.
- 69) Todd T. N., Carolan P.G., Tuda T., et al., The Study and Control of Error-Field Induced Locked Modes in Tokamaks, 14th International Conference on Plasma Physics and Controlled Nuclear Fusion Research (October, 1992).
- 70) Tokuda S., MHD stability of a small aspect ratio tokamak, US-Japan Workshop on Theory of High b Plasmas (November, 1992, San Diego).
- 71) Yamagiwa M., Effects of diffusive and direct losses on triton burnup, US-Japan Joint Workshop on Ion Orbit Losses in Toroidal Systems (December, 1992, Nagoya).
- 72) Obara K. and Murakami Y., "Fabrication and Performance Test of a Metal Gasket Applicable to both Knife-Edge-Type and V-Groove-Type Flanges", Proc. 8th Meeting on UHV Techniques for Accelerators and Storage Rings, (KFK, 1992) p.269.
- 73) Nishi M., Tsuji H., Ando T., et al., "Test Results of the DPC-TJ, a 24 kA-40 A/mm² Superconducting Test Coil for Fusion Machines", 17th Symposium on Fusion Technology (1992)
- 74) Yamamoto K., Yoshida K., Yasukawa Y., et al., "Design of the ITER Central Solenoid Scalable Model Coil", *ibid.*
- 75) Kato T., Takahashi T., Kawano K., et al., "Cryogenic Helium Pump System for the Development of Superconducting Magnets in a Fusion Experimental Reactor", *ibid.*
- 76) Tsukamoto H., Isono T., Hosono F., et al., "Development of the ITER Central Solenoid Scalable Model Coil", *ibid.*

- 77) Okumura Y., Fumelli M., Hanada M., et al., "Multi-Ampere D- Ion Source for Negative-Ion-Based Neutral Beam Injector", 17th Symp. on Fusion Technology, Rome, 1992.
- 78) Araki M., Suzuki S., Akiba M., et al., "Development and testing of divertor mock-ups for ITER/FER at JAERI", 17th Symposium on Fusion Technology, Rome, Italy Sep. 14-18, 1992
- 79) Yamazaki S., Ise H., Akiba M., et al., "Development of fabrication technologies for plasma facing components of ITER", 17th Symposium on Fusion Technology, Rome, Italy Sep. 14-18, 1992
- 80) Deschka S., Akiba M., Breibach G., et al., "Thermal response and fatigue behavior of brazed CFC/TZM/Mo41Re-divertor mock-ups under electron beam loading", 17th Symposium on Fusion Technology, Rome, Italy Sep. 14-18, 1992
- 81) Kurasawa T., Slagle O., Hollenberg G., et al., "BEATRIX-II : In-situ Tritium Recovery from a Thin-walled Li₂O Ring Irradiation in a Fast Neutron Flux", *ibid*
- 82) Isono T., Ando T., Tsuji H., "Development of 1kA-Class Go & Return High-Tc Superconducting Bus Bar"., Fifth International Symposium on Superconductivity
- 83) Okumura Y., "Development of a High Current H-/D- Ion Source", Proc. 1st Meeting on the Ion Engineering Society of Japan, Tokyo, 1992.
- 84) Okumura Y., Inoue T., Oguri H., et al., "Development of a High Brightness Ion Source for the Proton Linear Accelerator(BTA) at JAERI", 16th Inter. Linac Conference, Ottawa, 1992.
- 85) Mizumoto M., Hasegawa K., Yokobori H., et al., "High Intensity proton Accelerator for Nuclear Waste Transmutation", *ibid*.
- 86) Watanabe K., Hanada M., Inoue T., et al., "High Power Negative Ion Beam Development for Heating and Current Drive in Fusion Plasmas", IAEA 14th Inter. Conf. on Plasma Physics and Controlled Nuclear Fusion Research, Wurzburg, 1992.
- 87) Tsuji H., Akiba M., Tada E., et al., "Progress in the tokamak basic device development for the construction of the fusion experimental reactors", IAEA 14th International Conference on Plasma Physics and Controlled Nuclear Fusion Research, Wurzburg, Germany, Sep. 30-Oct. 7, 1992
- 88) Inoue T., Hanada M., Mizuno M., et al., "Development of a Multi-Ampere H- Ion Source at JAERI", 6th Inter. Symp. on the Production and Neutralization of Negative Ions and Beams, Brookhaven, 1992.
- 89) Watanabe K., Hanada M., Okumura Y., et al., "Cs Effects in a Large Multi-Ampere D- Ion Source", *ibid*.
- 90) Okumura Y., Araki M., Hanada M., et al., "Negative Ion Based Neutral Beam Injector for JT-60U", *ibid*.
- 91) Mizuno M., Hanada M., Inoue T., et al., " Multi-Second H- Ion Beam Production in a 350 keV Electrostatic Accelerator", *ibid*.
- 92) Hanada M., Tanaka M., Suzuki Y., et al., " Production of a Long Pulse Negative Ion Beam with Multi-Ampere", Proc. of the 3rd Symp. on Beam Engineering of Advanced Material Syntheses, Tokyo, 1992.
- 93) Maeno S., Hanada M., Inoue T., et al., "Production of 350 keV, 130 mA H- Ion Beams", *ibid*.
- 94) Saigusa, M., Moriyama, S., Fujii, T., et al., "Antenna Coupling Properties and Radiation Loss During ICRF Heating in JT-60U", Radio Frequency Heating and Current Drive of Fusion Devices, Europhysics Top. Conf. Brussels, (1992) 45.
- 95) Imai T., Ushigusa K., Ikeda Y., et al., "Performance of the LHCD in High Current Regime in JT-60U", Proc. of ICCP, Joint Conf. of 9th KIEV and 9th ICWIP combined with 19th European Conf. on Controlled Fusion and Plasma Physics Vol.16C, Part II, 953-956 (1992).
- 96) Kawasaki S., Kobayashi T., Sakamoto K., Kishimoto Y., Watanabe A., et al., "IREB transport in a focusing wiggler and FEL experiments at JAERI", Proc. of 9th Int. Conf. on High Power Particle Beams(1992).
- 97) Sakamoto K., Tsuneoka M., Maebara S., Kasugai A., Fujita H., et al., "Development of a high power gyrotron for ECH of tokamak plasma", Digest of 17th Int. Conf. on Infrared and MM Waves, 188 (1992).
- 98) Bolt H., Akiba M., Kikuchi K., et al., "Heat Flux Effects to Plasma Facing Materials", Proc. of Material Chemistry '92, April 1992 Tsukuba, JAPAN 25-38
- 99) Akiba M., Suzuki S. and Araki M., "Thermal Cycling Experiments of Monoblock Divertor Mock-ups for International Thermonuclear Experimental Reactor", Proc. of SPIE's 1992 Inter National Symposium on Optical Applied Science and Engineering (High Heat Flux), San Diego June 1992
- 100) Takatsu H., "Current Status of Blanket Activities in JAERI", International Workshop on Ceramic Breeder Blanket Interactions, Tokyo, 1992.
- 101) Kurasawa T., Slagle O., Hollenberg G., et al., "Tritium Mass Balance in the BEATRIX-II Experiment", *ibid*
- 102) Enoeda M., "Fabrication and Compatibility Measurement of Lithium Ceramics", *ibid*
- 103) Shibanuma K., Kondoh M., Kakudate S., et al., "Recent Development in Remote Maintenance for Fusion Experimental Reactor in JAERI", 14th IEEE/NPSS Symposium Proceeding, Vol.1.
- 104) Matsuda, S., "Status and Plans for Japanese FER/ITER Studies", 10th Topical Meeting on the Technology of Fusion Energy, Boston (USA).
- 105) Nishio, S., Takatsu, H., Koizumi, K., "Transient Electromagnetics in Tokamak Reactor", The 4th Electromagnetics Symposium Proceedings (in Japanese).

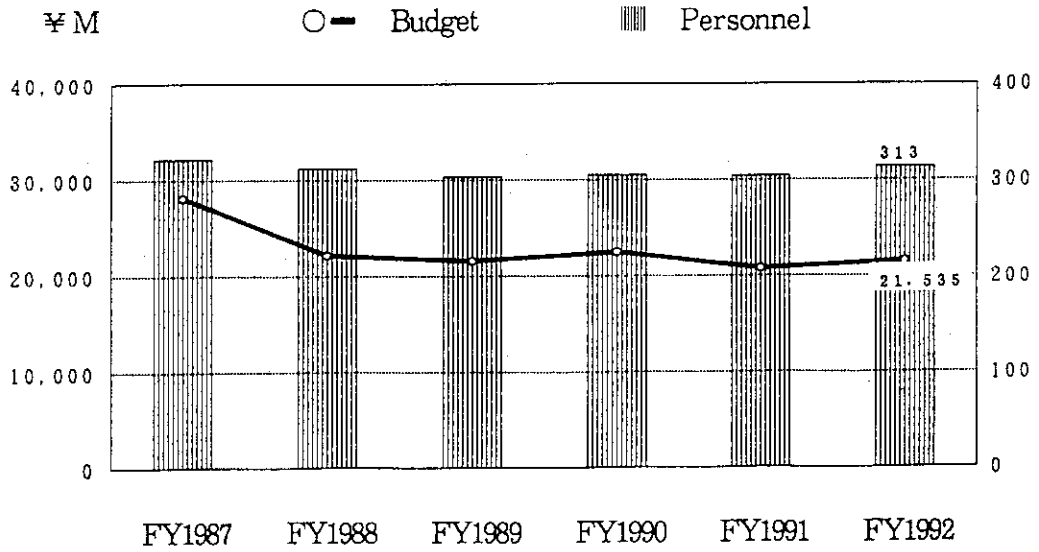
- 106) Koizumi, K., Tada, E., Takatsu, H., et al., "Development Program of Tokamak Fusion Experimental Reactor in JAERI", The first MAGDA Conference, 1992 (in Japanese).
- 107) Okazaki, T., Nishio, S., Shibui, M., et al., "Safety Considerations for divertor of fusion experimental Reactor", 17th SOFT (Sept.14-18, 1992, Roma).
- 108) Takatsu, H., Mori, S., Yoshida, H., et al., "Layered Pebble Bed concept for ITER breeding blanket", 17th SOFT (Sept.14-18, 1992, Roma).
- 109) Yoshida, H., Enoeda, M., Nagakura, M., et al., "Blanket Materials R&D from Engineering Aspects of Lithium Ceramic - Beryllium -Steel Systems in ITER Blanket ", 17th SOFT (Sept.14-18, 1992, Roma).
- 110) Tada, E., Nishio, S., Shibamura, M., et al., "Divertor Plate Supporting System for Fusion Experimental Reactor", 17th SOFT (Sept.14-18, 1992, Roma).
- 111) Shibamura, K., Kakudate, S., Kanamori, N., et al., "Feasibility Study of Blanket Handling System for Fusion Experimental Reactor", 17th SOFT (Sept.14-18, 1992, Roma).

A.1.4 List of other reports

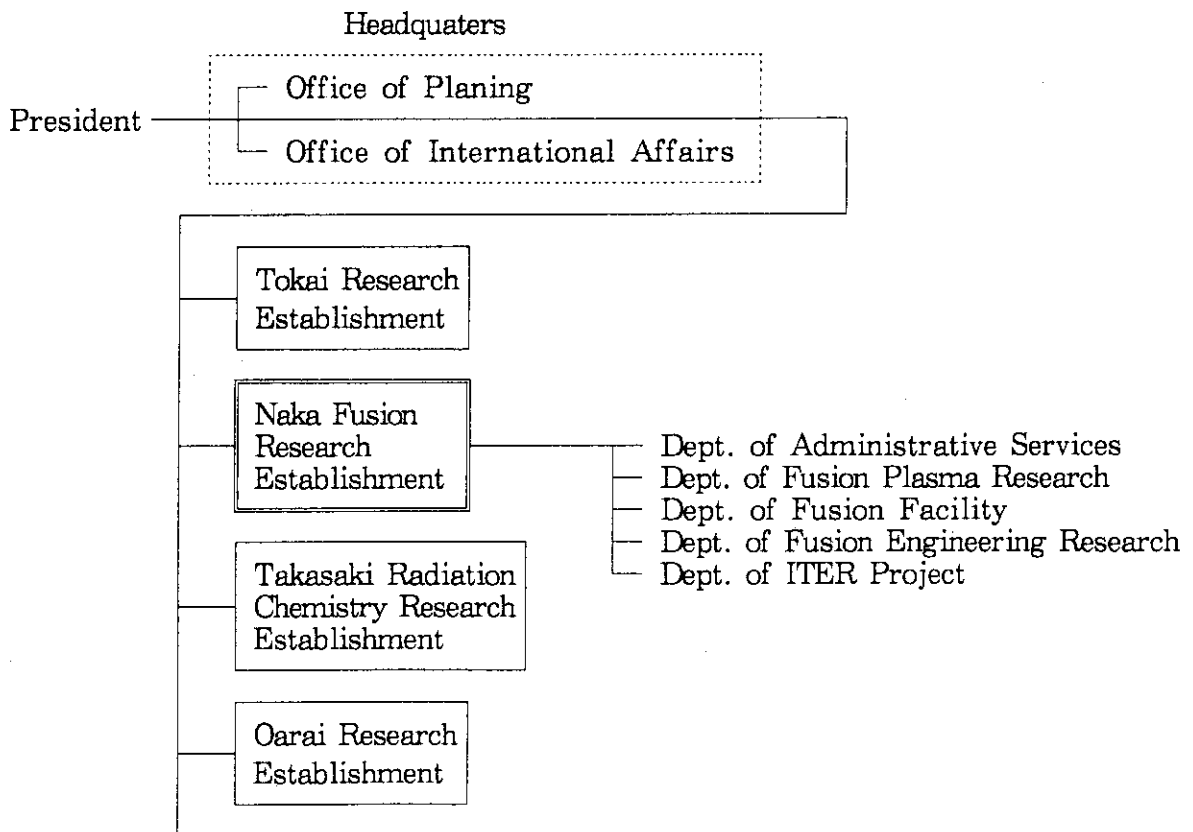
- 1) Roth J., Wilson K., Saidoh M., et al., "Plasma-Surface Interaction Data: Status and Requirements -- Working Group Report", INDC(NDS)-277 (1993) 29.
- 2) Itoh K., Itoh S.-I., Fukuyama A. et al., " Model of the L-Mode Confinement in Tokamaks", NIFS-187, 1992
- 3) Itoh K., Yagi M., Itoh S.-I. et al, "L-Mode Confinement Model Based on Transport-MHD Theory in Tokamaks", NIFS-192, 1992
- 4) Tanabe, T., Noda, N., Nakamura, H., "Review of High Z Materials for PSI Applications", NIFS-152 (1992).
- 5) Annaratone B.M., Shoji T., Maeda H., et al., "Fluid Velocity and Electromagnetic Forces Measured by a Rotating Langmuir Probe in the Scrape off Layer of JFT-2M", University of Oxford Report OUEL 1968/92.
- 6) Kishimoto Y., Tajima T., LeBrun M.J., et al., Self-organized profile relaxation by ion temperature gradient instability in toroidal plasmas, IFSR#589.
- 7) Matsuda, S. and Yamamoto, S., "Prospect of ITER EDA Program", Nuclear Engineering, 38 (1992) 32.
- 8) Matsuda, S. and Seki, M., "Present Status of ITER EDA and Reactor Technology", Nuclear Engineering, Vol.39 (1993) 32.

A.2 Personnel and Financial Data

A.2.1 Change in number of personnel and annual budged (FY1987-1992)



A.2.2 Organization chart (March 31,1993)



A.2.3 Scientific Staffs in the Naka Fusion Research Establishment (March 31, 1993)

Naka Fusion Research Establishment

SHIKAZONO Naomoto (Director General) SEKIGUCHI Tadashi (Scientific Advisor)
 TANAKA Masatoshi (Scientific Advisor)
 TOMABECHI Ken (Scientific Advisor)
 MIYAMOTO Goro (Scientific Advisor)

Department of Administrative Services

TEZUKA Kihachiro (Director)

Department of Fusion Plasma Research

TAMURA Sanae (Director) KISHIMOTO Hiroshi (Deputy Director)
 KANAZAWA Tetsuo (Administrative Manager)

Tokamak Program Division

KITSUNEZAKI Akio (Head)		
KISHIYA Kazuhiro(*28)	KONOSHIMA Sigeru	MIYA Naoyuki
NAKAJIMA Shinji(*28)	NINOMIYA Hiromasa	NISHITANI Takeo
OIKAWA Akira	TOYOSHIMA Noboru	USHIGUSA Kenkichi

Plasma Analysis Division

AZUMI Masafumi (Head)		
AOYAGI Tetsuo	HAGINOYA Hirofumi(*91)	HAMAMATSU Kiyotaka
OHSHIMA Takayuki	OZEKI Takahisa	NISHIMURA Yasutaro(*50)
SAITO Naoyuki	SAKATA Shinya	SATO Minoru
SHIRAI Hiroshi	TANI Keiji	TSUCHIYA Satoru(*85)
TSUJI Shunji	TSUGITA Tomonori	WAGURI Yasuhiro(*49)
YAGI Masahiro		

Large Tokamak Experiment Division I

FUNAHASHI Akimasa (Head)		
CHIBA Shinichi	DE HAAS Johannes(*90)	FUKUDA Takeshi
HATAE Takaki	HOSOGANE Nobuyuki	ISEI Nobuyuki
ISHIDA Shinichi	IWAHASHI Takaaki	KAMADA Yutaka
KIKUCHI Mitsuru	KITAMURA Shigeru	KOIDE Yoshihiko
KONDOH Takashi	MORI Masahiro	NAGASHIMA Keisuke
NAGAYA Susumu	NAITO Osamu	NEYATANI Yuzuru
NUMAZAWA Susumu	OHZEKI Masahiro	SAKUMA Takeshi
SATO Masayasu	SHITOMI Morimasa	SUNAOSHI Hidenori
TSUKAHARA Yoshimitsu	URAMOTO Yasuyuki	YAMASHITA Osamu
YOSHIDA Hidetoshi	YOSHINO Ryuji	WOLFE Sean(*89)

Large Tokamak Experiment Division II

NAGAMI Masayuki (Head)		
ASAKURA Nobuyuki	FUJITA Takaaki	HOEK Magnus(*89)
IDE Shunsuke	IMAI Tsuyoshi	ITAMI Kiyoshi
KAWANO Yasunori	KIMURA Haruyuki	KUBO Hirotaka
MIURA Sanae	MORIOKA Atsuhiko(*92)	NAGASHIMA Akira
NAKAMURA Hiroo	NEMOTO Masahiro	SAKASAI Akira
SHIMADA Michiya	SHIMIZU Katsuhiko	SUGIE Tatsuo
TAKEUCHI Hiroshi	TOBITA Kenji	
VAN BLOCLAND Arjen(*89)		

Plasma Theory Laboratory

TAKEDA Tatsuo (Head)	KISHIMOTO Yasuaki	KURITA Gen-Ichi
KAWANOBE Mitsuru(*49)	TAKIZUKA Tomonori	TOKUDA Shinji
NAKAMURA Yukiharu		TUDA Takashi
TSUNEMATSU Toshihide(ITER)		
YAMAGIWA Mitsuru		

Experimental Plasma Physics Laboratory

MAEDA Hikosuke (Head)	ASAHI Yoshihiro(*93)	HOSHINO Katsumichi
AIKAWA Hiroshi	KAWASHIMA Hisato	MAENO Katsuki
KAWAKAMI Tomohide	MORI Masahiro	MIURA Yukitoshi
MATSUDA Toshiaki	OGAWA Hiroaki	OGAWA Toshihide
ODAJIMA Kazuo	SEIKE Takamitsu(*79)	SHINA Tomio
OHASA Kazumi	TAMAI Hiroshi	UEHARA Kazuya
SHOJI Teruaki		
YAMAUCHI Toshihiko		

Department of Fusion Facility

TANAKA Yuji (Director)	OHTA Mitsuru (Deputy Director)
------------------------	--------------------------------

Fusion Facility Administration

KANAZAWA Tetsuo (General Manager)

JT-60 Facility Division I

KONDO Ikuo (Head)	AKIBA Kenichi(*79)	ARAKAWA Kiyotsugu
AKASAKA Hiromi	ISAKA Masayoshi	KAWAMATA Youichi
HISADA Kenji(*28)	KIUCHI Shigemi(*30)	KURIHARA Kenichi
KIMURA Toyooki	MATSUZAKI Yoshimi	MIYACHI Kengo
KUSAKA Makoto(*28)	NAKAKUKI Riichi(*49)	OMORI Kenichiro
MUTOH Mitugu	OMORI Yoshikazu	SEIMIYA Munetaka
OMORI Shunzo	TERAKADO Tsunehisa	TOTSUKA Toshiyuki
TAKAHASHI Minoru	YONEKAWA Izuru	YOSHIDA Michiharu
YAMAGISHI Koujiro		

JT-60 Facility Division II

SHIMIZU Masatugu (Head)	ARAI Takashi	HIRATSUKA Hajime
ANDO Toshiro	ICHIGE Hisashi	JIMBOU Ryutarou(*2)
HONDA Masao	KODAMA Kozo	KOIKE Tsuneyuki
KAMINAGA Atsushi	MIYAKE Kazuyuki(*39)	MIYO Yasuhiko
MATSUKAWA Makoto	OHUCHI Yutaka	SAIDOH Masahiro
OGIWARA Norio	SASAKI Noboru(*2)	TAKASAKI Manabu(*2)
SASAJIMA Tadashi	TSURUMI Satoshi(*2)	YAGYU Junichi
TANAKA Takejiro		

RF Facility Division

YAMAMOGO Takumi (Head)	FUJII Tsuneyuki	FUKUDA Hiromi
ANNOH Katsuto	IKEDA Yukiharu	KITAI Tatsuya(*28)
IKEDA Yoshitaka	MORIYAMA Shinichi	NIHONMATSU Yuuji(*28)
KIYONO Kimihiro	SEKI Masami	SHINOZAKI Shinichi
SAWAHATA Masayuki	SUZUKI Norio	TAKASA Akira
SUGANUMA Kazuaki	YOKOKURA Kenji	
TERAKADO Masayuki		

NBI Facility Division

KUNIEDA Toshisuke (Head)	KURIYAMA Masaaki (Deputy Head)	
AKINO Noboru	EBISAWA Noboru	ITOH Masaru(*31)
KAWAI Mikito	KASHIMURA Takanori(*30)	KAZAWA Minoru
MATSUOKA Mamoru	MIZUNO Makoto	MOGAKI Kazuhiko
OHGA Tokumichi	OOHARA Hiroshi	SHIMIZU Kazuhiko(*30)
TAKAHASHI Shunji	SUZUKI Yasuo(*28)	TAKAYASU Toshio(*79)
USAMI Hiroji(*2)	USUI Katsutomi	YAMAMOTO Masahiro

JFT-2M Facility Division

SUZUKI Norio (Head)		
HASEGAWA Koichi	HONDA Atsusi	KASHIWA Yoshitoshi
KIKUCHI Kazuo	KOMATA Masao	OKANO Fuminori
SAITO Masaya(*30)	SHIBATA Takatoshi	SUZUKI Sadaaki
TANI Takashi	TOKUTAKE Toshikuni	

Department of Fusion Engineering Research

SHIMAMOTO Susumu (Director)	SHOJI Kuniaki (Administrative Manager)
-----------------------------	--

Plasma Engineering Laboratory

MURAKAMI Yoshio (Head)		
ABE Tetsuya	HAMAZAKI Masanori(*30)	HIROKI Seiji
KASAI Satoshi		

Superconducting Magnet Laboratory

TSUJI Hiroshi (Head)		
ANDO Toshinari	EBISU Hideki(*18)	HAMADA Kazuya
HIYAMA Tadao	HOSONO Fumikazu(*87)	IWAMOTO Shuichi(*23)
KATO Takashi	KAWANO Katsumi	KOIZUMI Norikiyo
MIYAKE Akihiro(*14)	NAKAJIMA Hideo	NISHI Masataka
OSHIKIRI Masayuki(*30)	SASAKI Tomoyuki(*4)	SUGIMOTO Makoto
SEKI Shuichi(*30)	TAKAHASHI Yoshikazu	TAKANO Katsutoshi(*30)
TSUKAMOTO Hideo(*2)	WAKABAYASHI Hiroshi(*30)	WADAYAMA Yoshihide(*2)
YASUKAWA Yukio(*58)	YOSHIDA Kiyoshi	

NBI Heating Laboratory

OHARA Yoshihiro (Head)		
AKIBA Masato	ARAKI Masanori	DAIRAKU Masayuki
HANADA Masaya	INOUE Takashi	MAENO Shuichi(*59)
NAKAMURA Kazuyuki	NISHINO Yoshihiko	OKUMURA Yoshikazu
SATOH Kazuyoshi	SMID Ivica(*88)	SUZUKI Satoshi
TANAKA Masanobu(*2)	TANAKA Shigeru	WATANABE Kazuhiro
YOKOYAMA Kenji		

RF Heating Laboratory

IMAI Tsuyoshi (Head)		
SHIHO Makoto	TSUNEOKA Masaki	SAKAMOTO Keishi
SAIGUSA Mikio	MAEBARA Sunao	KASUGAI Atsushi
WATANABE Akihiko(*40)	FUJITA Hideo(*30)	KIKUCHI Masaya(*30)
STEPHEN Musyoki(*90)		

Tritium Engineering Laboratory

NARUSE Yuji (Head, ~92 Sep.)	OKUNO Kenji (Head, 92 Oct.~)	
AMANO Junzo(*23)	ASHIBE Kusuo(*4)	ENOEDA Mikio
HAYASHI Takumi	HIRATA Kazuhiro(*29)	HONMA Takashi
INOUE Masahiko(*23)	KONISHI Satoshi	KURASAWA Toshimasa
MATSUDA Yuji	MATSUMOTO Akihiko(*29)	NAKAMURA Hirofumi
OBATA Hiroyuki(*16)	SAKURABA Takayoshi(*2)	SHU Wei Min(*35)
SUZUKI Takumi	YAMADA Masayuki	YAMANISHI Toshihiko

Reactor Structure Laboratory

SHIMAMOTO Susumu (Head)		
TADA Eisuke	OBARA Kenjiro	NISHIO Satoshi
SHIBANUMA Kiyoshi	KURASAWA Toshimasa	KAKULATE Satoshi
SATO Satoshi	KANAMORI Naokazu(*2)	TERAKADO Takuya(*31)
OKA Kiyoshi	NAKAHIRA Masataka	

Fusion Reactor System Laboratory

SEKI Yasushi (Head)
AOKI Isao

Department of ITER Project

SHIKAZONO Naomoto (Head)
SHIMOMURA Yasuo SEKI Shogo

Administration Group

HINO Shunji

Project Management Group

MATSUDA Shinzaburo MATOBA Tohru TSUNEMATSU Toshihide

Joint Central Team Group

FUJISAWA Noboru	NAGASHIMA Takashi	TANAKA Shigeru
YOSHIDA Hiroshi	YAMAMOTO Shin	SUGIHARA Masayoshi
HORIIKE Hiroshi	MATSUMOTO Hiroshi	OKUNO Kiyoshi
SAJI Gen(*7)	MIZOGUCHI Tadanori(*2)	SHIMIZU Katsusuke(*23)
KONDOH Mitsunori(*4)	MORI Seiji(*16)	SATO Koichi(*83)

Home Team Design Group

TAKATSU Hideyuki	KOIZUMI Kouichi	OOKAWA Yoshinao
OKAZAKI Takashi(*2)	SASAKI Takashi(*15)	SHIBUI Masanao(*4)
MURAKAMI Yoshiki(*4)	NOMURA Yukio(*17)	HASHIMOTO Toshiyuki(*16)
SAWA Masafumi(*14)	HOTTA Masataka(*58)	ZIMIN Sergei(*90)

- *1 General Atomics, USA
- *2 Hitachi Ltd.
- *3 Lawrence Livermore National Laboratory, USA
- *4 Toshiba Corp.
- *5 Max-Planck Institute für Plasmaphysik, FRG
- *6 Massachusetts Institute of Technology, USA
- *7 Mitsubishi Atomic Power Industry Inc.
- *8 The University of Tokyo
- *9 Nagoya University
- *10 Okayama University
- *11 Kyoto University
- *12 Hiroshima University
- *13 Institute für Reaktorbauelemente, KfK, FRG
- *14 Ishikawajima-Harima Heavy Industries, Ltd.
- *15 Mitsubishi Electric Co., Ltd.
- *16 Kawasaki Heavy Industries, Ltd.
- *17 Hazama-gumi Ltd.
- *18 Kobe Steel Ltd.
- *19 Oak Ridge National Laboratory, USA
- *20 Century Research Center Corp.
- *21 Northwestern Laboratory
- *22 Institute of Plasma Physics, Nagoya University
- *23 Mitsubishi Heavy Industries, Ltd.
- *24 NAIG Nuclear Research Laboratory
- *25 Japan Atomic Industrial Forum
- *26 Central Research Institute for Electric Power
- *27 NEC Co.
- *28 Kaihatsu Denki Co.
- *29 Sumitomo Heavy Industries, Ltd.
- *30 Nuclear Engineering Co., Ltd.
- *31 Tomoe Shokai
- *32 Ibaraki Kohsan
- *33 Tokyo Nuclear Service Co., Ltd.
- *34 ULVAC Corp.
- *35 Kyushu University
- *36 Contract Researcher
- *37 Princeton Plasma Physics Laboratory, USA
- *38 LITEC Co., Ltd.
- *39 Japan Expert Clone Corp.
- *40 Nissei Sangyo Co., Ltd.
- *41 JET Joint Undertaking, UK
- *42 Hodaka Seiki Ltd.
- *43 Sumitomo Electric Industries, Ltd.
- *44 Nikon Corp.
- *45 National Laboratory for High Energy Physics
- *46 University of Tsukuba
- *47 Los Alamos National Laboratory, USA
- *48 Japan Radiation Engineering Co.
- *49 Nuclear Energy Data Center Co.
- *50 Osaka University
- *51 Imperial College, UK
- *52 Institute of Research Hydro-Quebec, Varenns, Canada
- *53 KFA-IPP, FRG
- *54 Ewic Engineering Co., Ltd.
- *55 ORC Manufacturing Co., Ltd.
- *56 Koike Sanso Kogyo Co., Ltd.
- *57 Hitachi Sanso Co., Ltd.

Tritium Engineering Laboratory

NARUSE Yuji (Head, ~92 Sep.)	OKUNO Kenji (Head, 92 Oct.~)	
AMANO Junzo(*23)	ASHIBE Kusuo(*4)	ENOEDA Mikio
HAYASHI Takumi	HIRATA Kazuhiro(*29)	HONMA Takashi
INOUE Masahiko(*23)	KONISHI Satoshi	KURASAWA Toshimasa
MATSUDA Yuji	MATSUMOTO Akihiko(*29)	NAKAMURA Hirofumi
OBATA Hiroyuki(*16)	SAKURABA Takayoshi(*2)	SHU Wei Min(*35)
SUZUKI Takumi	YAMADA Masayuki	YAMANISHI Toshihiko

Reactor Structure Laboratory

SHIMAMOTO Susumu (Head)		
TADA Eisuke	OBARA Kenjiro	NISHIO Satoshi
SHIBANUMA Kiyoshi	KURASAWA Toshimasa	KAKUDATE Satoshi
SATO Satoshi	KANAMORI Naokazu(*2)	TERAKADO Takuya(*31)
OKA Kiyoshi	NAKAHIRA Masataka	

Fusion Reactor System Laboratory

SEKI Yasushi (Head)
AOKI Isao

Department of ITER Project

SHIKAZONO Naomoto (Head)
SHIMOMURA Yasuo SEKI Shogo

Administration Group

HINO Shunji

Project Management Group

MATSUDA Shinzaburo MATOBA Tohru TSUNEMATSU Toshihide

Joint Central Team Group

FUJISAWA Noboru	NAGASHIMA Takashi	TANAKA Shigeru
YOSHIDA Hiroshi	YAMAMOTO Shin	SUGIHARA Masayoshi
HORIIKE Hiroshi	MATSUMOTO Hiroshi	OKUNO Kiyoshi
SAJI Gen(*7)	MIZOGUCHI Tadanori(*2)	SHIMIZU Katsusuke(*23)
KONDOH Mitsunori(*4)	MORI Seiji(*16)	SATO Koichi(*83)

Home Team Design Group

TAKATSU Hideyuki	KOIZUMI Kouichi	OOKAWA Yoshinao
OKAZAKI Takashi(*2)	SASAKI Takashi(*15)	SHIBUI Masanao(*4)
MURAKAMI Yoshiki(*4)	NOMURA Yukio(*17)	HASHIMOTO Toshiyuki(*16)
SAWA Masafumi(*14)	HOTTA Masataka(*58)	ZIMIN Sergej(*90)

- *58 Fuji Electric Co., Ltd.
- *59 Nissin Electric Co., Ltd.
- *60 Sandia National Laboratories, USA
- *61 JGC Corp.
- *62 Tokyo Institute of Technology
- *63 Nuclear Research Center Karlsruhe, FRG
- *64 Argonne National Laboratory, USA
- *65 ITER Team
- *66 Yokohama National University
- *67 Nihon Software Kaihatsu, Inc.
- *68 Kanazawa Computer Service Corp.
- *69 University of California at Los Angeles, USA
- *70 University of Texas, USA
- *71 Varian Company Co., Ltd.
- *72 Nagaoka University of Technology
- *73 Denki Kogyo Co., Ltd.
- *74 The NET Team
- *75 National Institute for Fusion Science
- *76 I.V. Kurchatov Institute of Atomic Energy
- *77 Keio University
- *78 Mitsubishi Cable Industries, Ltd.
- *79 Nippon Advanced Technology Co., Ltd.
- *80 Hamamatsu Photonics KK
- *81 University of California at San Diego, USA
- *82 University of Maryland
- *83 Atomic Data Service Corp.
- *84 Nihon Houshasen Engineering Co., Ltd.
- *85 ACE
- *86 Hitachi Works
- *87 Hitachi Cable, Ltd.
- *88 Austrian Research Center Seibersdorf
- *89 STA Fellowship
- *90 JAERI Fellowship
- *91 Nuclear Information Service Co.
- *92 Tokai University
- *93 Ibaraki Software